Acta Neurochir (2011) 153:1551–1559
DOI 10.1007/s00701-011-1050-1

REVIEW ARTICLE

Surgical management of glioneuronal tumors with drug-resistant epilepsy

Kareem A. Zaghloul · Johannes Schramm

Received: 6 May 2011 / Accepted: 9 May 2011 / Published online: 21 May 2011

Abstract In this review, we discuss the options for the surgical management of glioneuronal tumors (GNTs) associated with drug-resistant epilepsy, with an emphasis on the surgical issues involved in addressing the epileptogenic nature of these lesions. We briefly summarize the pathological hallmarks of these lesions in order to outline how these tumors contribute to seizure activity. Understanding the pathophysiology of these lesions is important in discussing the advantages and disadvantages of different surgical strategies. There have been a number of studies that have investigated the utility of different surgical approaches in improving seizure outcome, and we highlight some of these studies in order to shed light on surgical issues related to these tumors.

Keywords Glioneuronal tumors · Ganglioglioma · DNT · Epilepsy

Introduction

Glioneuronal tumors (GNT) are rare tumors of the central nervous system, comprised of both neuronal and glial elements [13, 20]. Despite their generally benign nature, however, these tumors have been increasingly implicated in causing medically intractable seizure disorders in children and young adults [41, 42, 59, 68]. Recent research over the past decade has advanced our understanding of these tumors, yet the optimal surgical management of patients with these tumors remains controversial.

Neuroepithelial neoplasms are found in up to 30% of patients with long-term medically refractory epilepsy lasting over 2 years [30, 37, 41, 64]. While higher grade glial tumors, such as astrocytomas and oligodendrogliomas, represent some of these tumors, the majority of tumors causing long-term medically refractory seizures can be classified as GNTs [29, 41, 43, 59, 68, 69]. According to the latest World Health Organization classification, there are 12 different types of glioneuronal tumors [40]. The majority of the literature investigating the role of GNTs in causing medically refractory seizures, however, focuses on gangliogliomas (GG) and dysembryoplastic neuroepithelial tumors (DNT), the most common types of GNTs.

Surgically addressing GNTs raises two important neurosurgical distinctions. First, a distinction must be made between GNTs associated with one or only a few seizures and GNTs associated with drug-resistant epilepsy, classically defined as a seizure disorder of a 2-year minimum duration despite maximal drug treatment. This review focuses on the surgical treatment of the latter class of GNTs. Secondly, unlike most neoplasms, the surgical goals for patients with GNTs associated with medically refractory epilepsy are not primarily oncologic in nature, but are firstly aimed at addressing the resultant seizure disorder. As such, the optimal surgical strategies one should use in addressing these tumors are focused on improving seizure outcome. Complete tumor removal is also a goal, but small residual remnants following resection are not considered truly dangerous and do not usually shorten life expectancy, as malignant GNTs have only rarely been described [43].

K. A. Zaghloul
Surgical Neurology Branch, NINDS, National Institutes of Health, Bethesda, MD, USA

J. Schramm (✉)
Department of Neurosurgery, University of Bonn,
Sigmund-Freud-Str. 25,
53105 Bonn, Germany
e-mail: Johannes.Schramm@ukb.uni-bonn.de

These strategies, although vigorously debated in the literature, are still not clearly defined. In this review, we briefly describe the pathophysiological basis of the epileptogenic nature of GNTs in order to understand how the epileptogenic nature of these lesions informs surgical decisions. We then focus the majority of this review on the debate surrounding the optimal surgical treatment of GNTs.

Histopathology of GNTs

Although GNTs share some of the features found in gliomas, they contain an additional neuronal component and only very rarely exhibit malignant progression [24]. GNTs lack the PTEN mutation commonly found in higher grade gliomas [24], which is likely one of the reasons for their generally benign nature. The majority of GNTs described in the literature are DNTs and GGs, and despite their low incidence, they account for a significant portion of tumors associated with long-term medically refractory epilepsy. Other types of GNTs include desmoplastic infantile gangliogliomas, papillary glioneuronal tumors, and rosetted glioneuronal tumors, which can all be epileptogenic in nature [2, 25, 40]. Because the pathophysiology for epileptogenicity in these lesions seems similar to both DNTs and GGs, the management of these other forms of GNTs will also likely be similar.

The histopathologic hallmark of DNTs, first described by Daumas-Duport [22], is the glioneuronal element. This entity is comprised of neurons floating in a myxoid interstitial fluid with oligodendrocyte-like cells attached to the bundles of axons [20], and can often be seen radiographically as multiple pseudocysts [13]. DNTs that contain only a glioneuronal element are classified as simple, whereas complex DNTs contain glial nodules and may contain both calcifications and hemorrhage [13, 21]. A nonspecific variant that lacks a glioneuronal element has been subsequently introduced [21], but this classification remains debated. Most DNTs are found in the temporal lobe, but frontal, parietal, and occipital DNTs, especially of the complex variety, have been reported [9, 13, 15].

The histopathological elements that define GGs, first described by Perkins [51], are dysplastic neurons and neoplastic glial cells. On gross specimen, GGs tend to be a yellow/brown firm mass that is well delineated, sometimes cystic, and occasionally calcified [43]. GGs can be predominantly neuronal or predominantly glial as both cell populations can exhibit marked heterogeneity [42]. Their precise pathogenesis is not well understood, and there have been cases reported associated with neurofibromatosis and Peutz-Jeghers syndrome [43]. Some authors contend that GGs fall on a more advanced end of a spectrum that includes focal cortical dysplasias (FCD) since both have similar radiographic appearances and both exhibit increased polymorphism of TSC2 [11, 67]. Although some GGs exhibit clear cell morphology that complicates their diagnosis, GGs express CD34, lack MAP2, and have a low Ki67, which often secures the diagnosis [12]. GGs represent 1.3% of all brain tumors and 0.4% of CNS tumors [42]. The vast majority of GGs are found in the temporal lobe, with most of these lying in temporomesial locations [34, 35, 41, 42, 46, 47, 62].

Pathophysiology of GNTs in medically refractory epilepsy

GNTs have been strongly implicated in causing long-term medically refractory seizures that are often the major clinical symptom that leads patients to present to their physician [12, 34, 42]. Roughly 30% of patients with medically refractory epilepsy have an underlying neoplastic lesion [41, 68], the majority of which are GNTs. Although only a subset of patients with medically refractory epilepsy exhibits an underlying GNT, the presence of GNTs is associated with refractory epilepsy in 90–100% of patients [55, 59]. For these patients where medical treatment has failed, the priority is reducing seizures or eliminating them altogether, as refractory epilepsy contributes to a worsening quality of life and higher incidences of morbidity.

GGs are the most common tumor in young patients who present with long-term medically refractory epilepsy [7, 19, 43, 62]. Between 20–40% of patients with chronic temporal lobe epilepsy have an underlying GG or DNT structural lesion [12, 41, 42, 62]. In one study, more than 85% of patients with GGs presented with chronic epilepsy lasting over 2 years [42]. However, despite their epileptogenic nature, there are cases when a GNT is not involved in seizure activity or when removal of a GNT does not improve seizure outcome [32]. A subset of patients, for example, exhibits additional cortical dysplasias or other foci of seizure activity [41]. Removal of the GNT in these patients may result in poor seizure outcomes, suggesting that the presence of a GNT in the setting of a seizure disorder does not obviate the need for a complete seizure workup to identify the best treatment strategy.

It is important to understand how GNTs can cause seizures, as such mechanisms will dictate surgical strategies. Although the precise pathological mechanisms for how GNTs cause seizures are not completely understood, proposed hypotheses center around how these tumors disrupt surrounding tissue. This critically affects how to think about these lesions from a surgical perspective, as the goal of surgery in these cases is an epileptological rather than an oncological one.

In general, tumors can affect surrounding brain tissue with edema, mechanical pressure, irritation, vascular insufficiency, irritation, and the induction of gliosis, and alterations in the

surrounding neuronal networks [63, 68, 70]. One possibility is that the neural component of GNTs contributes to the epileptogenic nature, but there is as yet no compelling evidence for this theory [10, 63]. More likely, low-grade intra-axial tumors, such as GNTs, can invade normal tissue, resulting in altered and overexpressed levels of neurotransmitters [70] and in inflammatory reactions with an accumulation of microglial cells [3]. Hypoxic effects on surrounding tissue may result in local irritation and abnormal neuronal growth [68].

Adjacent cortical areas may undergo dysplastic reorganization, which may lead to abnormal excitability [58, 59]. The complex epileptogenic networks that arise in areas adjacent to GNTs may result from alterations in the GABAergic system, as the density of inhibitory neuron subtypes has been shown to be reduced in areas adjacent to the tumor [4]. Furthermore, deafferentation of adjacent cortical regions can lead to denervation hypersensitivity [68]. MEG studies have demonstrated that adjacent cortical areas modify synchronization of local networks, which can lower thresholds for seizure activity [5, 54]. And neurotransmitters have been found to be overexpressed in adjacent cortical regions [58]. One common hypothesis is that seizures are primarily generated in the border zone (some use the term "collision zone") between solid tumor and normal brain structure. The precise extent of that presumed ictogenic zone remains unclear.

Clearly, for any patient presenting with a GNT with medically refractory seizures, a comprehensive approach to clarify the spatial relationships between the epileptogenic zone and the lesion is needed. That there is substantial evidence that these tumors can alter the surrounding brain tissue suggests that the best surgical outcome from an epileptogenic perspective must take this into account in order to reduce the frequency of postoperative seizures.

Surgical approaches to GNTs

The role of surgery for patients with GNTs is primarily focused on the epileptic nature of the disease. In routine oncological surgeries, the extent of resection is dictated by minimizing the likelihood for recurrence. Because of their benign nature, once removed, GNTs tend not to recur. Rates of recurrence and malignant progression for grade I GNTs, although not zero, range between 2 and 5% [41–43]. As such, surgical strategies instead focus on improving seizure outcome. If complete removal is easily achieved, it should be the goal of surgery. Even so, the optimal surgical strategies beyond this initial goal are vigorously debated in the literature, and no clear consensus has emerged.

The surgical approaches available for removing GNTs fall into one of three broad categories: surgical resection of the lesion only, surgical resection of the lesion with a surrounding rim of cortex, or surgical resection of the lesion with an additional corticectomy to maximize resection of the entire epileptogenic zone. Whereas the first two approaches can be guided with preoperative imaging and intraoperative visualization of the lesion, the latter approach involves a comprehensive approach to generate a three-dimensional spatial map of the entire epileptogenic zone.

For lesionectomies or for lesionectomies with an additional resection of a rim of surrounding cortex, MRI serves as the mainstay of preoperative diagnostic evaluations to guide the surgical approach. GNTs are most often found supratentorially, and among those, most often in the temporal lobes. In one study investigating 235 patients with temporomesiobasal tumors, 22% of lesions were found to be GGs or DNTs [60]. Tumors were classified based on location into purely mesiobasal tumors, lateral tumors, paramesial tumors, tumors with a combined mesial and paramesial component, and tumors that extended into the temporal stem and lateral insula. The vast majority of tumors were purely mesiobasal in location, which also portended a benign progression [60]. In another study focused on lesional mesial temporal lobe epilepsy (TLE), 78 patients with limited mesial temporal resections (out of 738 TLE patients) were followed for a mean of 49 months [17]. Forty-three of these 78 patients had developmental tumors, of which one had been overlooked in the preoperative MRI. Until recently, such mesial tumors were treated with biopsy and radiation, but with current advances in neurosurgical techniques, the available surgical options for tumors in these locations include a transsylvian approach, anterior temporal lobectomy, resection of the temporal pole, a subtemporal approach, and a transcortical approach. While the authors of this study were generally focused on temporomesiobasal tumors of all types, the approaches are still relevant for those temporobasal tumors that are classified as GNTs.

A separate study focused on outcomes following different types of resections for pediatric patients with temporal lobe epilepsy [18]. Almost half of these patients had a temporal lobe tumor that was presumed to be the causative agent in the patient's seizure disorder, and most of these were classified as GNTs. After following patients for a mean of 46 months, the authors concluded that temporal lobectomy followed closely by selective amygdalohippocampectomy offered the best seizure outcomes [18].

A number of other studies have examined the factors that affect seizure outcome following surgical resection of GGs in both temporal and extratemporal locations. In one study, patients who had a complete tumor resection had a 86% rate of seizure freedom following surgery compared to an 8% rate in those that had an incomplete resection, suggesting that the degree of resection correlates with the seizure outcome [35]. In other studies, patients had a better

seizure outcome following resection of temporal and extratemporal GGs when surgery was performed at a younger age and after a shorter duration of medically refractory epilepsy [33, 47]. Similarly, recent studies found that the most significant factors for seizure freedom are the completeness of resection and the duration of preoperative medically refractory epilepsy [31, 59, 71]. The fact that patients with a longer duration between epilepsy onset and tumor resection do worse than those with early resection makes sense when viewed in the context of data suggesting that tumors cause disruption and abnormal reorganization of adjacent tissue.

In a study comparing lesionectomy alone to lesionectomy with cortical resection for lateral and basal tumors, the authors adopted a strategy for addressing mesial temporal lobe structures [14]. Mesial structures were resected if the tumor involved these structures. However, in the cases when the mesial structures were radiologically normal in appearance, they were spared on the dominant side and only resected on the non-dominant side. Similarly, for lateral tumors that were in or near eloquent cortex, lesionectomy alone was performed. This strategy resulted in a 69% seizure-free rate [14]. In a separate study focusing on extratemporal tumors, however, structural resections of GNTs yielded better seizure outcomes than non-lesional frontal epilepsy surgery, but worse than surgery for temporal lobe epilepsy, suggesting that limitations imposed by functional cortex in extratemporal lobe locations and a possibly larger epileptogenic zone in these regions limit seizure freedom [72].

Most authors agree that gross total resection is better for seizure outcome [35, 50, 56], although there are reports that seizure outcomes are similar for gross and incomplete resections [38]. Some authors contend that medial temporal lobe tumors induce seizure activity in the adjacent mesial temporal structures, hence necessitating their removal [6, 26, 44, 45, 52, 57]. However, whether these structures remain epileptogenic after removal of an adjacent tumor remains unclear, although in one study, the authors contend that lesionectomy alone resulted in higher rates of re-operation with extension of the resection to include mesial structures to attain seizure freedom [9]. Clearly, if there is evidence of dual pathology on preoperative imaging, which can occur in 50–60% of patients with GNTs, then resection of the mesial structures is warranted [23, 46, 52]. Conversely, there are few who argue against simple lesionectomies for lateral temporal lobe tumors that seem to represent a different entity in regards to surgical strategy [62].

Finally, in a recent study investigating mesial temporal lobe GNTs, lesionectomy alone was compared to tailored resections to assess seizure outcome rates [29]. Medial temporal GNTs usually involve the uncus, amygdala, entorhinal cortex, and sometimes the hippocampus itself, suggesting that the tumor becomes involved in a wider epileptogenic network [1, 3, 4, 14, 15, 28, 29, 61, 66]. The tailored resections included resection of the tumor, temporal pole, hippocampus, and parahippocampal gyrus in an attempt to remove abnormal tissue contributing to seizure activity. The authors found a significant improvement in seizure outcome for those patients undergoing a tailored resection, suggesting that for medial temporal lobe tumors, the mesial structures are epileptogenic and should be resected even in the absence of imaging abnormalities [29]. In our own study of 78 patients who underwent a limited resection for lesional mesial temporal lobe epilepsy (43 patients with GG or DNT), various tailored resection types were employed resulting in an Engle class I outcome in 78% of patients [17].

Our own policy has always been to perform a lesionectomy with a surrounding rim of tissue, preferring that to a simple lesionectomy alone. Provided that the GNT is the only detectable lesion and is not located in or close to eloquent cortex and that seizure semiology or type does not suggest the involvement of larger cortical areas, our standard resection entails a lesionectomy with a surrounding rim of 0.5 to 1 cm of cortex. However, in cases when the lesion borders or lies within functionally important cortex, we restrict our resection to a simple lesionectomy without resection of a surrounding rim of tissue. Temporomesially located GNTs, i.e., tumors that are located in the amygdala or the hippocampal-parahippocampal areas, are also resected with a rim of a tissue as a minimum extent of resection (Fig. 1). An important dilemma arises with tumors that are not too big and are located along the axis of the hippocampal-parahippocampal block, where it may be possible to leave part of the hippocampus behind. Here, one must decide whether to perform a classical full mesial resection or whether to resect just the tumor with a small rim of adjoining hippocampus or parahippocampus. This decision can be facilitated by inserting depth electrodes along the length of the hippocampus to elucidate whether seizures also originate in a part of the hippocampal-parahippocampal bloc far from the lesion itself. Finally, we utilize the third type of resection, a lesionectomy, with an additional corticectomy of adjoining ictal cortex only in the case when invasive evaluation with strip or grid electrodes suggests that such a strategy would reduce seizure activity.

Any surgical strategy has a risk of complications, and these complications will depend upon the location of the GNT to be resected. Those tumors near functionally eloquent cortex increase the risk of postoperative neurological deficits, and in the event where a clear distinction cannot be made between tumor and eloquent cortex, intraoperative mapping and monitoring may be beneficial

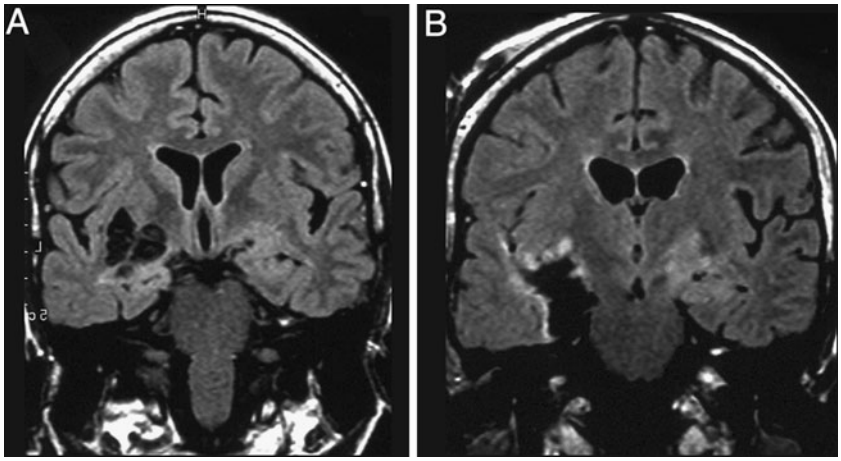

Fig. 1 **a** Coronal MRI of a 31-year-old female with a gangliogliomas under the insular cortex and in the temporal stem. **b** A postoperative MRI demonstrates that not only the tumor was removed, but also the amygdala. The hippocampus was left behind. Seizure outcome was ILAE 2 with a follow-up of 54 months

[48]. Complications of surgery for lesions in the mesial temporal lobe include hemiparesis, visual deficits, oculomotor disturbances, dysphasia, and vascular injury of vessels in the paramesencephalic cistern [6, 60].

In general, while no clear surgical strategy has been set forth, the first stages of a fragile consensus have emerged guiding surgical strategies for GNTs causing medically refractory epilepsy. First, there is relatively convincing evidence that GNTs invading mesial temporal structures warrant resection of those structures, both on the dominant and non-dominant side. Second, medial temporal lobe GNTs on the non-dominant side that do not invade mesial structures should be resected with the mesial structures, while those on the dominant side can be resected with a small rim but sparing much of the mesial structures. Although there is some evidence that radiologically normal mesial structures still contribute to the epileptogenic disorder, some authors believe the risks of resecting dominant mesial structures may outweigh the potential benefits. This is another situation where the insertion of a depth electrode into the hippocampus can facilitate the decision as to whether the dominant hippocampal structures should be taken or left behind. Third, lateral temporal lobe and extratemporal lobe tumors can be adequately addressed with lesionectomy alone as long as care is taken to respect functionally eloquent areas of cortex. From our own experience, we always prefer a lesionectomy with resection of a surrounding rim of tissue, arising out of our conviction that seizures originate in the border zone between the tumor proper and the surrounding normal cortex, although we are well aware that the advantages over a pure lesionectomy alone have not been demonstrated (Fig. 2). And finally, the completeness of tumor resection and pre-operative duration of medically refractory epilepsy are the most important factors in determining seizure outcome, suggesting a surgical strategy that is focused on early and *complete* intervention.

Invasive monitoring for GNTs

Because GNTs have been implicated in long-term medically refractory epilepsy, it is clear that the surgical management of these tumors must focus on the epileptogenic nature of the lesions rather than their oncological potential. Clearly, a complete resection should be one of the goals of surgery if it can be achieved without causing deficits. But from an epileptogenic perspective, resection of the epileptogenic zone is critical to ensure good seizure outcome. While preoperative imaging and intraoperative visualization alone may guide such resections, to develop a complete spatial map of the epileptogenic zone, some authors have utilized intraoperative electrocorticography (ECoG) and invasive monitoring with subdural electrodes in order to electrophysiologically delineate the epileptogenic zone. The contention is that this approach allows the surgeon to properly identify tissue that must be resected in order to eliminate seizure activity.

Invasive monitoring with ECoG has been used in a number of studies to tailor GNT resections. ECoG identifies areas of interictal spiking activity that would suggest involvement in an epileptogenic network. In many cases where ECoG has identified adjacent or other areas of epileptic activity, particularly in temporal lobe tumors [49, 68], patients were noted to have had a longer duration of medically refractory epilepsy, suggesting that with time more cortical areas are recruited into the epileptogenic zone [41]. However, in one study investigating post-excisional ECoG, no relationship was found between the presence of inter-ictal activity and seizure outcome [7].

In one of the earliest studies investigating the use of invasive monitoring to tailor resections, both intra-operative ECoG and invasive monitoring with subdural grids for those patients unable to tolerate an awake procedure were used to map functional areas of cortex and the epileptogenic zone [8]. After resection, the authors additionally used ECoG to document removal of the epileptogenic zone. With

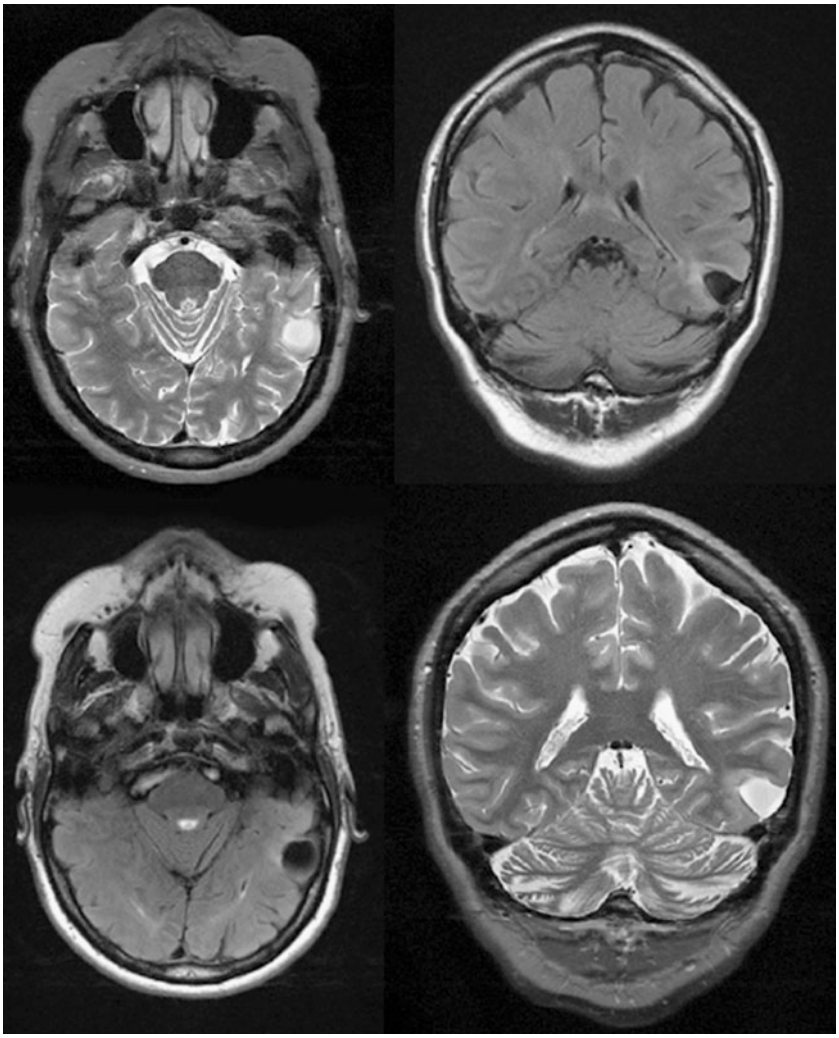

Fig. 2 Axial and coronal MRI cuts of a left temporo-occipito-lateral cystic lesion in the T3 gyrus in a 50-year-old patient with seizures for the past 44 years. A lesionectomy with resection of a rim of surrounding cortex of about 6–8 mm was performed, and histology proved it to be a ganglioglioma. There was no postoperative field defect. Follow-up is too short to provide reliable seizure outcome

seizure-freedom rates of over 90%, the authors of this study conclude that ECoG is an important tool in identifying multiple foci of epileptogenic activity and for improving seizure outcome, consistent with the simultaneous findings of another group [8, 53].

In a later study of temporal lobe tumors, ECoG was used to determine the location of interictal spiking activity in order to compare lesionectomy alone to ECoG tailored resections [36]. Similar to the earlier studies, the authors found a significantly high rate of seizure freedom for the ECoG group, suggesting that ECoG is an important adjunct in surgical planning for these types of lesions. More recently, intraoperative ECoG was used to delineate additional areas of abnormal electrical activity in the hippocampus and amygdala during the resection of temporal GNTs [65]. The authors noted considerable spiking activity in the hippocampus after resection, suggesting that this phenomenon may exist in resections without ECoG as well. What is unclear, however, is whether these spikes reach the stage of independent epileptogenicity and whether they influence clinical seizures. Despite this uncertainty, however, the authors conclude that seizure outcome will be improved with resection of mesial temporal structures with ECoG guidance [65], a strategy that has also been used for critically located gliomas [39].

Another important way to better define the ictogenic area is extra-operative monitoring with implanted depth, strip, or grid electrodes. A disadvantage of this approach is that a second surgery for the implantation of these electrodes is necessary. However, one great advantage is that one has the chance to record not only interictal ECoG, but to record seizures during the monitoring period that may last up to 2 weeks. Another advantage is that seizures can be recorded not only with surface electrodes, but also with electrodes that can be brought very close to the suspected lesion. A typical setup would involve two or three strip electrodes covering the borders of a lateral temporal lobe lesion close to the speech area in order to define the posterior extent of an additional corticectomy and how close that resection would come to eloquent speech areas. Another typical scenario would include the implantation of a grid over a

lesion and adjoining eloquent cortex, such as cortex involved in speech or motor function. A third typical scenario involves the implantation of depth electrodes in the hippocampus when lesions are located temporo-basally close to the hippocampus, and the surgical strategy requires a decision as to whether the hippocampus may be left behind or should be included in the resection. In a recent study investigating the use of motor-evoked potentials in 27 cases where a lesion was located close to the motor cortex, new deficits were shown to be more frequent without successful monitoring, whereas seizure control was significantly improved in successfully monitored cases [48].

In general, many authors report that tailored resections focusing on resection of the epileptogenic zone yields better seizure outcomes than standard resections [27, 29, 49, 59]. However, it is also important to recognize that numerous studies note that the use of intraoperative ECoG did not result in a significant difference in outcomes [13, 16, 34, 37, 47]. One potential confounder of these comparisons, however, is that ECoG may be employed for patients with poorer preoperative seizure control, which would suggest a favorable bias for those patients not receiving ECoG. The debate regarding invasive monitoring and ECoG remains to be settled, as invasive monitoring usually being restricted to recording interictal activity has yet to be convincingly shown to improve seizure outcome. In our center, surgical strategies are based on the hypothesis that invasive monitoring of ictal events with subdural or depth electrodes has many advantages. In cases where a difficult decision must be made, we prefer using such monitoring to simple intraoperative ECoG recordings. In all, the general consensus that is emerging is that surgical intervention for GNTs should be guided by the principles of epilepsy surgery rather than oncologic surgery, which in practice means that an epileptogenic zone should be preoperatively defined as clearly as possible to guide surgical resection.

Conclusion

Over the past 2 decades, glioneuronal tumors have been shown to play an increasingly important role as a causative agent in medically refractory epilepsy. The precise pathophsyiological evidence for how epileptogenicity arises in the context of these tumors remains unknown, but it is likely that these tumors cause disruptions in the organizational architecture of adjacent tissue. Hence, the surgical approaches to these tumors have evolved to focus on the epileptic nature of the disorders rather than on their oncological potential. Surgical strategies are still being refined, and no clear consensus as to the best surgical options has emerged. However, given the epileptic nature of these tumors, when in doubt a rather comprehensive approach that seeks to identify the epileptogenic zone to guide surgical resection appears to be the most promising strategy in attaining seizure freedom for patients with these tumors.

Conflicts of interest None.

References

1. Adachi Y, Yagishita A (2008) Gangliogliomas: characteristic imaging findings and role in the temporal lobe epilepsy. Neuroradiology 50(10):829–834
2. Allende DS, Prayson RA (2009) The expanding family of glioneuronal tumors. Adv Anat Pathol 16(1):33–39
3. Aronica E, Leenstra S, van Veelen CWM, van Rijen PC, Hulsebos TJ, Tersmette AC, Yankaya B, Troost D (2001) Glioneuronal tumors and medically intractable epilepsy: a clinical study with long-term follow-up of seizure outcome after surgery. Epilepsy Res 43(3):179–191
4. Aronica E, Redeker S, Boer K, Spliet W, Van Rijen P, Gorter J, Troost D (2007) Inhibitory networks in epilepsy-associated gangliogliomas and in the perilesional epileptic cortex. Epilepsy Res 74(1):33–44
5. Bartolomei F, Bosma I, Baayen J, Reijneveld J, Postma T, Heimans J, van Dijk B, de Munck J, de Jongh A, Cover K, Stam C (2006) How do brain tumors alter functional connectivity? A magnetoencephalography study. Ann Neurol 59(1):128–138
6. Bauer R, Dobesberger J, Unterhofer C, Unterberger I, Walser G, Bauer G, Trinka E, Ortler M (2007) Outcome of adult patients with temporal lobe tumours and medically refractory focal epilepsy. Acta Neurochir (Wien) 149(12):1211–1217
7. Benifla M, Otsubo H, Ochi A, Weiss SK, Donner EJ, Shroff M, Chuang S, Hawkins C, Drake JM, Elliott I, Smith ML, Snead OC, Rutka JT (2006) Temporal lobe surgery for intractable epilepsy in children. Neurosurgery 59(6):1203–1214
8. Berger MS, Ghatan S, Haglund MM, Dobbins J, Ojemann GA (1993) Low-grade gliomas associated with intractable epilepsy: seizure outcome utilizing electrocorticography during tumor resection. J Neurosurg 79(1):62–69
9. Bilginer B, Yalnızoglu D, Soylemezoglu F, Turanlı G, Cila A, Topçu M, Akalan N (2009) Surgery for epilepsy in children with dysembryoplastic neuroepithelial tumor: clinical spectrum, seizure outcome, neuroradiology, and pathology. Childs Nerv Syst 25(4):485–491
10. Blümcke I (2009) Neuropathology of focal epilepsies: A critical review. Epilepsy Behav 15(1):34–39
11. Blümcke I, Vinters H, Armstrong D, Aronica E, Thom M, Spreafico R (2009) Malformations of cortical development and epilepsies. Epileptic Disord 11(3):181–193
12. Blumcke I, Wiestler O (2002) Gangliogliomas: an intriguing tumor entity associated with focal epilepsies. J Neuropathol Exp Neurol 61(7):575–584
13. Campos AR, Clusmann H, Von Lehe M, Niehusmann P, Becker AJ, Schramm J, Urbach H (2009) Simple and complex dysembryoplastic neuroepithelial tumors (DNT) variants: clinical profile, MRI, and histopathology. Neuroradiology 51(7):433–443
14. Çataltepe O, Turanli G, Yalnizoglu D, Topçu M, Akalan N (2005) Surgical management of temporal lobe tumor-related epilepsy in children. J Neurosurg Pediatr 102(3):280–287
15. Chan C, Bittar R, Davis G, Kalnins R, Fabinyi G (2006) Long-term seizure outcome following surgery for dysembryoplastic neuroepithelial tumor. J Neurosurg 104(1):62–69

16. Chang EF, Christie C, Sullivan JE, Garcia PA, Tihan T, Gupta N, Berger MS, Barbaro NM (2010) Seizure control outcomes after resection of dysembryoplastic neuroepithelial tumor in 50 patients. J Neurosurg Pediatr 5(1):123–130
17. Clusmann H, Kral T, Fackeldey E, Blümcke I, Helmstaedter C, von Oertzen J, Urbach H, Schramm J (2004) Lesional mesial temporal lobe epilepsy and limited resections: prognostic factors and outcome. J Neurol Neurosurg Psychiatry 75:1589–1596
18. Clusmann H, Kral T, Gleissner U, Sassen R, Urbach H, Blümcke I, Bogucki J, Schramm J (2004) Analysis of different types of resection for pediatric patients with temporal lobe epilepsy. Neurosurgery 54(4):847–860
19. Clusmann H, Schramm J, Kral T, Helmstaedter C, Ostertun B, Fimmers R, Haud D, Elger CE (2002) Prognostic factors and outcomes after different types of resection for temporal lobe epilepsy. J Neurosurg 97:1131–1141
20. Daumas-Duport C, Scheithauer B, Chodkiewicz J, Laws E, Vedrenne C (1988) Dysembryoplasic neuroepithelial tumor: a surgically curable tumor of young patients with intractable partial seizure. Report of thirty-nine cases. Neurosurgery 23:545–556
21. Daumas-Duport C, Varlet P, Bacha S, Beuvon D, Cervera-Pierot P, Chodkiewicz J (1999) Dysembryoplastic neuroepithelial tumors: nonspecific histological forms–a study of 40 cases. J Neurooncol 41:267–280
22. Daumas-Duport C (1993) Dysembryoplastic neuroepithelial tumours. Brain Pathol 3(3):283–295
23. Drake J, Hoffman H, Kobayashi J, Hwang P, Becker L (1987) Surgical management of children with temporal lobe epilepsy and mass lesions. Neurosurgery 21(6):792–797
24. Duerr E, Rollbrocker B, Hayashi Y, Peters N, Meyer-Puttlitz B, Louis D, Schramm J, Wiestler O, Parsons R, Eng C (1998) PTEN mutations in gliomas and glioneuronal tumors. Oncogene 16 (17):2259
25. Edgar M, Rosenblum M (2007) Mixed glioneuronal tumors: recently described entities. Arch Pathol Lab Med 131(2):228–233
26. Fried I, Kim J, Spencer D (1994) Limbic and neocortical gliomas associated with intractable seizures: a distinct clinicopathological group. Neurosurgery 34(5):815–824
27. Giulioni M, Galassi E, Zucchelli M, Volpi L (2005) Seizure outcome of lesionectomy in glioneuronal tumors associated with epilepsy in children. J Neurosurg Pediatr 102(3):288–293
28. Giulioni M, Gardella E, Rubboli G, Roncaroli F, Zucchelli M, Bernardi B, Tassinari CA, Calbucci F (2006) Lesionectomy in epileptogenic gangliogliomas: Seizure outcome and surgical results. J Clin Neurosci 13(5):529–535
29. Giulioni M, Rubboli G, Marucci G, Martinoni M, Volpi L, Michelucci R, Marliani AF, Bisulli F, Tinuper P, Castana L, Sartori I, Calbucci F (2009) Seizure outcome of epilepsy surgery in focal epilepsies associated with temporomesial glioneuronal tumors: lesionectomy compared with tailored resection. J Neurosurg 111(6):1275–1282
30. Goldring S, Rich K, Picker S (1986) Experience with gliomas in patients presenting with a chronic seizure disorder. Clin Neurosurg 33:15–42
31. Hennessy MJ (2001) Predictors of outcome and pathological considerations in the surgical treatment of intractable epilepsy associated with temporal lobe lesions. J Neurol Neurosurg Psychiatry 70(4):450–458
32. Holmes M, Wilensky A, Ojemann G, Ojemann L (1999) Hippocampal or neocortical lesions on magnetic resonance imaging do not necessarily indicate site of ictal onsets in partial epilepsy. Ann Neurol 45(4):461–465
33. Iannelli A, Guzzetta F, Battaglia D, Iuvone L, Di Rocco C (2000) Surgical treatment of temporal tumors associated with epilepsy in children. Pediatr Neurosurg 32(5):248–254
34. Im S, Chung C, Cho B, Lee S (2002) Supratentorial ganglioglioma and epilepsy: postoperative seizure outcome. J Neurooncol 57:59–66
35. Johnson J Jr, Hariharan S, Berman J, Sutton L, Rorke L, Molloy P, Phillips P (1997) Clinical outcome of pediatric gangliogliomas: ninety-nine cases over 20 years. Pediatr Neurosurg 27(4): 203–207
36. Jooma R, Yeh H, Privitera MD, Gartner M (1995) Lesionectomy versus electrophysiologically guided resection for temporal lobe tumors manifesting with complex partial seizures. J Neurosurg 83 (2):231–236
37. Khajavi K, Comair Y, Wyllie E, Palmer J, Morris H, Hahn J (1999) Surgical management of pediatric tumor-associated epilepsy. J Child Neurol 14(1):15–25
38. Kirkpatrick PJ, Honavar M, Janota I, Polkey CE (1993) Control of temporal lobe epilepsy following en bloc resection of low-grade tumors. J Neurosurg Pediatr 78(1):19–25
39. Kral T, Kurthen M, Schramm J, Urbach H, Meyer B (2007) Stimulation mapping via implanted grid electrodes prior to surgery for gliomas in highly eloquent cortex. Neurosurgery 61:319–325
40. Louis D, Ohgaki H, Wiestler O, Cavenee W, Burger P, Jouvet A, Scheithauer B, Kleihues P (2007) The 2007 WHO classification of tumours of the central nervous system. Acta Neuropathol 114 (2):97–109
41. Luyken C, Blümcke I, Fimmers R, Urbach H, Elger C, Wiestler O, Schramm J (2003) The spectrum of long-term epilepsy-associated tumors: long-term seizure and tumor outcome and neurosurgical aspects. Epilepsia 44(6):822–830
42. Luyken C, Blümcke I, Fimmers R, Urbach H, Wiestler O, Schramm J (2004) Supratentorial gangliogliomas: Histopathologic grading and tumor recurrence in 184 patients with a median follow-up of 8 years. Cancer 101(1):146–155
43. Majores M, Von Lehe M, Fassunke J, Schramm J, Becker AJ, Simon M (2008) Tumor recurrence and malignant progression of gangliogliomas. Cancer 113(12):3355–3363
44. Mathern G, Babb T, Pretorius J, Melendez M, Levesque M (1995) The pathophysiologic relationships between lesion pathology, intracranial ictal EEG onsets, and hippocampal neuron losses in temporal lobe epilepsy. Epilepsy Res 21(2):133–147
45. Morioka T, Hashiguchi K, Nagata S, Miyagi Y, Yoshida F, Shono T, Mihara F, Koga H, Sasaki T (2007) Additional hippocampectomy in the surgical management of intractable temporal lobe epilepsy associated with glioneuronal tumor. Neurol Res 29(8):807–815
46. Morris H, Estes M, Gilmore R, Van Ness P, Barnett G, Tumbull J (1993) Chronic intractable epilepsy as the only symptom of primary brain tumor. Epilepsia 34(6):1038–1043
47. Morris H, Matkovic Z, Estes M, Prayson Y, Comair Y, Turnbull J, Najm I, Kotagal P, Wyllie E (1998) Ganglioglioma and intractable epilepsy: clinical and neurophysiologic features and predictors of outcome after surgery. Epilepsia 39(3):307–313
48. Neuloh G, Bien C, Clusmann H, von Lehe M, Schramm J (2010) Continuous motor monitoring enhances functional preservation and seizure-free outcome in surgery for intractable epilepsy. Acta Neurochir 152:1307–1314
49. Ogiwara H, Nordli DR, Dipatri AJ, Alden TD, Bowman RM, Tomita T (2010) Pediatric epileptogenic gangliogliomas: seizure outcome and surgical results. J Neurosurg Pediatr 5(3): 271–276
50. Park YS, Kim DS, Shim KW, Kim JH, Choi JU (2008) Factors contributing to resectability and seizure outcomes in 44 patients with ganglioglioma. Clin Neurol Neurosurg 110(7): 667–673
51. Perkins O (1926) Gangliogliomas. Arch Pathol Lab Med 2:11–17

52. Phi JH, Kim S-K, Cho B-K, Lee SY, Park SY, Park S-J, Lee SK, Kim KJ, Chung CK (2009) Long-term surgical outcomes of temporal lobe epilepsy associated with low-grade brain tumors. Cancer 115(24):5771–5779
53. Pilcher WH, Silbergeld DL, Berger MS, Ojemann GA (1993) Intraoperative electrocorticography during tumor resection: impact on seizure outcome in patients with gangliogliomas. J Neurosurg 78(6):891–902
54. Ponten S, Daffertshofer A, Hillebrand A, Stam C (2010) The relationship between structural and functional connectivity: Graph theoretical analysis of an EEG neural mass model. Neuroimage 52 (3):985–994
55. Prayson R (2010) Diagnostic challenges in the evaluation of chronic epilepsy-related surgical neuropathology. Am J Surg Pathol 34(5):1–13
56. Rades D, Zwick L, Leppert J, Bonsanto MM, Tronnier V, Dunst J, Schild SE (2010) The role of postoperative radiotherapy for the treatment of gangliogliomas. Cancer 116(2):432–442
57. Radhakrishnan A, Abraham M, Radhakrishnan VV, Sarma SP, Radhakrishnan K (2006) Medically refractory epilepsy associated with temporal lobe ganglioglioma: characteristics and postoperative outcome. Clin Neurol Neurosurg 108(7):648–654
58. Rajneesh KF, Binder DK (2009) Tumor-associated epilepsy. Neurosurg Focus 27(2):E4
59. Rudà R, Trevisan E, Soffietti R (2010) Epilepsy and brain tumors. Curr Opin Oncol 22(6):611–620
60. Schramm J, Aliashkevich A (2007) Surgery for temporal mediobasal tumors: experience based on a series of 235 patients. Neurosurgery 60(2):285–295
61. Schramm J, Clusmann H (2008) The surgery of epilepsy. Neurosurgery 62:463–481
62. Schramm J, Kral T, Grunwald T, Blümcke I (2001) Surgical treatment for neocortical temporal lobe epilepsy: clinical and surgical aspects and seizure outcome. J Neurosurg 94(1):33–42
63. Shamji MF, Fric-Shamji EC, Benoit BG (2009) Brain tumors and epilepsy: pathophysiology of peritumoral changes. Neurosurg Rev 32(3):275–285
64. Spencer D, Spencer S, Mattson R, Williamson P (1984) Intracerebral masses in patients with intractable partial epilepsy. Neurology 34(4):432
65. Sugano H, Shimizu H, Sunaga S (2007) Efficacy of intraoperative electrocorticography for assessing seizure outcomes in intractable epilepsy patients with temporal-lobe-mass lesions. Seizure 16 (2):120–127
66. Takahashi A, Hong S, Dae W, Seung B, Lee M, Suh Y (2005) Frequent association of cortical dysplasia in dysembryoplastic neuroepithelial tumor treated by epilepsy surgery. Surg Neurol 64(5):419–427
67. Urbach H, Binder D, von Lehe M, Podlogar M, Bien C, Becker A, Schramm J, Kral T, Clusmann H (2007) Correlation of MRI and histopathology in epileptogenic parietal and occipital lobe lesions. Seizure 16(7):608–614
68. van Breemen M, Wilms E, Vecht C (2007) Epilepsy in patients with brain tumours: epidemiology, mechanisms, and management. Lancet Neurol 6(5):421–430
69. Wolf H, Campos M, Zentner J, Hufnagel A, Schramm J, Elger C, Wiestler O (1993) Surgical pathology of temporal lobe epilepsy. Experience with 216 cases. J Neuropathol Exp Neurol 52(5):499
70. Wolf H, Roos D, Blümcke I, Pietsch T, Wiestler O (1996) Perilesional neurochemical changes in focal epilepsies. Acta Neuropathol 91:376–384
71. Yang I, Chang EF, Han SJ, Barry JJ, Fang S, Tihan T, Barbaro NM, Parsa AT (2011) Early surgical intervention in adult patients with ganglioglioma is associated with improved clinical seizure outcomes. J Clin Neurosci 18(1):29–33
72. Zaatreh M, Firlik K, Spencer D, Spencer S (2003) Temporal lobe tumoral epilepsy: characteristics and predictors of surgical outcome. Neurology 61(5):636–641

Acta Neurochir (2011) 153:1561–1572
DOI 10.1007/s00701-011-0985-6

CLINICAL ARTICLE

A software tool for interactive exploration of intrinsic functional connectivity opens new perspectives for brain surgery

Joachim Böttger · Daniel S. Margulies · Peter Horn · Ulrich W. Thomale · Ilana Podlipsky · Irit Shapira-Lichter · Shereen J. Chaudhry · Christine Szkudlarek · Karsten Mueller · Gabriele Lohmann · Talma Hendler · Georg Bohner · Jochen B. Fiebach · Arno Villringer · Peter Vajkoczy · Alexander Abbushi

Received: 23 June 2010 / Accepted: 18 February 2011 / Published online: 3 April 2011

Abstract
Background Functional connectivity analysis of resting-state functional magnetic resonance imaging data (fcrs-fMRI) has been shown to be a robust non-invasive method for localization of functional networks (without using specific tasks) and to be promising for presurgical planning. However, in order to transfer the approach to everyday clinical practice, fcrs-fMRI needs to be further validated and made easily accessible to neurosurgeons. This paper addresses the latter by presenting a software tool designed for neurosurgeons for analyzing and visualizing fcrs-fMRI data.

Methods A prototypical interactive visualization tool was developed to enable neurosurgeons to explore functional connectivity data and evaluate its usability. The implementation builds upon LIPSIA, an established software package for the assessment of functional neuroimaging data, and integrates the selection of a region-of-interest with the computation and visualization of functionally connected areas. The tool was used to explore data from a healthy participant and eight brain lesion patients. The usability of the software was evaluated with four neurosurgeons previously unacquainted with the methodology,

Joachim Böttger and Daniel S. Margulies contributed equally.

Electronic supplementary material The online version of this article (doi:10.1007/s00701-011-0985-6) contains supplementary material, which is available to authorized users.

J. Böttger (✉) · P. Horn · U. W. Thomale · C. Szkudlarek · P. Vajkoczy · A. Abbushi
Department of Neurosurgery, Charité-Universitätsmedizin Berlin,
Augustenburger Platz 1,
13353 Berlin, Germany
e-mail: joachim@visualistics.de

D. S. Margulies · S. J. Chaudhry · A. Villringer
Mind & Brain Institute and Berlin School of Mind and Brain,
Humboldt Universität,
Berlin, Germany

D. S. Margulies · S. J. Chaudhry · K. Mueller · G. Lohmann · A. Villringer
Max Planck Institute for Human Cognitive and Brain Sciences,
Leipzig, Germany

I. Podlipsky · I. Shapira-Lichter · T. Hendler
Wohl Institute for Advanced Imaging,
Tel-Aviv Sourasky Medical Center,
Tel Aviv, Israel

T. Hendler
Sackler Faculty of Medicine,
Tel Aviv University,
Tel Aviv, Israel

G. Bohner
Department of Neuroradiology,
Charité-Universitätsmedizin Berlin,
Berlin, Germany

J. B. Fiebach
Center for Stroke Research Berlin,
Charité-Universitätsmedizin Berlin,
Berlin, Germany

who were asked to identify prominent, large-scale cortical networks.
Findings With this novel tool, previously published findings, such as tumor displacement of the sensorimotor cortex and other disturbances of functional networks, were reproduced. The neurosurgeons were able to consistently obtain results similar to the results of an expert, with the exception of the language network. Immediate feedback helped to pinpoint functional networks quickly and intuitively, with even inexperienced users requiring less than 3 min per network.
Conclusions Although fcrs-fMRI is a nascent method still undergoing evaluation with respect to established standards, the interactive software is nonetheless a promising tool for non-invasive exploration of individual functional connectivity networks in neurosurgical practice, both for well-known networks and for those less typically addressed.

Keywords Resting-state · fMRI · Visualization · Interactivity · Surgical planning

Introduction

The outcome of neurosurgical interventions benefits from knowledge about the location of specific functional areas in the brain. For example, pre-surgical identification of circumscribed functional regions in relation to a tumor can be a substantial advantage in surgical planning. The gold standard method for such functional localization, intraoperative electrical stimulation mapping, is invasive and limited to the localization of a few main cortical functional areas accessible during intracranial interventions. In contrast, a non-invasive imaging technique, "task-based" functional magnetic resonance imaging (fMRI), is capable of non-invasively showing the location of a diverse array of functional regions by using task paradigms to identify the implicated areas [38].

Although seemingly of great promise for clinical application, task-based fMRI has seen limited integration into the technical repertoire of neurosurgical planning because of several practical constraints: special experimental setup, relatively long measuring time, high demand on patients for cooperation, and the substantial training and expertise required for processing the data (for a detailed review of these limitations, see [6]). Furthermore, localization of each functional area using task-based fMRI requires a specialized task.

A novel technique in functional neuroimaging termed "resting-state fMRI," in contrast to traditional task-based fMRI, measures changes in the blood oxygen-level dependent (BOLD) signal without the patient being subjected to any task (i.e., spontaneous fluctuations). A formidable body of research in brain and neurological science over the past 15 years has demonstrated the feasibility of using spontaneous fluctuations in fMRI data to map functional systems. The methodology has recently been applied to presurgical planning; however, the current design of the software used for analysis is more suitable for brain researchers rather than being programmed specifically for daily neurosurgical practice.

The purpose of this article is to address this obstacle by introducing a novel interactive visualization tool designed for neurosurgical use in exploring resting-state fMRI data. Because of the relative novelty of the method for neurosurgery, we first review the resting-state methodology, especially as it is applied to neurosurgical patients. Following that, we describe the development of our prototypical software, our experience while applying the tool to explore eight brain lesion cases, as well as a first evaluation of its usability for neurosurgeons previously unacquainted with resting-state analysis.

Introduction to resting-state fMRI

Previous research points out that resting-state fMRI has several practical advantages over task-based fMRI in the clinical setting [8, 9, 24, 35, 39]. Firstly, no stimulation devices are required, and acquisition time can be as little as 5 min. Furthermore, no demands are made of the patient other than to lie motionless throughout the duration of the scan. The patients are usually instructed to rest with their eyes either opened or closed and to simply remain still and not think of anything in particular. The utility of the method does not depend on the precise condition; it has also been successfully used for sleeping [11, 12], sedated [14] and anesthetized [21] participants.

Various functional areas and networks throughout the entire brain can be mapped using a single resting-state fMRI scan. The basic underlying observation is that, even in a task-independent state, the fMRI activity of the brain reveals spontaneous fluctuations that are far from random. The correlation between spontaneous fluctuations across different regions reflects areas that are functionally relevant to each other and can be described as "functionally connected" [10]. The resulting methodology is termed "functional connectivity analysis of resting-state fMRI" (fcrs-fMRI). The classic method for the analysis of functional connectivity is based on taking the signal from a region-of-interest (ROI) and assessing its correlation with all other regions of the brain (termed: "seed-based" functional connectivity [1]). See Fig. 1A for a visual overview of the methodology.

Functional connectivity can be used to describe distributed networks that subserve cohesive functional roles. Such networks are not restricted to the cortex and have been applied to the brainstem [29], thalamus [40], striatum [7], and cerebellum [15, 23, 31]. Nevertheless, the most promising

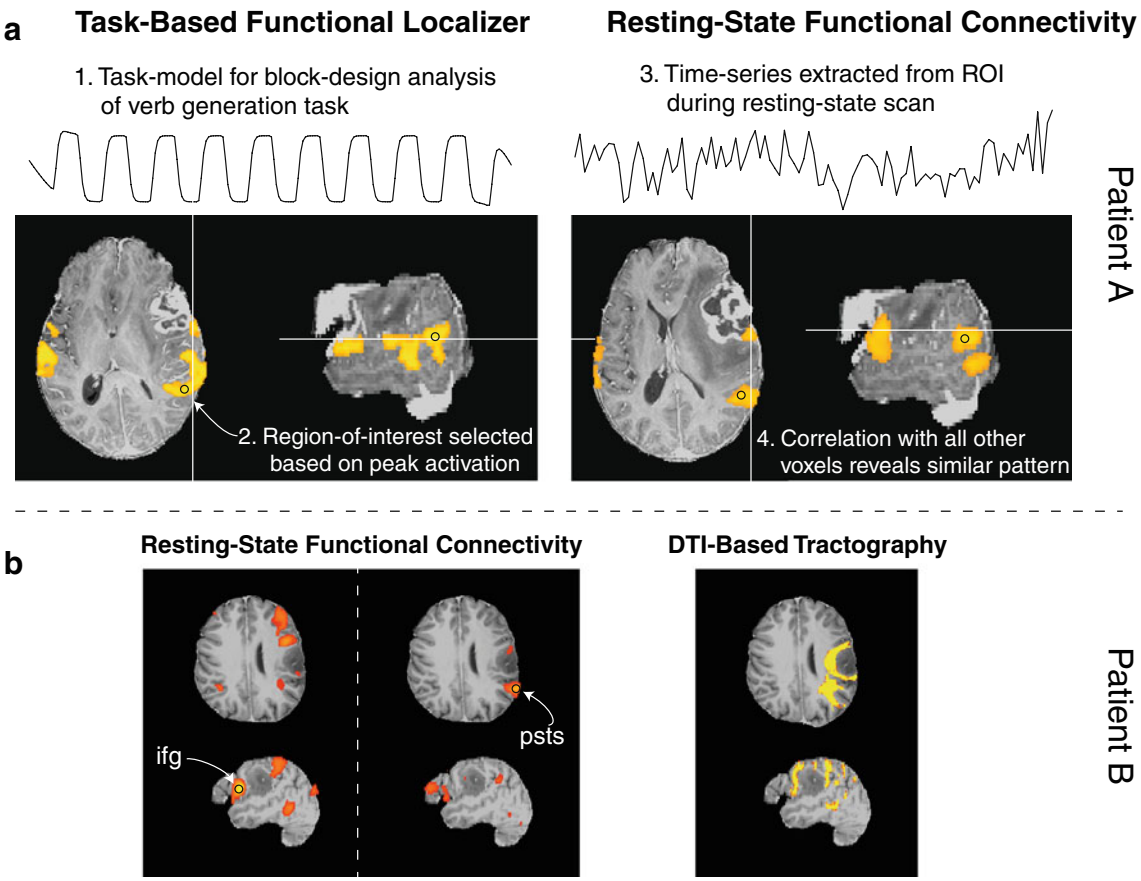

Fig. 1 (**A**) Significant functional activation during performance of a verb generation task (left). The peak region of the posterior superior temporal sulcus (psts) was taken as a region-of-interest and used for subsequent functional connectivity analysis (right). Note the spatial similarity of the two maps, particularly the shift of the inferior frontal gyrus (ifg) portion of the network anterior to the tumor. (**B**) Functional connectivity in another patient from regions-of-interest located in the ifg and psts (left). Diffusion tensor-based tractography from the same patient (right). More information can be found in Online Resource 1

area of clinical application so far is the individual mapping of prominent networks in the cortex, whose architecture is consistent in healthy populations [3–5, 18] and can vary significantly across various patient populations (for reviews, see [13, 22]). While the number of networks varies across studies, here we selected four stable and reproducible networks to explore (see Fig. 2):

- The *sensorimotor network* is located in the pre- and post-central cortex and supplementary motor area [18].
- The *language network* consists of functional connectivity between Broca's and Wernicke's areas [16, 26].
- The *dorsal-attention network* consists of the lateral frontal and parietal cortex [4, 5]. This network has been associated with top-down orienting and conscious direction of attention ("executive control") [34, 37].
- The *default-mode network* consists of the posterior cingulate cortex, medial prefrontal, and medial temporal cortex, and has been associated with self-related processing, mind-wandering, and autobiographical memory [2, 33].

Supporting evidence for the validity of using fcrs-fMRI to identify these networks stems from the comparison of functional connectivity with diffusion direction of white matter, as derived from tractography using diffusion tensor imaging (DTI) data. Van den Heuvel et al. [19] have been able to show that major fcrs-fMRI networks of the healthy brain are indeed interlinked by anatomically well-known DTI tractography. We have reproduced these findings for the language system of a tumor patient, as can be seen in Fig. 1B, and described more fully in the Supplementary Material (Online Resource 1).

Neurosurgical applications

While fcrs-fMRI has been widely used for the characterization of the healthy brain and neurological diseases, its application to neurosurgery is rather recent [9]. In a pioneering study, Shimony and colleagues [35] demonstrated the utility of resting-state fMRI for the resection of tumors close to functional centers. Their new paradigm for neurosurgical

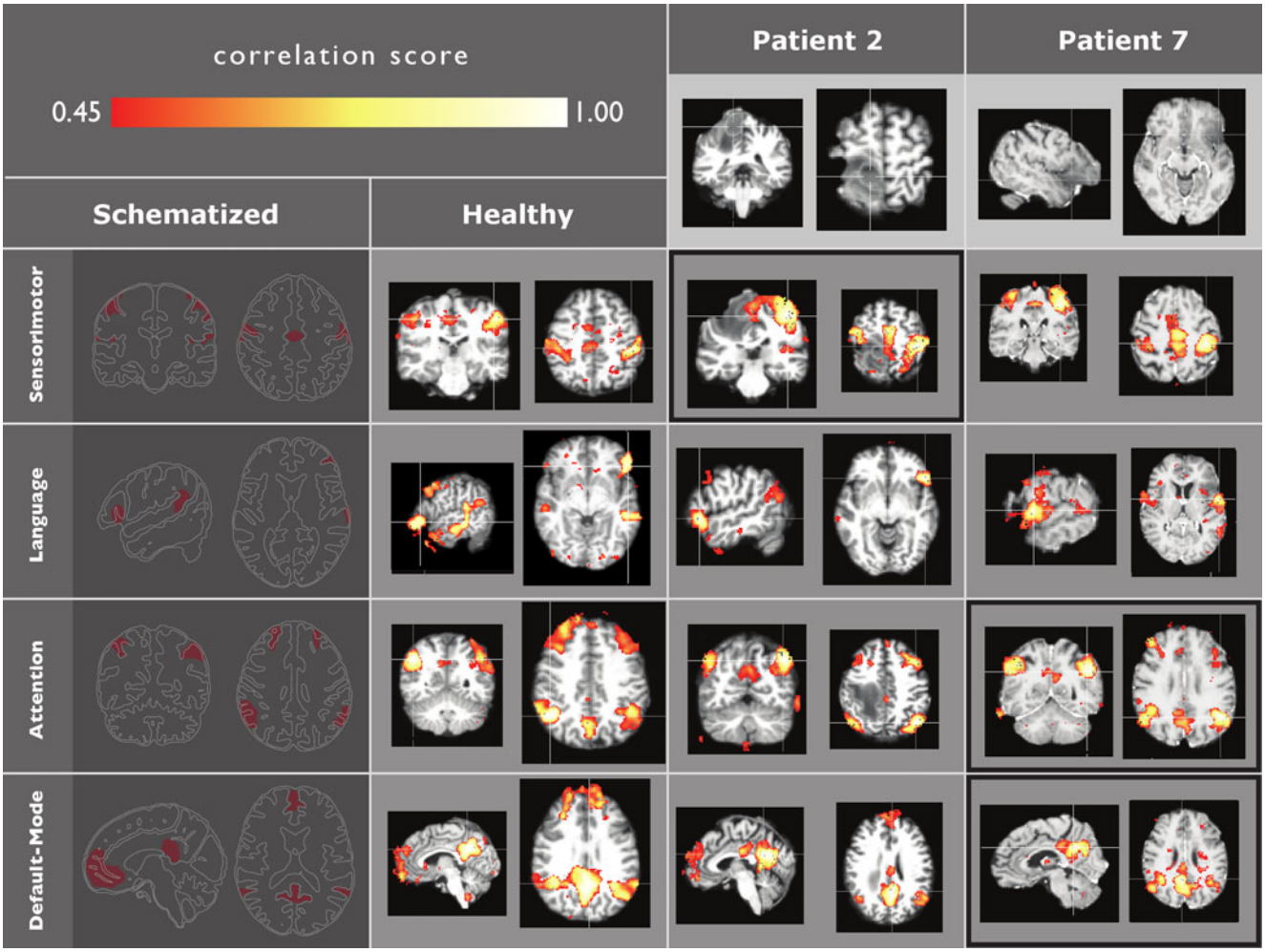

Fig. 2 Four schematized (left) intrinsic functional connectivity networks, and reference networks for our data with manually selected seed regions-of-interest in a healthy individual brain and two example pathological cases (right). Abnormal networks in the patients emphasized with black frame

application took advantage of the high degree of bilateral symmetry in the sensorimotor network [1, 19, 30, 36]. An ROI was chosen in the motor cortex of the healthy hemisphere using specific anatomical landmarks, and the BOLD signal from that region was extracted. Then, the contralateral precentral cortex, in which severe distortion prohibited localization of equivalent landmarks, was localized by looking for areas with highly similar fluctuations in signal. In the extended description of the same work, Zhang et al. demonstrated good overlap with task-based fMRI and the gold standard, intraoperative cortical stimulation [39].

Liu et al. [24] also indirectly localized cortical hand and tongue motor areas in a lesion patient using anatomical landmarks and functional connectivity, and compared these results with task-based fMRI measurements. Taking into account six typical cases, they report highly similar activations, sufficient selectivity to distinguish between hand and tongue centers, and robustness across different imaging resolutions. Their comparison in one case with direct cortical stimulation showed substantial consistency with fcrs-fMRI.

Summarizing, fcrs-fMRI seems to be able to localize even displaced eloquent cortex with resolution comparable to task-based fMRI, but with many practical advantages in the clinical setting. Despite these advantages, applying fcrs-fMRI in a clinical setting remains impractical without the ability to analyze the data quickly and efficiently. For example, as Shimony and colleagues explain [35], in one case the region of interest had to be "determined empirically by shifting […] until the normal spatial pattern of the sensorimotor network was seen," for a distance of approximately 2 cm. With the commonly available processing tools, this trial-and-error process is tedious and could benefit from the development of specialized interactive visualization tools designed with attention to clinical needs.

Thus, building upon the fMRI data analysis toolbox LIPSIA, we developed an interactive tool for rapid and convenient exploration of functional connectivity in the

human brain [25]. The impact of the software is illustrated with neurosurgical case examples and an evaluation. The ultimate goal of the prototypical implementation is to make it easy for neurosurgeons to directly explore the functional connectivity of different ROIs selected in real-time and to localize functional networks for assistance in presurgical planning.

Methods and technical development

We report here on our development of a prototypical tool for fcrs-fMRI exploration. This is followed by its application to eight case examples with lesions close to functionally relevant cortical areas, reproducing alterations of main functional connectivity networks that are similar to previously reported findings (see above). Additionally, the usability of the tool was evaluated with four neurosurgeons without previous expertise in the methodology.

Software implementation

We implemented a prototypical interactive exploration tool building on LIPSIA, a freely available MRI data processing suite. LIPSIA already implements certain pre-computation steps as well as the masking-out of voxels outside the brain in order to optimize correlation computation. We chose to implement real-time interaction using a further restriction of correlation computation to only three currently visible slices present in the standard LIPSIA triplanar visualization. The combination of these approaches yields redraw rates of approximately 0.1 s during a shift of the seed ROI, which is sufficiently fast for fluent interaction.

AFNI recently introduced interactive functional connectivity visualization as part of its standard distribution. Using highly optimized computational methods, "InstaCorr" (afni.nimh.nih.gov/pub/dist/doc/misc/instacorr.pdf) achieves comparable speed of calculation while conducting correlation across the whole brain. While AFNI's computational methods are more sophisticated than our current method, our tool is streamlined for the singular purpose of rapid exploration of functional connectivity with minimal prior knowledge.

Application of the software

Data acquisition and patient selection

Resting-state fMRI data were acquired from eight patients (age 31–69, 6 male, 2 female) with lesions localized close to components of the default-mode, attention, or sensorimotor networks. The lesions include metastases and gliomas located in the frontal or parietal lobes. In Table 1, clinical symptoms and signs as well as the histopathology and the age of the patients at the time when the rs-fMRI scan was performed are described. In addition, data from a healthy 35-year-old male were acquired for the evaluation. All protocols were approved by the Charité hospital ethics board and have, therefore, been performed in accordance with the ethical standards of the Declaration of Helsinki (1964). Informed consent was received from all participants prior to the scan.

All participants were instructed to "think of nothing in particular" and remain still with their eyes open. Subjects were scanned at different hospitals equipped with two different MR scanner systems, and the following parameters were established to optimize measurements on each system, respectively. On a GE 3-T scanner equipped with an eight-channel head coil, fMRI was acquired using a standard echo-planar imaging sequence (repetition time=2,500 ms, echo time=30, flip angle=83º, voxel dimensions=1.71873×1.71873×4 mm). High-resolution "anatomical" images were obtained using a T1-weighted pulse sequence (MPRAGE, TR=7,224 s; TE=3.1 ms; TI=900 ms; flip angle=8; 154 slices, FOV=240 mm). On a Siemens 3-T Tim Trio scanner equipped with a 12-channel head coil, fMRI was acquired using a standard echo-planar imaging sequence (repetition time=2,300 ms, echo time=30, flip angle=90º, voxel dimensions=3×3×4 mm). Anatomical scans were obtained using a T1-weighted pulse sequence (MPRAGE, TR=1,900/2,300 ms; TE=2.52/2.98 ms; TI=900 ms; flip angle=9; 192/176 slices, FOV=256 mm).

Data preprocessing

The data were preprocessed using a combination of Freesurfer (http://surfer.nmr.mgh.harvard.edu/), AFNI (http://afni.nimh.nih.gov/), and FSL (http://www.fmrib.ox.ac.uk/fsl/)—all freely available standard data analysis packages. Preprocessing for the functional data, which has been described previously [7, 27], included: slice-timing correction for interleaved slice acquisition and motion correction in six degrees-of-freedom (AFNI). The six motion components and a "global" signal (extracted from the average signal over the entire brain) were used as covariates in a general linear model. The residual data were then bandpass-filtered between 0.02–0.08 Hz and spatially smoothed using a 6-mm full-width half-maximum Gaussian kernel (AFNI).

The anatomical volume was skull stripped using the standard Freesurfer processing path. A single functional volume was then registered to the skull-stripped anatomical volume using FSL's linear registration tool, and the resulting transformation matrix was applied to the entire functional data set. Both data sets were co-registered to Montreal Neurological Institute (MNI152) space.

The preprocessing takes advantage of the availability of technically matured software tools and usually requires no manual intervention.

Table 1 Eight focal lesion cases with clinical patient information and observations of abnormal fcrs-fMRI networks (see Fig. 4)

Patient no.	Age	Sex	Signs and symptoms	MRI findings/diagnosis	fcrs-fMRI network observations
1	66	F	Personality changes with reduced impulsion, disorientation	Right frontal lesion (38 × 30 × 39 mm)/ astrocytoma IV°	Sensorimotor: functional connectivity correlation borders the edema around the lesion Attention: strongly diminished correlation on the frontal component on the lesion side Default-mode: correlation appears with a laterally shifted and diminished frontal component next to the lesion
2	50	M	Simple partial motor seizures in the left leg	Right central lesion (17 × 20 × 27 mm)/ metastasis of a malignant melanoma	Sensorimotor: displaced and weakened functional connectivity correlation of the motor region anterior to the lesion
3	52	M	Focally induced generalized tonic-clonic seizures, no persisting sensorimotor deficits	Left pre-central lesion (32 24 22 mm)/menin gioma WHO grade I	Sensorimotor: displaced and weakened functional connectivity correlation of the motor component on the lesion side
4	47	M	Tonic-clonic seizures, right-sided lower extremity plegia and upper extremity paresis	Left central, paramedian lesion (32 × 25 × 35 mm)/astrocytoma WHO IV°	Sensorimotor: substantially diminished functional connectivity signal in the left paramedian motor cortex
5	69	M	Hypesthesia mainly of the right, upper extremity, with impaired coordination and fine motor skills	Left post-central subcortical lesion (27 × 27 × 20 mm)/ astrocytoma WHO IV°	Sensorimotor: substantially diminished functional connectivity of the motor network on the lesion side, especially in the hand region Default-mode: lateral component of the default-mode network displaced
6	31	M	Right-sided hemiplegia	Left central lesion (23 × 28 × 28 mm)/ resulting from bridging vein thrombosis	Sensorimotor: absence of functional connectivity correlation of the sensorimotor system of the right arm and hand
7	49	M	Secondary generalized tonic clonic seizures	Lesion in the left frontal operculum (no clear contour)/astrocytoma WHO III°	Attention: reduced degree of functional connectivity correlation of the frontal component ipsilateral to the lesion Default-mode: disconnection between frontal and posterior components
8	42	F	Auto-motor and grand mal epileptic seizures with bilateral tonic-clonic seizures and affective disorders (frontal brain syndrome), slight mental retardation (caused by perinatal asphyxia), intermittent tremor of the right hand	Bilateral frontobasal lesion (70 × 60 × 50 mm)/atypical menigioma WHO II°	Default-mode: frontal component almost not visible

Interactive exploration

Our tool was then used by an experienced fcrs-fMRI researcher to interactively explore the preprocessed data. In the process, previously described observations, as well as other observations described below, were reproduced. Towards this aim, the four functional systems depicted in Fig. 2 were explored: sensorimotor, language, dorsal-attention, and default-mode networks. The quick redraw rates yielded a fluent interaction, which let the user conveniently maximize correlation patterns. See Fig. 3 for the example of the motor network and also Online Resource 2 for a video of the interactive exploration of the networks described below.

To detect the **sensorimotor network**, the mouse cursor was placed on the lateral motor cortex, anterior to the

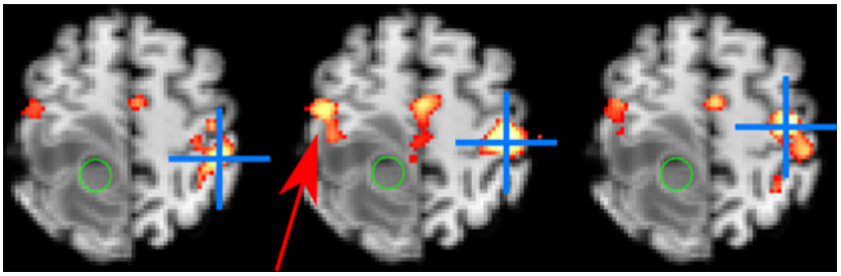

Fig. 3 Interactive movement of the region-of-interest (marked with blue coordinate cross) makes it possible to quickly maximize the functional connectivity patterns, such as in this case example for the bilateral motor network: Dragging the ROI in the anterior-posterior axis on the healthy side contralateral from the tumor (marked green) results in an optimal delineation of the component ipsilateral from the tumor (middle, marked with arrow)

central sulcus, and the ROI shifted until a symmetrical network appeared across the pre- and post-central gyri, as well as supplementary motor area. For the **language network**, the mouse cursor was placed in the left inferior frontal gyrus, adjacent to the precentral sulcus, which corresponds to Broca's area (anterior operculum). By shifting the location slightly, it was possible to detect functional connectivity in the sagittal plane to the posterior portion of the superior temporal gyrus (Wernicke's area) and adjacent to the inferior parietal cortex. For the **dorsal-attention network**, the cursor was placed in the superior frontal gyrus and shifted until functional connectivity in the axial slice was visible bilaterally in both frontal regions and the intraparietal sulcus. The **default-mode network** was identified with the cursor placed in the posterior cingulate. Functional connectivity from this region was visible in the medial prefrontal cortex along the sagittal plane, as well as in the bilateral inferior parietal cortex along the coronal plane. During the exploration, it was possible to manually adjust a threshold for the visualization of correlation using a slider.

Usability evaluation

Two representative cases (patient 2 and 7, see below) were then picked for an evaluation of the usability of our tool. Four neurosurgeons without previous knowledge of the functional connectivity literature were recruited to interactively explore the data. For familiarization, the schematic diagrams and anatomical localization of the four standard networks in Fig. 2 were presented, and the basic method was explained. The group of neurosurgeons was then asked to localize the networks in the one healthy and two representative pathological brain data sets. During this exploration, we recorded the seed ROIs they picked for optimal delineation of the networks for the different cases (for later visual comparison of the resulting correlation maps), the time for the respective searches, and any unprompted special observations made.

Results

Interactive exploration of the clinical cases

An experienced fcrs-fMRI researcher used the procedure described above to explore the four different networks in the eight patients with focal brain lesions. In Table 1, the specific networks that were shifted, or otherwise disturbed, are described.

Six cases of disturbance within the motor network were found (see Fig. 4), ranging from displacement of the functional region by the lesion in patients 1–3 (see Table 1) to the substantial absence of bilaterality in the network in patients 4–6 (see Table 1). These findings are consistent with those in the previous literature [24, 35, 39].

Furthermore, six examples of lesion effects on the default-mode network in patients 1, 5, 7, and 8 (see Table 1, and also Fig. 4) and attention network in patients 1 and 7 (see Table 1, and also Fig. 4) were observed. In patient 1, the frontal component of the default-mode network appeared displaced and weakened. In patient 5, the tumor-side lateral component of the default-mode network appeared dorsally displaced. In patients 7 and 8, components of the default-mode network, and in patients 1 and 7, components of the attention network appeared substantially weakened. For the figures, a threshold was manually chosen in order to match the spatial extent of networks traditionally observed.

Additionally, interactive exploration of tumors and their surroundings reproduced another previously described observation [8]: that functional connectivity can differentiate edema from surrounding healthy grey matter (for an example, see Online Resource 3).

Usability evaluation

Two representative cases were picked for the evaluation: patient 2 because the case presented a clear displacement of the functional motor cortex, which is valuable information

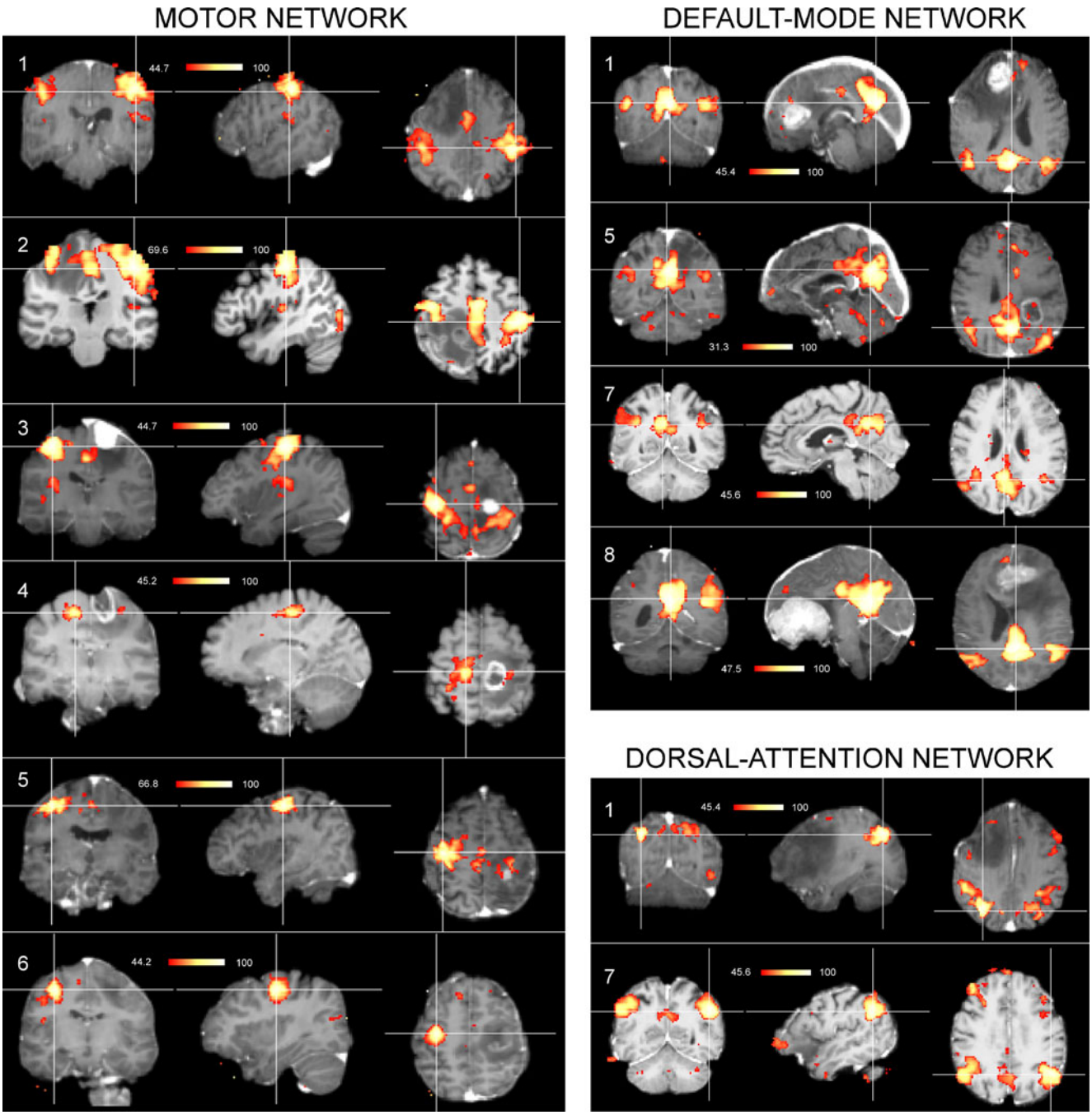

Fig. 4 Clinical cases with network changes. Motor network: patients 1-6 are ordered from weakest (top) to strongest (bottom) disturbance. Default network: patient 1 displays a distorted frontal component, patient 5 shows a displaced lateral lesion-side component, patient 7 lacks the frontal component, and patient 8 has a weak frontal component. Attention network: patient 1 shows a weakened frontal lesion-side component, and the tumor below the location of the missing frontal component in patient 7 appears to disturb the network

in the planning of a resection, and patient 7, since the case contains a visible change in two other large-scale networks that are often not well known to neurosurgeons. The exploration of these two cases by an experienced user resulted in our 12 reference networks, shown in Fig. 2, used for the evaluation.

The evaluation sessions with the neurosurgical users typically lasted 20 min. After familiarization with the software and the introduction of the schematic figures, seed ROIs for the four described networks were selected in all three data sets. The neurosurgeons were able to quickly and consistently reproduce most of the reference networks

with a high degree of similarity (see Fig. 5). The longest exploration time was needed to identify the language network, which does not stand out as clearly as the others. The solutions for this network were also not as similar to one another as for the other networks. Some neurosurgical users were able to pinpoint attention and default-mode networks in the pathological cases in less than 30 s and the sensorimotor cortex in less than 20 s.

All neurosurgical users consistently reported displacement of the motor cortex in patient 2. In patient 7, after observing the "normal" pattern of the attention network, a missing frontal component ipsilateral to the tumor was reported by all participants without prompting, while a disturbance of the default-mode network was seen by three of four neurosurgical users.

Discussion

In this paper, a novel interactive software tool is presented. The tool enables the analysis and visualization of functional connectivity using "resting-state fMRI" data at a speed that allows for real-time exploration. As an improvement over the classical iterative analysis of fcrs-fMRI data, it could be demonstrated that this tool enables experienced researchers to reproduce previously described effects like displacement or weakening of functional networks in less than 30 s in eight case examples of lesioned brains. Furthermore, after a short introduction, neurosurgeons without previous experience in the methodology were also able to rapidly explore functional connectivity data, requiring less than 2 min on average to localize functional networks.

Other studies have utilized fcrs-fMRI for the localization of functional areas: Liu et al. [24] in a study with six, and Zhang et al. [39] with four patients. These studies report high overlap with task-based fMRI and good consistency with direct cortical stimulation, making it a promising functional localization method.

Utility of interactive software

Previous studies predominantly used anatomical landmarks as a guide for functional connectivity. However, spatial disagreement of anatomical landmarks versus functional networks argues for the individual assessment of functional brain organization rather than relying on "average" landmarks [32]. For example, in the study by Shimony et al. [35] it was necessary to shift the ROI on the healthy side, which was initially placed in the hand knob, in order to discern the sensorimotor network. The data processing necessary for such an analysis required a technical expert. Our tool can facilitate intuitive and simple access of

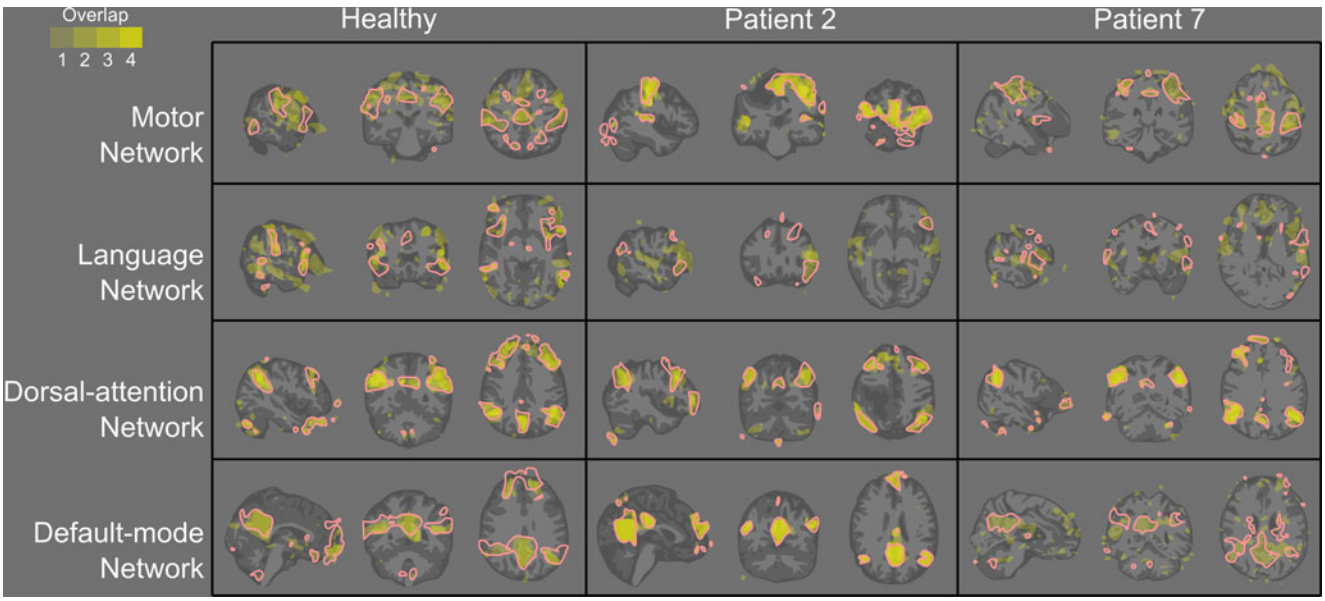

Fig. 5 The reference networks (in red, solid line) have been consistently reproduced for sensorimotor, attention and default-mode networks by a group of four neurosurgeons without previous knowledge of the relevant literature (marked in a gradient, representing the overlap of the four neurosurgeons' solutions) and allowed for identification of the abnormal networks. The language network seems to be harder to identify, as witnessed by large differences in solutions exhibited in the second row. The abnormal structure of the default-mode network in patient 7 also showed more variability in the selected networks; nevertheless, all but one neurosurgeon detected the abnormality in its structure

clinicians to resting-state fMRI data and differs from other analysis software in that it was designed specifically for use in neurosurgical practice.

Fine movements (of the seed ROI) inside networks enable users to maximize correlation patterns and thereby pinpoint the maxima of a functional connectivity network. This mode of interaction is shown in Fig. 3 and in the video (Online Resource 2). Searching for a functional area in the vicinity of, for example, a tumor is thus rendered intuitive. The mouse pointer is used like a searchlight that is moved around within an ROI until typical connection patterns appear.

More advanced users tend to localize functional networks in less time than novices. Although there is a learning curve involved in developing an intuitive understanding and expertise for such a new modality, this is no different than for other explorative visualization diagnostics such as ultrasonography.

During the evaluation of the tool with a neurosurgical user group, it seemed that the symmetrical appearance of most networks, such as in the case of the motor network, makes it particularly easy to identify them and to observe disturbances of the underlying functional connectivity. Even for the "default-mode network" and the "attention network" (both of which might not be well known in a neurosurgical context) a short introduction was sufficient for most of the neurosurgical users to find the networks quickly and observe changes in their appearance. This concept may explain the "relative" difficulty in detecting the lateralized language network. Additionally, the language network has been shown [20] to present more complexly in fcrs-fMRI data than in the classical Broca/Wernicke model of two distinct centers prevalent in neurosurgery. Therefore, it is not surprising that exploring this network in our data proved difficult.

While our prototype was sufficient to test the applicability of interactive visualization for neurosurgery, it certainly has its limitations. The restriction to perpendicular planes in a triplanar view does not allow for an optimal overview. A logical next step therefore will be the development of our tool into a three-dimensional surgery planning system. We also plan to incorporate more advanced analytic methodologies. Statistical comparisons between individual pathological cases and a normative sample may also prove to be a valuable means of assessing localized damage of clinical relevance.

Clinical findings of the motor network

One further concern is the validity of fcrs-fMRI localization for the case of lesions, which destroy functional connectivity patterns instead of displacing components of functional networks. Liu et al. [24] reported as a preliminary finding one case of a diminished right motor cortex component, accompanied with clinical symptoms of the left hand. While not the focus of this paper, eight lesion cases were explored in order to support that fcrs-fMRI is effective in facilitating the presurgical localization of functional networks.

In seven of the eight described patients (that is, with the exception of patient 6), the sensorimotor cortex was bilaterally identifiable with fcrs-fMRI. The changes observed in the central region range from strong spatial displacement (patients 1–3) to substantially weakened correlation (patients 4 and 5) to complete interhemispheric asymmetry (patient 6).

While patients 1–3 showed no sensorimotor deficits, patients 4–6 suffered from different degrees of pareses. The most severe clinical symptom was observed in the case of absent bilateral functional connectivity in patient 6, who indeed had a total plegia of the right upper limb. The weakened functional connectivity in this case prohibited localization of the motor cortex ipsilateral to the lesion.

Although still only descriptive at this point, we can confirm Liu et al.'s observation of a connection between weakening of the connectivity and the severity of clinical symptoms. While this means that fcrs-fMRI seems to be most applicable in cases of non-infiltrated, lesion-displaced motor areas, further quantitative studies are required to assess the implications of weakened or missing functional connectivity.

Other fcrs-fMRI networks

In most of the described cases, the more complex networks, which are largely not taken into account in neurosurgery today (attention and default-mode), present with normal appearance. However, there are four cases where they seem to get displaced or their connections seem weakened by lesions (patients 1, 5, 7, and 8). Patient 1 presented clinically with changes in personality, reduced drive and disorientation, and diminished components in both the attention and the default-mode network.

Although at this point the clinical relevance of these specific networks is still not clear, research supports that brain functions rely on distributed networks rather than single areas, emphasizing the need for an assessment of such networks [28]. The clinical relevance of large-scale networks in brains with localized lesions has, for example, already been demonstrated in stroke patients [17], but must be further established for neurosurgical patients through future studies. We believe that interactive visualization might then become a viable option for easy network localization by neurosurgeons.

Similar to the clinical relevance of the attention and default-mode networks, the fcrs-fMRI methodology clearly has to be further evaluated with respect to accuracy and reliability with surgical patients and to be extensively compared with standard methods like direct cortical

stimulation. By correlating clinical findings with observed changes in functional networks, we hope that neurosurgery will be able not only to establish fcrs-fMRI in clinical everyday practice, but also to contribute to basic neuroscience.

Conclusion

In this paper, we presented a novel tool for the interactive exploration of functional connectivity using resting-state fMRI data. As others have pointed out [9, 24, 35, 39], fcrs-fMRI has significant practical advantages in a clinical setting over activation-based, preoperative fMRI (e.g., less scanning time necessary, no task or need for a cooperative patient, and several networks can be assessed simultaneously). Given the limitations imposed on data collection in the clinical setting, the efficiency of this approach makes it a prime candidate for functional localization of distributed large-scale networks throughout the brain. In this way, this method can help to understand disturbances of functional areas surrounding a pathological structure and to contribute another tool to pre-surgical planning. Nonetheless, while the use of such networks may no doubt be of service to neurosurgical planning, rigorous future research is still necessary to assess how these functional connectivity-determined areas spatially relate to eloquent cortex, as defined by gold standard intraoperative cortical stimulation.

The interactive tool presented here is capable of quickly and easily reproducing previously reported findings such as the delineation of edema [8], the shift of cortical areas by tumors [24, 35, 39], and the impairment of large-scale networks [39] by clinical neurosurgeons without previous expertise in fcrs-fMRI. The tool is intended to be a step out of the ivory tower of basic neuroscience into the clinical realm of practicing neurosurgeons.

Conflicts of interest None.

References

1. Biswal B, Yetkin FZ, Haughton VM, Hyde JS (1995) Functional connectivity in the motor cortex of resting human brain using echo-planar MRI. Magn Reson Med 34:537–541
2. Buckner RL, Andrews-Hanna JR, Schacter DL (2008) The brain's default network: anatomy, function, and relevance to disease. Ann NY Acad Sci 1124:1–38
3. Chen S, Ross TJ, Zhan W, Myers CS, Chuang K, Heishman SJ, Stein EA, Yang Y (2008) Group independent component analysis reveals consistent resting-state networks across multiple sessions. Brain Res 1239:141–151
4. Damoiseaux JS, Rombouts SARB, Barkhof F, Scheltens P, Stam CJ, Smith SM, Beckmann CF (2006) Consistent resting-state networks across healthy subjects. Proc Natl Acad Sci 103:13848–13853
5. De Luca M, Beckmann C, De Stefano N, Matthews P, Smith S (2006) fMRI resting state networks define distinct modes of long-distance interactions in the human brain. Neuroimage 29:1359–1367
6. Desmond JE, Annabel Chen SH (2002) Ethical issues in the clinical application of fMRI: factors affecting the validity and interpretation of activations. Brain Cogn 50:482–497
7. Di Martino A, Scheres A, Margulies D, Kelly A, Uddin L, Shehzad Z, Biswal B, Walters J, Castellanos F, Milham M (2008) Functional connectivity of human striatum: a resting state fMRI study. Cereb Cortex 18:2735–2747
8. Feldman S, Chu D, Schulder M, Barry M, Cho E, Liu W (2009) The blood oxygen level-dependent functional MR imaging signal can be used to identify brain tumors and distinguish them from normal tissue. AJNR Am J Neuroradiol 30:389–395
9. Fox MD, Greicius M (2010) Clinical applications of resting state functional connectivity. Front Syst Neurosci 4:19
10. Fox MD, Raichle ME (2007) Spontaneous fluctuations in brain activity observed with functional magnetic resonance imaging. Nat Rev Neurosci 8:700–711
11. Fukunaga M, Horovitz SG, van Gelderen P, de Zwart JA, Jansma JM, Ikonomidou VN, Chu R, Deckers RHR, Leopold DA, Duyn JH (2006) Large-amplitude, spatially correlated fluctuations in BOLD fMRI signals during extended rest and early sleep stages. Magn Reson Imaging 24:979–992
12. Fukunaga M, Horovitz SG, de Zwart JA, van Gelderen P, Balkin TJ, Braun AR, Duyn JH (2008) Metabolic origin of BOLD signal fluctuations in the absence of stimuli. J Cereb Blood Flow Metab 28:1377–1387
13. Greicius M (2008) Resting-state functional connectivity in neuropsychiatric disorders. Curr Opin Neurol 24:424–430
14. Greicius MD, Kiviniemi V, Tervonen O, Vainionpää V, Alahuhta S, Reiss AL, Menon V (2008) Persistent default-mode network connectivity during light sedation. Hum Brain Mapp 29:839–847
15. Habas C, Kamdar N, Nguyen D, Prater K, Beckmann CF, Menon V, Greicius MD (2009) Distinct cerebellar contributions to intrinsic connectivity networks. J Neurosci 29:8586–8594
16. Hampson M, Peterson BS, Skudlarski P, Gatenby JC, Gore JC (2002) Detection of functional connectivity using temporal correlations in MR images. Hum Brain Mapp 15:247–262
17. He BJ, Snyder AZ, Vincent JL, Epstein A, Shulman GL, Corbetta M (2007) Breakdown of functional connectivity in frontoparietal networks underlies behavioral deficits in spatial neglect. Neuron 53:905–918
18. van den Heuvel M, Mandl R, Hulshoff Pol H (2008) Normalized cut group clustering of resting-state FMRI data. PLoS ONE 3: e2001
19. Heuvel MPVD, Mandl RC, Kahn RS, Pol HEH (2009) Functionally linked resting-state networks reflect the underlying structural connectivity architecture of the human brain. Hum Brain Mapp 30:3127–3141
20. Kelly C, Uddin LQ, Shehzad Z, Margulies DS, Castellanos FX, Milham MP, Petrides M (2010) Broca's region: linking human brain functional connectivity data and non-human primate tracing anatomy studies. Eur J Neurosci 32:383–398
21. Kiviniemi V, Kantola J, Jauhiainen J, Hyvärinen A, Tervonen O (2003) Independent component analysis of nondeterministic fMRI signal sources. Neuroimage 19:253–260
22. Kiviniemi V, Starck T, Remes J, Long X, Nikkinen J, Haapea M, Veijola J, Moilanen I, Isohanni M, Zang Y, Tervonen O (2009) Functional segmentation of the brain cortex using high model order group PICA. Hum Brain Mapp 30:3865–3886
23. Krienen FM, Buckner RL (2009) Segregated fronto-cerebellar circuits revealed by intrinsic functional connectivity. Cereb Cortex 19:2485–2497
24. Liu H, Buckner RL, Talukdar T, Tanaka N, Madsen JR, Stufflebeam SM (2009) Task-free presurgical mapping using

functional magnetic resonance imaging intrinsic activity. J Neurosurg 111:746–754
25. Lohmann G, Muller K, Bosch V, Mentzel H, Hessler S, Chen L, Zysset S, von Cramon DY (2001) Lipsia-a new software system for the evaluation of functional magnetic resonance images of the human brain. Comput Med Imaging Graph 25:449–457
26. Lohmann G, Hoehl S, Brauer J, Danielmeier C, Bornkessel-Schlesewsky I, Bahlmann J, Turner R, Friederici A (2010) Setting the frame: the human brain activates a basic low-frequency network for language processing. Cereb Cortex 20:1286–1292
27. Margulies DS, Kelly AC, Uddin LQ, Biswal BB, Castellanos FX, Milham MP (2007) Mapping the functional connectivity of anterior cingulate cortex. Neuroimage 37:579–588
28. Mesulam M (2009) Defining neurocognitive networks in the BOLD new world of computed connectivity. Neuron 62:1–3
29. Nioche C, Cabanis E, Habas C (2009) Functional connectivity of the human red nucleus in the brain resting state at 3T. AJNR Am J Neuroradiol 30:396–403
30. Nir Y, Mukamel R, Dinstein I, Privman E, Harel M, Fisch L, Gelbard-Sagiv H, Kipervasser S, Andelman F, Neufeld MY, Kramer U, Arieli A, Fried I, Malach R (2008) Interhemispheric correlations of slow spontaneous neuronal fluctuations revealed in human sensory cortex. Nat Neurosci 11:1100–1108
31. O'Reilly JX, Beckmann CF, Tomassini V, Ramnani N, Johansen-Berg H (2010) Distinct and overlapping functional zones in the cerebellum defined by resting state functional connectivity. Cereb Cortex 20:953–965
32. Pouratian N, Bookheimer SY (2010) The reliability of neuroanatomy as a predictor of eloquence: a review. Neurosurg Focus 28:E3
33. Raichle ME, MacLeod AM, Snyder AZ, Powers WJ, Gusnard DA, Shulman GL (2001) A default mode of brain function. Proc Natl Acad Sci USA 98:676–682
34. Seeley WW, Menon V, Schatzberg AF, Keller J, Glover GH, Kenna H, Reiss AL, Greicius MD (2007) Dissociable intrinsic connectivity networks for salience processing and executive control. J Neurosci 27:2349–2356
35. Shimony JS, Zhang D, Johnston JM, Fox MD, Roy A, Leuthardt EC (2009) Resting-state spontaneous fluctuations in brain activity: a new paradigm for presurgical planning using fMRI. Acad Radiol 16:578–583
36. Stark DE, Margulies DS, Shehzad ZE, Reiss P, Kelly AMC, Uddin LQ, Gee DG, Roy AK, Banich MT, Castellanos FX, Milham MP (2008) Regional variation in interhemispheric coordination of intrinsic hemodynamic fluctuations. J Neurosci 28:13754–13764
37. Vincent JL, Kahn I, Snyder AZ, Raichle ME, Buckner RL (2008) Evidence for a frontoparietal control system revealed by intrinsic functional connectivity. J Neurophysiol 100:3328–3342
38. Vlieger E, Majoie CB, Leenstra S, den Heeten GJ (2004) Functional magnetic resonance imaging for neurosurgical planning in neurooncology. Eur Radiol 14:1143–1153
39. Zhang D, Johnston JM, Fox MD, Leuthardt EC, Grubb RL, Chicoine MR, Smyth MD, Snyder AZ, Raichle ME, Shimony JS (2009) Preoperative sensorimotor mapping in brain tumor patients using spontaneous fluctuations in neuronal activity imaged with functional magnetic resonance imaging. Neurosurgery 65:ons226–ons236
40. Zhang D, Snyder AZ, Fox MD, Sansbury MW, Shimony JS, Raichle ME (2008) Intrinsic functional relations between human cerebral cortex and thalamus. J Neurophysiol 100:1740–1748

Acta Neurochir (2011) 153:1573–1578
DOI 10.1007/s00701-011-0997-2

CLINICAL ARTICLE

Analysis of hemorrhagic risk factors during deep brain stimulation surgery for movement disorders: comparison of the circumferential paired and multiple electrode insertion methods

Jin Hoon Park · Sun Ju Chung · Chong Sik Lee · Sang Ryong Jeon

Received: 20 December 2010 / Accepted: 10 March 2011 / Published online: 9 April 2011

Abstract
Background The most serious complication of deep brain stimulation (DBS) surgery is intracranial hemorrhage. The authors have assessed risk factors for hemorrhage in DBS surgery and compared two types of microelectrode insertion technique on hemorrhagic risk.
Methods A total of 171 DBS procedures were performed on 110 patients (58 females, 52 males) by the same neurosurgeon at a single center between May 2005 and May 2010. We used two microelectrode insertion methods: multiple microelectrode insertion (MMI) and circumferential paired microelectrode insertion (CPMI). We analyzed the correlation between bleeding rates and gender, age, hypertension, target location, simultaneous bilateral procedure and electrode insertion method.
Results Of the 171 DBS procedures, 138 were on 85 patients with Parkinson's disease, 16 were in 15 patients with essential tremor and 17 were on ten patients with dystonia. There were nine postoperative hemorrhagic events (5.26%), of which three were symptomatic (1.75%), and one permanent neurological deficit event (0.58%). Compared with the bleeding rate in the MMI method (9/106, 8.5%), there was no instance of bleeding with the CPMI method (0/65, 0%) (p=0.04). In other factors, the correlation with hemorrhage was not found.
Conclusion Use of the CPMI method significantly decreased the rate of bleeding. This new surgical technique seems to be safe and accurate and may be recommended as another surgical option.

Keywords Deep brain stimulation · Hemorrhage · Risk Factors · Microelectrode insertion · Circumferential paired insertion

J. H. Park · S. R. Jeon (✉)
Center for Parkinson and Alzheimer's Disease,
Department of Neurological Surgery, Asan Medical Center,
University of Ulsan College of Medicine,
388–1 Pungnap-2dong, Songpa-gu,
Seoul 138–736, Korea
e-mail: srjeon@amc.seoul.kr

S. J. Chung · C. S. Lee
Center for Parkinson and Alzheimer's Disease,
Department of Neurology, Asan Medical Center,
University of Ulsan College of Medicine,
Seoul, Korea

Introduction

Deep brain stimulation (DBS) is a widely accepted procedure used to treat patients with movement disorders, including Parkinson's disease, dystonia, and essential tremors. The most serious complication associated with DBS is intracranial hemorrhage, which occurs in 0.6–6.0% of the patients treated and includes intracerebral hemorrhage (ICH), intraventricular hemorrhage (IVH), subdural hemorrhage (SDH), and venous infarction [1, 3, 4, 6, 9, 10, 14, 15]. Factors affecting the risk of hemorrhage include patient age, gender, hypertension, anatomic target, and the number of microelectrodes [1, 2, 4, 9, 13, 15].

In this study, the authors retrospectively investigated the factors possibly affecting the risk of hemorrhage during DBS surgery, including a new surgical procedure, the circumferential paired microelectrode insertion (CPMI) method, which we developed.

Materials and methods

Patient characteristics

A total of 171 DBS procedures were performed on 110 patients (58 females, 52 males) by the same neurosurgeon at a single medical center between May 2005 and May 2010. The 110 patients included 85 diagnosed with Parkinson's disease, 15 with essential tremor, and ten with dystonia; 59 patients underwent bilateral implantation and 51 underwent unilateral implantation. Revision surgery was required for two patients due to incorrect electrode positioning. Thirteen patients had a history of hypertension, although the intraoperative blood pressure of all patients was strictly controlled during all procedures in order to maintain it within the normal range.

Microelectrode insertion procedures

We used two microelectrode insertion methods, i.e., the circumferential paired microelectrode insertion (CPMI) method, which we developed and used for 65 DBS procedures, and the multiple microelectrode insertion (MMI) method, which we used for 106 DBS procedures.

All patients were prepared for surgery using the same method. Briefly, a Leksell series G stereotactic frame was attached to each patient, mostly using local anesthesia, but with the 11 patients with dystonia under general anesthesia. Magnetic resonance imaging (MRI) (1.5 T) was performed, and imaging data were transferred to a Surgiplan (ELEKTA, Stockholm, Sweden) system in order to determine the optimal target based on the known anatomical coordinates. Using three-dimensional reconstructions created using double-dose, enhanced MRI data, we determined the safest pathway, i.e., avoiding vasculature, from the surface to the target. During this time, the patient was prepared for surgery. The patient was placed in a semirecumbent position, both for patient comfort and to allow a neurologist to easily monitor neurological changes. At the location indicated by the Surgiplan system, a single burrhole (10–15 mm) was made using a high-speed drill. After making the dura opening, an arachnoid incision was made, followed by pial coagulation. Electrodes were inserted using the MMI or CPMI method, shown schematically in Figs. 1, 2 and described below.

With the CPMI method, two microelectrodes were inserted simultaneously, one in the center and the other 2 mm anterior to the center, followed by evaluation of the microelectrode recording (MER) signals in order to determine that the correct target had been reached, in which case, no further insertions were performed. If not, the anterior electrode was removed and another electrode was inserted 2 mm lateral to the center. These procedures were repeated, with the second electrode placed 2 mm posterior or medial to the central electrode, until the MER signals indicated that the correct target had been reached. Although this procedure could potentially be performed from any of five alternate trajectories, only those trajectories which the Surgiplan planning had shown no risk of vessel injury were used. Any trajectory with a risk of vessel injury was not used. We found that the mean number of electrodes inserted during this procedure was 3.21 (range 2–4). The central electrode was inserted repeatedly so as to prevent any brain shift caused by leakage of cerebrospinal fluid during the removal and insertion of other electrodes. After insertion of at least one electrode showing appropriate MER of the target, electrical stimulation was performed. A neurologist subsequently evaluated each patient's symptomatic improvement and side effects. This was followed by insertion of a permanent electrode (3387 or 3389, Medtronic, Minneapolis, MN, USA) under fluoroscopic guidance.

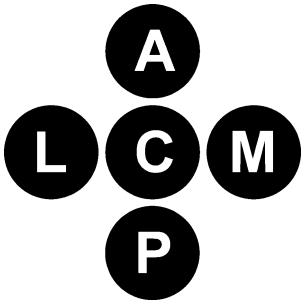

Fig. 1 Pattern of simultaneous insertion of five microelectrodes in the MMI technique. *A* Anterior electrode, *C* central electrode, *M* medial electrode, *L* lateral electrode, *P* posterior electrode

During the MMI procedure, five electrodes were inserted simultaneously. This procedure used the same methods as those described above, including enhanced three-dimensional MR, trajectory planning using Surgiplan, and MER.

A battery was implanted into the pectoralis muscle under general anesthesia. Postoperative skull X-rays and computed tomography (CT) were then performed in all patients within 24 h.

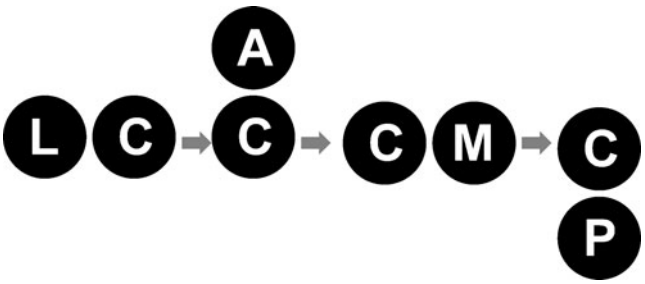

Fig. 2 Sequence of microelectrode insertion used in the CPMI technique. This procedure is repeated until MER signals indicate correct target. *A* Anterior electrode, *C* central electrode, *M* medial electrode, *L* lateral electrode, *P* posterior electrode

Statistical analysis

Univariate and multivariate logistic regression analyses were used to determine the association between bleeding and patient gender, age, the presence of hypertension, target location, simultaneous bilateral procedure, and electrode insertion methods. A p value<0.05 was considered statistically significant. All statistical analyses were performed using SAS (version 8.1; SAS Institute, Cary, NC, USA) and SPSS (release 10.1.4; SPSS, Chicago, IL) software.

We analyzed the bleeding risk factors using the univariate and multivariate logistic regression test. We also compared the clinical outcomes of Parkinson's patients in two, different surgical groups, i.e., the CPMI and MMI groups, using the changes of the Unified Parkinson's Disease Rating Scale (UPDRS) and the levodopa equivalent dose (LED) reduction rate both before surgery and 12 months after surgery.

Results

Of the 171 DBS procedures, 138 were performed on 85 patients with Parkinson's disease, 16 on 15 patients with essential tremor, and 17 on ten patients with dystonia. There were nine, postoperative hemorrhagic events (5.26%), of which three were symptomatic (1.75%), and one permanent neurological deficit event (0.58%). The nine postoperative hemorrhagic events consisted of two IVHs, one venous hemorrhagic infarction along the electrode, and six ICHs (Table 1).

We performed univariate logistic regression analysis in order to identify the factors associated with bleeding complications (Table 2). There were 92 procedures on females and 79 on males, with bleeding occurring in six and three of those procedures, respectively. Statistical analysis showed no significant relationship between bleeding and gender (female patient odds ratio=1.77; $p>0.05$). Similarly, an age threshold of 60 years or the presence of hypertension did not affect the bleeding rate. Analysis of the target location showed that eight instances of bleeding occurred in the subthalamic nucleus (STN), one in the ventral intermediate nucleus (Vim), and none in the nucleus of the globus pallidus interna (Gpi); however, statistical analysis showed no significant difference in the bleeding rates among these three target sites. The bleeding rates were higher following simultaneous, bilateral procedures than unilateral procedures, although the difference was not statistically significant.

In contrast to these factors, our univariate logistic regression analysis showed that the microelectrode insertion method was the only significant factor affecting bleeding ($p=0.02$). Multivariate logistic regression analysis also showed that the bleeding risk was significantly reduced when using the CPMI method compared with the MMI technique ($p=0.04$) (Table 3).

Regarding the total number of Parkinson's patients ($n=85$), the CPMI and MMI groups included 40 and 45 patients respectively. The changes in the clinical results of both groups were compared before surgery and 12 months after surgery using DBS. The mean total UPDRS of both groups changed from 76.8±15.9 to 28.4±15.2 in the CPMI group and from 65.2±17.2 to 32.3±14.3 in the MMI group ($p=0.17$). The mean UPDRS III of both groups changed from 41.4±9.1 to 17.3±10.5 in the CPMI group and from 34.3±10.1 to 18.9±8.9 in the MMI group ($p=0.21$). The mean LED reduction rates were 21±5.8% in the CPMI group and 23±6.2% in the MMI group ($p=0.32$). There was no statistically significant difference in clinical outcomes between the two groups.

Table 1 Profiles of nine cases associated with hemorrhage during DBS surgery

Patient	Age (years)/ gender	Hx of HTN	Dx	Target	Procedure	Trajectory planning	Electrode insertion method	Type of bleeding	Location	Size (mm^2)	Outcome
1	64/F	-	PD	Bi STN	SB	+	MMI	ICH	Rt Thal	31.0 × 18.5	Permanent sequelae
2	55/M	-	PD	Lt STN	U	+	MMI	IVH	Lt Lat V	32.5 × 9.5	Asymptomatic
3	59/F	-	PD	Bi STN	SB	+	MMI	IVH	Rt Lat V	13.0 × 5.0	Asymptomatic
4	59/M	-	PD	Bi STN	SB	+	MMI	ICH	Rt Fr	18.5 × 11.0	Temporary deficit
5	54/F	-	PD	Bi STN	SB	+	MMI	HVI	Rt Fr	17.5 × 12.0	Temporary deficit
6	67/M	+	ET	Lt Vim	U	+	MMI	ICH	Lt BG	14.0 × 12.0	Temporary deficit
7	65/F	-	PD	Lt STN	U	+	MMI	ICH	Lt Thal	14.0 × 11.0	Temporary deficit
8	54/F	+	PD	Rt STN	U	+	MMI	ICH	Rt BG	4.5 × 7.5	Temporary deficit
9	60/F	-	PD	Lt STN	U	+	MMI	ICH	Lt Fr	6.5 × 10.0	Temporary deficit

M male, *F* female, *Hx* history, *Dx* daignosis, *PD* Parkinson's disease, *ET* essential tremor, *HTN* hypertension, *Rt* right, *Lt* left, *Bi* bilateral, *STN* subthalmic nucleus, *Vim* ventral intermediate nucleus, *SB* simultaneous bilateral, *U* unilateral, *ICH* intracerebral hemorrhage, *IVH* intraventricular hemorrhage, *HVI* hemorrhagic venous infarction, *Thal* thalamus, *Lat.* lateral, *V* ventricle, *Fr* frontal, *BG* basal ganglia

Table 2 Results of univariate logistic regression analysis to identify factors that affect bleeding

Factor	Character	Total (hemorrhage)/ n=171 (9)	Odds ratio	p value
Gender	F	92 (6)	1.77	0.47
	M	79 (3)		
Age	<60	100 (5)	0.88	0.14
	≥60	71 (4)		
HTN	Hx (+)	20 (2)	2.29	0.68
	Hx (−)	151 (7)		
Location of target	STN	138 (8)	0.92	0.65
	GPi	17 (0)	0	
	Vim	16 (1)		
Procedure	SB	45 (4)	2.36	0.71
	U (including staged bilateral)	126 (5)		
Microelectrode insertion method	CPMI	65 (0)	0	0.02
	MMI	106 (9)		

Discussion

DBS is a well-established procedure used to alleviate the symptoms of movement disorders, such as Parkinson's disease, essential tremor, and dystonia [7, 8, 11, 12]. Although many hemorrhagic complications have been reported, the incidence and causes of bleeding have not yet been determined. Hypertension, the total number of electrodes, target, patient age and sex, and the amount of radiofrequency thermocoagulation have been reported to be risk factors for bleeding, athough many of these studies have reported contradictory results and there is no consensus regarding the risk factors for bleeding [3, 5, 9]. In the present study, we also assessed possible risk factors for bleeding in patients undergoing DBS surgery and found that the only factor that reduced the risk of hemorrhage was the use of our CPMI technique, which caused no difference in the clinical outcome.

When we performed simultaneous, bilateral surgeries on the same day, we observed bleeding in four patients, thus suggesting that simultaneous, bilateral surgery may cause bleeding. This bleeding may have been caused by brain shifting resulting from the leakage of cerebrospinal fluid during surgery at the first site and thus resulting in a vascular violation. However, the results of our statistical analysis did not show any significance regarding this factor.

In the medical literature, bleeding has been associated with the total number of electrodes inserted during the procedure [9], thus suggesting that a single electrode inserted multiple times may increase the risk of hemorrhage. In contrast, our results indicate that the number of electrodes inserted simultaneously is related to the hemorrhagic risk. This increase in bleeding risk when simultaneous multiple electrodes inserted may be due to the rod-like volume effect of multiple electrodes which causes significant tissue damage. In addition, the dead space created by simultaneous, multiple, microelectrode insertions reduces tissue pressure which otherwise acts as a compression force to reduce bleeding. The findings in the patient described in Fig. 3 (patient 1 in Table 1) support this hypothesis. In this patient,

Table 3 Multivariate logistic regression analysis of microelectrode insertion method to identify the bleeding risk

Factor	Character	Total (hemorrhage)/ n=171 (9)	Rate (%)	p value
Gender	F	92 (6)	6.5	0.70
	M	79 (3)	3.8	
Age	<60	100 (5)	5.0	0.72
	≥60	71 (4)	5.6	
HTN	Hx (+)	20 (2)	1.0	0.80
	Hx (−)	151 (7)	4.6	
Location of target	STN	138 (8)	5.8	0.81
	GPi	17 (0)	0	
	Vim	16 (1)	6.3	
Procedure	SB	45 (4)	8.9	0.87
	U (including staged bilateral)	126 (5)	4.0	
Microelectrode insertion method	CPMI	65 (0)	0	0.04
	MMI	106 (9)	8.5	

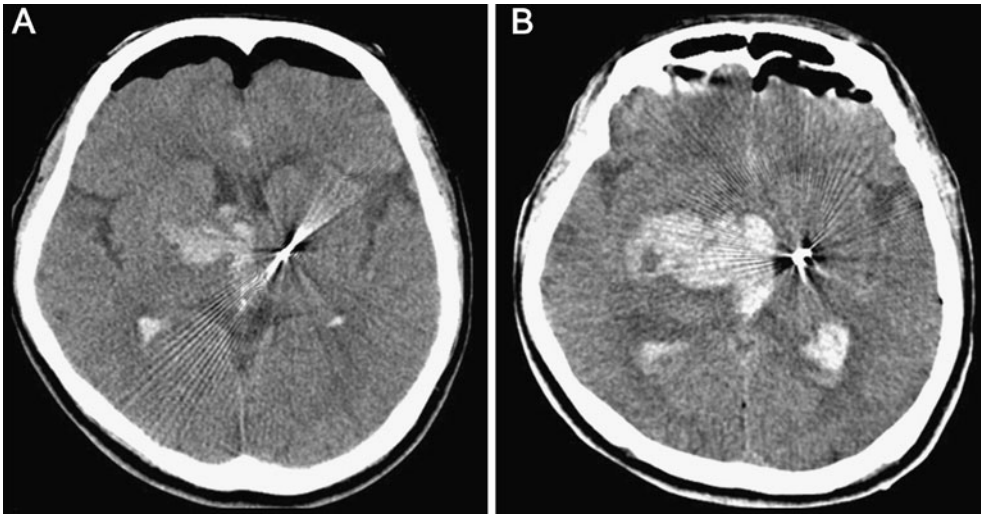

Fig. 3 CT findings in patient 1 of Table 1. **A** Immediate postoperative CT. Note the small amount of bleeding in the right thalamus. **B** CT finding 2 h after first CT shows a marked increase in bleeding, likely due to induced dead space and lowered tissue pressure

immediate, postoperative CT showed slight bleeding (Fig. 3A), whereas repeat CT performed 2 h later showed a markedly increased amount of bleeding apparently caused by induced dead space and lowered tissue pressure (Fig. 3B). Simultaneous insertion of multiple electrodes may act like a rod and causing greater tissue damage and dead space, thereby reducing the tissue pressure essential for compressive force.

Our new surgical technique, CPMI, reduced the bleeding risk compared with the MMI method as simultaneously inserting only two microelectrodes may reduce the risk of tissue damage and dead space. In addition, the central electrode prevents brain shifting during electrode change, which is beneficial compared with the single electrode insertion method. Future comparisons of single and circumferential, paired electrode insertion may help to determine the efficacy of our new surgical technique. In addition, we believe that a prospective randomized comparative study between the CPMI and MMI methods is needed to show the efficacy of our insertion method. However, our retrospective analysis showed that the CPMI method was safer than the MMI method regarding the possible risk of bleeding. Due to our results, we face the ethical dilemma of whether we should conduct a prospective, randomized, comparative study. Alternatively, we can demonstrate the safety of the new CPMI technique with further surgical cases.

The authors do not consider that the decrese of bleeding risk in the CPMI method, compared with the MMI method, is caused by time-dependent development of surgical skill. There was no special inclusion criterion for the use of the new CPMI method. When we used the MMI method during DBS surgery, we experienced bleeding in nine patients. Therefore, we substituted the electrode insertion method with the new CPMI method. We used the same software (Surgiplan), same MRI protocol including double-dose enhancement, and also same other surgical instruments were used in the two different methods (CPMI and MMI). Actually, the nine patients who experienced bleeding with the MMI method did do so only during the early period but bleeding was evenly distributed over the entire series of the MMI method. In addition, we had performed previous DBS surgeries during the previous 5 years before using these standardized, microelectrode insertion techniques, CPMI and MMI. Therefore, our surgical skills were not those of a beginner when we initiated the present comparative analysis. Because of the reasons described above, we believe that a surgical skill might not be a significant confounding factor.

We unexpectedly found that hypertension and the simultaneous, bilateral procedure, although having high odds ratios for bleeding, did not significantly affect the bleeding rate. Moreover, gender, age, and target location were not significant determinants of the bleeding risk.

Conclusion

The results of this study suggest that the number of electrodes inserted simultaneously was the only significant risk factor for bleeding during DBS surgery. The circumferential paired microelectrode insertion (CPMI) method was associated with a reduced bleeding risk when compared with multiple electrode insertion. However, further surgical cases will be needed in order to verify the safety and efficacy of CPMI method during DBS surgery.

Acknowledgements This paper was supported by KRCF National Agenda Project.

Conflicts of interest None.

References

1. Ben-Haim S, Asaad WF, Gale JT, Eskandar EN (2009) Risk factors for hemorrhage during microelectrode-guided deep brain stimulation and the introduction of an improved microelectrode design. Neurosurgery 64:754–762, discussion 762–753
2. Binder DK, Rau G, Starr PA (2004) Hemorrhagic complications of microelectrode-guided deep brain stimulation. Stereotact Funct Neurosurg 80:28–31
3. Binder DK, Rau GM, Starr PA (2005) Risk factors for hemorrhage during microelectrode-guided deep brain stimulator implantation for movement disorders. Neurosurgery 56:722–732, discussion 722–732
4. Chan DTM, Zhu XL, Yeung JHM, Mok VCT, Wong E, Lau C, Wong R, Lau C, Poon WS (2009) Complications of deep brain stimulation: a collective review. Asian J Surg 32:258–263
5. Gorgulho A, De Salles AA, Frighetto L, Behnke E (2005) Incidence of hemorrhage associated with electrophysiological studies performed using macroelectrodes and microelectrodes in functional neurosurgery. J Neurosurg 102:888–896
6. Kenney C, Simpson R, Hunter C, Ondo W, Almaguer M, Davidson A, Jankovic J (2007) Short-term and long-term safety of deep brain stimulation in the treatment of movement disorders. J Neurosurg 106:621–625
7. Krack P, Batir A, Van Blercom N, Chabardes S, Fraix V, Ardouin C, Koudsie A, Limousin PD, Benazzouz A, LeBas JF, Benabid AL, Pollak P (2003) Five-year follow-up of bilateral stimulation of the subthalamic nucleus in advanced Parkinson's disease. N Engl J Med 349:1925–1934
8. Kupsch A, Kuehn A, Klaffke S, Meissner W, Harnack D, Winter C, Haelbig TD, Kivi A, Arnold G, Einhaupl KM, Schneider GH, Trottenberg T (2003) Deep brain stimulation in dystonia. J Neurol 250(Suppl 1):I47–I52
9. Sansur CA, Frysinger RC, Pouratian N, Fu KM, Bittl M, Oskouian RJ, Laws ER, Elias WJ (2007) Incidence of symptomatic hemorrhage after stereotactic electrode placement. J Neurosurg 107:998–1003
10. Seijo FJ, Alvarez-Vega MA, Gutierrez JC, Fdez-Glez F, Lozano B (2007) Complications in subthalamic nucleus stimulation surgery for treatment of Parkinson's disease. Review of 272 procedures. Acta Neurochir Wien 149:867–875, discussion 876
11. The Deep-Brain Stimulation for Parkinson's Disease Study Group (2001) Deep-brain stimulation of the subthalamic nucleus or the pars interna of the globus pallidus in Parkinson's disease. N Engl J Med 345:956–963
12. Vaillancourt DE, Sturman MM, Verhagen Metman L, Bakay RA, Corcos DM (2003) Deep brain stimulation of the VIM thalamic nucleus modifies several features of essential tremor. Neurology 61:919–925
13. Vesper J, Haak S, Ostertag C, Nikkhah G (2007) Subthalamic nucleus deep brain stimulation in elderly patients—analysis of outcome and complications. BMC Neurol 7:7
14. Voges J, Waerzeggers Y, Maarouf M, Lehrke R, Koulousakis A, Lenartz D, Sturm V (2006) Deep-brain stimulation: long-term analysis of complications caused by hardware and surgery–experiences from a single centre. J Neurol Neurosurg Psychiatry 77:868–872
15. Xiaowu H, Xiufeng J, Xiaoping Z, Bin H, Laixing W, Yiqun C, Jinchuan L, Aiguo J, Jianmin L (2010) Risks of intracranial hemorrhage in patients with Parkinson's disease receiving deep brain stimulation and ablation. Parkinsonism Relat Disord 16:96–100

Acta Neurochir (2011) 153:1579–1585
DOI 10.1007/s00701-011-1036-z

TECHNICAL NOTE

A role of diffusion tensor imaging fiber tracking in deep brain stimulation surgery: DBS of the dentato-rubro-thalamic tract (drt) for the treatment of therapy-refractory tremor

Volker A. Coenen · Niels Allert · Burkhard Mädler

Received: 1 March 2011 / Accepted: 18 April 2011 / Published online: 8 May 2011

Abstract
Introduction Deep brain stimulation (DBS) can alleviate tremor of various origins. A number of regions are targeted. In recent work our group was able to show the involvement of the dentato-rubro-thalamic tract (drt) in tremor control with fiber tracking techniques. Here we report for the first time the successful use of magnetic resonance tractography in combination with traditional landmark-based targeting techniques to perform the implantation of a bilateral DBS system in a patient with dystonic head tremor.
Methods We report on a 37-year-old female with long-standing pure head tremor from myoclonus dystonia. She was identified as a candidate for thalamic DBS. The use of head fixation in a stereotactic frame would blur target symptoms (head tremor) during surgery and was therefore avoided. Her dentate-rubro-thalamic tracts were visualized with preoperative diffusion tensor imaging (DTI) and tractography, and then directly targeted stereotactically with DBS electrodes.
Results Three months after implantation, tremor control was excellent (>90%). A close evaluation of the active electrode contact positions revealed clear involvement of the drt.
Conclusion This is the first time that direct visualization of fiber tracts has been employed for direct targeting and successful movement disorder tremor surgery. In the reported case, additional knowledge about the position of the drt, which previously has been shown to be a structure for modulation to achieve tremor control, led to a successful implantation of a DBS system, although there was a lack of intra-operatively testable tremor symptoms. In concordance with studies in optogenetic neuromodulation, fiber tracts are the emerging target structures for DBS. The routine integration of DTI tractography into surgical planning might be a leading path into the future of DBS surgery and will add to our understanding of the pathophysiology of movement disorders. Larger study populations will have to prove these concepts in future research.

Keywords Deep brain stimulation · Dentato-rubro-thalamic tract · Diffusion tensor imaging · Fiber tracking · Myoclonus dystonia · Subthalamus · Thalamus · Tractography · Tremor

Introduction

Background

Medically refractory tremor can be treated effectively with deep brain stimulation (DBS) in the ventral lateral thalamus. The ventral intermediate nucleus of the thalamus (Vim) is the traditional target [2, 9, 13, 15, 20]. However, in the past years there have been reports about the benefit of the posterior STN region and the caudal zona incerta (cZI) as better target regions for certain distinct tremor forms [12, 18, 19]. Recent reports in rodents suggest that DBS preferably acts through an activation of fiber tracts afferent to targeted nuclei [10]. Diffusion tensor imaging combined

The results have not been presented before.

V. A. Coenen (✉) · N. Allert · B. Mädler
Division of Stereotaxy and MR-based Operative Techniques/
Department of Neurosurgery, University of Bonn,
Sigmund Freud Straße 25,
53105 Bonn, Germany
e-mail: volker.coenen@ukb.uni-bonn.de

N. Allert
Neurological Rehabilitation Center Godeshoehe,
Bonn, Germany

with deterministic fiber tracking (DTI-FT) can show individual fiber tracts in the living human brain because of preferential water diffusion in central nervous system tissue, explicitly in white matter [7, 14, 16, 22]. DTI-FT has been employed to interpret unexplained side effects of STN DBS with the activation of distinct fiber tracts [8] to understand the (patho-) physiology of emotion processing [11, 21] and has helped to determine the dentate-rubro-thalamic tract (drt) as the possible true candidate structure for tremor reduction through DBS [6]. Other groups have also investigated the usefulness of DTI in movement disorder surgery. In our opinion they come to rather vague assumptions with regard to brain anatomy while completely leaving out possibilities of therapeutic options [1]. Our experience from DTI studies in tremor is that symptoms can be alleviated if the active electrode contact is located inside or in the vicinity of the individual drt [6]. In this report we present a patient who underwent bilateral thalamic DBS to alleviate her dystonic head tremor. Due to the absence of an extremity tremor, we decided to directly target her bilateral drt instead of purely relying on anatomical landmarks and intraoperative testing for side effects (paraesthesia and internal capsule activation).

We hypothesize that direct high-resolution DTI-based targeting of the drt for stereotactic DBS electrode implantation will eventually lead to sufficient tremor control. This is the first report on direct DTI-based fiber tract targeting in DBS surgery for the treatment of tremor.

Materials and methods

A 37-year-old, otherwise healthy female presented to our service with a 19-year history of myoclonic head tremor and a slight dystonic rotation to the right. Her tremor showed a slight rotational component. Previously she had been treated with botulinum toxin type A until the development of antibodies. A trial with botulinum toxin type B was not effective. Similarly, several trials with medication were not successful or tolerated. An alleviation of the tremor was observed after alcohol consumption. Interestingly, her 6-year younger brother also had a head tremor. However, the patient refused genetic testing, most notably for myoclonus-dystonia syndrome (DYT 11). She felt socially isolated by her tremor and was identified as a candidate for thalamic DBS surgery. Since her tremor showed no testable extremity tremor, we felt that fixation in the stereotactic frame would blur all target symptoms. One way to perform surgery would be to rely solely on the side effect spectrum. We offered to visualize her drt in order to directly target it. The patient agreed and gave written informed consent.

The evaluation of the DTI imaging together with clinical effects and the publication of data were approved by the institutional ethics board of the University of Bonn (no. 199/09). Tremor rating scales were applied pre- and postoperatively (at 3 months) to give an objective outcome measure.

MR imaging

One day prior to surgery, MR imaging studies were performed without a stereotactic frame and with the patient under mild sedation (5 mg Midazolam, Hoffmann-La Roche, Ltd).

MRI data were acquired on a 3-T MR imaging system (Philips Healthcare, Best, The Netherlands) comprising an isotropic T2-weighted fast spin echo (FSE), diffusion-weighted SE EPI, and 3D inversion prepared T1-weighted gradient echo sequences (MPRAGE). All images were conducted in axial orientation.

A T2-weighted FSE sequence was acquired (12,646-ms TR, 100-ms TE, 254-mm FOV, 176×176 matrix, 120 slices, 1.44-mm slice thickness, 3:44-min acquisition time). The resulting data were reconstructed to 1.44 mm^3 isotropic voxels.

For DTI, a sensitivity encoded (SENSE, factor 2.9) spin-echo echo-planar imaging (SE-EPI) pulse sequence was applied (13,188-ms TR, 84-ms TE, 256-mm FOV, 128×128 matrix; 70 slices, 2-mm slice thickness, 32 gradient directions, 1,000-s/mm^2 b-value, 7:54-min acquisition time). The sequence resulted in 2-mm^3 isotropic reconstructed voxels.

The T1-weighted 3D-MPRAGE sequence was acquired after contrast administration (gadolinium DTPA) with a SENSE factor of 4 (8.5-ms TR, 3.8-ms TE, 8° flip angle, 256-mm FOV, 256×256 matrix, 160 slices, 2-mm slice thickness, 1-mm spacing between slices, 4:17-min acquisition time). It resulted in 1-mm^3 reconstructed voxels.

For CT imaging, preoperative stereotactic CT scans were acquired on a 16-row multidetector scanner (Brilliance 8000, Philips Medical Systems, Best, The Netherlands). Parameters were as follows: 120-kV tube voltage, 350-mA tube current, 16×0.75-mm collimation, 1-s tube rotation time, 0.942 pitch, 512×512 matrix, 1.5-mm slice thickness, and 1.5-mm increment.

Postoperative CT scans were acquired with the following parameters: 120-kV tube voltage, 350-mA tube current, 16×0.75-mm collimation, 0.75-s tube rotation time, 0.688 pitch, 512×512 matrix, 2-mm slice thickness, and 1-mm increment. The different postoperative CT scanning parameters were chosen for better electrode metal artifact suppression.

Fiber tracking

For details regarding the data processing and FT procedure, please refer to our previous publication [6]. Deterministic

fiber tracking was performed on a stand-alone Linux workstation using the StealthViz DTI software application (Medtronic Navigation, Louisville, CO). Fiber tracking of the bilateral pyramidal tract (pt) was carried out as described elsewhere [3]. For the dentato-rubro-thalamic tract (drt), fiber tracking was performed, with a fractional anisotropy (FA) level of 0.2. Minimal fiber length was set to 20 mm. Seed density was held at 5.0. Maximal directional change of fibers was chosen at 52°. The fiber tracking started with a cubic VOI (volume of interest) defining the cerebellar dentate nucleus (DN) on the high-resolution T2-weighted MRI. The resulting fibers that followed the superior cerebellar peduncle were included with a second VOI box (end region) around the fibers that reached the precentral gyrus, as identified according to the Yousry criteria [23]. The medial lemniscus was tracked with a VOI in the midbrain as for drt. The ending VOI was set in the corresponding postcentral gyrus. The resulting fiber tracts were fused to the T2-weighted and T1-weighted MRI sequences and transferred to the stereotactic planning system (FrameLink 5.0, Medtronic, USA) (Fig. 1) for direct targeting.

Stereotactic procedure

A Leksell Model G stereotactic frame was mounted on the patient's head under local anesthesia. After stereotactic CT acquisition, the image data were transferred to a FrameLink 5.0 workstation (Medtronic, USA) and fused to the preoperative MR images (T1-weighted and T2-weighted). The target for left thalamic DBS was planned (Fig. 1) according to standard landmarks. The resulting position was then adjusted to the individual drt position in the previously manipulated and altered imaging sequence (Fig. 1). The patient was placed on the operating table in a half-sitting position. Bilateral coronal burr holes were made under local anesthesia. A macro-electrode with a 2-mm exposed tip (Cosman, USA) was inserted over a microdrive (FHC, Bowdoin, ME). The target area was tested beginning 6 mm superficially to the planned target. Intraoperative effects were briefly tested and were felt not to be helpful. The side effect spectrum was tested (reflecting medial lemniscus and pyramidal tract affection). Bilateral trajectories were chosen as planned based on direct visualization of the drt. The DBS electrodes (model 3389, 28 cm, Medtronic, USA) were implanted under fluoroscopic guidance (Fig. 1, superimposed). After removal of the stereotactic frame, a rechargeable internal neural stimulator (ACTIVA RC, Medtronic, USA) was placed subcutaneously in the right abdominal region under general anesthesia in the same session. Four days after the implantation of the DBS system, each electrode contact was tested clinically to determine generator settings that yielded the best therapeutic effects (reduction of tremor) and avoided side effects.

Determination of DBS electrode position and fiber tracts

A helical CT scan of the head was performed postoperatively to confirm the targeted individual DBS electrode

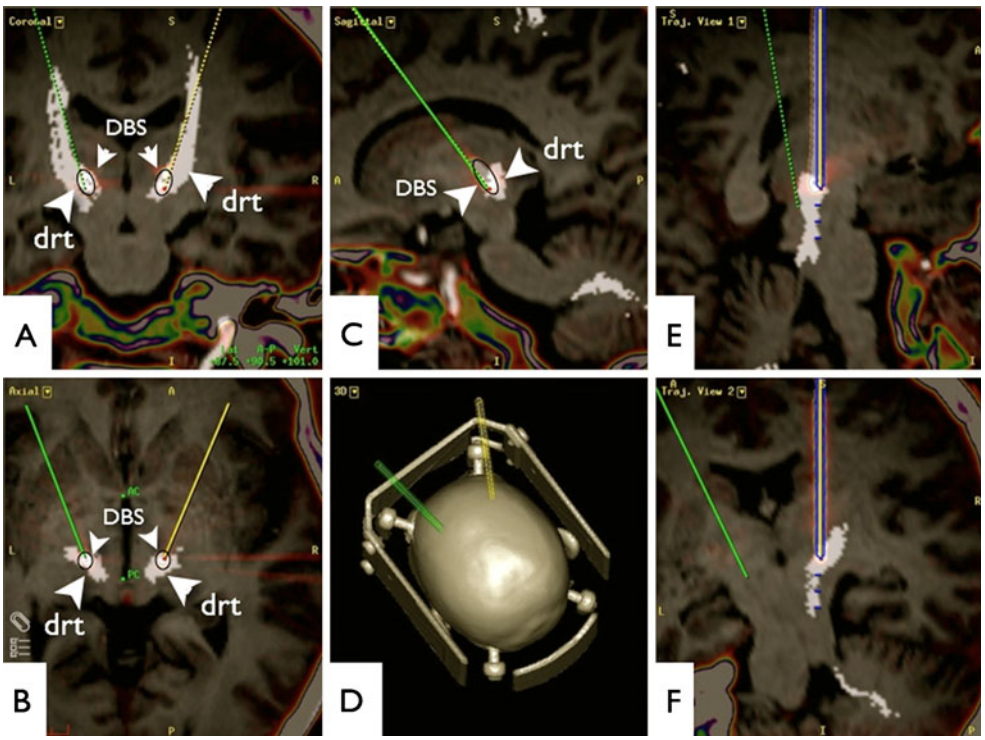

Fig. 1 DTI fiber tracking-based direct targeting of the drt. Superimposition with a postoperative helical CT (artifact from DBS electrodes, DBS). **A** Coronal; **B** axial; **C** sagittal views. **E**, **F** Trajectory views of left electrode path

Table 1 Position of effective DBS electrode contacts (EC) expressed in mid-commissural point (MCP) coordinates

	Left	Right
MCP coordinates	EC 1	EC 9
Laterality (X)	-10.9	+10.4
Anterior-posterior (Y)	-4.8	-5.3
Verticality (Z)	+1	+3

contact locations. The CT data were automatically fused to the planning data. Fusion quality was evaluated by visual inspection in the three orthogonal image planes (axial, coronal, sagittal). Effective DBS electrode contacts (EC) were determined and expressed in mid-commissural point (MCP) coordinates (Table 1). Multimodal data sets containing information from fiber tracking. MRI and CT were evaluated and reconstructed perpendicular to the implanted DBS electrodes. Minimal distances of the individual effective DBS contacts (EC) to fiber tract structures in their proximity (ml, pt, drt) were evaluated and visualized in an individual thalamic/subthalamic anatomical fiber tract map (Fig. 2). The center of the CT-derived artifact for the DBS electrode was identified. The electrophysiological distance was obtained according to the proposal of Butson et al. (2006) using their "impedance model" of a finite-element reconstruction [4]. This distance represents the estimated electric field (EF) size around the individual activated contact, depending on the voltage used and the actual impedance measured during INS programming (Fig. 3).

Results

Tremor in this patient was effectively alleviated. Stimulation parameters were as follows: right side, 4.0 V, case positive, 9 negative (monopolar), 180 Hz, 60 μs; left side, 4.5 V, 1 negative, 2 positive (bipolar), 60 μs. The score on the Essential Tremor Rating Scale (ETRS) improved by 18% (preoperatively, 11; postoperatively, 9). However, the patient showed excellent control of the head tremor (>90%) 3 months after surgery. This improvement was not well expressed by the ETRS scores because of the pure head tremor. Effective DBS electrode contact positions were expressed in MCP coordinates (Table 1). Fiber tracking allowed detailed depiction of fiber tracts traversing the subthalamic/thalamic region (Figs. 2, 3 and 4).

The dentato-rubro-thalamic tract (drt) was located in the environment of the pyramidal tract (pt) and the medial lemniscus (ml). It was shown to traverse the three typical stereotactic target regions for tremor surgery: the ventral intermediate nucleus of the thalamus (Vim), posterior STN region (pSTN), and caudal zona incerta (cZI) (Fig. 2). The fusion of the postoperative helical CT data revealed the exact DBS electrode location with respect to adjacent fiber structures (Figs. 2, 3 and 4). Evaluation of the electric fields (EFs) surrounding the effective contacts (Fig. 3, left shown only) allowed identifying the drt as the target structure for

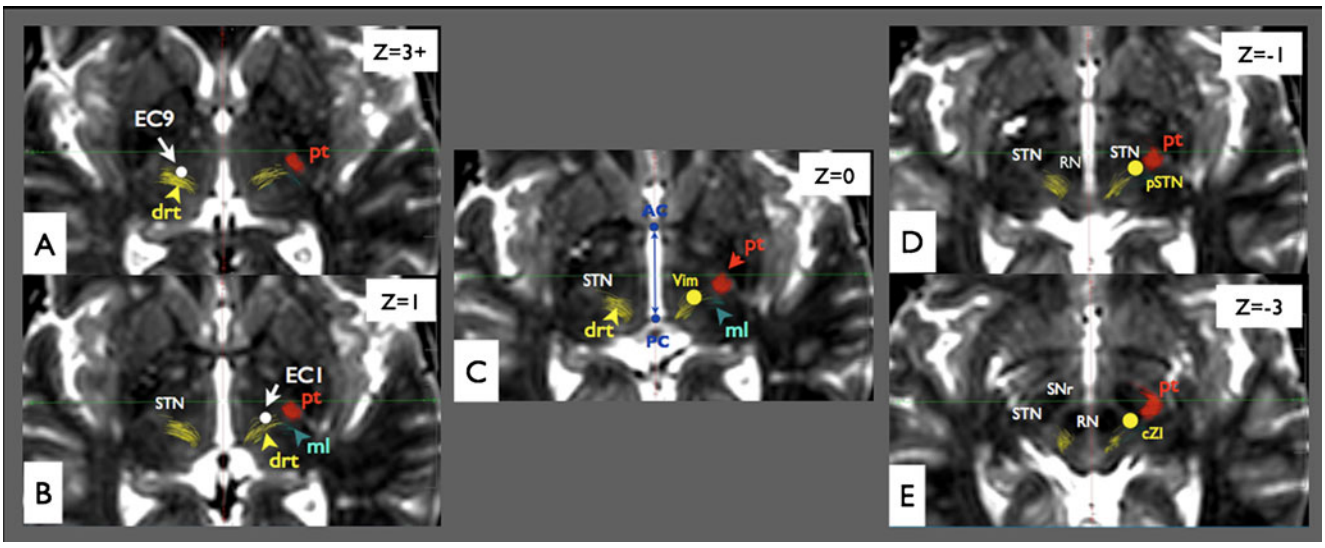

Fig. 2 Individual fiber map of the thalamic (**A**–**C**) and subthalamic (**D**–**E**) regions in axial T2-weighted high-resolution display. **A**,**B** Effective electrode contact positions (EC9, EC1) in our patient, with clear contact to the anterior part of the drt. **c** Traditional target level (z=0) for thalamic DBS. Note how these three target regions (Vim, pSTN, cZI; yellow) are interconnected by the drt at the thalamic/subthalamic level.

Abbreviations: AC= anterior commissure, cZI= caudal Zona incerta, drt= dentato-rubro-thalamic tract, EC1= effectice DBS contact 1, EC9= effective DBS contact 9, ml= medial lemniscus, PC= posterior comissure, pSTN= posterior subthalamic nucleus, pt= pyramidal tract, RN= red nucleus, STN= subthalamic nucleus, SNr= substantia nigra, Vim= ventral intermediate nucleus of thalamus

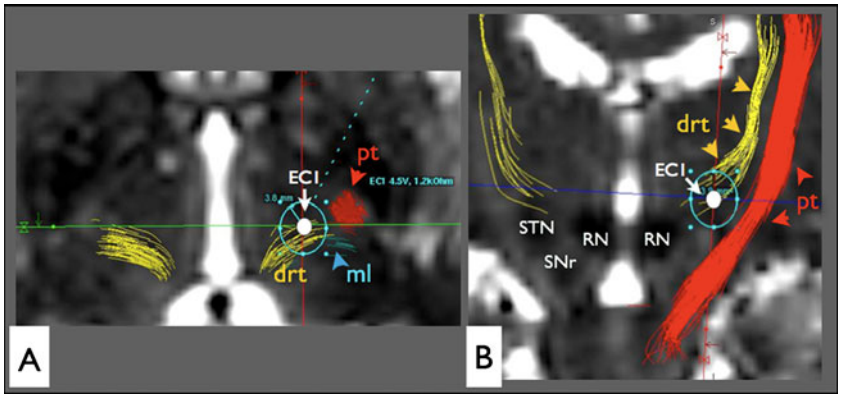

Fig. 3 Estimation of the volume of tissue activated (VTA) at the effective electrode contact (EC1). Left VTA shown only, green circle. **A** axial; **B** coronal. VTA, shown as idealized ball-shaped green structure, includes the complete cross section of the drt inside without reaching adjacent fiber structures. For abbreviations, see Fig. 2

tremor reduction, whereas the EFs did not reach the adjacent structures (ml, pt) either in the imaging studies or clinical effects.

Discussion

Functionally, the drt is concerned with coordination of somatomotor function. It is the main fiber bundle that forms the superior cerebellar peduncle (scp) and consists mainly of axon fibers that arise from the dentate (DN), emboliform, and globose nuclei. The fibers form a compact bundle that ascends dorsolaterally in the wall of the fourth ventricle. Most fibers cross at the level of the upper pons or inferior colliculus, and surround and enter the contralateral red nucleus (RN) after this decussation. The minor parts terminate in the RN. Most fibers project to the thalamus and terminate in the ventralis oralis posterior nucleus (VOP) and the nucleus ventralis intermedius (Vim). These nuclei then project to the primary motor cortex [5, 6, 13].

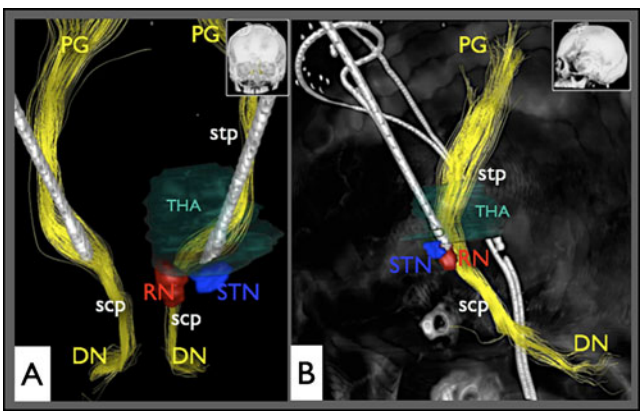

Fig. 4 Three-dimensional depiction of DBS electrode positions (from CT) and anatomical structures (from MRI). Note how DBS electrodes traverse the thalamus to reach the subthalamic level. Detailed anatomy is shown on the left side only for better overview. **A** Frontal view; **B** lateral view. Lack of crossing of the drts under the RN level is due to limitations of the fiber tracking technique. Abbreviations: Same as in Fig. 2. DN=dentate nucleus, PG=precentral gyrus, scp=superior cerebellar peduncle, stp=superior thalamic radiation, THA=thalamus

The complete incorporation of the dentato-rubro-thalamic tract into the lesion during the lesion era for complete and lasting tremor control has long been reported [3]. In reverse, the same effect is given as the reason for increased proximal limb tremor control in more inferior (ventral) target locations (cZI, pSTN) as compared to the more superficial thalamic target (VIM), which needs larger voltages and at the same time presumably causes more side effects (paraesthesia, motor symptoms) because of involvement of its functional environment (ml, pt). Plaha suggested that tremor control at low voltages in the posterior subthalamic (pSTN) region might be attributable to an affection of the dentato-rubro-thalamic tract (drt) in a deeper position where it crosses the pSTN or caudal zona incerta (cZI) [18, 19]. Our findings strongly substantiate this suggestion. Moreover, our results show that the drt crosses (or interconnects) these deep-seated DBS targets (Fig. 2), making the drt an even better candidate for tremor control. In our case it is clear that a thalamic target (resembling Vim) (Table 1) as opposed to a deeper target (cZI, pSTN) has been implanted with Z-values (verticality) of +1 and +3, respectively. Electric field analysis (Fig. 3) shows that the utilized voltages needed to achieve tremor control lead to an electric field (EF) extension that covers the drt's complete cross section. This electric field does, however, not touch surrounding critical structures like the medial lemniscus (ml) or the pyramidal tract (pt). This is in accordance with the clinical response of this patient and the complete lack of side effects. It is also in line with our previous work [6].

By identifying the effective contact coordinates, the location and volume of the electric field around the electrode can be estimated by the applied voltage and the impedance. This electric field influences the target structure and results in the desired clinical outcome (tremor reduction). At the same time it can cause side effects if other neuronal structures in its proximity are touched (Figs. 2 and 3). The application of this mapping technique depends on the accuracy that can be achieved for DTI-FT and for the fusion of preoperative MRI with postoperative

CT data. Our group has shown in a previous study that an accuracy of 3 mm is realistic when applying diffusion-weighted-imaging-derived fiber tract portrayal alone [7]. The combined accuracy (DTI-FT and fusion to postoperative CT data) was found to be as low as 1.5–2 mm with the same techniques as applied in this report. These are results of a newer, not yet published study. Other groups have shown that the localization of DBS electrodes in postoperative CT is accurate and might even be superior to postoperative MRI. Helical CT can be acquired for exclusion of perioperative bleeding and later be post-processed and fused to planning data for localization needs [17]. The electrode artifact's center should represent the exact radial center of the DBS electrode in the brain. DTI-FT visualizes fiber tracts according to the anisotropy of water diffusion in the brain tissue. It is not able to differentiate afferent and efferent fibers or synapses. This is the reason why the drt appears as a bundle that penetrates the thalamus, although synapses in the thalamus are known to exist in this functional projection [5, 13].

We are aware of the principal limitations posed by the deterministic fiber tracking algorithm (FACT), such as termination of tracking in areas of reduced FA (due to increased intermingling of fibers, approaching the subcortical boundaries, and partial volume effects), the ambiguity of following the correct connection pathways in dense areas of crossing, and kissing or branching fibers (limitation of single diffusion tensor model), combined with a relatively low spatial resolution (ca. 2 mm isotropic voxel dimension). Nevertheless, we could verify that our achieved reproducible accuracy approaches this intrinsic resolution very closely [14, 16, 22].

There is a possibility to scrutinize the target region with electrophysiological detection of tremor cells during microelectrode recording (MER). However, in our group's experience, targeting and clinical outcomes are not enhanced by this technique. Like many groups in the world, we stopped performing MER for tremor surgery years ago, and now solely rely on the direct stimulation results and the side effect spectrum. We certainly admit that MER in this case would have been a valuable adjunct to the imaging technique.

Conclusion

To our knowledge, this is the first report on direct visualization, targeting, and implantation of the drt through the application of magnetic resonance tractography to alleviate tremor in a human subject. It provides evidence for the general concept of improved DBS target structure assignment for stereotactic DBS implantation by the combination of high-resolution anatomical MRI, CT, and individual white matter fiber tracking. As previously shown by our group, modulation of the drt is the most likely physiological effect of DBS in the thalamic/subthalamic region that leads to alleviation of tremor [6, 12, 18, 19]. This includes the notion that probably the traditional DBS targets (Vim, cZI, pSTN) are effective, because they are interconnected by the drt or actually resemble different parts of it. Moreover, the combination of preoperative DTI imaging with postoperative helical CT and the evaluation of the electrophysiological environment of distinct DBS electrode contacts with EF modulation lead to individual detailed fiber maps [6, 8]. Fiber tracts are most likely the true anatomical structures that are influenced by the DBS technology [6, 8, 10]. In the future, traditional atlas information for stereotactic surgical strategies will likely prove to be inferior to individual fiber tract anatomy, as shown here. DTI tractography will probably have an important role in the future of DBS surgery not only for patient safety in reducing brain perforating tracts while searching for the effective target region, but also for the understanding of physiological and anatomical circuits involved in the generation of movement disorders. However, this all will only hold true if these results can be replicated in a larger study group.

Conflicts of interest Dr. Coenen and Dr. Allert have received honoraries for lecturing and consulting services (Medtronic, Europe). Dr. Coenen was a clinical collaborator in the development of StealthViz DTI (Medtronic, Navigation, USA).

References

1. Barkhoudarian G, Klochkov T, Sedrak M, Frew A, Gorgulho A, Behnke E, De Salles A (2010) A role of diffusion tensor imaging in movement disorder surgery. Acta Neurochir (Wien) 2089–2095
2. Benabid AL, Pollak P, Gao D, Hoffmann D, Limousin P, Gay E, Payen I, Benazzouz A (1996) Chronic electrical stimulation of the ventralis intermedius nucleus of the thalamus as a treatment of movement disorders. J Neurosurg 84:203–214
3. Burgel U, Madler B, Honey CR, Thron A, Gilsbach J, Coenen VA (2009) Fiber tracking with distinct software tools results in a clear diversity in anatomical fiber tract portrayal. Cen Eur Neurosurg 70:27–35
4. Butson CR, Maks CB, McIntyre CC (2006) Sources and effects of electrode impedance during deep brain stimulation. Clin Neurophysiol 117:447–454
5. Carpenter MB (1991) Core Text of Neuroanatomy. Williams and Wilkins, Baltimore
6. Coenen V, Mädler B, Schiffbauer H, Urbach H, Allert N (2011) Individual fiber anatomy of the subthalamic region revealed with DTI—A concept to identify the DBS target for tremor suppression. Neurosurgery 2011 Jan 19. [Epub ahead of print]
7. Coenen VA, Fromm C, Kronenburger M, Rohde I, Reinacher PC, Becker R, Marks B, Gilsbach JM, Rohde V (2006) Electrophysiological proof of diffusion-weighted imaging-derived depiction

of the deep-seated pyramidal tract in human. Zentralbl Neurochir 67:117–122
8. Coenen VA, Honey CR, Hurwitz T, Rahman AA, McMaster J, Burgel U, Madler B (2009) Medial forebrain bundle stimulation as a pathophysiological mechanism for hypomania in subthalamic nucleus deep brain stimulation for Parkinson's disease. Neurosurgery 64:1106–1114, discussion 1114–1105
9. Deuschl G, Bain P, Brin M (1998) Consensus statement of the Movement Disorder Society on Tremor. Ad Hoc Scientific Committee. Mov Disord 13(Suppl 3):2–23
10. Gradinaru V, Mogri M, Thompson K, Henderson J, Deisseroth K (2009) Optical deconstruction of parkinsonian neural circuitry. Science 324(5925):354–359
11. Gutman DA, Holtzheimer PE, Behrens TE, Johansen-Berg H, Mayberg HS (2009) A tractography analysis of two deep brain stimulation white matter targets for depression. Biol Psychiatry 65:276–282
12. Hamel W, Herzog J, Kopper F, Pinsker M, Weinert D, Muller D, Krack P, Deuschl G, Mehdorn HM (2007) Deep brain stimulation in the subthalamic area is more effective than nucleus ventralis intermedius stimulation for bilateral intention tremor. Acta Neurochir Wien 149:749–758, discussion 758
13. Hassler R, Mundinger F, Riechert T (1979) Stereotaxis in Parkinson Syndrome. Springer, Berlin, Heidelberg
14. Kreher BW, Mader I, Kiselev VG (2008) Gibbs tracking: a novel approach for the reconstruction of neuronal pathways. Magn Reson Med 60:953–963
15. Lozano AM (2000) Vim thalamic stimulation for tremor. Arch Med Res 31:266–269
16. Mori S, Kaufmann WE, Davatzikos C, Stieltjes B, Amodei L, Fredericksen K, Pearlson GD, Melhem ER, Solaiyappan M, Raymond GV, Moser HW, van Zijl PC (2002) Imaging cortical association tracts in the human brain using diffusion-tensor-based axonal tracking. Magn Reson Med 47:215–223
17. Pinsker MO, Herzog J, Falk D, Volkmann J, Deuschl G, Mehdorn M (2008) Accuracy and distortion of deep brain stimulation electrodes on postoperative MRI and CT. Zentralbl Neurochir 69:144–147
18. Plaha P, Khan S, Gill SS (2008) Bilateral stimulation of the caudal zona incerta nucleus for tremor control. J Neurol Neurosurg Psychiatry 79:504–513
19. Plaha P, Patel NK, Gill SS (2004) Stimulation of the subthalamic region for essential tremor. J Neurosurg 101:48–54
20. Schaltenbrand G, Wahren W (1977) Atlas of Stereotaxy of the Human Brain. Thieme
21. Schoene-Bake JC, Parpaley Y, Weber B, Panksepp J, Hurwitz TA, Coenen VA (2010) Tractographic analysis of historical lesion surgery for depression. Neuropsychopharmacology 35(13):2553–2563, Epub 2010 Aug 25
22. Wakana S, Jiang H, Nagae-Poetscher LM, van Zijl PC, Mori S (2004) Fiber tract-based atlas of human white matter anatomy. Radiology 230:77–87
23. Yousry TA, Schmid UD, Alkadhi H, Schmidt D, Peraud A, Buettner A, Winkler P (1997) Localization of the motor hand area to a knob on the precentral gyrus. A new landmark. Brain 120(Pt 1):141–157

Comment

Targeting in functional neurosurgery traditionally has been based on the Stereotatic Atlas, direct anatomical targeting (image-based, generally MRI), and neurophysiological MER (microelectrode recording). Most centers in the world use a combination of the above-mentioned modalities to insert electrodes (or perform a lesioning procedure) in different anatomical nuclei (STN, VIM, Gpi, etc.). Destruction or high frequency stimulation of these gray matter nuclei seems to reduce the abnormal firing activity and indirectly restore normal (or semi-normal) functioning of different neuronal circuits (STN, cortico-striato-pallido-thalamo-cortical; VIM, cerebello-rubro-thalamic, etc.).

DTI as a targeting modality, alongside the traditional methods, offers a new opportunity in DBS surgery or lesioning (4).

With this modality, it is possible to visualize white matter tracts with better anatomical placement of the electrode (decreased incidence of side effects); moreover, a new target may emerge allowing the possibility of stimulating axons in white matter tracts. This is true in movement disorder surgery, but also in psychosurgery and possibly in epilepsy.

In this very interesting paper, the authors report a case of dystonic head tremor treated with DBS-drt (dentato-rubro-thalamic). The author visualized the drt tract with DTI and directly targeted this area. The postoperative electrode position was confirmed with CT-MRI fusion. Ninety percent head tremor control was achieved at 3 months.

Jibril Osman Farah
Liverpool, UK

Acta Neurochir (2011) 153:1587–1590
DOI 10.1007/s00701-011-1051-0

CASE REPORT

Improvement of hand dexterity induced by stimulation of the peduncolopontine nucleus in a patient with advanced Parkinson's disease and previous long-lasting bilateral subthalamic DBS

Angelo Franzini · Giuseppe Messina · Edvin Zekaj · Luigi Romito · Roberto Cordella

Received: 1 March 2011 / Accepted: 12 May 2011 / Published online: 3 June 2011

Abstract We report the case of a patient already submitted to bilateral deep-brain stimulation (DBS) of the subthalamic nucleus (STN) who started to develop gait impairment, postural imbalance and frequent falls in the course of the disease and who subsequently underwent DBS of the right pedunculopontine nucleus (PPN) at our institute. An immediate clinical benefit in hand dexterity was observed with acute external stimulation and maintained after the definitive implant of the internal pulse generator (IPG) at 6 months' follow-up. The benefit on hand dexterity seemed to be related to the interactions between the PPN low-frequency stimulation and the bilateral STN high-frequency stimulation.

Introduction

The role of the pedunculopontine nucleus (PPN) in the control of gait and voluntary movements has been demonstrated in experimental primate models, suggesting its therapeutic application since 1998 [1].

PPN chronic stimulation in man was patented in the USA in 2002 by Lozano and Rise [4] but the first implants in human beings was published by Mazzone et al. [6] and by Plaha and Gill [10], who reported their work in the same issue of *Neuroreport* in 2005.

Nevertheless, the clinical research on PPN is still in a preliminary stage and the available published series suggest applications aimed at improving gait and axial symptoms in advanced Parkinson's disease [2, 9, 12]. PPN stimulation has been used in patients affected by Parkinson's disease with previous subthalamic nucleus (STN) implants or as a stand-alone application in patients with Parkinson's disease whose gait and posture impairment were the prevailing symptoms [7, 11].

We describe a patient with Parkinson's disease who had been harbouring a bilateral STN implant for 8 years and who, after acute and chronic PPN stimulation, obtained marked improvement of hand dexterity bilaterally. An appropriate evaluation scale for hand dexterity (DASH) [3] and another scale for quality of life (SF 36) were applied, together with the conventional Unified Parkinson's Disease Rating Scale (UPDRS) evaluation.

This case report suggests a clinical application of PPN stimulation not only targeted for gait and for freezing but also for the possibility of obtaining further clinical improvements in patients with a long-lasting disease who have had benefits from STN DBS.

Case report

This 66-year-old woman, a Roman Catholic nun, started to complain of tremor and bradykinesia of the right side about 10 years before admittance to our institute. After the diagnosis of Parkinson's disease was made, the patient started treatment with levodopa with mild improvement of bradicinesia and rigidity, but without improvement of right upper limb tremor. In 2001 she underwent unilateral left STN deep-brain stimulation (DBS), with an 80% improvement on the UPDRS motor sub score and the disappearance of tremor of upper right limb. Three years later, tremor also

A. Franzini · G. Messina (✉) · E. Zekaj · L. Romito · R. Cordella
Fondazione IRCCS Istituto Nazionale Neurologico "Carlo Besta",
Via Celoria 11,
20133 Milan, Italy
e-mail: giusmex@gmail.com

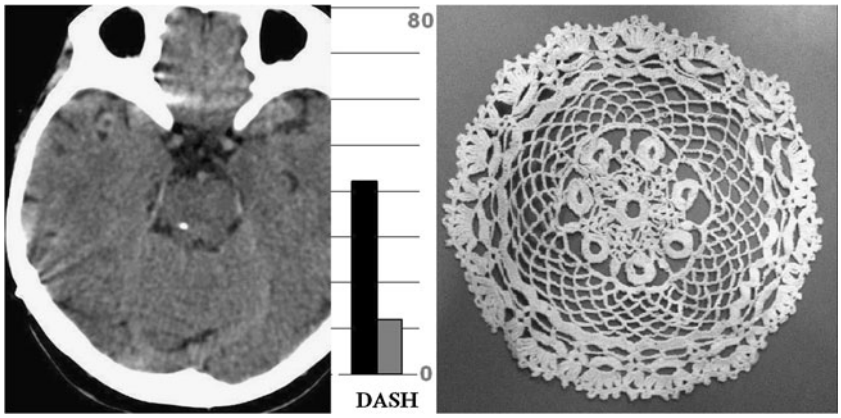

Fig. 1 *Left*: CT scan showing the tip of the deep-brain electrode, placed in the following coordinates (X 5, Y −18, Z −15) with respect to the midcomissural point. In the *middle* of the diagram is the DASH score that revealed an amelioration of the hand dexterity (*black* preop, *grey* follow-up). *Right*: a photograph of a crocheted lace doily made by the patient after surgery

appeared on the left hemibody and the patient was subsequently submitted to right STN DBS that resulted in control of controlateral tremor.

In the following years the patient presented progressive worsening of gait, with onset of postural imbalance and daily falls. Furthermore, hand dexterity gradually diminished, and the patient also started to complain of not being able to perform normal daily activities, such as cooking, dressing and needlework. The worsening of hand dexterity was mainly due to progression of upper limb's distal bradykinesia. These symptoms were refractory to both modification of drug therapy and of stimulation parameters. In 2010, DBS of the right PPN was performed, aimed at reducing postural imbalance and falls [7, 11]. Surgical intervention was performed under local anaesthesia; with the Leksell frame (Elekta, Stockholm, Sweden) computerized tomography (CT) exam scan in stereotactic conditions being performed for the targeting procedure. We also used the probabilistic Franzini atlas, updated with a specific program for PPN (www.angelofranzini.com/BRAIN.HTM). We took into account a previously published manuscript by Zrinzo et al. [13] about the position of the PPN relative to the anterior commissure-posterior commissure (AC-PC) line and the ventricular floor line (VFL). The definitive coordinates relaive to the midcomissural point (MCP) were: 5 mm lateral from the midline, 18 mm behind the mid-commissural point along the AC-PC line, and 15 mm below the MCP.

The definitive electrode (3389, Medtronic) was positioned after macrostimulation at the target site that elicited contralateral sensory responses (consistent with PPN's proximity to the medial lemniscus) with stimulation at 3 V, 30 Hz, 90-μs pulse width, monopolar mode.

In the following days the stimulation parameters were tested through an external stimulator, and finally set to 25 Hz, 60 μs and 2 V. Acute stimulation induced immediate improvement of hand dexterity, witnessed by the regained

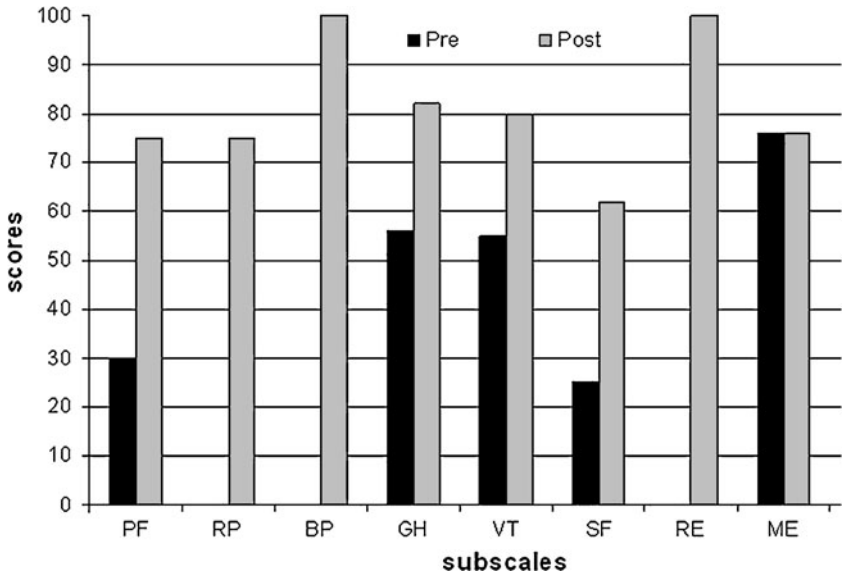

Fig. 2 Preoperative and postoperative subscores of SF 36 scale relative to last clinical follow-up (6 months). *PF* physical functioning, *RP* role limitations due to physical problems, *BP* bodily pain, *GH* general health perceptions, *VT* vitality, *SF* social functioning, *RE* role-limitations due to emotional problems, *ME* mental health

ability to create beautifully executed needlework (Fig. 1). The patient was unaware of the beginning of the electrical stimulation and no subjective sensation was reported during the acute turning on and off of the stimulator .

A few days later, the patient underwent, in general anaesthesia, a surgical procedure of positioning of an internal pulse generator (Soletra, Medtronic), which was connected to the deep-brain PPN electrode. Gait instability and postural imbalance were significantly reduced from the first week of definitive stimulation . In a few days, the patient also reported a significant reduction of the number of falls.

The patient was re-evaluated at follow-up 6 months later. The DASH score and the quality of life evaluation scale (SF 36) were applied together with the conventional UPDRS evaluation. A stable improvement in overall DASH score was noticed. The UPDRS scale part III improved from 29 to 15. Finally, the quality of life score also improved as assessed by the SF 36 scale (Fig. 2); this positive outcome on the quality of life was mainly due to improvement of the dexterity of the hand, which allowed the patient to perform several activities which were not possible before PPN DBS.

Discussion

This case confirms that PPN DBS should be taken into account as an adjunctive therapeutic option in the hands of trained neurosurgeons and neurologists involved in the treatment of movement disorders. In the literature, a small series of patients who underwent bilateral or unilateral electrode implantation within the PPN to improve freezing, gait, posture and axial symptoms in Parkinson disease [4, 6] have been reported. Also, in this specific case, the aim of the PPN implant was the improvement of gait and the reduction of falls; however, the clinical results not only achieved this goal but also an unexpected improvement of bilateral hand dexterity appeared acutely when the stimulator was turned on. This effect is chronically maintained by the PPN stimulation. The patient spent most of the day praying and making crocheted doilies and small pieces of needlework. For many years, about 80% of her finalistic movements concerned the hands, and the disease progressively slowed fine finger movements without real impairment of any specific movements, which were all possible but slow. The role of the concomitant STN stimulation is evident by the fact that when we turned off the STN IPG (unilaterally and/or bilaterally), most of the improved hand dexterity effect was lost. When we turned off the PPN IPG we immediately and completely lost the hand dexterity effect even, if STN DBS was still on. It is very difficult in a single case to explain this bizarre interaction between brainstem and mesencephalic nuclei involved in the control of movements. The PPN has a potential role in modulation of the basal ganglia output structures and of spinal neurons (with which it harbours bilateral connections), although most of the data available refer to studies on non-human primates, rodents and cats [8]; PPN neurons have been shown to modify their firing rates in response to movements of contralateral and ipsilateral arm in normal monkeys [5], and to voluntary and passive movements of both upper and lower limbs in humans [12]; it is then possible that the modulatory role of this nucleus is not limited to neuronal pathways involving the lower limbs.

We have only performed two implants of deep-brain electrodes into the PPN target so far; the other one was implanted as a stand-alone target (monolateral implant, right side) in a patient affected by iatrogenic Parkinson's disease (because of long-term use of neuroleptic drugs), whose main symptom was postural imbalance and appendicular tremor, and not hand dexterity.

We may comment that STN DBS gave the presented patient about a decade of well being and autonomy, and now PPN stimulation has given an additional chance to this woman, who would otherwise be condemned to worsen and to progressively lose her motor and creative abilities. In this report we suggest to add to the conventional UPDRS evaluation the use of other evaluation scales aimed at evaluating functions, such as hand dexterity and the quality of life, as in this case.

Conflicts of interest None.

References

1. Aziz TZ, Davies L, Stein J, France S (1998) The role of descending basal ganglia connections to the brain stem in parkinsonian akinesia. Br J Neurosurg 12(3):245–249
2. Ferraye MU, Debû B, Fraix V, Goetz L, Ardouin C, Yelnik J, Henry-Lagrange C, Seigneuret E, Piallat B, Krack P, Le Bas JF, Benabid AL, Chabardès S, Pollak P (2010) Effects of pedunculopontine nucleus area stimulation on gait disorders in Parkinson's disease. Brain 133(Pt 1):205–214
3. Hudak PL, Amadio PC, Bombardier C (1996) Development of an upper extremity outcome measure: the DASH (disabilities of the arm, shoulder and hand) [corrected]. The Upper Extremity Collaborative Group (UECG). Am J Ind Med 29(6):602–608
4. Lozano AM, Rise T (2002) Method of treating movement disorders by electrical stimulation and/or drug infusion of the penduncolopontine nucleus. US patent no. 6356784, United States Patent Office, Alexandria
5. Matsumura M (2005) The pedunculopontine tegmental nucleus and experimental parkinsonism. A review. J Neurol 252(Suppl 4): IV5–IV12
6. Mazzone P, Lozano A, Stanzione P, Galati S, Scarnati E, Peppe A, Stefani A (2005) Implantation of human pedunculopontine nucleus: a safe and clinically relevant target in Parkinson's disease. Neuroreport 16(17):1877–1881

7. Moro E, Hamani C, Poon YY, Al-Khairallah T, Dostrovsky JO, Hutchison WD, Lozano AM (2010) Unilateral pedunculopontine stimulation improves falls in Parkinson's disease. Brain 133(Pt 1):215–224
8. Pahapill PA, Lozano AM (2000) The pedunculopontine nucleus and Parkinson's disease. Brain 123(Pt 9):1767–1783
9. Peppe A, Pierantozzi M, Chiavalon C et al (2010) Deep brain stimulation of the pedunculopontine tegmentum and subthalamic nucleus: effects on gait in Parkinson's disease. Gait Posture 32 (4):512–518
10. Plaha P, Gill SS (2005) Bilateral deep brain stimulation of the pedunculopontine nucleus for Parkinson's disease. Neuroreport 16 (17):1883–1887
11. Stefani A, Lozano AM, Peppe A, Stanzione P, Galati S, Tropepi D, Pierantozzi M, Brusa L, Scarnati E, Mazzone P (2007) Bilateral deep brain stimulation of the pedunculopontine and subthalamic nuclei in severe Parkinson's disease. Brain 130(Pt 6):1596–1607
12. Weinberger M, Hamani C, Hutchison WD, Moro E, Lozano AM, Dostrovsky JO (2008) Pedunculopontine nucleus microelectrode recordings in movement disorder patients. Exp Brain Res 188 (2):165–174
13. Zrinzo L, Zrinzo LV, Tisch S, Limousin PD, Yousry TA, Afshar F, Hariz MI (2008) Stereotactic localization of the human pedunculopontine nucleus: atlas-based coordinates and validation of a magnetic resonance imaging protocol for direct localization. Brain 131(Pt 6):1588–1598

Acta Neurochir (2011) 153:1591–1592
DOI 10.1007/s00701-011-1066-6

LETTER TO THE EDITOR

Newly developed back pain after subthalamic nucleus stimulation in Parkinson's disease

Atsushi Umemura · Yuichi Oka · Atsuhiko Okura · Kenji Okita · Kazuo Yamada

Received: 4 February 2011 / Accepted: 26 May 2011 / Published online: 9 June 2011

Dear editor,

Deep brain stimulation (DBS) of the subthalamic nucleus (STN) has been widely performed for medically refractory Parkinson's disease (PD). We have encountered patients with newly developed back pain after successful STN-DBS surgery. In this report, we review these cases and discuss the pathogenesis of newly developed back pain after STN-DBS.

Between November 2003 and December 2008, 148 patients with medically refractory PD underwent implantation of bilateral STN-DBS electrodes in Nagoya City University Hospital, Nagoya, Japan. STN-DBS was indicated in most patients for significant motor complications from levodopa such as fluctuation and dyskinesia. Among these patients, seven complained of newly developed back pain in the early period after STN-DBS despite having had no experience of back pain before STN-DBS. None of the patients showed camptocormia. The demographic details for all patients are shown in Table 1. STN-DBS yielded marked improvement in the UPDRS III motor score and UPDRS IV dyskinesia/fluctuation score, and reduced the need for dopaminergic medication in all patients. The time until they complained of back pain varied from 2 weeks to 5 months after surgery. Imaging study of lumbar X-ray, CT or MRI revealed various lumbar spine pathologies such as lumbar disc herniation, lumbar spinal stenosis, scoliosis, spondylolisthesis, and old compression fracture. Two patients subsequently underwent lumbar surgery for their lumbar pathology. We performed lumbar laminectomy and discectomy for disc herniation, and laminectomy and pedicle screw-rod fixation for spondylolisthesis. One patient was treated with epidural injections, and the other four patients were treated conservatively with analgesic medication. Consequently, the back pain was controlled well in all of the patients.

Several types of pain occur frequently in PD. Ford classified pain in PD into several categories: musculoskeletal pain, radicular or neuropathic pain, dystonia-related pain, central or primary pain, and akathitic discomfort [2]. The most prevalent painful sensations in PD seem to be musculoskeletal pain and dystonia-related pain. Depression in PD may also confound and aggravate pain.

Back problems in particular seem to be common in PD. Broetz et al. reported that the prevalence of back pain in PD (74%) was significantly higher than in control patients (27%) [1]. Postural abnormalities or truncal dystonia in PD seem to put stress on the lumbar disc structures and cause lumbar disc herniation. Increased muscle tone and reduced flexibility of the spine may also cause nonradicular back pain originating from the muscle, soft tissues, and skeletal structures.

Some previous studies demonstrated that STN-DBS improved fluctuating pain, namely, pain in the "off" period [3, 6]. STN-DBS also improves painful "off" period dystonia [4]. Nevertheless, we showed that a significant incidence (approximately 5%) of newly developed back pain occurs after STN-DBS in spite of the marked improvement of cardinal PD symptoms. Kim et al. also reported that new pain developed in some patients

A. Umemura (✉) · Y. Oka · A. Okura · K. Yamada
Department of Neurosurgery,
Nagoya City University Graduate School of Medicine,
1 Kawasumi, Mizuho-ku,
Nagoya 467-8601, Japan
e-mail: aume@med.nagoya-cu.ac.jp

K. Okita
Department of Neurology,
Nagoya City University Graduate School of Medicine,
Mizuho-ku,
Nagoya 467–8601, Japan

Table 1 Clinical features of seven patients with newly developed back pain after DBS

Case no.	Age (years), sex	Duration of PD (years)	UPDRS III			UPDRS IV (32–39)		Time to back pain after DBS	Lumber spine pathology	Treatment
			Pre-DBS (On meds)	Pre-DBS (Off meds)	Post-DBS	Pre-DBS	Post-DBS			
1	57, F	7	17	30	9	10	1	5 months	Disc herniation	Lumber surgery
2	58, M	6	23	41	18	2	0	3 months	Disc herniation	Medication
3	59, F	12	28	60	26	7	2	1 month	Disc herniation, scoliosis	Epidural injection
4	74, F	12	7	32	9	8	4	1 month	Spinal stenosis, scoliosis	Medication
5	65, M	12	4	39	6	2	0	2 weeks	Spondylolisthesis	Lumber surgery
6	59, F	9	5	20	4	9	5	5 months	Old compression fracture	Medication
7	76, F	6	7	18	5	9	2	1 month	Old compression fracture	Medication

after STN-DBS [3]. There could be several speculations for the pathogenesis of newly developed back pain. Firstly, as all patients had some lumbar pathology, back pain may have been masked by the immobility of PD. Increased motor activity after STN-DBS may cause back pain to develop. Secondly, alleviation of rigidity in the paraspinal muscles may promote instability of spinal components and cause back pain to develop. Thirdly, weight gain after STN-DBS is a common complication and may also contribute to the deterioration of back pain [5]. In addition, back pain in PD is often overlooked or underestimated before STN-DBS due to distress from motor symptoms [1].

In conclusion, we should pay more attention to back pain as a probable complication in STN-DBS for PD. As shown in this study, all patients who developed back pain had some asymptomatic pathology in the lumbar spine. Therefore, preoperative evaluation of the lumbar spine is essential for candidates of STN-DBS to predict postoperative back pain. It is also useful for further refinement of patient selection and patient education.

Conflicts of interest None.

References

1. Broetz D, Eichner M, Gasser T, Weller M, Steinbach JP (2007) Radicular and nonradicular back pain in Parkinson's disease: a controlled study. Mov Disord 22:853–856
2. Ford B (2010) Pain in Parkinson's disease. Mov Disord 25(Suppl 1):S98–S103
3. Kim HJ, Paek SH, Kim JY, Lee JY, Lim YH, Kim MR, Kim DG, Jeon BS (2008) Chronic subthalamic deep brain stimulation improves pain in Parkinson disease. J Neurol 255:1889–1894
4. Krack P, Pollak P, Limousin P, Benazzouz A, Deuschl G, Benabid AL (1999) From off-period dystonia to peak-dose chorea. The clinical spectrum of varying subthalamic nucleus activity. Brain 122:1133–1146
5. Macia F, Perlemoine C, Coman I, Guehl D, Burbaud P, Cuny E, Gin H, Rigalleau V, Tison F (2004) Parkinson's disease patients with bilateral subthalamic deep brain stimulation gain weight. Mov Disord 19:206–212
6. Witjas T, Kaphan E, Régis J, Jouve E, Chérif AA, Péragut JG, Azulay JP (2007) Effect of chronic subthalamic stimulation on nonmotor fluctuations in Parkinson's disease. Mov Disord 22:1729–1734

Acta Neurochir (2011) 153:1593–1599
DOI 10.1007/s00701-011-1009-2

CLINICAL ARTICLE

Foramen ovale cannulation guided by intra-operative computed tomography with integrated neuronavigation for the treatment of trigeminal neuralgia

Martin Hsiu-Chu Lin · Ming-Hsueh Lee · Ting-Chung Wang · Yu-Kai Cheng · Chen-Hsing Su · Chia-Mao Chang · Jen-Tsung Yang

Received: 3 January 2011 / Accepted: 29 March 2011 / Published online: 20 April 2011

Abstract
Background Radiofrequency rhizotomy of the Gasserian ganglion for the treatment of trigeminal neuralgia via percutaneous cannulation of the foramen ovale is facilitated by various localization modalities. In our preliminary study, we described the feasibility of computed tomography (CT) using an integrated neuronavigation system to cannulate the foramen ovale.
Methods Analysis was performed on 42 consecutive patients who underwent cannulation of the foramen ovale for radiofrequency trigeminal rhizotomy guided by CT using an integrated neuronavigation system. The reproducibility and safety of the neuronavigation-guided procedure were evaluated.
Results Overall, the average dimension of the foramen ovale was 7.1 (1.5)×4.7 (1.1) mm, and it was successfully cannulated by neuronavigation guidance in 31 (73.8%) patients with a mean cannulation time of 3.1 (0.7) min and an overall procedure time of 68.2 (16.4) min. The remaining 11 (26.2%) patients required subsequent CT guidance for successful puncture of the foramen ovale.
Conclusions These data demonstrate that neuronavigation-guided cannulation of the foramen ovale can be executed both quickly and safely on an outpatient basis. Additionally, the use of CT with integrated neuronavigation technology provides superior visual-spatial information compared to conventional fluoroscopy, the process of CT scanning, object planning, and neuronavigation-guided intervention can be completed in the same locale, and its application is easy to master and has the potential to enhance procedure tolerability of awake patients.

Keywords Gasserian ganglion · Trigeminal neuralgia · Neuronavigation · Percutaneous rhizotomy

Introduction

Idiopathic trigeminal neuralgia, the most common craniofacial pain syndrome, has significant morbidity. To date, surgical microvascular decompression has remained the most efficacious treatment modality with regard to response and recurrence [25, 30]. Indications for less-invasive percutaneous ablative techniques have evolved for unfit or unwilling surgical candidates, to become a primary treatment modality and been offered as a salvage procedure following unsuccessful microvascular decompression or recurrences [15, 24].

Haertel's technique has stood the test of time since its original description in 1912 [12]. Its three cutaneous reference points—the cheek point, zygomatic point, and mid-pupillary point—guide the cannulation of the foramen ovale. The needle is typically advanced under a fluoroscope utilizing a combination of the anteroposterior, lateral, and oblique submental views [29]; however, visualization of the foramen ovale under such circumstances can be inadequate and inadvertent injury to the surrounding neurovascular

This work has not been presented nor is it under evaluation for publication elsewhere.

M. H.-C. Lin · M.-H. Lee · T.-C. Wang · Y.-K. Cheng · C.-H. Su · C.-M. Chang · J.-T. Yang (✉)
Department of Neurosurgery, Chang Gung Memorial Hospital,
6 Sec West, Chia Pu Rd,
Pu Tz City, Chia-Yi, Taiwan
e-mail: jents716@ms32.hinet.net

J.-T. Yang
College of Medicine, Chang Gung University,
Tao-Yuan, Taiwan

structures can result in catastrophic complications [1, 4, 6, 11, 14, 20, 21, 27, 31, 32]. Several localization modalities have been explored thus far, including computed tomography (CT) guidance, high-speed real-time CT fluoroscopy, neuronavigation, and stereotaxy, all of which are intended to avoid multiple needle passes to minimize cannulation-related complications and improve procedure tolerability of awake patients [3–5, 8, 9, 13, 17–19, 22, 23, 26, 34]. CT images are by far superior, when combined with neuronavigation, which allows trajectory visualization in three dimensions and multiple planes at the surgeon's choosing, and use of real-time cannulation. Here, we report our preliminary experience on the use of intra-operative CT with integrated neuronavigation for cannulation of the foramen ovale.

Methods

From August to November 2010, 42 consecutive patients diagnosed with medically refractory idiopathic trigeminal neuralgia were treated by percutaneous radiofrequency rhizotomy at our institution's newly established BrainSUITE® iCT (Siemens and Brainlab, Germany). All procedures were performed on an outpatient basis by a single surgeon (M. Lin). The workflow is as follows: with the patient lying supine, the ENT reference array (Kolibri™ ENT System, Brainlab, Germany) is strapped firmly to the patient's forehead. The head is positioned in slight extension on a snug-fitting horseshoe headrest in order to avoid excessive movement during image acquisition and to facilitate optimal cannulation trajectory (Fig. 1). A head CT scan is performed at 1.5-mm intervals, 120 kV, 120 mAs, with the Somatom Sensation Open sliding gantry CT scanner (Siemens, Germany), the acquired images are sent to the iPlan® 2.0 platform (Brainlab, Germany) for planning with the Cranial essential & unlimited® 1.0 software (Brainlab, Germany), the foramen ovale and the lateral pterygoid plate are marked on all axial slices with contrasting colors, and the plan is then exported to the VectorVision Sky Navigation System® (Brainlab, Germany) and fused with the registered images for neuronavigation. The accuracy of the registration is verified through placement of the pointer on the facial bony features before sterile preparation of the operative field. The instrument adaptor is attached to the hub of a 100-mm-long, 20-gauge radio–frequency-insulated cannula with a 5-mm active tip (Diros Technology Inc. Canada); the needle tip and its trajectory is calibrated and verified with the instrument calibration matrix; and tip deviation <0.3 mm and trajectory deviation <0.3° are considered acceptable. Adjustment of the entry point as defined by the landmarks of the Haertel's technique is made to accommodate the individual geometric variability of the foramen ovale for an unobstructed linear pathway toward the Gasserian ganglion. Xylocaine (1%) is infiltrated, and cannulation is done under guidance by the standard 4-window display showing the 3-D skin probe eye view, inline sagittal view, inline coronal view, and probe eye view (Fig. 2).

Fig. 1 The strap-on ENT reference array (**a**); From *top to bottom*: instrument calibration matrix, instrument adaptor attached to the rhizotomy needle, and pointer (**b**); and patient set-up showing the left side approach, the instrument adaptor has been removed from the rhizotomy needle (**c**)

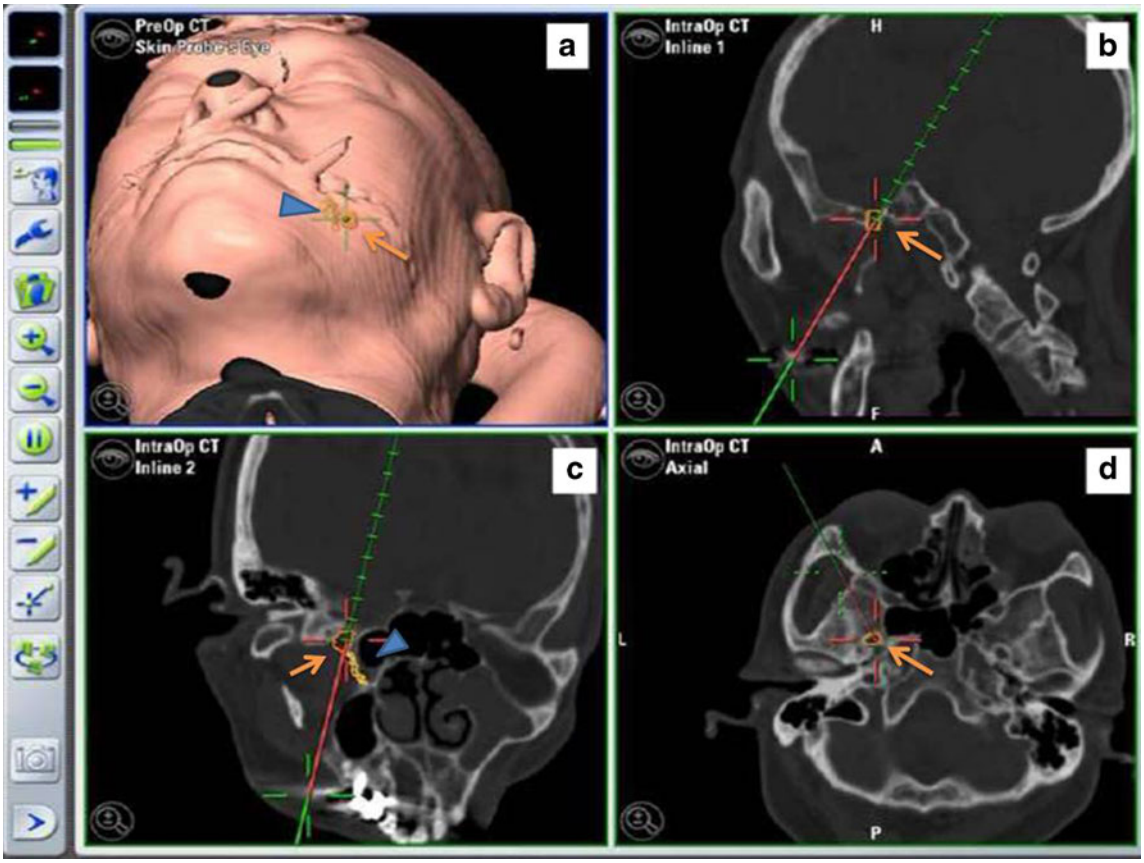

Fig. 2 The standard four-window display in real time during the cannulation process in which the foramen ovale (*arrow*) and lateral pterygoid plate (*arrowhead*) have been marked for distinction. The 3-D skin probe eye view (**a**), inline sagittal view (**b**), inline coronal view (**c**) and probe eye view (**d**)

Upon successful cannulation, the instrumentation adaptor is removed from the needle hub and needle tip placement is confirmed by a focused CT scan (Fig. 3). Advancement of the needle tip 6 mm beyond the foramen ovale on the endocranial surface is optimal, and fine adjustments are made accordingly. If cannulation cannot be achieved by neuronavigation, then it is performed under sequential CT guidance. A Tew electrode kit and a Radionics RTG-3CF generator is used (Radionics, Burlington, MA, USA), and test stimulation begins through application of 50 Hz, 1 ms,

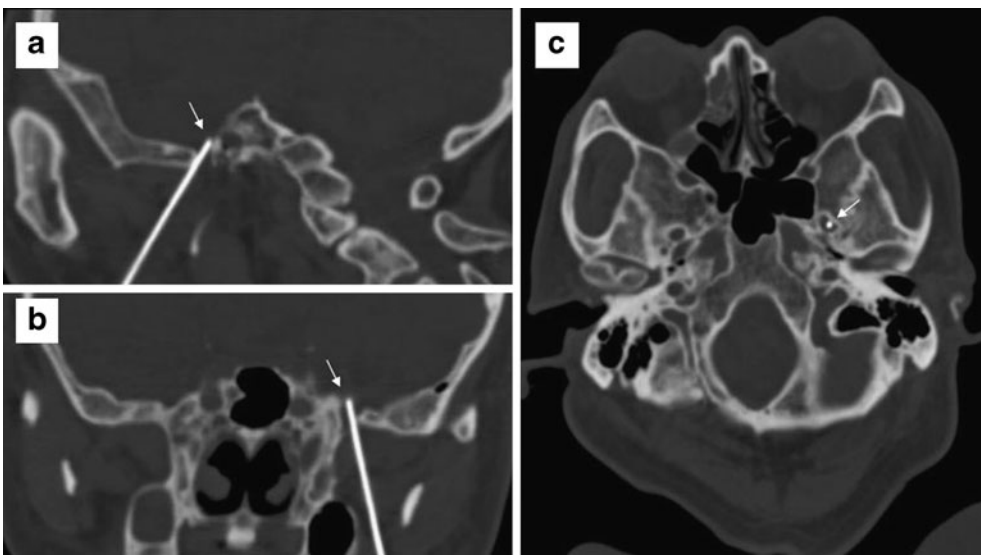

Fig. 3 Computed tomography scan confirming that the needle (*arrow*) is well placed within the foramen ovale in the sagittal (**a**), coronal (**b**), and axial views (**c**)

and 0–1 V until paresthesia in the distribution of the involved trigeminal division is produced or the masticatory response is elicited when appropriate. Further adjustment to the needle is made if required in accordance to the electrophysiologic response. The patient is monitored throughout the procedure by pulse oximetry, continuous electrocardiography, and blood pressure. A prophylactic nasal airway is placed and supplemental oxygen is given via a nasal cannula. Intravenous fentanyl (25–50 μg q 5–10 min) or midazolam (1–2 mg q 5–10 min) is given for analgesia during cannulation and lesioning is performed under propofol sedation (1%, 1–1.5 mg/kg, titrated to effect) at 60-70°C for 60–90 s.

The results are presented as mean (SD). Statistical analysis was carried out using SPSS version 13 (SPSS Inc. Chicago, IL, USA); normality was assessed using the Kolmogorov-Smirnov test; and the independent samples test was used to compare differences in mean procedure time and foramen dimension of both patients in whom cannulation was successful by neuronavigation and those who require further sequential CT guidance. Differences were considered statistically significant when $p<0.05$.

Results

There were 42 consecutive patients in this preliminary study. The patient characteristics are summarized in Table 1. There were 15 (36%) males and 27 (64%) females and the mean age was 60.2 (12.9) years old. The right side was involved in 23 (55%) patients and the left side was involved in 19 (45%) patients. The V_2 and or the V_3 distributions were predominantly affected ($n=33$, 76%). All patients had medically refractory idiopathic trigeminal neuralgia; 29 (69%) were taking a single medication, seven (17%) were taking more medications, and six (14%) were intolerant to medical treatment. A total of 14 (33%) patients had previous surgery or ablative intervention.

The procedure characteristics are summarized in Table 2. The registration head CT scan for neuronavigation was completed using a single scan in 40 (95%) patients and using two scans in two (5%) patients due to inaccuracies from slippage of the reference array. The foramen ovale was successfully punctured under neuronavigation in 31 (74%) patients, with use of one needle pass in 27 (87%) patients and two needle passes in four (13%) patients. Bony hindrances within the foramen ovale precluding optimal needle placement were encountered in five (16%) patients. In addition to the registration scan for neuronavigation, post-insertion, most patients required 1 scan (n=10; 32%) or 2 scans (n=18, 58%) for confirmation of needle placement. In 11 (26%) patients, the foramen ovale could not be cannulated by neuronavigation; on average, 5.2 scans were required for the subsequent correct needle placement under CT -guidance. In all cases, the appropriate sensory or motor responses were elicited by test stimulation before lesioning (mean voltage, 0.17 [0.09] V). The neuronavigation-guided cannulation took 3.1 (0.7) min; the entire procedure took 68.2 (16.4) min; and when required, sequential CT guidance took significantly more time (87.0 [28.5] min; $p<0.011$). The longitudinal and transverse dimensions of the foramen ovale on the exocranial surface in relation to the long axis of the petrous temporal bone were 7.1 (1.5) mm and 4.7 (1.1) mm, respectively. There were no significant differences in the foramen dimensions between patients who could and could not be cannulated by neuronavigation.

Table 1 Patient characteristics

Patient characteristics	$n=42$
Gender (*n*)	
Male	15
Female	27
Age (years)	60.2±12.9 (20–80)
Affected side (*n*)	
Right	23
Left	19
Symptom distribution (n)	
V_2	13
V_3	6
$V_{1,2}$	7
$V_{2,3}$	14
$V_{1,2,3}$	3
Prior intervention (n)	
Nil	28
Surgery	4
Surgery and stereotactic radiosurgery	1
Stereotactic radiosurgery	4
Radiofrequency rhizotomy	5
Current medication (*n*)	
Single	29
Multiple	7
Intolerance	6

Discussion

Percutaneous ablative or compressive techniques have been well accepted for the treatment of idiopathic trigeminal neuralgia. In our series, percutaneous radiofrequency trigeminal rhizotomy was offered to 42 patients as the primary treatment for medically refractory or recurrent idiopathic trigeminal neuralgia. The therapeutic outcome

Table 2 Procedure characteristics

Procedure characteristics			
Registration error (*n*)		2	
Foramen dimensions (mm)		7.1±1.5×4.7±1.1	
Test stimulation voltage (V)		0.17±0.09	
Successful neuronavigation (*n*=31)		Additional sequential CT guidance (*n*=11)	
Scans following needle adjustment (*n*)			
1 Scan 10		~	
2 Scans 18		~	
3 Scans 2		~	
4 Scans 1		~	
Average no. of scans 2.8		5.2	
Foramen dimension (mm)			
Longitudinal	7.2±1.3	6.8±0.7	*p*=0.410
Transverse	4.8±1.9	4.5±1.0	*P*=0.393
No. of passes	1.1	1	
Bony hindrance	5	0	
Cannulation time (min)	3.1±0.7	~	
Total procedure time (min)	68.2±16.4	87.0±28.5	*p*=0.011*

and the avoidance of cannulation-related complications is greatly dependent on the precise placement of the needle with minimal needle passages [33]; although rare, complications such as caroticocavernous fistula; temporary or persistent cranial nerve neuropathy; cerebrospinal fluid fistula; bacterial meningitis; and subdural, subarachnoid and intracerebral hemorrhage have been reported [2, 28, 30]. Image-guided cannulation is crucial in avoiding these complications; based on cadaveric studies, the Gasserian ganglion is approximately 6 mm beyond the endocranial opening of the foramen ovale, and advancement of the needle tip >10 mm risk injury to the internal carotid artery or the abducent nerve and lesioning near the lateral wall of the cavernous sinus can result in cranial nerve injuries [16]. Hence, a penetration depth of no more than 6 mm is ideal. Reliable imaging is also important in circumstances in which general anesthesia with endotracheal intubation is required but where the needle location cannot be confirmed electrophysiologically.

There are several disadvantages with the fluoroscopic guided technique; the foramen ovale and related landmarks can be difficult to identify with the standard projections and needle placement cannot always be confirmed reliably. In addition to being cumbersome to operate, the views are limited to biplanar at the most, and are dependent on the resting position of the patient's head. However, the coaxial fluoroscopic projection recently described by Grunert shows distinct advantages over standard projections as it overcomes the difficulties of obtaining an adequate submental view from a sub-optimally reclined head position due to cervical spine stiffness or large chest volume. The coaxial projection offers an unobstructed view of the foramen ovale from the mandible through which the needle can be advanced directly under real-time imaging. Comparable to that of the probe eye view of neuronavigation but free of the possible inaccuracies from bending of the flexible needle, time and cost associated with neuronavigation, the results of this new technique appeared to be promising [7]. In contrast, CT with integrated neuronavigation offers superior resolution of the skull base osseous structures and becomes particularly useful in cases with abnormal bony anatomy at the level of the foramen ovale. The simultaneous display in real-time multiplanar and 3-D reconstructed images is much more visuo-spatially informative for surgeons regardless of the patient's position. Furthermore, needle placement can be confirmed accurately, and it also has the advantage of sparing the surgeon and ancillary staff unnecessary radiation exposure.

The idea of using neuronavigation or serial CT for the foramen ovale cannulation is not novel, and the feasibility of the neuronavigation-guided procedure has been reported to have remarkable success [5, 13, 23, 33, 34]; however, these reports are limited by their relatively small case numbers, so the reliability of their successes has probably been over-rated. This is the largest study to date to evaluate the reproducibility of the neuronavigation-guided cannulation of the foramen ovale. As rightly stated in previous reports, several factors are inherent to the design of the neuronavigation system and rhizotomy needle, which can be problematic for achieving a successful cannulation, mainly due to slippage of the reference array leading to erroneous registration and distortion of the needle during its passage through the soft tissues [13, 23]. We have found the ENT reference array (Kolibri™ ENT System, Brainlab,

Germany) both simple to apply and reliable, and its use eliminates the disadvantages of the invasive head clamp reference systems and the sophistication and bulkiness of the stereotactic systems. In experienced hands, failure to cannulate the foramen ovale is rarely encountered; however, it cannot be overstated that in our series, although the foramen ovale was eventually cannulated in all patients with two needle passes at most, which compares favorably with the failure rate of up to 15% in historical fluoroscopy-guided series [10], the neuronavigation-guided procedure was successful in only 31 (74%) patients. Possible registration error could have occurred during the cannulation process in the remaining patients who were unable to be cannulated by neuronavigation alone, however, in these patients needle placements were near the foramen ovale to enable free-hand puncture guided by sequential CT. Failed neuronavigation attempts were unrelated to the foramen ovale dimensions and were more likely related to bending of the flexible needle as it was advanced toward the intended target. A more rigid needle has been suggested to prevent this problem; however, a flexible needle better conforms to the geometry of the foramen ovale and is more forgiving with respect to the selected trajectory into the Gasserian ganglion without bony hindrance. No cannulation-related complications occurred in any of the patients in the current study and the appropriate electrophysiological response was elicited through the use of stimulating voltage comparable to that in other studies. The entire procedure can be completed in a timely manner in the BrainSUITE® iCT, the integrated OR solution that allows CT scanning, object planning, and neuronavigation-guided intervention to be performed in the same locale with full OR and anesthesiology personnel support. The unsophisticated preparatory steps that utilizes the basic components of the neuronavigation system can be easily mastered. Information acquired during the first treatment session can be stored for future reference, and registration can be performed with the surface match method should further treatment sessions be required.

Concerns over the amount of radiation exposure during these CT-based procedures have been raised by Koizuka et al., and it appears that such exposure can be limited and offset by the speed at which the foramen ovale can be accurately cannulated, so it may even be less than what conventional fluoroscopy entails [18]. However, how this will compare to our treatment protocol remains to be elucidated. Our future goal is to shift away from the heavy reliance on CT imaging without compromising safety to a greater emphasis on an electrophysiologically based localization protocol to keep patient radiation exposure to a minimum. With regard to clinical efficacy, the long-term outcome of this present series for comparison with our historical data will be the subject of future analysis.

Conclusions

The present study indicated that use of the neuronavigation-guided technique is feasible with sequential CT guidance as a secondary localization modality and that the foramen ovale can be successfully cannulated without complications. The system utilizes neuronavigational components that are available in most modern neurosurgical suites, plus this technology allows the procedure to be performed quickly with the potential to reduce cannulation-related complications and improve the overall patient procedure tolerability.

Acknowledgments We thank Yi-Chen Lee for help in performing this operative technique.

Conflicts of interest None.

References

1. Agazzi S, Chang S, Drucker MD, Youssef AS, Van Loveren HR (2009) Sudden blindness as a complication of percutaneous trigeminal procedures: mechanism analysis and prevention. J Neurosurg 110:638–641
2. Arrese I, Lobato RD, Alén JF, Lagares A, Miranda P (2005) Acute subdural and intratemporal hematoma as a complication of percutaneous compression of the Gasserian ganglion for trigeminal neuralgia. Neurocirugia (Astur) 16:177–182
3. Bale RJ, Laimer I, Martin A, Schlager A, Mayr C, Rieger M, Czermak BV, Kovacs P, Widmann G (2006) Frameless stereotactic cannulation of the foramen ovale for ablative treatment of trigeminal neuralgia. Neurosurgery 59:394–401
4. Brown JA (1997) Direct carotid cavernous fistula after trigeminal balloon microcompression gangliolysis: case report. Neurosurgery 40:886
5. Daszkiewicz P, Zwoliński P, Roszkowski M (2009) Neuronavigation-guided implantation of foramen ovale electrodes in a child. J Neurosurg Pediatr 4:47–49
6. Egan RA, Pless M, Shults WT (2001) Monocular blindness as a complication of trigeminal radiofrequency rhizotomy. Am J Ophthalmol 131:237–240
7. Grunert P, Glaser M, Kockro R, Boor S, Oertel J (2010) An alternative projection for fluoroscopic-guided needle insertion in the foramen ovale: technical note. Acta Neurochir 152:1785–1792
8. Gusmão S, Magaldi M, Arantes A (2003) Trigeminal radiofrequency rhizotomy for the treatment of trigeminal neuralgia: results and technical modification. Arq Neuropsiquiatr 61:434–440
9. Gusmão S, Olivera M, Tazinaffo U, Honey CR (2003) Percutaneous trigeminal nerve radiofrequency rhizotomy guided by computerized tomography fluoroscopy: technical note. J Neurosurg 99:785–786
10. Hakanson S (1981) Trigeminal neuralgia treated by the injection of glycerol into the trigeminal cistern. Neurosurgery 9:638–646
11. Harrigan MR, Chandler WF (1998) Abducens nerve palsy after radiofrequency rhizolysis for trigeminal neuralgia: case report. Neurosurgery 43:623–625
12. Haertel F (1912) Die Leitungsanästhesie und Injektionsbehandlung des Ganglion Gasseri und der Trigeminusstaemme. Arch Klin Chir 100:193–292, Ger

13. Ivanov M, Brodbelt A, Ianovici N, Ciurea AV, Poeata I, Gramada FM (2010) Neuronavigation in the percutaneous treatment of trigeminal neuralgia. Technical note. Rom Neurosurg 27:166–170
14. James EA, Kibbler CC, Gillespie SH (1995) Meningitis due to oral streptococci following percutaneous glycerol rhizotomy of the trigeminal ganglion. J Infect 31:55–57
15. Kanpolat Y, Savas A, Bekar A, Berk C (2001) Percutaneous controlled radiofrequency trigeminal rhizotomy for the treatment of idiopathic trigeminal neuralgia: 25-year experience with 1,600 patients. Neurosurgery 48:524–532
16. Kaplan M, Erol FS, Ozveren MF, Topsakal C, Sam B, Tekdemir I (2007) Review of complications due to foramen ovale puncture. J Clin Neurosci 14:563–568
17. Koizuka S, Saito S, Kubo K, Tomioka A, Takazawa T, Sakurazawa S, Goto F (2006) Percutaneous radio-frequency mandibular nerve rhizotomy guided by CT fluoroscopy. AJNR Am J Neuroradiol 27:1647–1648
18. Koizuka S, Saito S, Sekimoto K, Tobe M, Obata H, Koyama Y (2009) Percutaneous radio-frequency thermocoagulation of the Gasserian ganglion guided by high-speed real-time CT fluoroscopy. Neuroradiology 51:563–566
19. Koizuka S, Saito S, Tobe M, Sekimoto K, Obata H, Koyama Y (2010) Technical communication: percutaneous radiofrequency mandibular nerve rhizotomy guided by high-speed real-time computed tomography fluoroscopy. Anesth Analg 111:763–767
20. Kuether TA, O'Neill OR, Nesbit GM, Barnwell SL (1996) Direct carotid cavernous fistula after trigeminal balloon microcompression gangliolysis: case report. Neurosurgery 39:853–855
21. Langford P, Holt ME, Danks RA (2005) Cavernous sinus fistula following percutaneous balloon compression of the trigeminal ganglion. Case report. J Neurosurg 103:176–178
22. Liu M, Wu CY, Liu YG, Wang HW, Meng FG (2005) Three-dimensional computed tomography-guided radiofrequency trigeminal rhizotomy for treatment of idiopathic trigeminal neuralgia. Chin Med Sci J 20:206–209
23. Mandat T, Brozyna B, Krzymanski G, Podgorski JK (2009) An image-guided, noninvasive method of cannulation of the foramen ovale for awake, percutaneous radiofrequency rhizotomy. J Neurosurg 111:1223–1225
24. Moraci A, Buonaiuto C, Punzo A, Parlato C, Amalfi R (1992) Trigeminal neuralgia treated by percutaneous thermocoagulation. Comparative analysis of percutaneous thermocoagulation and other surgical procedures. Neurochirurgia (Stuttg) 35:48–53
25. Pagni CA, Fariselli L, Zeme S (2008) Trigeminal neuralgia. Non-invasive techniques versus microvascular decompression. It is really available any further improvement? Acta Neurochir Suppl 101:27–33
26. Patil AA (2010) Stereotactic approach to the trigeminal ganglion using a stereotactic frame and intraoperative computed tomography scans: technical note. Stereotact Funct Neurosurg 88:277–280
27. Rath GP, Dash HH, Bithal PK, Goyal V (2009) Intracranial hemorrhage after percutaneous radiofrequency trigeminal rhizotomy. Pain Pract 9:82–84
28. Savas A, Sayin M (2010) Subarachnoid bleeding into the superior cerebellopontine cistern after radiofrequency trigeminal rhizotomy: case report. Acta Neurochir 152:561–562
29. Taha J (2004) Trigeminal neuralgia: percutaneous procedures. Semin Neurosurg 15:115–134
30. Tatli M, Satici O, Kanpolat Y, Sindou M (2008) Various surgical modalities for trigeminal neuralgia: literature study of respective long-term outcomes. Acta Neurochir 150:243–255
31. Torroba L, Moreno S, Lorenzana L, Buzon L (1987) Purulent meningitis after percutaneous radiofrequency trigeminal rhizotomy. J Neurol Neurosurg Psychiatry 50:1081–1082
32. Ugur HC, Savas A, Elhan A, Kanpolat Y (2004) Unanticipated complication of percutaneous radiofrequency trigeminal rhizotomy: rhinorrhea: report of three cases and a cadaver study. Neurosurgery 54:1522–1524
33. Xu SJ, Zhang WH, Chen T, Wu CY, Zhou MD (2006) Neuronavigator-guided percutaneous radiofrequency thermocoagulation in the treatment of intractable trigeminal neuralgia. Chin Med J (Engl) 119:1528–1535
34. Yang Y, Shao Y, Wang H, Liu Y, Zhu S, Wu C (2007) Neuronavigation-assisted percutaneous radiofrequency thermocoagulation therapy in trigeminal neuralgia. Clin J Pain 23:159–164

Acta Neurochir (2011) 153:1601–1609
DOI 10.1007/s00701-011-1026-1

CLINICAL ARTICLE

Computed tomography-guided gamma knife stereotactic radiosurgery for trigeminal neuralgia

Kyung-Jae Park · Hideuki Kano · Oren Berkowitz · Nasir R. Awan · John C. Flickinger · L. Dade Lunsford · Douglas Kondziolka

Received: 14 March 2011 / Accepted: 6 April 2011 / Published online: 3 May 2011

Abstract
Background Gamma knife stereotactic radiosurgery (GKSR) is an effective minimally invasive option for the treatment of medically refractory trigeminal neuralgia (TN). Optimal targeting of the retrogasserian trigeminal nerve target requires thin-slice, high-definition stereotactic magnetic resonance imaging (MRI). The purpose of this study was to evaluate management outcomes in TN patients ineligible for MRI and who instead underwent GKSR using computed tomography (CT).
Methods The authors reviewed their experience with CT-guided GKSR in 21 patients (median age: 75 years) with idiopathic TN. Contraindications to MRI included implanted pacemakers (n=16), aneurysm clips (n=2), cochlea implants (n=1), metallic vascular stents (n=1) or severe obesity (weight of 163 kg, n=1). Contrast-enhanced CT at 1- or 1.25-mm intervals was acquired in all patients. One patient also underwent CT cisternography. The median target dose for GKSR was 80 Gy. The median follow-up was 35 months after GKSR. Treatment outcomes were compared to 459 patients who underwent MRI-guided GKSR for TN at our institute in the same time interval.
Results Targeting of the trigeminal nerve guided by CT scan was feasible in all patients. Stereotactic frame titanium pin-related artifacts that interfered with full visualization of the trigeminal nerve were found in one patient who had the ipsilateral posterior pin placed near the inion. After GKSR, 90% of patients achieved initial pain relief that was adequate or better, with or without medication (Barrow Neurological Institute pain scores I-IIIb). Median time to pain relief was 2.6 weeks. Pain relief was maintained in 81% at 1 year, 66% at 2 years, and 46% at 5 years. Eight (42%) of 19 patients who achieved initial pain relief reported some recurrent pain at a median of 18 months after GKSR. Some degree of facial sensory dysfunction occurred in 19% of patients within 24 months of GKSR. These results are comparable to those of patients who had MRI-guided GKSR.
Conclusions CT-guided GKSR provides a similar rate of pain relief as MRI-guided radiosurgery. The posterior pins should be placed at least 1 cm away from the inion to reduce pin and frame-related artifacts on the targeting CT scan. This study indicates that GKSR using CT targeting is appropriate for patients with medically refractory TN who are unsuitable for MRI.

Keywords Computed tomography · Gamma knife · Radiosurgery · Trigeminal neuralgia

K.-J. Park · H. Kano · O. Berkowitz · N. R. Awan · J. C. Flickinger · L. D. Lunsford · D. Kondziolka (✉)
Departments of Neurological Surgery, University of Pittsburgh, Center for Image-Guided Neurosurgery, Suite B-400, UPMC Presbyterian, 200 Lothrop Street, Pittsburgh, PA 15213, USA
e-mail: kondziolkads@upmc.edu

J. C. Flickinger
Departments of Radiation Oncology, University of Pittsburgh, Center for Image-Guided Neurosurgery, Suite B-400, UPMC Presbyterian, 200 Lothrop Street, Pittsburgh, PA 15213, USA

K.-J. Park
Department of Neurosurgery, College of Medicine, Korea University, Seoul, Korea

Introduction

Gamma knife stereotactic radiosurgery (GKSR) is a minimally invasive option for refractory trigeminal neural-

gia (TN). It has been used as an alternative or addition to microvascular decompression (MVD) and percutaneous rhizotomy. Typically frame-based stereotactic radiosurgery is based on magnetic resonance imaging (MRI) guidance because of the higher contrast resolution of intracranial structures using MRI. However, not all patients can undergo MRI due to contraindications such as implanted pacemakers, aneurysm clips, or claustrophobia.

Computed tomography (CT) provides spatially accurate images under stereotactic conditions, but anatomic structure resolution is inferior to that achieved using MRI [2, 11, 12, 20]. This report discusses our experience in the use of CT-guided GKSR for TN in patients ineligible for MRI. In addition, we compare the outcomes in this subset of TN patients to the outcomes achieved when using MRI-guided radiosurgery.

Methods

Patient population

Between July 1996 and May 2010, 854 GKSR procedures were performed in 705 patients with medically refractory TN at the University of Pittsburgh Medical Center. Twenty-two patients underwent GKSR using intraoperative CT imaging instead of MRI. The contraindications to MRI included: presence of a pacemaker (n=17), ferrous metallic foreign bodies (including MRI non-compatible aneurysm clips (n=2), cochlea implants (n=1), endovascular stents (n=1) and severe obesity (weight of 163 kg, n=1). One patient was lost to follow-up after GKSR. The remaining 21 patients were included in this Institutional Review Board–approved study. All patients had recurrent pain resistant to medical management with typical agents such as carbamazepine, phenytoin, baclofen, or gabapentin.

The clinical information for these 21 patients is shown in Table 1. There were 11 male and ten female patients. The median patient age at GKSR was 75 years (range, 53–93 years). The median symptom duration was 72 months (range, 2–300 months). At GKSR, the pain was predominantly distributed in the V2 and V3 distributions of trigeminal nerve (33%), followed by V3 (29%), V2 alone (19%), V1 plus V2 (14%), and all trigeminal distributions (5%). Five patients (24%) had undergone various surgical procedures prior to their GKSR. These procedures included percutaneous retrogasserian glycerol rhizotomy in three patients, percutaneous balloon microcompression in one patient, and percutaneous glycerol rhizotomy plus radiofrequency lesioning in one patient. Three patients had undergone multiple surgical procedures. All patients had typical tic douloureux (Type I TN), and two patients (10%) reported sensory disturbances (paresthesias) preoperatively. No patient had tumor or multiple sclerosis-related TN.

Radiosurgical procedure

Various models of the gamma knife (models U, B, C, 4 C, and Perfexion, Elekta Instruments) were used during this 17-year study. After application of the Leksell Model G stereotactic frame (Elekta Instruments) under local anesthesia, all patients underwent stereotactic contrast-enhanced CT imaging to identify the trigeminal nerve. At the time of frame application, we attempted to place the posterior titanium or steel-tipped aluminum frame fixation pin 5–43 mm below or above the inion to minimize artifact. A wide field of view (FOV 25) was used in order to visualize the stereotactic fiducials needed for target definition. Thin slice thickness (1 or 1.25 mm) was selected to image the entire posterior fossa and brainstem.

One patient had improved identification of the trigeminal nerve within the cisternal space after lumbar intrathecal administration of 6 cc of non-ionic iodinated contrast media into the cerebrospinal fluid. The patient was then placed on a tilt table to allow for cephalad migration of the intrathecal contrast. Each patient's treatment plan was generated using Leksell Gamma Plan (Elekta, Inc, Norcross, Georgia). A single 4-mm isocenter was used in all patients, and the target was 3–8 mm anterior to the junction of the trigeminal nerve and pons. The isocenter was usually located so that the brainstem surface was irradiated at the 20% isodose line or less. The maximum target doses varied from 75 to 85 Gy (median: 80 Gy).

Follow-up and evaluation of treatment outcome

Serial follow-up information was obtained via direct contact with the patient or their family. We evaluated the degree of pain relief, latency interval until pain relief, need for further surgical procedures, continued requirement for medication, and development of new symptoms or signs. The median follow-up period was 35 months (range, 3–138 months) after the radiosurgical procedure. The pain outcome was evaluated using the Barrow Neurological Institute (BNI) pain intensity scoring criteria as follows: grade I, no pain, no medication; grade II, occasional pain, not requiring medication; grade IIIa, no pain, but continued medication; grade IIIb, pain present, but adequately controlled with medication; grade IV, pain present, but not adequately controlled with medication; and grade V, severe pain despite medication [19]. We considered BNI pain scores I to IIIb as successful treatment (adequate pain relief), representing pain improvement without requirement for further surgical management. Treatment failure was defined as BNI pain scores IV and V. We also sought information about the patient's corneal sensation and whether there was any difficulty with mastication. We used the same criteria in our comparative evaluation of outcomes after MRI-guided GKSR.

Table 1 Clinical information on 21 patients included in the present study

Case no.	Age/ gender	Duration of symptoms (years)	Pain side	Pain distribution	Prior surgical management	Preexisting facial sensory change	Cause of CT	Cisternography	Maximum GKSR dose (Gy)
1	89/F	5	Right	V3	None	No	Pacemaker	No	80
2	77/M	4.5	Right	V2	None	No	Pacemaker	No	80
3	88/M	5	Right	V2 + V3	None	No	Pacemaker	No	80
4	68/F	10	Right	V3	None	No	Pacemaker	No	85
5	75/M	10	Left	V2 + 3	PRGR	No	Cochlea implant	No	80
6	73/F	6	Right	V2	None	No	Pacemaker	No	80
7	85/F	15	Right	V1 + V2 + V3	None	No	Pacemaker	No	80
8	79/F	6	Right	V1 + V2	None	No	Pacemaker	No	80
9	75/M	25	Left	V2 + V3	None	No	Vascular stent (aorta)	No	85
10	62/M	12	Left	V2 + V3	None	No	Aneurysm clip	No	80
11	93/M	25	Right	V3	PRGR + PRFL	Paresthesia	Pacemaker	No	80
12	90/F	6	Left	V2 + V3	PRGR	Paresthesia	Pacemaker	No	75
13	53/M	2	Right	V2	PRGR	No	Pacemaker	No	85
14	75/M	20	Right	V1 + V2	None	No	Pacemaker	No	80
15	68/M	10	Left	V1 + 2	None	No	Overweight	No	80
16	80/F	0.2	Left	V3	None	No	Pacemaker	No	80
17	88/F	1.5	Left	V2+V3	None	No	Pacemaker	No	80
18	74/M	5	Left	V3	None	No	Aneurysm clip	Yes	85
19	55/M	5	Right	V2	None	No	Pacemaker	No	80
20	55/F	25	Left	V2 + V3	PBM	No	Pacemaker	No	80
21	75/F	5	Left	V3	None	No	Pacemaker	No	80

CT computed tomography; *GKSR* gamma knife stereotactic radiosurgery; *PBM* percutaneous balloon microcompression; *PRFL* percutaneous radiofrequency lesioning; *PRGR* percutaneous retrogasserian glycerol rhizotomy

Statistical analysis

The rates of pain improvement were calculated and the maintenance rate of pain improvement for patients showing initial response was evaluated using the Kaplan–Meier method. We examined the relationship between outcomes and various factors (including age, gender, presence of previous surgical procedures, pain distribution, new development or worsening of preexisting sensory abnormality, and maximum target dose) by univariate analyses. The outcomes of CT-guided GKSR were also compared to those of MRI-guided GKSR using a log-rank test, Fisher's exact test, and Mann–Whitney *U* test. All statistical analysis was performed using SPSS 17 software (SPSS, version 17.0; SPSS, Inc., Chicago, IL, USA), and $p < 0.05$ was considered to be statistically significant.

Results

CT-guided radiosurgical targeting of the trigeminal nerve was feasible in all patients. The outcomes of this experience are outlined in Fig. 1. The responses to GKSR of individual patients are shown in Table 2.

Trigeminal nerve identification

Twenty patients underwent intravenous contrast-enhanced CT scans (without cisternography); eight patients (40%) had excellent visualization of their affected trigeminal nerves for the entire length of the cisternal nerve segment. For these patients, the target was 3–8 mm anterior from the junction of the trigeminal nerve and pons (Fig. 2a). In 12 patients (60%), CT imaging could not clearly define the entire cisternal segment of the nerve, but we could identify the distal cisternal component of the nerve as it entered into Meckel's cave. The target of these patients was directed to 2-3 mm posterior from the entry into Meckel's cave (Fig. 2b). One patient with an MRI non-compatible right middle cerebral artery bifurcation aneurysm clip had significant metallic artifacts extending to the trigeminal nerve identified on their preradiosurgery CT scan. This patient underwent CT cisternography to define the trigeminal nerve (Fig. 2c).

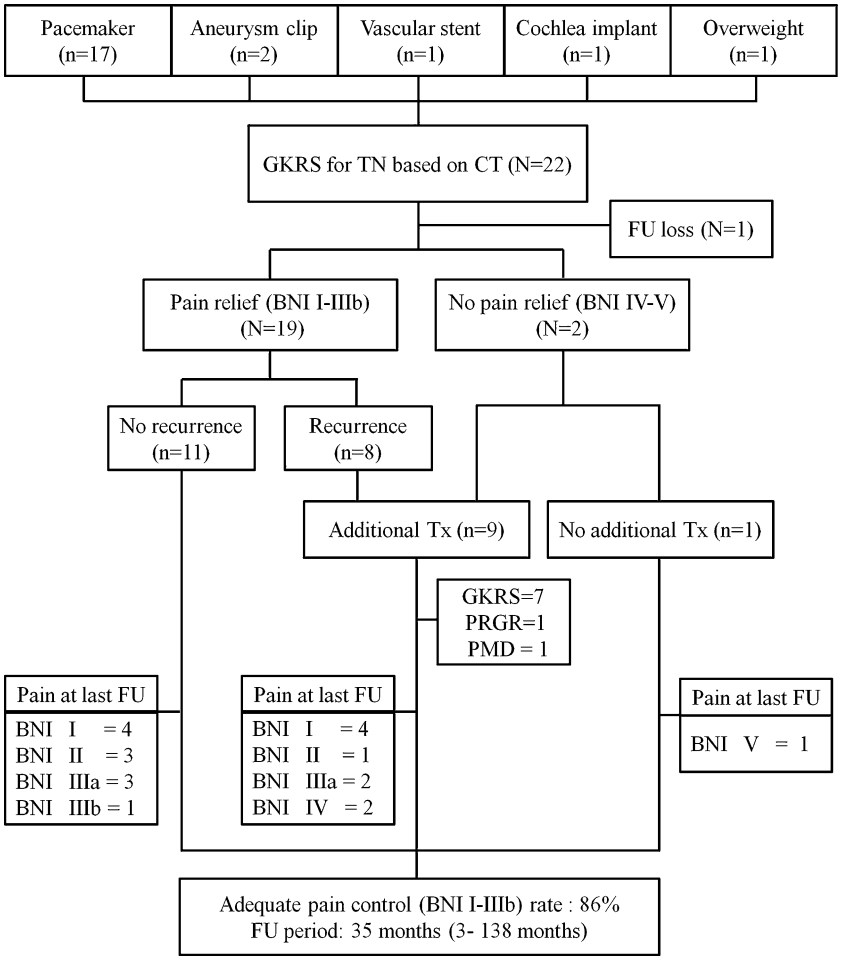

Fig. 1 Schematic drawing of patient population and brief outcomes of computed tomography-based gamma knife stereotactic radiosurgery for trigeminal neuralgia. *BNI* Barrow Neurological Institute; *CT* computed tomography; *FU* follow-up; *GKSR* gamma knife stereotactic radiosurgery; *PBM* percutaneous balloon microcompression; *PRFL* percutaneous radiofrequency lesioning; *PRGR* percutaneous retrogasserian glycerol rhizotomy; *TN* trigeminal neuralgia; *Tx* treatment

Pin-related artifacts that interfered with full visualization of the trigeminal nerve were noted in one patient who had their posterior stereotactic frame pin inadvertently located too close to the inion (Fig. 3). The inion is a palpable skull landmark that we use to identify the general level of axial plane location of the trigeminal nerve. Fortunately, the trigeminal nerve in this patient was detected at the distal part of the cisternal segment, which we found sufficient to complete stereotactic targeting. When the posterior pin was placed within some distance of the inion (range: 14–43 mm), frame and pin-related artifacts did not affect target recognition (Table 2).

Initial pain response to GKSR

Nineteen (90%) patients had improvement in their pain level (BNI score I-IIIb) after GKSR. Ten patients (48%) achieved complete initial pain relief (BNI score I). Two patients (10%) had insufficient pain relief after the procedure. The median interval time until pain improvement was 2.6 weeks after radiosurgery (range: 1 day–8 months). Eighteen patients (86%) experienced pain improvement within 3 months.

Maintenance of pain relief after radiosurgery

Although 19 patients had initial successful pain management, eight patients (42%) eventually experienced pain recurrence. The median time to recurrence was 18 months (range: 4–84 months). The duration of pain relief after the initial response was evaluated using the Kaplan–Meier method. The probability of maintaining pain relief (BNI pain scores I–IIIb) was 81% at 1 year, 66% at 2 years, 57% at 3 years, and 46% at 5 years (Fig. 4).

The variables of age, gender, symptom duration, presence of prior surgical treatment, pain distribution, target dose, post-radiosurgery sensory change, and degree of trigeminal nerve visualization were not associated with pain recurrence after GKSR.

Sensory dysfunction after radiosurgery

No patient sustained a perioperative complication after GKSR. During the follow-up interval, four patients (19%) developed new or increased trigeminal sensory dysfunction between 2 and 24 months after GKSR. All of these patients

Table 2 Outcomes of 21 patients who underwent gamma knife radiosurgery based on computed tomography

Case no.	Visibility of trigeminal nerve on CT	Pin-related artifact	Vertical distance between posterior pin and inion	Initial pain outcome after GKSR*	Facial sensory change after GKSR	Interval between GKRS and pain recurrence (months)	Additional treatment for poor response or recurrent pain	Interval between initial GKSR and additional Treatment (months)	Final pain score*	Follow-up (months)
1	Partial	No	42 mm	BNI I	Yes	No recurrence	No	NA	BNI I	6.7
2	Partial	No	19 mm	BNI IIIa	No	6.0	Repeat GKSR	14.7	BNI I	28.6
3	Definite	No	20 mm	BNI IIIa	No	No recurrence	No	NA	BNI IIIa	33.6
4	Partial	No	25 mm	BNI I	Yes	No recurrence	No	NA	BNI II	90.2
5	Definite	No	31 mm	BNI II	No	No recurrence	No	NA	BNI II	6.6
6	Partial	No	19 mm	BNI II	No	No recurrence	No	NA	BNI II	92.0
7	Partial	No	43 mm	BNI I	Yes	No recurrence	No	NA	BNI I	24.9
8	Partial	No	20 mm	BNI I	Yes	13.5	Repeat GKSR	15.5	BNI IIIa	21.3
9	Partial	No	21 mm	BNI I	No	No recurrence	No	NA	BNI IIIa	14.1
10	Partial	Yes	5 mm	BNI I	No	4.0	Repeat GKSR	8.4	BNI I	35.3
11	Definite	No	15 mm	BNI II	No	No recurrence	No	NA	BNI IIIa	7.1
12	Partial	No	21 mm	BNI IIIa	No	42.0	Repeat GKSR	53.5	BNI IV	99.3
13	Definite	No	20 mm	BNI I	No	84.0	Repeat GKSR	90	BNI IIIa	138.0
14	Definite	No	17 mm	BNI IV	No	No pain relief	PRGR + PBM	13 (PRGR), 24 (PBM)	BNI IV	48.5
15	Partial	No	19 mm	BNI V	No	No pain relief	No	NA	BNI V	6.5
16	Definite	No	14 mm	BNI IIIa	No	36.0	Repeat GKSR	40.0	BNI I	56.9
17	Partial	No	23 mm	BNI I	No	No recurrence	No	NA	BNI I	39.2
18	Definite	No	16 mm	BNI I	No	24.0	Repeat GKSR	28.1	BNI II	86.0
19	Definite	No	32 mm	BNI I	No	No recurrence	No	NA	BNI I	89.1
20	Partial	No	14 mm	BNI IIIa	No	8.0	PRGR	9.0	BNI I	65.0
21	Definite	No	21 mm	BNI IIIb	No	No recurrence	No	NA	BNI IIIb	3.0

BNI Barrow Neurological Institute, *CT* computed tomography, *GKSR* gamma knife stereotactic radiosurgery, *NA* not available, *PBM* percutaneous balloon microcompression, *PRGR* percutaneous retrogasserian glycerol rhizotomy, *TN* trigeminal neuralgia

*Pain outcome was scored using BNI pain intensity scoring criteria as follows: grade I, no pain, no medication; grade II, occasional pain, not requiring medication; grade IIIa, no pain, but continued medication; grade IIIb, pain present, but adequately controlled with medication; grade IV, pain present, but not adequately controlled with medication; and grade V, severe pain despite medication

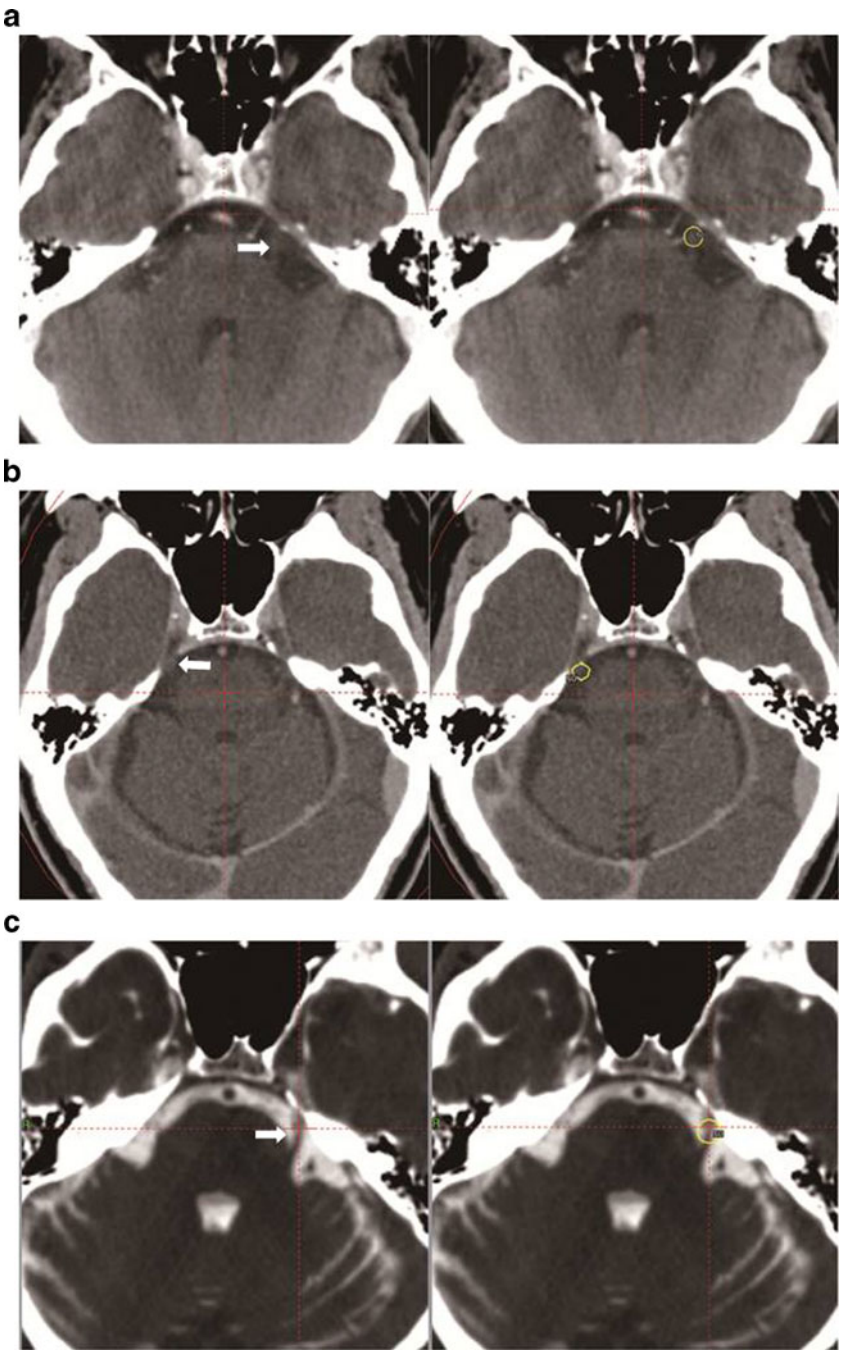

Fig. 2 Computed tomography (CT) obtained at the radiosurgical procedure. On the *right* is the dose planning image, and the *yellow circle* indicates the 50% of isodose line. **a** The cisternal segment of left trigeminal nerve (*arrow*) is well visualized (case 5). **b** The right trigeminal nerve (*arrow*) is seen partially at the entry of Meckel's cave (case 8). **c** The left trigeminal nerve (*arrow*) on CT cisternography is clearly identified (case 18)

found this sensory dysfunction to be not bothersome. Sensory dysfunction was transient in one (5%) patient and persisted in three (14%) patients. No patient developed corneal sensory loss, a trigeminal motor deficit, or other cranial nerve deficits after GKSR.

Comparison to the outcomes of GKSR guided by MRI

Recently, we reported a series of 503 patients who underwent GKSR for idiopathic TN [10]. From this database, we identified the 459 patients with classical TN (type I TN) who were treated with GKSR based on MRI. We then compared the outcomes of the CT based GKSR (group I) to those of the MRI based GKSR (group II). The baseline characteristics and outcomes of these two groups are summarized in Table 3. There were no significant differences between the two groups in the rates of initial pain relief (BNI pain score I: p=0.655, BNI pain scores I–IIIb; p=0.992), recurrence of facial pain (p=0.922) and postoperative sensory changes (p=0.303), time to initial pain relief (p=0.533) and pain recurrence (p=0.718). The probability of maintaining pain relief (BNI pain scores I–

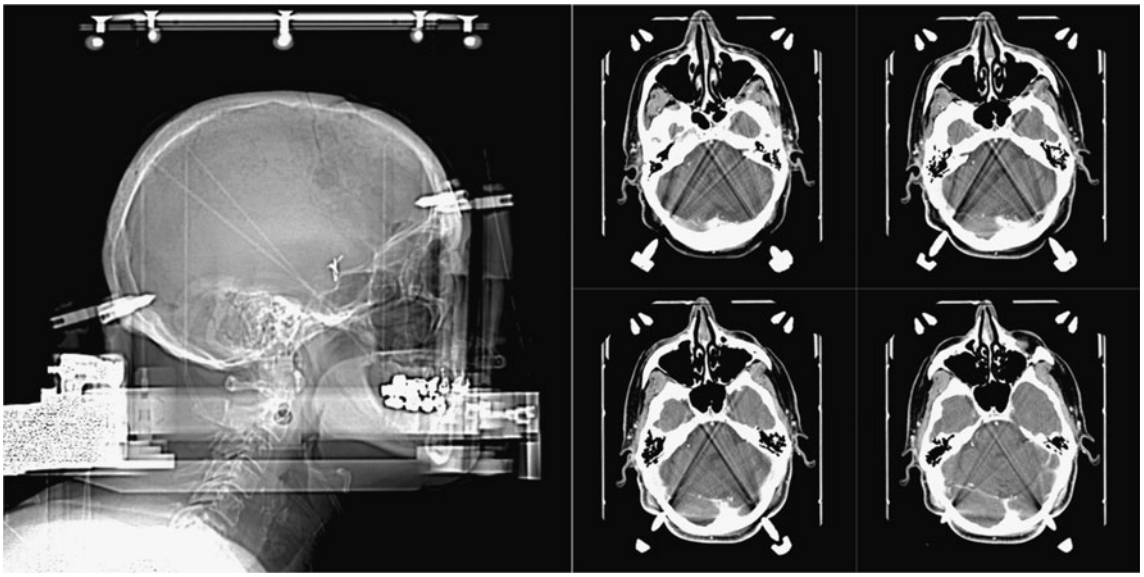

Fig. 3 Computed tomography demonstrating the pin-related artifact (case 10). Posterior pin was located too close to the inion (**a**), which caused artifact in the region of the trigeminal nerve (**b**)

IIIb) in MRI based GKSR was 81% at 1 year, 75% at 2 years, 60% at 3 years, and 46% at 5 years. These results were comparable to CT-based GKSR (p=0.987).

Additional Management after GKSR

Ten patients had either insufficient initial pain control (BNI IV-V) (n=2) or recurrent pain (BNI IV-V) after initial relief (n=8). Nine of these ten patients underwent an additional surgical procedure at a median of 16 months (range: 4–90 months) after initial GKSR. Seven (33%) had a repeat GKSR, one (5%) had a glycerol rhizotomy, and one (5%) had both a glycerol rhizotomy and balloon microcompression. One patient did not undergo any further surgery at the time of final follow-up. At the last follow-up (including additional surgical treatment), 18 patients (86%) had satisfactory pain control (BNI pain score I-IIIb). Eight patients (38%) achieved BNI pain score I, four patients (19%) score II, five patients (24%) score IIIa, one patient (5%) score IIIb. Three patients (14%) continued to have uncontrolled or severe pain (BNI pain score IV-V) (Fig. 1).

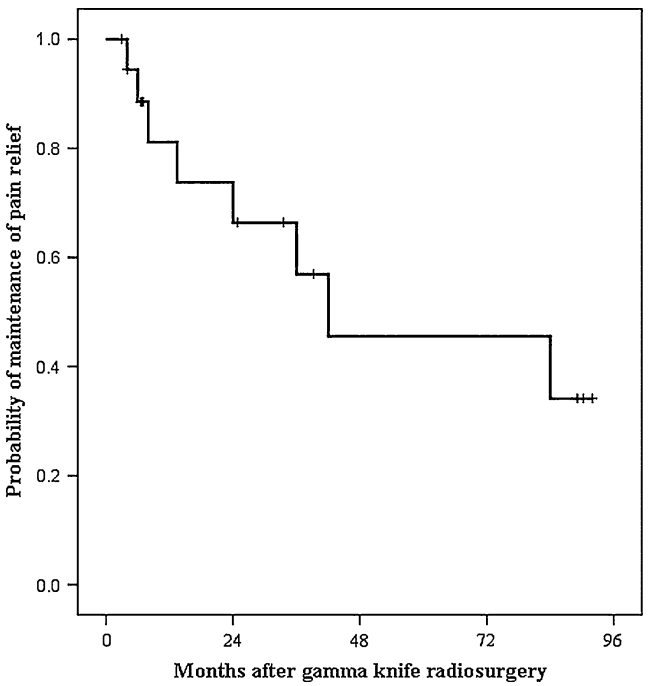

Fig. 4 Kaplan–Meier estimate of maintaining pain relief (Barrow Neurological Institute pain score I-IIIb) after computed tomography-based gamma knife stereotactic radiosurgery for 21 patients

Discussion

Microvascular decompression of the trigeminal nerve is considered by many as an often definitive surgical intervention for medically refractory TN, providing up to 90% of patients with early postoperative pain relief. At ten or more years after the procedure, 68% maintained persistent pain relief [3]. Because TN commonly affects people with advanced age and/or significant comorbid medical conditions, many are not suitable candidates for a major posterior fossa surgical procedure under general anesthesia [13]. In such patients, other less-invasive options are necessary.

Gamma knife surgery for TN is a minimally invasive and effective alternative surgical procedure, especially for patients who are either higher risk or failures of prior MVD. With the evolution of imaging technology that allowed the trigeminal system to be visualized more clearly during the 1990s, the early experience with GKSR for TN achieved

Table 3 Comparisons of outcomes in a group of patients who were treated with gamma knife radiosurgery for idiopathic trigeminal neuralgia (type I) based on computed tomography or magnetic resonance image

	CT-based GKSR group (n=21)	MRI-based GKSR group (n=459)	p value
Characteristics			
Age (median, ranges)	75 years (53–93)	72 years (26–95)	0.068
Gender (male vs. female)	52%/48%	40%/60%	0.264
Symptom duration (median, range)	6 years (0–25)	7.3 years (0–44)	0.679
Pain distribution (single vs. multiple)	48%/52%	29%/71%	0.088
Maximum dose (median, ranges)	80 Gy (75–85)	80 Gy (60–90)	0.197
Presence of prior operation	24%	44%	0.074
Follow-up period (median, ranges)	35 months (3–138)	24 months (3–156)	0.247
Outcomes after GKSR			
Initial pain relief*			
Complete relief (BNI score I)	10 (48%)	192 (42%)	0.655
Adequate relief (BNI score I-IIIb)	19 (90%)	415 (90%)	0.992
Time to pain relief (median, range)	2.6 weeks (1 day–8 months)	3 weeks (1 day–12 months)	0.533
Recurrence of pain	8 (42%)	179 (43%)	0.922
Time to recurrence (median, range)	18 months (4–84)	21 months (3–123)	0.718
Probability of maintaining pain relief			
1 years	81%	81%	0.987
2 years	66%	75%	
3 years	57%	60%	
5 years	46%	46%	
Postoperative sensory change	4 (19%)	56 (12%)	0.303

BNI Barrow Neurological Institute; *CT* computed tomography; *GKSR* gamma knife stereotactic radiosurgery, *MRI* magnetic resonance image. *Pain outcome was scored using BNI pain intensity scoring criteria as follows: grade I, no pain, no medication; grade II, occasional pain, not requiring medication; grade IIIa, no pain, but continued medication; grade IIIb, pain present, but adequately controlled with medication; grade IV, pain present, but not adequately controlled with medication; and grade V, severe pain despite medication

promising clinical results, with high rates of pain relief and a low risk of complications [8, 9, 16, 17]. Since then, the number of patients with TN who undergo radiosurgery has increased dramatically.

The routine technique of GKSR for TN requires the placement of a single 4-mm isocenter targeted at the retrogasserian trigeminal nerve. Because this structure is generally well visualized by MRI, intraoperative frame-based MRI rapidly became the preferred method to perform GKSR. Stereotactic CT is an alternative high-resolution axial plane imaging technique that must be used in patients with a pacemaker, an internal defibrillator, or ferrous metallic foreign bodies. In addition, it may be preferred in some patients who are severely claustrophobic or morbidly obese. The use of CT-guided target localization for stereotactic neurosurgery is a well-accepted technique that is supported by studies which confirm clinical and anatomic accuracy [2, 11, 12, 20]. Currently, CT or CT cisternography (often fused with a preoperative MRI) has been utilized when non-frame-based linear accelerator technologies are used to perform radiosurgery [1, 4, 6, 21]. Frame-based GKSR requires clear definition of the target using CT despite potential artifacts from the frame or the skull fixation pins. Poor placement of the pins, or preexisting metallic artifacts in the patient, can obscure the anatomic detail necessary for visualization of the nerve. In selected cases, nerve visualization can be achieved by CT cisternography. This method, requiring intrathecal injection of iodinated contrast medium that results in the nerve appearing as a negative filling defect within the cistern, was introduced by Worthington et al. in 2000 [22].

In the present series, we could identify the whole length of the cisternal segment of trigeminal nerve in 40% of the patients. In 60% of the patients, we could identify the distal end of the retrogasserian nerve as it entered Meckel's cave. Once we were confident that the simple CT-based targeting was feasible based on our initial experience, the use of CT cisternography for this purpose was abandoned except for a single patient with an aneurysm clip that affected the visualization of the trigeminal nerve on a prior CT scan. A pin-related artifact disturbing good visualization of trigeminal nerve was noted in a single patient who had a posterior pin inserted too close to the inion, a reliable external landmark that allows us to obtain low artifact imaging when the skull pin is placed well above or below this axial plane level. The posterior pin should be placed at least 1 cm

below or above the inion to reduce pin related artifacts at the level of the trigeminal nerve.

After GKSR, we found that 90% of the patients had an improvement in their pain level (BNI pain score I-IIIb); 48% of patients achieved a BNI pain score I. The majority of patients (86%) had pain relief within 3 months (median: 2.6 weeks, range 1 day–8 months). During the median follow-up of 35 months, 42% of patients experienced some level of pain recurrence, and 19% developed new or increased trigeminal sensory loss between 2 and 24 months after GKSR. Eighty one percent of patients who achieved initial pain relief maintained pain control (BNI pain score I – IIIb) at 1 year, 57% at 3 years, and 46% at 5 years. These results are comparable to the results that we confirmed for 459 patients who underwent MRI-guided GKSR at our center (Table 3).

Outcome results of TN radiosurgery are quite dependent upon pre-treatment factors such as the patient age, pain characteristics (typical vs. atypical), comorbid conditions (TN associated with tumor or multiple sclerosis), radiation dose, the number of failed prior operations, and potentially the radiosurgical target location (i.e., closer to the brainstem vs. closer to Meckel's cave) [5, 7, 10, 14, 15, 18]. Although our experience with CT-based GKSR is much smaller than our experience with MRI-based TN management, we found no significant differences in initial response or delayed recurrence rates.

Conclusions

CT-based stereotactic frame-based targeting for TN provides sufficient anatomic resolution to visualize and target the trigeminal nerve when MRI is not feasible. The posterior pins should be placed at least 1 cm away from inion to reduce pin-related CT artifacts. The treatment outcomes in those patients who underwent CT-guided GKSR for TN were comparable to those of the patients who were treated by MRI-guided GKSR.

Conflicts of interest Drs. Lunsford and Kondziolka are consultants with Elekta Instruments, Inc. Dr. Lunsford is a stockholder in AB Elekta.

References

1. Adler JR Jr, Bower R, Gupta G, Lim M, Efron A, Gibbs IC, Chang SD, Soltys SG (2009) Nonisocentric radiosurgical rhizotomy for trigeminal neuralgia. Neurosurgery 64:A84–90
2. Asakura T, Uetsuhara K, Kanemaru R, Hirahara K (1985) An applicability study on a CT-guided stereotactic technique for functional neurosurgery. Appl Neurophysiol 48:73–76
3. Barker FG 2nd, Jannetta PJ, Bissonette DJ, Larkins MV, Jho HD (1996) The long-term outcome of microvascular decompression for trigeminal neuralgia. N Engl J Med 334:1077–1083
4. Borchers JD 3rd, Yang HJ, Sakamoto GT, Howes GA, Gupta G, Chang SD, Adler JR Jr (2009) Cyberknife stereotactic radiosurgical rhizotomy for trigeminal neuralgia: anatomic and morphological considerations. Neurosurgery 64:A91–95
5. Brisman R (2000) Gamma knife radiosurgery for primary management for trigeminal neuralgia. J Neurosurg 93(Suppl 3):159–161
6. Fariselli L, Marras C, De Santis M, Marchetti M, Milanesi I, Broggi G (2009) CyberKnife radiosurgery as a first treatment for idiopathic trigeminal neuralgia. Neurosurgery 64:A96–101
7. Han JH, Kim DG, Chung HT, Paek SH, Kim YH, Kim CY, Kim JW, Jeong SS (2009) Long-term outcome of gamma knife radiosurgery for treatment of typical trigeminal neuralgia. Int J Radiat Oncol Biol Phys 75:822–827
8. Kondziolka D, Lunsford LD, Flickinger JC, Young RF, Vermeulen S, Duma CM, Jacques DB, Rand RW, Regis J, Peragut JC, Manera L, Epstein MH, Lindquist C (1996) Stereotactic radiosurgery for trigeminal neuralgia: a multiinstitutional study using the gamma unit. J Neurosurg 84:940–945
9. Kondziolka D, Perez B, Flickinger JC, Habeck M, Lunsford LD (1998) Gamma knife radiosurgery for trigeminal neuralgia: results and expectations. Arch Neurol 55:1524–1529
10. Kondziolka D, Zorro O, Lobato-Polo J, Kano H, Flannery TJ, Flickinger JC, Lunsford LD (2010) Gamma Knife stereotactic radiosurgery for idiopathic trigeminal neuralgia. J Neurosurg 112:758–765
11. Laitinen LV (1985) CT-guided ablative stereotaxis without ventriculography. Appl Neurophysiol 48:18–21
12. McKean JD, Allen PB, Filipow LJ, Miller JD (1987) CT guided functional stereotaxic surgery. Acta Neurochir (Wien) 87:8–13
13. Oh IH, Choi SK, Park BJ, Kim TS, Rhee BA, Lim YJ (2008) The treatment outcome of elderly patients with idiopathic trigeminal neuralgia: micro-vascular decompression versus gamma knife radiosurgery. J Korean Neurosurg Soc 44:199–204
14. Park SH, Hwang SK, Kang DH, Park J, Hwang JH, Sung JK (2010) The retrogasserian zone versus dorsal root entry zone: comparison of two targeting techniques of gamma knife radiosurgery for trigeminal neuralgia. Acta Neurochir (Wien) 152:1165–1170
15. Pollock BE, Phuong LK, Foote RL, Stafford SL, Gorman DA (2001) High-dose trigeminal neuralgia radiosurgery associated with increased risk of trigeminal nerve dysfunction. Neurosurgery 49:58–62, discussion 62–64
16. Regis J, Bartolomei F, Metellus P, Rey M, Genton P, Dravet C, Bureau M, Semah F, Gastaut JL, Peragut JC, Chauvel P (1999) Radiosurgery for trigeminal neuralgia and epilepsy. Neurosurg Clin N Am 10:359–377
17. Regis J, Manera L, Dufour H, Porcheron D, Sedan R, Peragut JC (1995) Effect of the gamma knife on trigeminal neuralgia. Stereotact Funct Neurosurg 64(Suppl 1):182–192
18. Regis J, Metellus P, Hayashi M, Roussel P, Donnet A, Bille-Turc F (2006) Prospective controlled trial of gamma knife surgery for essential trigeminal neuralgia. J Neurosurg 104:913–924
19. Rogers CL, Shetter AG, Ponce FA, Fiedler JA, Smith KA, Speiser BL (2002) Gamma knife radiosurgery for trigeminal neuralgia associated with multiple sclerosis. J Neurosurg 97:529–532
20. Tasker RR, Dostrovsky JO, Dolan EJ (1991) Computerized tomography (CT) is just as accurate as ventriculography for functional stereotactic thalamotomy. Stereotact Funct Neurosurg 57:157–166
21. Villavicencio AT, Lim M, Burneikiene S, Romanelli P, Adler JR, McNeely L, Chang SD, Fariselli L, McIntyre M, Bower R, Broggi G, Thramann JJ (2008) Cyberknife radiosurgery for trigeminal neuralgia treatment: a preliminary multicenter experience. Neurosurgery 62:647–655, discussion 647–655
22. Worthington C, Hutson K, Boulware R, Neglia W, Gibbons JP, Clark R, Rand J (2000) Computerized tomography cisternography of the trigeminal nerve for stereotactic radiosurgery. Case report. J Neurosurg 93(Suppl 3):169–171

Acta Neurochir (2011) 153:1611–1619
DOI 10.1007/s00701-011-1021-6

CLINICAL ARTICLE

Early and long-term outcome of surgically treated giant internal carotid artery aneurysms—comparison with smaller aneurysms

Tomasz Szmuda · Pawel Sloniewski

Received: 27 July 2010 / Accepted: 5 April 2011 / Published online: 15 May 2011

Abstract
Background Internal carotid artery (ICA) is predominant localization of giant intracranial aneurysms (GIAs). The rupture of GIA is supposed to be related to higher risk of poor clinical outcome. Although endovascular techniques are still being developed, they seem to be unsatisfactory in the mean of GIAs.
Methods Included in the retrospective analysis were 78 giant and 250 smaller surgically treated ICA aneurysms. Exclusion criteria were multiple and blood blister-like aneurysms. Neurological deficit on admission, clinical and radiological presentation, gender, age, segment of ICA, surgical methods, accessory techniques and complications were analyzed. Death rate and short- and long-term outcome of giant aneurysms were compared with smaller aneurysms and risk factors for mortality, unfavorable short- and long-term outcome were determined.
Results There was no difference in general and surgical complications between ICA aneurysm size groups, as well as in occurrence of newly diagnosed neurological deficit after the operation. There were similar mortality rates, proportion of unfavorable outcome, and low health related quality of life for giant and smaller aneurysms. A 12.2% death rate for all ICA aneurysms was achieved. Trapping method as well as Fisher grades 3 and 4 increased mortality risk in the smaller aneurysm group. No significant factors were related to an unfavorable outcome in the ruptured giant aneurysm group. Patients older than 65, Hunt-Hess grades 4 and 5, Fisher grade 4, and newly diagnosed deficit after operation were connected with unfavorable outcome in the ruptured smaller aneurysm group. Newly diagnosed neurological deficit was also an unfavorable outcome risk factor in both giant and smaller ICA unruptured aneurysms. No difference was noted in long-term health-related quality of life between the giant and smaller ICA groups. Higher age and presence of concomitant disease were independent factors affecting quality of life, although obtained data were incomplete.
Conclusions The study breaks the stereotype of unfavorable giant ICA aneurysms treatment results. Mortality rate, short- and long-term outcome after the operation of giant and smaller ICA aneurysms are similar. Higher age, patients' condition at admission, and the amount of extravasated blood and trapping method are poor prognostic factors in patients with smaller ICA aneurysm.

Keywords Internal carotid artery · Intracranial aneurysm · Giant cerebral aneurysm · Outcome · Quality of life

Presentation at a conference This paper was presented at the "Annual Conference of Polish Neurosurgery Society" in Poland (Mikolajki) at 2009.

Clinical Trial Registration number if required Not applicate.

This study was approved by the Ethical Comity of the Medical University of Gdansk (No: NKEBN/209/2008).

T. Szmuda (✉) · P. Sloniewski
Neurosurgery Department, Medical University of Gdansk, Poland,
Debinki 7,
Gdansk, Poland 80–952
e-mail: smalec7@wp.pl

P. Sloniewski
e-mail: pslonie@gumed.edu.pl

Introduction

Localization of giant intracranial aneurysms (GIAs) (defined as a dimension exceeding 25 mm [18]) is different compared to smaller ones. Although 20–40% of GIAs are found in posterior circulation, the internal carotid artery (ICA) is the predominant localization of GIAs [16, 17]. Up to 67% of GIAs are localized on the ICA [17].

The etiology of GIAs is similar to the smaller ones [16]. However, apart from the enlargement of small aneurysms, de novo development of GIAs is described [2]. Krings et al. [14] indicate that the formation of GIAs (proximal ICA and vertebral artery) may differ from the others. Repeated subadventitial hemorrhages from the vasa vasorum play an important role in the pathogenesis of GIAs. Therefore, GIAs can be regarded as a "proliferative disease of the vessel wall induced by extravascular activity" [14].

Approximately two-thirds of GIAs are diagnosed before rupture, causing mass effect, while most of the patients with smaller aneurysms are admitted due to subarachnoid hemorrhage (SAH) [17]. Regardless of how thick the wall of the GIA is, rupture causes extravasation of a greater amount of blood than happens in smaller aneurysms [8, 16]. This may result in poor clinical presentation in patients with GIAs. The ISUIA study [29] showed a 40% risk of rupture in case of giant ICA aneurysms. Kassell [9] noticed that the large size of the aneurysm is one of the prognostic factors related to postoperative mortality. The two studies above [9, 29] warrant treatment of both ruptured and unruptured giant ICA aneurysms [4].

Endovascular and surgical techniques are the options considered in treatment of giant ICA aneurysms. Since the first attempt of excluding giant ICA aneurysms from circulatory system in 1885 [5], a great many surgical occlusion and accessory techniques have been developed and described [17]. Current endovascular techniques are regarded as having lower risks for the patient [28]. Despite the fact that these techniques are being constantly developed, in GIAs, these still seem to be unsatisfactory in terms of durability of aneurysm occlusion [24, 28]. Parkinson [23] suggests that the results of surgical techniques should be the "gold standard" with which other techniques, including endovascular treatment, are compared.

Untreated GIAs have a poor natural history, as the mortality rate after 2 years of observation can reach 100% [13, 20, 25]. Even treated, favorable results usually did not exceed 80% in previous series [3, 10, 13, 15, 25, 27].

Reviewing neurosurgical literature regarding methods used for measuring outcome, the Glasgow outcome scale (GOS) and Rankin scale are mostly mentioned. Kim also reported the application of quality-of-life scale SF-36 in the intracranial aneurysm group [12]. Doctor's and patient's evaluation of treatment may differ, thus patient's self-assessment scale should be used [6].

There is not enough data in the literature describing the results of treatment and quality of life in patients with giant ICA in comparison to smaller ones. Surprisingly, factors influencing quality of life several years after operation have not been reported in the ICA aneurysm group. For this reason, the current study was performed to compare the prognosis after treatment of giant and smaller ICA aneurysms as well as to determine which factors influence postoperative mortality, early and long-term outcome separately in patients with giant and smaller type of aneurysm.

Materials and methods

Patient population and data collection

Between 1997 and 2006, 1,035 surgical intracranial saccular aneurysms securing procedures were performed in the Neurosurgery Department at the Medical University of Gdansk in Poland. Angiography and CT scans were analyzed, and surgical results, demographics, and other factors were evaluated retrospectively in 328 cases of saccular ICA aneurysms. The group was selected as 62 multiple and four blood blister-like aneurysms were excluded. GOS was used in patients' evaluation on the day of discharge. Postoperative mortality (GOS 1) was divided into perioperative (before 48 h) and postoperative (after 48 h after surgery) [19]. In the study, postoperative mortality analysis referred only to the in-hospital period. Favorable short-term outcome was defined as GOS grade 4 and 5, and unfavorable if GOS was 1, 2, or 3. Long-term outcome was assessed using the quality-of-life SF-36 scale. The query was sent to the patients in 2008 or collected during visits. If total SF-36 scores were under 50 points, low health-related quality of life was established.

Patients' characteristic and condition

The group consisted of 119 (36.28%) small, 81 (24.70%) medium, 50 (15.24%) large and 78 giant (23.78%) ICA aneurysms. For the statistics, small, medium, and large constituted one group of 250 smaller ICA aneurysms.

All of the giant aneurysms were operated on by senior author (SP). Over half (n=42; 53.85%) of the giant ICA aneurysms were diagnosed based on mass effect signs, while 82.40% (n=206) of the smaller aneurysms were operated on after rupture (p<0.01) (Fig. 1).

Age of the treated patients ranged from 17 to 83, mean 51.20 (SD±12.73). No difference in age was noted between the groups, as for the giant, the mean was 50.53 (SD± 10.12) and for the smaller ICA aneurysms 51.42 (SD± 13.46). Female predomination was observed in both groups. There were significantly (p=0.03) more females (85.90%) in the giant than in the smaller ICA aneurysm group (74.00%). Statistically, the proportion of education and habitation (village/town) was similar in both groups, as well as the percentage of concomitant diseases.

For 242 patients who presented SAH (36 giant and 206 smaller ICA aneurysms), Hunt-Hess, Fisher, GCS, WFNS grading and neurological deficit on admission was assessed.

In these regards, the giant group did not differ from the smaller ICA aneurysm group.

In 86 patients with unruptured aneurysm (42 giant and 44 smaller aneurysms), neurological deficit was also assessed on admission. Third nerve paresis was diagnosed on admission in seven patients (15.91%) with smaller ICA aneurysm group. There were 13 smaller ICA aneurysm of PCoA origin, five of them (38.46%) presented oculomotor nerve paresis. All of patients with smaller intracavernous aneurysms (n=2) had third nerve paresis (Table 1).

Most (85.71%) of the intracavernous aneurysms were giant, 11 unruptured (all patients were symptomatic) and 1 ruptured (clinical presentation was epistaxis). All smaller intracavernous aneurysms (n=2) were unruptured. The posterior wall aneurysms (AChA, PCoA) were usually small. One-fourth of the ICA aneurysms were localized in the bifurcation segment. The different localizations of the giant and smaller aneurysms were significant (p<0.01) (Fig. 2).

Treatment

The surgical methods and accessory techniques used in the treatment of the giant and smaller ICA aneurysms are shown in Table 2. The pterional approach was applied in all cases of giant and smaller, ruptured and unruptured ICA aneurysms. Extraduraly lesser wing of sphenoid bone partial removal and decompression of supraorbital fissure were performed in all cases of pterional craniotomy.

In both of the smaller and the one giant intracavernous aneurysm, direct clipping was performed in deep hypothermic circulatory arrest. In the remaining nine cases of intracavernous aneurysm, high-flow bypass was done.

For all clinoid and ophthalmic artery origin aneurysms, the additionally ipsilateral cervical carotid bifurcation exposure was prepared for proximal ICA control as well as intradural anterior clinoid process removal. When deemed necessary, optic strut removal was performed. In the four cases of clinoid giant aneurysms, retrograde suction was accessory. If the surgeon found that direct clipping impossible, bypass was offered afterwards. Unfortunately, in four cases, low-flow by-passes (STA-MCA and SThA-MCA) were found to be insufficient.

Direct surgical clipping was performed in the majority of supraclinoid aneurysms. If this method appeared difficult or insufficiently safe intraoperatively, then the wrapping or trapping technique was a possibility. For inoperable aneurysms, by-pass was the treatment option.

One temporary by-pass and one temporary balloon occlusion occurred to be invaluable accessory techniques in the authors' opinion, and therefore neglected. Microvascular Doppler ultrasonography was regularly used intraoperatively.

During the study years (1997–2006), there were no endovascular procedures performed in either giant or smaller ICA aneurysms. Patients were offered only a surgical treatment option.

For ruptured aneurysms, timing of the surgery was not assessed in the study. The angiogram was performed on admission and the operation took place on the next day. It referred to the majority of the ruptured ICA aneurysm, including those patients in a worse condition (Hunt-Hess grade IV). Patients in grade V were operated on if a mass effect caused of aneurismal intracerebral hemorrhage was diagnosed (Table 2).

Only significant surgery complications were analyzed, and were divided into three types: general (pneumonia, pulmonary embolism, heart attack, etc.), surgical (infectious, hematoma, CSF leakage, etc.) and neurological (conscious deterioration, ischemia in CT, etc.).

Outcome risk factors

Patient characteristics, including gender, age, education, habitation, and concomitant diseases, were analyzed to determine the relationship to outcome. Localization of aneurysm, surgical method, accessory techniques, complications, and diagnosis of new neurological deficit were analyzed for both ruptured and unruptured aneurysms. In the case of patients who presented SAH, Fisher, WFNS, and Hunt–Hess grading were taken into consideration in predicting the outcome.

Statistical methods

For categorical values, Chi-square and its nonparametric equivalents, for numerical values t and Mann–Whitney U tests were applied. Multivariate analysis was performed by logistic regression. Probability values less than 0.05 were used to determine significance.

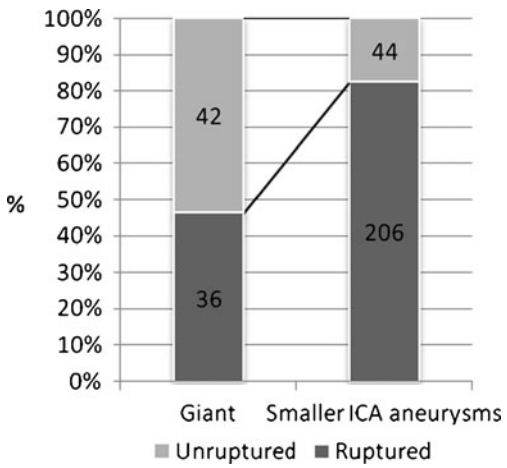

Fig. 1 Ruptured and unruptured aneurysms in giant and smaller aneurysm group

Table 1 Patients' characteristics at admission

Neurological deficit in the SAH group	Giant ICA aneurysm group [*n*; %]	Smaller ICA aneurysm group [*n*; %]	Fisher scale	Giant ICA aneurysm group [*n*; %]	Smaller ICA aneurysm group [*n*; %]
Hemiparesis	3; 8.33%	14; 6.80%	1	2; 5.56%	5; 2.43%
Aphasia	1; 2.78%	7; 3.40%	2	17; 47.22%	116; 56.31%
Oculomotor nerve					
Paresis	4; 11.11%	9; 4.37%	3	16; 44.44%	66; 32.04%
Abducens nerve paresis	1; 2.78%	0; 0.00%	4	1; 2.78%	19; 9.22%
Undefined visual symptoms	0; 0.00%	5; 2.43%			
Without neurological deficits	26; 72.22%	173; 83.98%			
WFNS scale			Hunt-Hess grading		
I	19; 52.78%	129; 62.62%	1	7; 19.44%	42; 20.39%
II	2; 5.56%	8; 3.88%	1A	2; 5.56%	8; 3.88%
III	3; 8.33%	9; 4.37%	2	8; 22.22%	80; 38.83%
IV	9; 25.00%	47; 22.82%	3	8; 22.22%	35; 16.99%
V	3; 8.33%	13; 6.31%	4	7; 19.44%	30; 14.56%
			5	4; 11.11%	11; 5.34%
Neurological deficit in unruptured group					
Hemiparesis	2; 4.76%	0; 0.00%			
Hemi-body numbness	0; 0.00%	1; 2.27%			
Seizures	1; 2.38%	2; 4.55%			
Oculomotor nerve					
Paresis	10; 23.81%	7; 15.91%			
Abducens nerve paresis	3; 7.14%	1; 2.27%			
Undefined visual symptoms	4; 9.52%	0; 0.00%			
Without neurological deficits	23; 54.76%	33; 75.00%			

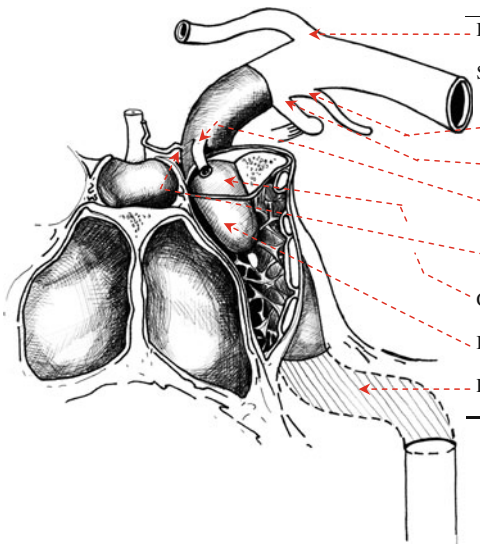

Fig. 2 Localization of giant and smaller ICA aneurysms

Segment of ICA	*Giant ICA aneurysm group* *[n; %]*	*Smaller ICA aneurysm group* *[n; %]*
Bifurcation	21; 26,92%	61; 24,40%
Supraclinoid	32; 41,03%	180; 72,00%
AChA	*0; 0,00%*	*13; 5,20%*
PCoA	*13; 16,67%*	*139; 55,60%*
OpthA	*16; 20,51%*	*25; 10,00%*
„Carotid cave"	*3; 3,85%*	*3; 1,20%*
Clinoid	13; 16,67%	7; 2,80%
Intracavernous	12; 15,38%	2; 0,80%
Petrous	0; 0,00%	0; 0,00%

Table 2 The surgical methods and accessory techniques used in the treatment of giant and smaller ICA aneurysms

Surgical methods	Giant ICA aneurysm group [*n*; %]	Smaller ICA aneurysm group [*n*; %]
Clipping	57; 73.08%	235; 94.00%
Trapping	2; 2.56%	3; 1.20%
Wrapping	1; 1.28%	5; 2.00%
Not secured	3; 3.85%	5; 2.00%
STA-MCA by-pass	2; 2.56%	1; 0.40%
ECA-MCA by-pass	10; 12.82%	0; 0.00%
ICA-MCA by-pass	2; 2.56%	1; 0.40%
SThA-MCA by-pass	1; 1.28%	0; 0.00%
Accessory techniques		
Temporary STA-MCA by-pass	1; 1.28%	0; 0.00%
Retrograde suction	4; 5.13%	0; 0.00%
Temporary balloon occlusion	1; 1.28%	0; 0.00%
Deep hypothermic circulatory arrest	2; 2.56%	1; 0.40%

Results

Complications

General and surgical complications occurred in 8.23% (n=27) of cases. Surgical complications referred to 4.40% (n=11) and general ones to 3.60% (n=9). After surgery, new neurological deficit was diagnosed in 8.54% of cases (n=28) (Table 3). There was an insignificantly higher percentage of patients with new deficits in giant (10.26%; n=8) in proportion to the smaller ICA aneurysm group (8.00%; n=20). No difference between aneurysm size groups was observed in the means of general and surgical complications.

There was no rebleeding from treated or other aneurysm observed in our series

Postoperative mortality

No perioperative death was recorded. There were 40 postoperative deaths, resulting in a total mortality rate of 12.20% in the entire group of 328 patients. No significant difference was observed in mortality between groups (12.82% in giant and 12.00% in smaller aneurysm group). Gender, age, education, habitation, segment of ICA, presence of concomitant disease, and complications did not determine postoperative mortality in whole analyzed ICA aneurysm group. Patients who died after leaving the Neurosurgery Department were lost to follow-up, as there were no such data obtained in the queries sent to the patients.

Ruptured aneurysms There were similar mortality rates for different sizes of ruptured ICA aneurysms. Death occurred in 16.67% (n=6) and 14.56% (n=30) of the giant and smaller ICA aneurysms, respectively. In the giant ICA group, only GCS was the mortality determining factor, thus multivariate analysis was not performed. Uni- and multivariate analyses of significant factors related to death were shown in Table 3. Multivariate analysis revealed that Fisher grade 3 and 4 increases mortality six times and the trapping method, 13 times (Table 4).

Unruptured aneurysms The risks of mortality for unruptured giant and small aneurysms were statistically similar, although four of 42 patients (9.52%) with giant ICA aneurysm died and all with smaller unruptured aneurysm survived (n=44). No factors related to death in the giant and smaller unruptured ICA aneurysms were found.

Short-term outcome

The analysis of short-term outcome, based on *GOS*, revealed that one-third (n=218; 33.54%) of the patients has an unfavorable outcome. Gender, education, habitation, segment of ICA, surgical method, surgical complications and presence of concomitant disease had no influence on short-term outcome in ruptured and unruptured, and both giant and smaller ICA aneurysms.

Ruptured aneurysms No statistical difference in short-term outcome rates between the giant and the smaller ICA aneurysm group was observed. 61.11% (n=22) of the giant and 57.77% (n=119) of the smaller ICA aneurysm cases had a favorable outcome (four and five in *GOS*).

Unruptured aneurysms In the unruptured aneurysm group, unfavorable outcome rates between giant (n=6; 14.29%) and small aneurysms (n=3; 6.82%) did not statistically differ (p=0.26). Newly diagnosed neurological deficit after surgery of giant or smaller ICA aneurysms (n=8) was related to unfavorable outcome occurrence.

Uni- and multivariate analyses of factors related to unfavorable outcome in ruptured and unruptured, giant and smaller ICA aneurysms are shown in Table 4. Multivariate analyses revealed four independent factors related to an unfavorable outcome in smaller ICA aneurysm group: patients' age over 65, Fisher grade 4, Hunt-Hess grades 4 and 5, and newly diagnosed neurological deficit after operation. A total of 63.33% (n=19) of patients over 65 years old, while only 38.64% (n=68) of younger patients had an unfavorable outcome in smaller ICA aneurysms group (Table 5).

Table 3 New neurological deficit in ruptured and unruptured, giant and smaller ICA aneurysm groups

	SAH		Unruptured	
New neurological deficit after the operation	Giant ICA aneurysm group	Smaller ICA aneurysm group	Giant ICA aneurysm group	Smaller ICA aneurysm group
	[*n*; %]	[*n*; %]	[*n*; %]	[*n*; %]
Hemiparesis	2; 5.56%	12; 5.82%	1; 2.38%	1; 2.27%
Upper extremity paresis	1; 2.78%	0	1; 2.38%	0
Aphasia	1; 2.78%	2; 0.97%	2; 4.76%	0
Oculomotor nerve				
Paresis	0	4; 1.94%	2; 4.76%	0
Without new neurological deficits after the operation	32; 88.89%	187; 90.78%	38; 90.48%	43; 97.73%

Long-term outcome

In the group of patients with an unfavorable short-term outcome (GOS grades 2 or 3), the investigators encountered problems with collecting SF-36 queries (only 35.7% of response), although the quality of life was assessed in 73.5% of patients with favorable short-term outcome. Summarily, there were 206 of 288 patients evaluated (71.5%). The mean follow-up did not differ between aneurysm size groups and was over 6 years (76.3 months), ranging from 15 to 133 months. SF-36 summary components as well as subscale scores of the giant aneurysm group did not significantly differ from the smaller aneurysm group {(Fig. 3)

A total of 41.2% of patients with giant and 45.1% of patients with smaller ICA aneurysms showed high health-related quality of life (p=0.62). The quality of life few years after the operation of giant or smaller ICA aneurysms, was not affected by gender, education, habitation, segment of ICA, method of operation, or complications. There was a significant influence of two factors: age and the presence of concomitant disease on the quality of life in the entire ICA aneurysm group. In the separate analysis of giant and smaller aneurysms, only the presence of concomitant disease was related to low health-related quality of life in the smaller ICA aneurysm group.

Ruptured aneurysms No difference in the SF-36 scores between the aneurysm size groups was noted, although 27.3% of the giant and 45.2% of the smaller ICA aneurysm group had low health-related quality of life. In both groups, no correlation between functional status at admission (regarding Fisher, WFNS, and Hunt-Hess grading) and SF-36 scores was observed.

Unruptured aneurysms A few years after surgical treatment of the unruptured smaller or giant ICA aneurysms, half of the patients had low health-related quality of life, namely 54.8% and 48.3% of giant and smaller aneurysm groups, respectively. No factors related to quality of life were found.

Table 4 Uni- and multivariate analyses of significant factors related to death in ruptured ICA aneurysms

Mortality risk factor	Univariate analysis *p*	Multivariate analysis *p*	OR (odds ratio)
Ruptured giant ICA aneurysms			
GCS scale	p=0.02	Not performed	1.03
Ruptured smaller ICA aneurysms			
Hunt-Hess grading	p<0.01	p=0.11	1.65
GCS scale	p<0.01	p=0.64	1.07
WFNS scale	p<0.01	p=0.31	1.42
Fisher scale	p<0.01	3 i 4 vs. 1 i 2 grade in Fisher scale	
		p<0.01	6.28
		4 vs. 1. 2 i 3 grade in Fisher scale	
		p=0.54	1.44
Trapping method	p=0.04	p=0.04	13.79

Table 5 Uni- and multivariate analyses of significant factors related to an unfavorable outcome in ruptured smaller and unruptured giant and smaller ICA aneurysms

Unfavorable outcome risk factor	Univariate analysis p	Multivariate analysis p	OR (odds ratio)
Ruptured smaller ICA aneurysms			
Hunt-Hess grading	$p<0.01$	4, 5 vs. 1, 2, 3 grade in Hunt-Hess scale	
		$p<0.01$	1.04
GCS scale	$p<0.01$	$p=0.58$	1.14
WFNS scale	$p<0.01$	$p=0.79$	1.11
Fisher scale	$p<0.01$	3, 4 vs. 1, 2 grade in Fisher scale	
		$p=0.10$	1.96
		4 vs. 1, 2, 3 grade in Fisher scale	
		$p<0.01$	10.93
Age	$p<0.01$	$p<0.01$	1.04
Newly diagnosed neurological deficit after operation	$p<0.01$	$p=0.01$	8.10
Unruptured giant and smaller ICA aneurysms			
Newly diagnosed neurological deficit after operation	$p<0.01$	Not performed	-

Discussion

The above study was based on a single-center and a single-surgeon series of surgically treated (both ruptured and unruptured) saccular ICA aneurysms. After excluding multiple and blood blister-like aneurysms, the analyzed group consisted of 23.78% giant aneurysms, a higher percentage than published [1, 11, 28]. This was due to the fact that some patients with diagnosed GIAs were admitted from other neurosurgical wards that do not have much experience in surgical treatment of GIAs. Since most of the smaller aneurysms were diagnosed after their rupture, giant causing mass effect or asymptomatically, thus separate comparisons of ruptured and unruptured ICA aneurysms were carried out.

Complications

An insignificantly higher percentage of newly diagnosed neurological deficits after operation was found in giant ICA aneurysm patients. The surgery of GIAs is supposed to be a more difficult and complicated entity than smaller aneurysms [28]. A thorough analysis of general and surgical complications was not the purpose of this study. Le Roux indicates that the complication rate can reach even up to 100%, depending on established criteria [17].

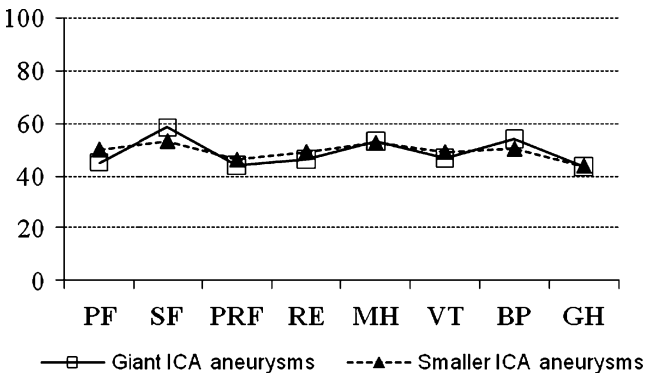

Fig. 3 SF-36 subscale scores of the giant and smaller ICA aneurysm groups

There was no rebleeding observed in the entire analyzed group. The risk of rupture from a secured aneurysm is low. In the ISAT study [22], 0.10% neurosurgically treated patients experienced rebleeding from the target aneurysm in 4 years of follow-up. On the other hand, in our series, rebleeding might not occur due to losing patients during the follow-up.

Postoperative mortality

Surgical mortality rates for GIAs may vary from 4 to 21%, with an average of 10% [27]. In the presented series of ICA aneurysms, similar death rates for giant and smaller were obtained, resulting in a 12% overall mortality rate. A considerable number of 328 patients enabled the analysis of multivariate factors which influence mortality, indicating that not aneurysm size, but the amount of blood (Fisher grade) and the trapping method were increasing the number of deaths. Kassell's [9, 10] publications, based on large series, signified that aneurysm size is one of the death prognostic factors. He also indicated that level of consciousness and age was related to higher mortality rate, which our study did not confirm in the ruptured ICA aneurysm population. Consecutive improving of surgical techniques contributed to a significant decrease in the mortality and that was also confirmed by the authors in the present study.

Short-term outcome

In author's opinion [9, 10], short-term outcome after surgical treatment of ruptured giant aneurysms is worse than smaller ones. Although the presented series partially confirmed the above opinion, it is worth mentioning that the difference was not significant. In giant unruptured aneurysms, the percentage of favorable short-term outcome was similar to smaller aneurysms. The surgical treatment of unruptured smaller ICA aneurysms revealed that up to 7% of patients may have an unfavorable short-term outcome, but natural history and consequences [29] of rupture excuse intervention. The analysis of factors influencing short-term outcome in the smaller aneurysm group confirmed well-known [8] unfavorable prognostic factors: Fisher grade 4, Hunt-Hess grades 4 and 5 and patients' higher age. It also acknowledges current status, indicating the amount of blood as the strongest prognostic factor [8–10]. Newly diagnosed neurological deficit after the operation of both ruptured and unruptured smaller ICA aneurysms was connected to unfavorable outcomes. In giant aneurysms, conventional endovascular therapy or use of dimethyl sulfoxide (Onyx) is related to 8% morbidity [21].

Long-term outcome

In the authors' opinion, the use of the SF-36 questionnaire in patients with unfavorable outcome on discharge (GOS grade 2 or 3) a few years after surgery is debatable. However, response rate can attain 100% in a similar group [26]. There are no published reports comparing quality of life between giant and smaller ICA aneurysms. The presented study revealed that the long-term outcome of different aneurysm size groups is similar. Moreover, in opposition to Scharbrodt's publication [26], the quality of life does not depend on functional status at admission in the ruptured aneurysm group. Higher age and presence of concomitant disease were the only two factors related to low health-related quality of life a few years after the operation of giant or smaller ICA aneurysms. Despite the fact that age may influence the brain's ability to recover [26], other factors (social, economic) determine age-related quality of life [7]. As a matter of fact, concomitant diseases may affect health-related quality of life, which has been acknowledged in the presented series.

In conclusion, the analysis of the surgically treated 78 giant and 250 smaller ICA suggests that mortality, morbidity, and short and long-term outcomes of these patients are similar. These novel results are at variance with some standard neurosurgical reports from highly experienced neurovascular surgeons worldwide [1, 15, 16, 25]. Most papers considering the outcomes of surgically treated giant ICA aneurysms are dated to the late 1980s and 1990s of the previous century [1, 9, 15–17, 23, 25, 28] and they rarely exceeded 80% of good results. A few successors, taught by the formers' experience, showed that surgical treatment still remains a gold standard, publishing that outcome could be better. They achieved up to 90% good results [4, 27, 30]. Proper, individualized case selection and surgical strategy including accessory techniques, preoperative assessment of vascular anastomoses, temporary parent vessel occlusion, retrograde suction decompression, and microvascular Doppler ultrasonography can substantially improve microsurgical outcome [27, 30]. Therefore, we believe that our innovative conclusions could encourage other scientists to share their results and would open the discussion on this particularly interesting topic.

The unique peculiarity of giant ICA aneurysms requires extensive comprehension of the treatment strategies to achieve better results. An experienced neurovascular surgeon should be accustomed to all surgical techniques for giant ICA aneurysms [23].

Acknowledgements I thank my advisor and teacher Professor M.D. Pawel Sloniewski, the Head of Neurosurgery Department of Medical University of Gdansk in Poland, for his continuous support in the PhD program and great help in preparing this paper.

Conflicts of interest None.

References

1. Barrow DL, Alleyne C (1995) Natural history of giant intracranial aneurysms and indications for intervention. Clin Neurosurg 42:214–244
2. Barth A, de Tribolet N, Barth A, de Tribolet N (1994) Growth of small saccular aneurysms to giant aneurysms: presentation of three cases. Surg Neurol 41:277–280
3. Dolenc V (1999) Extradural approach to intracavernous ICA aneurysms. Acta Neurochir Suppl 72:89–106
4. Doormaal TP, Zwan A, Verweij BH, Langer DJ, Tulleken CA (2006) Treatment of giant and large internal carotid artery aneurysms with a high-flow replacement bypass using the excimer laser-assisted nonocclusive anastomosis technique. Neurosurgery 59 (4 Supl 2):328–334; discussion 334–335
5. Flamm ES (1997) Cerebral aneurysms and subarachnoid hemorrhage history of neurovascular surgery. In: Greenblatt S (ed) History of neurological surgery. AANS Publishers, Park Ridge
6. Janse AJ, Gemke RJ, Uiterwaal CS, van der Tweel I, Kimpen JL, Sinnema G (2004) Quality of life: patients and doctors don't always agree: a meta-analysis. J Clin Epidemiol 57:653–661
7. Jokela M, Singh-Manoux A, Ferrie JE, Gimeno D, Akbaraly TN, Shipley MJ, Head J, Elovainio M, Marmot MG, Kivimaki M (2010) The association of cognitive performance with mental health and physical functioning strengthens with age: the Whitehall II cohort study. Psychol Med 40(5):837–845

8. Juvela S, Siironen J, Varis J, Poussa K, Porras M (2005) Risk factors for ischemic lesions following aneurysmal subarachnoid hemorrhage. J Neurosurg 102(2):194–201
9. Kassell NF, Torner JC, Haley EC Jr, Jane JA, Adams HP, Kongable GL (1990) The International Cooperative Study on the Timing of Aneurysm Surgery. Part 1. Overall management results. J Neurosurg 73(1):18–36
10. Kassell NF, Torner JC, Jane JA, Haley EC Jr, Adams HP (1990) The International Cooperative Study on the Timing of Aneurysm Surgery. Part 2. Surgical results. J Neurosurg 73(1):37–47
11. Khurana VG, Piepgras DG, Whisnant JP (1998) Ruptured giant intracranial aneurysms: Part I - A study of rebleeding. J Neurosurg 88:425–429
12. Kim DH, Haney CL, Van Ginhoven G (2005) Utility of outcome measures after treatment for intracranial aneurysms: a prospective trial involving 520 patients. Stroke 36(4):792–6
13. Kodama N, Suzuki J (1982) Surgical treatment of giant aneurysms. Neurosurg Rev 5:155–160
14. Krings T, Piske RL, Lasjaunias PL (2005) Intracranial arterial aneurysm vasculopathies: targeting the outer vessel wall. Neuroradiology 47:931–937
15. Lawton MT, Spetzler RF (1995) Surgical management of giant intracranial aneurysms: experience with 171 patients. Clin Neurosurg 42:245–266
16. Lemole GM, Henn J, Spetzler RF, Riina HA (2000) Surgical management of giant aneurysms. Oper Tech Neurosurg 3(4):239–254
17. Le Roux PD (2004) Management of cerebral aneurysms. Saunders, Pennsylvania
18. Locksley HB (1966) Natural history of subarachnoid hemorrhage, intracranial aneurysms and arteriovenous malformations: based on 6368 cases in the cooperative study. J Neurosurg 25:219–239
19. Lokato EB, Gravenstein N, Kirby RR (2007) Complications in anesthesiology, ed.3. Wolters Kluwer Health. Lippincott Williams & Wilkins, p 4
20. Michel WF (1974) Posterior fossa aneurysms simulating tumours. J Neurol Neurosurg Psychiatry 37:218–223
21. Molyneux AJ, Cekirge S, Saatci I, Gal G (2004) Cerebral Aneurysm Multicenter European Onyx (CAMEO) trial: results of a prospective observational study in 20 European centers. AJNR Am J Neuroradiol 25:39–51
22. Molyneux AJ, Kerr RS, Yu LM, Clarke M, Sneade M, Yarnold JA, Sandercock P (2005) International subarachnoid aneurysm trial (ISAT) of neurosurgical clipping versus endovascular coiling in 2143 patients with ruptured intracranial aneurysms: a randomised comparison of effects on survival, dependency, seizures, rebleeding, subgroups, and aneurysm occlusion. Lancet 366 (9488):809–17
23. Parkinson RJ, Eddleman CS, Batjer HH, Bendok BR (2006) Giant intracranial aneurysms: endovascular challenges. Neurosurgery 59 (5 Suppl. 3):103–12; discussion 3–13
24. Pavlisa G, Ozretic D, Murselovic T, Pavlisa G, Rados M (2010) Sole stenting of large and giant intracranial aneurysms with self-expanding intracranial stents-limits and complications. Acta Neurochir (Wien) 152(5):763–9
25. Peerless SJ, Wallace MC, Drake CG (1990) Giant intracranial aneurysms. In: Youmans JR (ed) Neurological surgery: a comprehensive reference guide to the diagnosis and management of neurological problems. WB Saunders, Philadelphia, pp 1742–63
26. Scharbrodt W, Stein M, Schreiber V, Böker DK, Oertel MF (2009) The prediction of long-term outcome after subarachnoid hemorrhage as measured by the Short Form-36 Health Survey. J Clin Neurosci 16(11):1409–13
27. Sharma BS, Gupta A, Ahmad FU, Suri A, Mehta VS (2008) Surgical management of giant intracranial aneurysms. Clin Neurol Neurosurg 110(7):674–81
28. Wehman JC, Hanel RA, Levy EI, Hopkins LN (2006) Giant intracranial aneurysms: endovascular challenges. Neurosurgery 59 (5 Suppl 3):125–138
29. Wiebers DO, Whisnant JP, Huston J, Meissner I, Brown RD Jr, Piepgras DG (2003) Unruptured intracranial aneurysms: natural history, clinical outcome, and risk for surgical and endovascular treatment. (ISUIA). The Lancet 12:362,9378:103.
30. Xu BN, Sun ZH, Romani R, Jiang JL, Wu C, Zhou DB, Yu XG, Hernesniemi J, Li BM (2010) Microsurgical management of large and giant paraclinoid aneurysms. World Neurosurg 73 (3):137–146

Comment

Somewhat surprisingly, this single-center series of 78 patients with giant and 250 with smaller ICA aneurysms operated on by a single surgeon had similar outcomes after surgery. However, the series was rather selective with a very short and incomplete follow-up. Even if there are some biases in the series, it still shows that microsurgical techniques are developing constantly, and in experienced hands, aneurysms can be safely operated on. This addresses the importance of patients being treated in dedicated neurovascular centers not forgetting the collaboration between microsurgical and endovascular surgeons.

Mika Niemelä
Hanna Lehto
Juha Hernesniemi
Helsinki, Finland

Acta Neurochir (2011) 153:1621–1623
DOI 10.1007/s00701-011-1022-5

EDITORIAL

Mortality rates for giant aneurysms

Zakaria Hakma · Raghu Ramaswamy · Christopher Miranda Loftus

Received: 4 April 2011 / Accepted: 5 April 2011 / Published online: 15 May 2011

In this issue, Szmuda and coworkers present a series of internal carotid artery (ICA) (only) aneurysms, all treated with open surgery, in which there is no material difference in morbidity and mortality figures between routine small aneurysms and giant aneurysms. This finding is in contradistinction to previous surgical reports and accepted surgical teachings, and this variance merits our further consideration here.

Giant intracranial aneurysms (GIAs)—defined as those greater than 2.5 cm in diameter—often pose a unique and challenging problem in their microsurgical or endovascular treatment. They are relatively infrequent, comprising approximately 5% of all aneurysms in most series [2, 4].

The size definition (>2.5 cm) came from Locksley's pivotal work that classified the aneurysms according to size and their rate of morbidity and mortality [7].

Giant aneurysms are dangerous. The mortality rates for untreated giant aneurysms have been reported to be as high as 65 and 100% after 2–5 years of follow-up [5, 9], with a rupture rate for conservatively treated intradural giant aneurysms roughly around 8–10% per year [10].

Morphologically, giant aneurysms are divided into saccular and fusiform types, with fusiform aneurysms arising more commonly in the vertebrobasilar and middle cerebral territories [1].

The treatment of GIAs, like smaller aneurysms, is generally directed toward complete exclusion of the lesion from the circulation, with preservation of flow in all parent arteries. This can be accomplished with direct clip reconstruction, aneurysm trapping with or without surgical bypass, acute proximal vessel occlusion with or without surgical bypass, and Selverstone clamping (delayed proximal occlusion). The reported modern surgical mortality rates for the treatment of both ruptured and unruptured giant aneurysms vary between 6% and 22% [3, 6]

From an endovascular perspective, these lesions are often not favorable because they frequently have broad necks, distorting the anatomy of the parent vessel, incorporating branch arteries at the base, and there is a high incidence of intraluminal thrombosis. These anatomic factors make giant aneurysms difficult to coil and obliterate completely, leading to residual or recurrent aneurysms, multiple retreatments, occasional rehemorrhages, and neurological deterioration from progressive aneurysm enlargement.

Current endovascular techniques (coil embolization with or without balloon assistance, neck remodeling with stents, liquid embolics, etc.) for the treatment of giant cerebral aneurysms still have significant periprocedural risks for the patients. These risks are only compounded by the severity of their cerebral vascular pathology, and many times are not satisfactory in terms of the long-term durability of aneurysm occlusion.

Flow diversion approaches to intracranial aneurysm treatment have offered many promising early results; but some apparently successful treatments have been complicated by later aneurysm hemorrhage. Combined microsurgical and endovascular strategies have been used for more than a decade to treat complex intracranial aneurysms with varying degrees of success [8].

Szmuda and Sloniewski, in this issue, report similar mortality rates, short-term outcomes, and long-term outcomes after surgery for giant and smaller ICA aneurysms.

Z. Hakma · R. Ramaswamy · C. M. Loftus (✉)
Department of Neurosurgery, Temple University,
3401 N. Broad Street, Parkinson C-540,
Philadelphia, PA 19140, USA
e-mail: cloftus@temple.edu

They did not offer their patients an endovascular option during this study period. In a retrospective review of 328 ICA aneurysms with a high fraction of "giant" lesions (78 giant, 250 smaller), 242 were ruptured and 86 were unruptured. Hunt and Hess scores, Fisher grades, Glasgow Coma Scale (GCS), and World Federation of Neurological Surgeons (WFNS) scores did not differ between giant and smaller aneurysms. There were no significant differences in complication rates between these two groups and the mortality rates were similar. In regards to the occurrence of complications in the short-term, three independent risk factors were found: general complications in the giant aneurysm group, Fisher grade 4 status, and the presence of a new postoperative neurologic deficit following surgery of smaller aneurysms. The long-term outcome after surgery was influenced by factors of age and of concomitant disease.

The authors espouse that while surgery of giant aneurysms is generally felt—as discussed above—to be more dangerous than for smaller aneurysms, complication rates—assessed in their series by short-term and long-term outcome—can be similar between the two groups.

As we mentioned, this is a single institution, single surgeon experience, and while excellent and provocative, it is not reflective of the experience of the neurosurgical community as a whole.

Limitations of this study include the absence of the endovascular option, as none of these patients were offered an endovascular procedure. The authors were not in a position to offer newer technologies for these challenging aneurysms (especially flow diversion with Pipeline or SILK that might be a viable option for some of these unruptured aneurysms).

The timing of surgery after rupture was not presented. Timing of surgery is an important factor when discussing surgical results, to eliminate selection bias and bring into focus the crossing lines of surgical morbidity (higher with early surgery) versus rebleeding and management morbidity (higher with delayed surgery). Timing of surgery also affects the ability to aggressively treat vasospasm, depending on the presence of a secured versus an unsecured aneurysm.

In this study, many patients were lost to follow-up; in fact, in the group of patients with unfavorable short-term outcome [Glasgow Outcome Scale (GOS) grade 2 or 3], the authors collected SF-36 queries from 7%, while the quality of life was assessed in 73.5% of patients with good short-term outcomes. This creates an issue for interpreting the long-term outcomes and assessing the rate of rebleeding after surgical treatment.

Let us consider the differences in populations that may explain this inability to assign higher perioperative risk to giant ICA aneurysms. First, giant aneurysms in this series were less likely to present with subarachnoid hemorrhage (SAH) (46% of giant lesions, 83% of smaller ones), and we feel that SAH portends a higher treatment morbidity. Second, 15% of giant lesions were intracavernous, but only 0.8% of smaller lesions, and the treatment in most cases was flow diversion with high-flow bypass (9/78 or 12% of giant aneurysms, only 2/250 or 0.8% of smaller aneurysms); once again direct clipping is most likely associated with a higher perioperative risk than flow diversion techniques. These considerations skew the risk away from the giant population, and may lull us into a false sense of security that GIA morbidity approaches that of smaller lesions, contrary to conventional surgical dogma.

Table 2 is lucid, and explains clearly that alternatives to direct clipping, probably less morbid in nature, were used in 20% more of the GIA cases. Indirect treatment proved to be an excellent strategy, as there was no rebleeding in the series, and we are not critical of this, but we do feel that it lowered the risk profile in the GIA group.

While we do not dispute the results here in any way, we recognize that these results are at variance with results of highly experienced neurovascular surgeons and we caution to generalize these results yet; we encourage surgeons to continue to report their results on this challenging disease. We believe that the authors' statistics are credible and valid, and that their conclusions are reasonable considering the data provided. We believe that the variance with accepted teaching is best explained by the group differences between SAH rate, aneurysm location, and direct versus indirect approach. We would also be curious to know if the authors' experience with posterior circulation GIAs could reproduce these results?

This is an interesting article by experienced surgeons and a worthwhile contribution that challenges the notion of unfavorable giant ICA aneurysm treatment results, and adds to the knowledge base of the treatment of this difficult condition.

Conflicts of interest None.

References

1. Barrow DL, Alleyne C (1995) Natural history of giant intracranial aneurysms and indications for intervention. Clin Neurosurg 42:214–244
2. Drake CG (1979) Giant intracranial aneurysms: experience with surgical treatment in 174 patients. Clin Neurosurg 26:12–95
3. Gewirtz RJ, Awad IA (1996) Giant aneurysms of the anterior circle of Willis: management outcome of open microsurgical treatment. Surg Neurol 45:409–421
4. Hosobuchi Y (1979) Direct surgical treatment of giant intracranial aneurysms. J Neurosurg 51:743–756

5. Kodama N, Suzuki J (1982) Surgical treatment of giant aneurysms. Neurosurg Rev 5:155–160
6. Lawton MT, Spetzler RF (1995) Surgical management of giant intracranial aneurysms: experience with 171 patients. Clin Neurosurg 42:245–266
7. Locksley HB (1966) Natural history of subarachnoid hemorrhage, intracranial aneurysms and arteriovenous malformations. Based on 6368 cases in the cooperative study. J Neurosurg 25:219–239
8. Mizoi K, Takahashi A, Yoshimoto T, Fujiwara J, Koshu K (1993) Combined endovascular and neurosurgical approach for paraclinoid internal carotid artery aneurysms. Neurosurgery 33:986–992
9. Peerless SJ, Wallace MC, Drake CG (1990) Giant intracranial aneurysms. In: Youmans JR (ed) Neurological surgery: a comprehensive reference guide to diagnosis and management of neurological problems. Saunders, Philadelphia, pp 1742–1763
10. Wiebers DO, Whisnant JP, Huston J 3rd, Meissner I, Brown RD Jr, Piepgras DG, Forbes GS, Thielen K, Nichols D, O'Fallon WM, Peacock J, Jaeger L, Kassell NF, Kongable-Beckman GL, Torner JC; International Study of Unruptured Intracranial Aneurysms Investigators (2003) Unruptured intracranial aneurysms: natural history, clinical outcome and risks of surgical and endovascular treatment. Lancet 362:103–110

Acta Neurochir (2011) 153:1625–1631
DOI 10.1007/s00701-011-0999-0

CLINICAL ARTICLE

A retrieval thrombectomy technique with the Solitaire stent in a large cerebral artery occlusion

Hyun Park · Gyo jun Hwang · Sung-Chul Jin · Cheol-kyu Jung · Jae Seung Bang · Moon Ku Han · Hee Jun Bae · Ghee young Choe · Chang Wan Oh · O-Ki Kwon

Received: 11 January 2011 / Accepted: 14 March 2011 / Published online: 10 April 2011

Abstract
Background To describe preliminary experiences and the procedural details of retrieval thrombectomy using a self-expanding and fully retrievable Solitaire stent (ev 3 Inc., CA, USA) in acute ischemic stroke (AIS) patients with large artery occlusions.
Methods Eight patients with AIS were treated by mechanical thrombectomy using a self-expanding, fully retrievable stent (Solitaire, ev 3 Inc., CA, USA). The stent was deployed to cover the whole intra-arterial clot and then it was slowly retrieved while occluding the internal cerebral artery (ICA) with a balloon guiding catheter. Additionally, continuous negative pressure was applied through the balloon guiding catheter with a specially designed gun device. Occlusion sites were M1 in six cases including one combined supraclinoid ICA occlusion and the other combined M2 occlusion, M2 in 1 case and one basilar artery top.
Results Complete recanalization was achieved in all patients. Procedure time was 45 min or less in seven cases and 70 min in one case. Distal emboli occurred in one case in which the balloon guide catheter was not used. Only in this case was intraarterial fibrinolytics infusion necessary. There was no post-operative intracranial hemorrhage.

This study was supported by grant no. 02-2010-021 from the SNUBH Research Fund.

H. Park
Department of Neurosurgery, Jeju National University School of Medicine, Jeju National University Hospital,
Ara-1-dong,
Jeju-Si, Jeju Self-Governing Province 690–716, Korea

J. S. Bang · C. W. Oh · O.-K. Kwon (✉)
Department of Neurosurgery, Seoul National University College of Medicine, Bundang Hospital,
166 Gumi-ro Bundang-gu Seongnam-si,
Gyeonggi-do 463–707, Korea
e-mail: kwonoki@snubh.org

M. K. Han · H. J. Bae
Neurology, Seoul National University College of Medicine,
Bundang Hospital,
Seongnam, Korea

C.-k. Jung
Radiology, Seoul National University College of Medicine,
Bundang Hospital,
Seongnam, Korea

G. j. Hwang
Department of Neurosurgery, Chuncheon Sacred Heart hospital,
Hallym University and Graduate school of Kangwon University,
Seongnam, Korea

S.-C. Jin
Department of Neurosurgery, Cerebrovascular Center,
Inje University, Haeundae Paik Hospital,
Pusan, Korea

G. y. Choe
Pathology, Seoul National University College of Medicine,
Bundang Hospital,
Seongnam, Korea

Conclusions In our experience, retrieval thrombectomy with the Solitaire stent was a simple and effective method for reopening large cerebral arteries in AIS patients.

Keywords Acute · Stroke · Stent · Mechanical · Thrombolysis · Thrombectomy

Introduction

The Solitaire system (ev3 Inc, Irvine, CA, USA) is a self-expanding, electrically detachable stent for cerebral vessels. It is retrievable even after complete deployment if not detached [4]. In addition, thanks to its closed cell design and softness, it could be also retrievable even without resheathing the stent. Recently, we used this device for capturing and removing clots in patients with acute stroke. A balloon guiding catheter to block internal cerebral artery (ICA) flow and a simple device for applying constant negative pressure through the guiding catheter were used for reducing distal migration of the captured thrombi during retrieval. In this report, we describe our experience of retrieval thrombectomy using the Solitaire stent system for revascularization of acute stroke.

Materials and methods

Eight consecutive patients with acute ischemic stroke (AIS) caused by large artery occlusion were treated by endovascular retrieval thrombectomy with Solitaire devices. Our intra-arterial mechanical thrombolysis criteria was as follows: [1] clinical symptoms of acute ischemic stroke; [2] intracranial large arterial occlusion visible on brain magnetic resonance (BMR) angiograms or brain computed tomography (BCT) angiograms; [3] definite mismatch on diffusion MR and perfusion MR; [4] within 8 h of onset; and [5] within a time window of 3 h, the patients exhibited no response on BMR angiograms to intravenous tissue plasminogen activator (tPA) treatment. Patients who had intracranial hemorrhages (ICH), broad infarctions (middle cerebral artery territory ≥1/3), or severe brain edema were excluded.

Common interventional techniques

Endovascular procedures were performed through the femoral artery under local anesthesia. A biplane angiography unit (Integris Allura 12/12, Philips, Netherlands) was used. No heparin was given during the procedure. After placing a femoral sheath, diagnostic cerebral angiography was performed to visualize the occlusion site and the collateral channels. A 9Fr balloon guiding catheter (Cello, Fuji Systems Corp. Japan) was then introduced. The extent of occluding clot was visualized by selective angiography using a microcatheter (Prowler Select Plus; Cordis Corp., Bridgewater, NJ, USA), which was passed through the clot and placed distally. A Prowler Select Plus microcatheter (Cordis Corp., Bridgewater, NJ, USA) was also used for the Solitaire stent. A Solitaire stent was advanced and fully deployed from a few millimeters distal to the clot. In our cases, the clot length was shorter than the stent length (20 mm), so the stent covered the whole clot. In all cases, immediate but partial flow restoration was observed after stent deployment. The stent was kept there for 30 s to 1 min to fully expand into the clot. The microcatheter and the stent were then withdrawn together slowly with the balloon of the guiding catheter inflated to block ICA flow. Simultaneously, we applied negative suction pressure with a gun-like aspiration device (Fig. 1, Aspiration Gun, Taesung, Seoul, Korea) to reduce distal migration of the thrombi during retrieval.

Periprocedural work-up

Histological examination of the retrieved clots was performed to understand structural features of the retrieved clots and to determine whether endothelial components were contained in the clot. The etiology of the AIS was classified according to the Trial of Org 10172 in Acute Stroke Treatment (TOAST) classification system. At an initial and immediate postprocedural examination, the presence of neurological deficits was evaluated by a stroke neurologist according to the National Institutes of Health Stroke Scale (NIHSS).

Recanalization was assessed and scored by the Thrombosis in Cerebral infarction (TICI) scale. We regarded TICI grades 2 and 3 as recanalization and complete recanalization was defined as TICI grades 2b or 3. If an intracranial hemorrhage was suspected, BCT was performed immediately after the procedure. A symptomatic hemorrhage was defined as a neurological deterioration greater than or equal to four points on the follow-up NIHSS score compared to

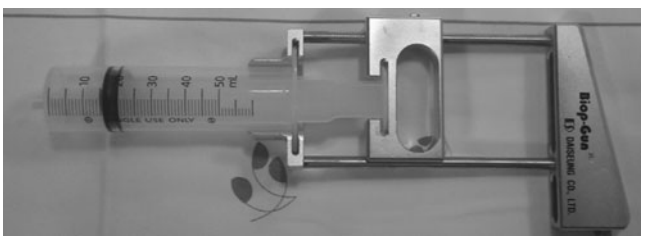

Fig. 1 Photograph of gun-like aspiration device with tooth-like locking system

that of the initial examination and a hemorrhage visible on follow-up imaging. Clinical outcome at 90 days was evaluated according to the modified Rankin-scale (mRS) and a good long-term outcome was defined as mRS ≤2 at 90 days.

Results

The characteristics of the eight patients and procedural results are summarized in Table 1. Five patients were treated with intravenous tissue plasminogen activator (IVtPA) before the intra-arterial thrombolysis. The mean initial NIHSS score was 18.3±6.3 (range 8–24), and unfavorable and favorable mean initial NIHSS was 22.3 ±2.4 (range 19–24) and 14.3±6.7 (range 8–20), respectively. Mean immediate post-operative NIHSS score was 12.3±7.3 (range 0–20). The median procedure time (from femoral puncture to recanalization of occlusive site) was 41.5±15.1 min (range 17–70 min). The mean number of passes until achieving maximal recanalization runs was 1.5 (range 1–3). Successful recanalization was achieved in all patients and complete recanalization (defined as thrombolysis in cerebral infarction grade 3, 2b) was achieved in all patients.

The Solitaire system was used as the first thrombolytic method for large vessel occlusion in all patients. Histopathological examination of the retrieved clots from the first three cases resulted in no endothelial component in the clots. Emergent angioplasty and stenting of extracranial internal cerebral artery (ICA) was needed because of severe stenosis of proximal ICA before mechanical thrombectomy in one patient. Distal emboli occurred in one case in which the balloon guide catheter was not used because of vessel tortuousness. Only in this case was intraarterial fibrinolytics infusion necessary and distal emboli were completely resolved. There was no intra-operative dissection, arterial rupture, and post-operative intracranial hemorrhage. The favorable functional outcome (mRS 0–2) at 3 months was 50% (four of eight cases), which were 1 of mRS 0, 2 of mRS 1, and 1 of mRS 2. The mortality was 0%.

Illustrative cases

Case 2

This 76-year-old male patient presented with the clinical signs of stroke including right-side weakness and a drowsy mental status. The initial NIHSS score was 24. Diffusion MR showed an acute infarction in the left basal ganglia and the corona radiata. There was a large diffusion-perfusion mismatch and so an emergency IAT was decided. Angiograms showed occlusion of the proximal M1 (Fig. 2a). A

Table 1 Summary of the characteristics of the patients, procedural results, and occlusion location

Patient no.	Age	Sex	Location	TOAST	Initial NIHSS	TFTF (min)	Procedure time (min)	IVtPA dose(mg)	IAUK dose(U)	No. of runs	TICI grade	Sx he	Immediate post-operative NIHSS	90 days mRS	Path.
1	81	M	MCA(M1)	CE	22	120	17	39	N	1	3	N	17	5	Y
2	76	M	MCA(M1)	CE	24	105[d]	30	No	N	1	3	N	19	3	Y
3	89	F	MCA(M1)	CE	20	207	45	28.6	N	1	3	N	17	2	Y
4	77	F	MCA(M2)	CE	8	210	43	27.9	N	1	3	N	5	1	N
5	78	F	MCA(M1)[b]	CE	24	335[d]	70	30.5	200 K	2	3	N	20	4	N
6	74	F	ICA[a]+MCA(M1)	CE	19	60	40	N	N	3	2B	N	15	4	N
7	71	M	BT-PCA	CE	20	135	37	32.6	N	2	3	N	0	0	N
8	65	M	MCA(M1+M2) [c]	LAA	9	270	45	N	N	1	2B	N	5	1	N

NIHSS National Institutes of Health Stroke scale; *TOAST* Trials of Org 10172 in Acute Stroke Treatment; *TFTF* time from onset of symptom to femoral puncture; *IVtPA* intravenous tissue plasminogen activator; *IA UK* intraarterial urokinase; *TICI* thrombolysis in cerebral infarction; *Sx* symptomatic; *he* hemorrhage; *mRS* modified Rankin-scale; *M* male; *MCA* middle cerebral artery; *BT* basilar tip; *PCA* posterior cerebral artery; *CE* cardiac embolism; *N* no; 20K=200,000; *Path* histopathology

[a] distal internal cerebral artery (tandem lesion)

[b] fragmented thrombus migrated from M1 to M2 after retrieval thrombectomy

[c] emergent extracranial angioplasty and stenting at proximal ICA because of severe stenosis

[d] in case with awaken stroke, TFTF was defined as time from first abnormal finding of neurologic status to femoral puncture

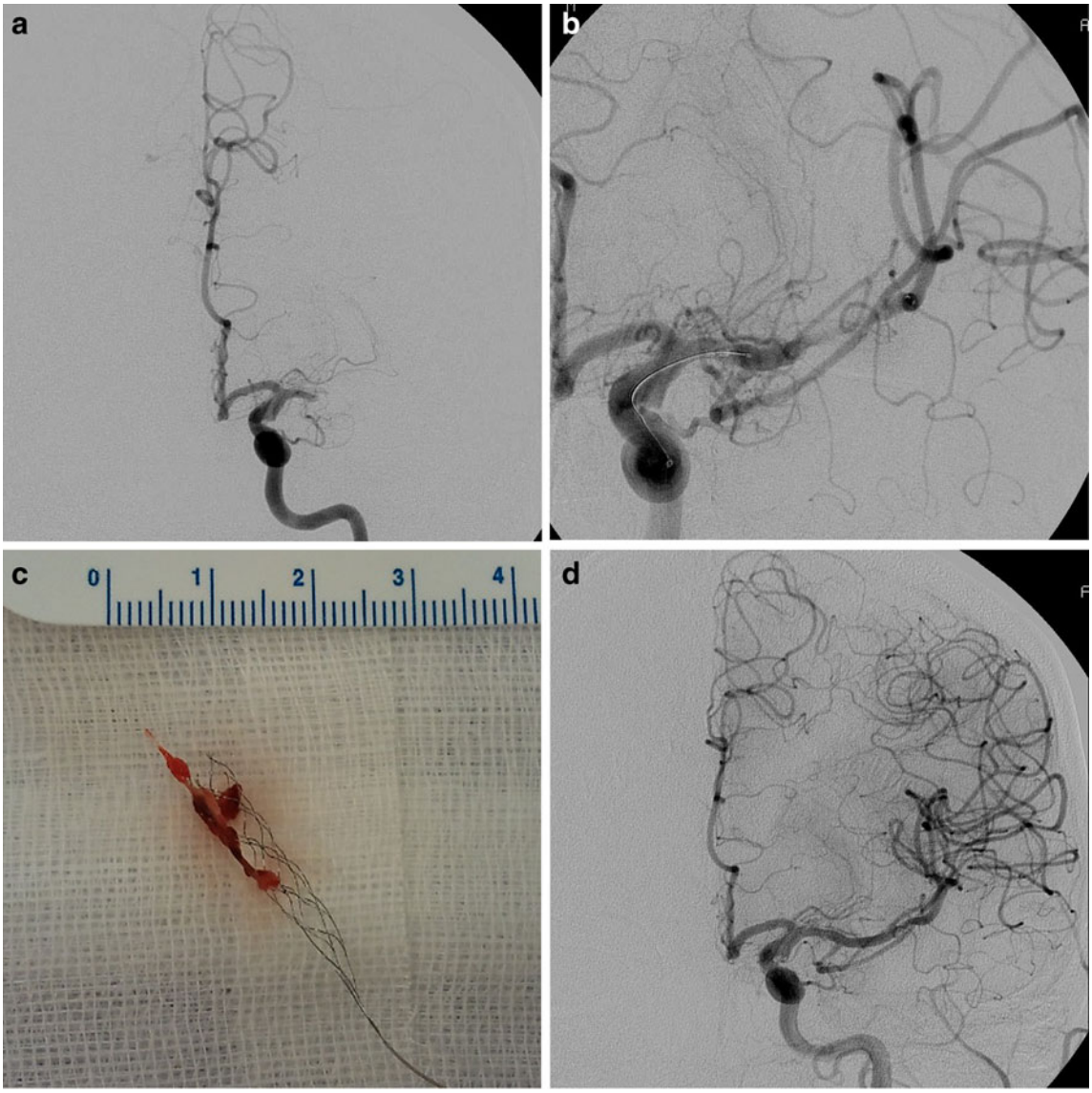

Fig. 2 **a** Initial angiogram of the left middle cerebral artery. **b** Temporary reperfusion flow after the deploying of the stent. **c** Captured thrombus with stent. **d** Final angiogram with complete recanalization and no distal emboli

microcatheter (prowler plus; Cordis, MA, Florida, USA) was advanced to the thrombus under the guidance of a microwire. A Solitaire stent was deployed over the whole length of the thrombus. Partial recanalization was observed immediately after stent deployment (Fig. 2b). The stent was carefully withdrawn together with the microcatheter. The whole clot was successfully removed with the stent (Fig. 2c). Complete recanalization of TICI grade 3 was achieved (Fig. 2d). No emboli were found in angiograms. The whole procedural time was 30 min from femoral puncture to recanalization. No intra-arterial fibrinolytic drug was used. The immediate post-procedural NIHSS score improved to 19. His 3-month mRS was 3. Histopathologic study of the retrieved clot revealed thrombi with laminations called lines of Zahn. Lines of Zahn represent pale platelet and fibrin deposits alternating with darker red blood cell-rich layers (Fig. 3).

Case 7

This 71-year-old male patient presented with stuporous mental status. The initial NIHSS score was 20. Diffusion MR showed no definite acute infarction, but, a decrease of perfusion at pons, midbrain, and Lt PCA territory was observed on perfusion MR. There was a large diffusion-perfusion mismatch. Basilar artery occlusion was found in MR angiograms and conventional angiography (Fig. 4a). IAT was decided. A microcatheter (prowler plus; Cordis,

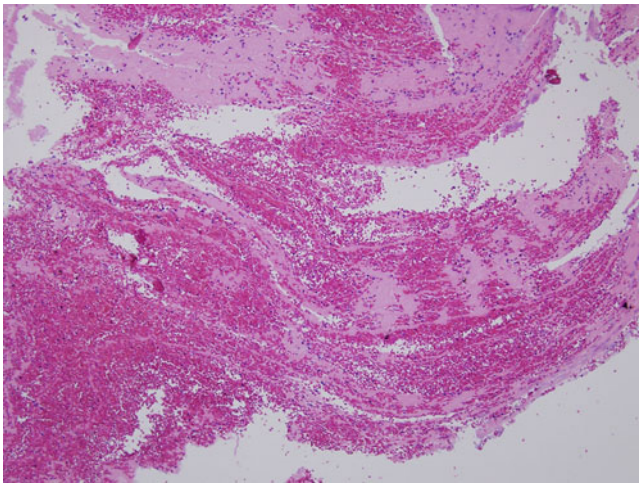

Fig. 3 Photomicrograph of captured thrombi. Note apparent laminations called lines of Zahn, which represent pale platelet and fibrin deposits alternating with darker red blood cell-rich layers like a cement and gravel (H&E, ×100)

MA, Florida, USA) was advanced to the thrombus under the guidance of a microwire. A Solitaire stent was deployed from right PCA to BT. Partial recanalization was observed immediately after stent deployment (Fig. 4b). The stent was carefully withdrawn together with the microcatheter. A small clot was retrieved. Main thrombi were still observed from BT to left PCA. The same procedure was repeated through left PCA (Fig. 4c). The remaining clot was successfully removed. Angiograms showed complete recanalization of TICI grade 3 (Fig. 4d). The whole procedural time was 34 min. No intra-arterial fibrinolytic was used. The immediate post-procedural NIHSS score improved to 0. His mRS was 0 at discharge and at 3-month follow-up.

Discussion

Mechanical thrombolysis has been introduced due to limitations of pharmacological IAT, which takes time to open the vessels and is often ineffective [1, 3, 9, 13]. Various mechanical devices have been used including wires, coils, balloons, stents, and capture-aspiration devices. Theoretically and practically, removing the occluding thrombi from the cerebral arteries is the fastest and most effective way to reopen occluded arteries. In this report, we present a new thrombectomy method using the Solitaire stent, which is a newly introduced self-expandable, detachable, and retrievable stent. The thrombectomy method presented in this article is technically simple and effective in reopening the vessels. In our series, advancing and retrieving the device was not difficult even in elderly patients with tortuous vessels.

The retrieved clots had an elastic consistency. They were not easily torn or broken. Histopathologic examinations showed that the thrombi had laminations composed of amorphous area of fibrin and alternating layers of red blood cell-rich parts. Two components appear to be mixed like cement and gravels. The histologic findings seem to show sticky characteristics of the thrombi. These characteristics of thrombi may explain why the whole thrombi were easily caught and removed by the stent system.

One of the advantages of this technique is the short recanalization time. The time for recanalization was 45 min or less in all cases except one, in which 70 min was taken. The initial flow restoration time, if partial recanalization of the occluded vessels were included, was shorter. As timely reperfusion is critical for brain survival [5, 6, 11], the present technique has an overt advantage. However, in our study, in spite of the short recanalization time, unfavorable outcomes at 90 days were observed in about a half of the cases. These results were similar to previously published literature [2, 12] and may be caused by the initial high NIHSS score.

Another advantage of this technique is that intra-arterial thrombolytic drugs are not often necessary, as our series shows. In our cases, fibrinolytics was only used for one case in which distal emboli developed. It could be a merit of this technique because symptomatic cerebral hemorrhage is a critical factor for bad outcomes in AIS patients [7, 14]. Less fibrinolytics are associated with less cerebral hemorrhage [10, 15, 16]. In addition, no stent is left in cerebral arteries, therefore we should not be concerned about early and delayed stent-related complications. The solitaire stent is a laser-cut, self-expanding, fully retrievable and electrically detachable nitinol device, and its open-slit, closed-cell design gives optimal radial force with good kink resistance and maximizes the opportunity for trapping the clot [8]. By trapping the clot, partial recanalization of the occluded vessels with temporary flow can be achieved in AIS. Compared to other thrombectomy devices, for example the Penumbra system (Penumbra Inc, Alameda, CA, USA), a microcatheter with a smaller profile is used for delivering the Solitaire stent, which allows easier navigation in tortuous cerebral vessels. Compared to Merci retriever (Concentric Medical, Mountain View, CA, USA), the basic architecture of stents (tubular structure, array of struts, and expanding nature) may provide a better chance for effective clot capture.

Like other mechanical thrombectomy techniques, the present method has the risk of fragmentation and distal migration of the thrombi. Distal emboli are usually difficult to resolve. In our series, we used a balloon guiding catheter to block the antegrade flow during clot retrieval. Additionally, we used a device to apply continuous negative pressure through the guiding catheter. This gun-like device is composed of 50-cc syringe, a tooth-like locking system, and a handle to control. This device is attached to a side hole of

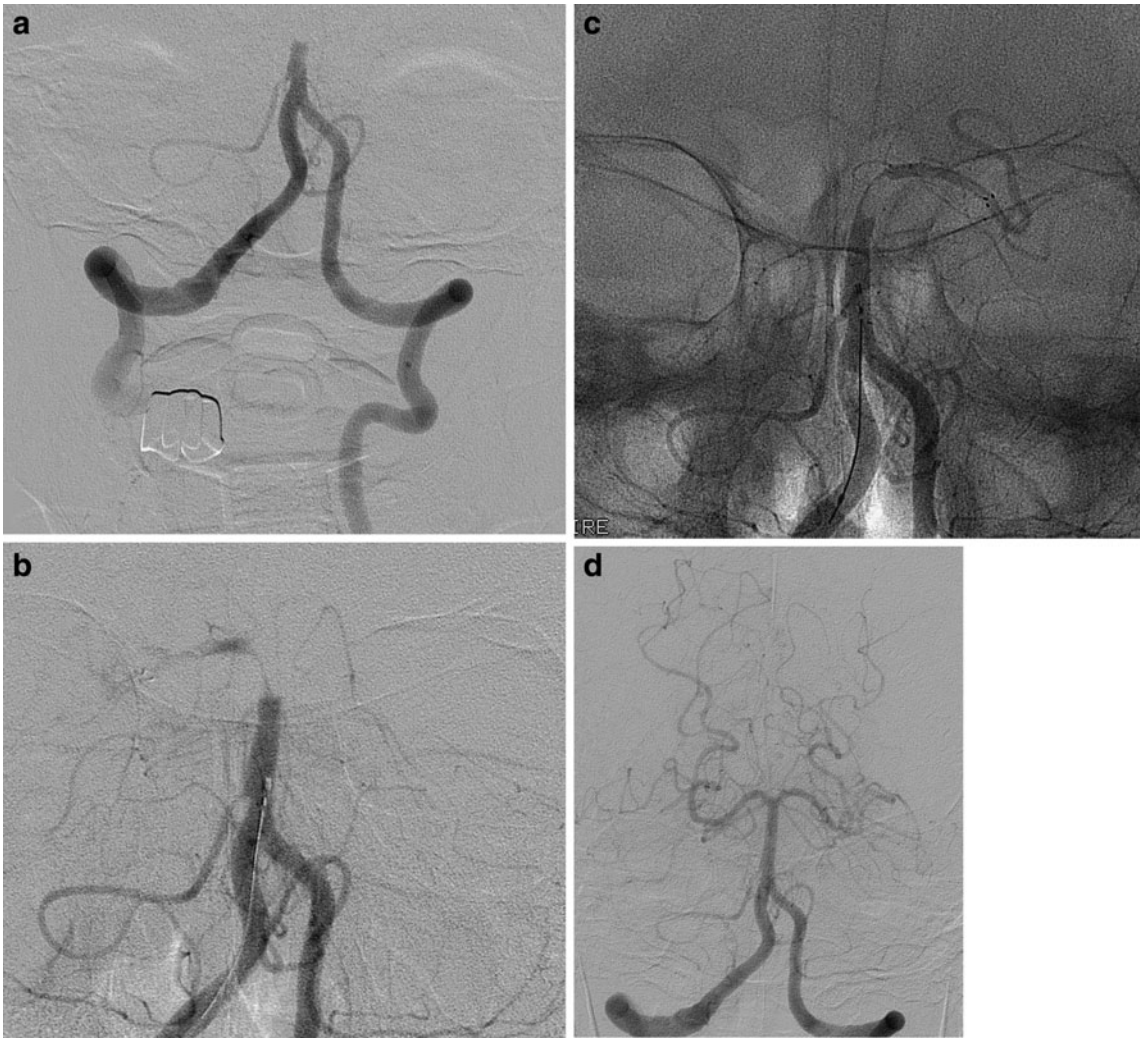

Fig. 4 **a** Initial angiogram of basilar artery. **b** Insufficient partial recanalization was observed after stent placement. **c** The stent was redeployed from BA to left PCA and certain flow restoration was observed after stent placement. **d** Final angiogram showed complete recanalization with no distal emboli

three-way connector of the guiding catheter. By pulling the gun handle, we are able to apply continuous negative suction pressure and maintain the pressure during the retrieval the stent and the clot with the locking system (Fig. 5).

Fig. 5 Photograph of proximal portion of balloon guide catheter set with Aspiration-gun (**a**) connected through three-way and in-deflator composed of three-way and 3-cc lock-syringe (**b**)

We do not believe that this stent has sufficient radial force to dilate preexisting tight stenosis from atherosclerosis, so it will not be recommendable to use this technique for thrombotic occlusion at the pre-existing arterial stenosis.

A prospective study including more patients is necessary to confirm the safety and effectiveness of this mechanical thrombectomy technique, but we believe that our series have shown the potentials of the retrieval thrombectomy method using the Solitaire stent system.

Conclusions

Retrieval thrombectomy technique with the Solitaire system is a simple, rapid, safe, and feasible thrombolytic method for AIS patients with large artery occlusion.

Conflicts of interest None.

References

1. (1995) Tissue plasminogen activator for acute ischemic stroke. The National Institute of Neurological Disorders and Stroke rt-PA Stroke Study Group. N Engl J Med 333:1581–1587
2. Castano C, Dorado L, Guerrero C, Millan M, Gomis M, Perez de la Ossa N, Castellanos M, Garcia MR, Domenech S, Davalos A (2010) Mechanical thrombectomy with the Solitaire AB device in large artery occlusions of the anterior circulation: a pilot study. Stroke 41:1836–1840
3. Furlan A, Higashida R, Wechsler L, Gent M, Rowley H, Kase C, Pessin M, Ahuja A, Callahan F, Clark WM, Silver F, Rivera F (1999) Intra-arterial prourokinase for acute ischemic stroke. The PROACT II study: a randomized controlled trial. Prolyse in Acute Cerebral Thromboembolism. JAMA 282:2003–2011
4. Henkes H, Flesser A, Brew S, Miloslavski E, Doerfler A, Felber S, Monstadt H, Kuehne D (2003) A novel microcatheter-delivered, highly-flexible and fully-retrievable stent, specifically designed for intracranial use. Technical note. Interv Neuroradiol 9:391–393
5. Jansen O, Schellinger P, Fiebach J, Hacke W, Sartor K (1999) Early recanalisation in acute ischaemic stroke saves tissue at risk defined by MRI. Lancet 353:2036–2037
6. Khatri P, Abruzzo T, Yeatts SD, Nichols C, Broderick JP, Tomsick TA (2009) Good clinical outcome after ischemic stroke with successful revascularization is time-dependent. Neurology 73:1066–1072
7. Khatri P, Wechsler LR, Broderick JP (2007) Intracranial hemorrhage associated with revascularization therapies. Stroke 38:431–440
8. Mpotsaris A, Bussmeyer M, Loehr C, Oelerich M, Buchner H, Weber W (2011) Mechanical thrombectomy in severe acute stroke: preliminary results of the Solitaire stent. J Neurol Neurosurg Psychiatry (in press)
9. Nogueira RG, Schwamm LH, Buonanno FS, Koroshetz WJ, Yoo AJ, Rabinov JD, Pryor JC, Hirsch JA (2008) Low-pressure balloon angioplasty with adjuvant pharmacological therapy in patients with acute ischemic stroke caused by intracranial arterial occlusions. Neuroradiology 50:331–340
10. Patel SC, Mody A (1999) Cerebral hemorrhagic complications of thrombolytic therapy. Prog Cardiovasc Dis 42:217–233
11. Rha JH, Saver JL (2007) The impact of recanalization on ischemic stroke outcome: a meta-analysis. Stroke 38:967–973
12. Roth C, Papanagiotou P, Behnke S, Walter S, Haass A, Becker C, Fassbender K, Politi M, Korner H, Romann MS, Reith W (2010) Stent-assisted mechanical recanalization for treatment of acute intracerebral artery occlusions. Stroke 41:2559–2567
13. Smith WS, Sung G, Saver J, Budzik R, Duckwiler G, Liebeskind DS, Lutsep HL, Rymer MM, Higashida RT, Starkman S, Gobin YP, Frei D, Grobelny T, Hellinger F, Huddle D, Kidwell C, Koroshetz W, Marks M, Nesbit G, Silverman IE (2008) Mechanical thrombectomy for acute ischemic stroke: final results of the Multi MERCI trial. Stroke 39:1205–1212
14. Vora NA, Gupta R, Thomas AJ, Horowitz MB, Tayal AH, Hammer MD, Uchino K, Wechsler LR, Jovin TG (2007) Factors predicting hemorrhagic complications after multimodal reperfusion therapy for acute ischemic stroke. AJNR Am J Neuroradiol 28:1391–1394
15. Yokogami K, Nakano S, Ohta H, Goya T, Wakisaka S (1996) Prediction of hemorrhagic complications after thrombolytic therapy for middle cerebral artery occlusion: value of pre- and post-therapeutic computed tomographic findings and angiographic occlusive site. Neurosurgery 39:1102–1107
16. Yoneyama T, Nakano S, Kawano H, Iseda T, Ikeda T, Goya T, Wakisaka S (2002) Combined direct percutaneous transluminal angioplasty and low-dose native tissue plasminogen activator therapy for acute embolic middle cerebral artery trunk occlusion. AJNR Am J Neuroradiol 23:277–281

Acta Neurochir (2011) 153:1633–1640
DOI 10.1007/s00701-011-1055-9

EXPERIMENTAL RESEARCH

The adverse effects of flow-diverter stent-like devices on the flow pattern of saccular intracranial aneurysm models: computational fluid dynamics study

Tamer Hassan · Yasser Mohamed Ahmed · Amr Ali Hassan

Received: 29 December 2010 / Accepted: 18 May 2011 / Published online: 8 June 2011

Abstract
Background Stent deployment across the aneurysmal neck has been established as one of the endovascular methods to treat intracranial aneurysms with or without coils.
Objective The purpose is to study the possible adverse effects of deployment of the new flow-diverter stent-like devices (FD) on the flow characteristics of saccular aneurysm models.
Methods Numerical simulations of the blood flow patterns in the artificial models of three aneurysms were studied. One model was designed without an FD stent, the second model with one FD stent, and the third model with two stents. Numerical simulation for incompressible laminar blood flow was conducted in the three artificial cerebral aneurysm models by means of computational fluid dynamics.
Results There was a noticeable increase in the values of the circumferential pressure distributed on the walls of the aneurysm after stent deployment; this led to an increase the tension of the aneurysm surface and was considered to be an adverse effect. This pressure increase was further aggravated by the deployment of another stent. However, there is a beneficial effect of using FD stents, translating into the reduction of the flow velocity inside the aneurysm and wall shear stress at the inflow zone. This reduction decreases further with the deployment of another stent.
Conclusion Aneurysms become tenser after the deployment of one flow-diverter stent and (more tense still) after after the deployment of another stent. This principle should be kept in mind when choosing which group of aneurysms is the best candidate for such a treatment strategy. This study recommends deploying several FD stents during endovascular procedures until complete arrest of the blood flow occurs during the procedure; otherwise, the aneurysm may become tenser and dangerous if a slow blood flow jet still exists inside it at the end of the procedure.

Keywords Computational fluid dynamics · Aneurysm · Flow diverters · Stent

T. Hassan (✉)
Department of Neurosurgery,
Alexandria University School of Medicine,
Elazarita, Shambeleon Street,
Alexandria, Egypt
e-mail: Neurocatheter@yahoo.com

T. Hassan
e-mail: Tamer.shihata@alexmed.edu.eg

Y. M. Ahmed
Department of Naval Architecture and Marine Engineering,
Faculty of Engineering, Alexandria University,
Alexandria, Egypt
e-mail: yahmed@alex.edu.eg

A. A. Hassan
Head of Marine Engineering Department,
College of Engineering, Arab Academy for Science,
Technology and Maritime Transport (AASTMT),
Alexandria, Egypt

Introduction

Blood flow dynamics are thought to be an important factor in the pathogenesis and treatment of cerebral aneurysms [3]. The application of stent implants for the treatment of intracranial aneurysms was first proposed in the early 1990s [11, 16, 17]. Stents have three potential mechanisms of action: they improve anatomical reconstruction of the parent artery, modify the flow across the neck of the aneurysm, and allow the possible biological repair of the aneurysm neck by endothelial overgrowth [16].

The early application of stent-assisted aneurysm therapy was primarily focused on geometric reconstruction of the parent artery through improved coil packing of the aneurysm to decrease the rate of coil compaction. A few clinical case reports, however, suggested that improved outcomes associated with the use of stents may be attributable to stent-induced modification of flow within and around the aneurysm [1, 5, 9].

A new generation of flexible self-expanding, microcatheter-delivered stent-like devices with high metal surface area coverage has emerged, which represents a fundamentally different approach to the endovascular treatment of brain aneurysms. These flow-diverting devices are designed to achieve aneurysm occlusion by the endoluminal reconstruction of the diseased segment of the parent artery. These devices promote the thrombosis of aneurysms without filling the aneurysm cavity by shifting the blood flow away from the aneurysmal neck. This approach can avoid recanalization because the stability of the device within the parent artery is able to establish a stable hemodynamic environment that is not subject to displacement by the pulsatile blood flow, as is the situation with endosaccular coils. Two flow diversion devices are available for patient use: the Silk device (Balt, Montmorency, France) and the Pipeline Embolic Device (ev3, Irvine, CA) [6, 7, 10, 13, 15].

The purpose of this study was to study the possible adverse effects of deployment of the new flow-diverter stent-like devices (FD) on the flow characteristics of a saccular aneurysm model.

Methods

Geometries and grids

Case A represents the aneurysmal model without an FD stent. **Case B** represents the aneurysmal model after the deployment of one FD stent. **Case C** represents the aneurysmal model after deployment of two FD stents. Because of the flexibility of the FD stents and for the purpose of facilitating the procedure of computational calculation accuracy, the stent itself was not entirely represented in the geometry. However, a piece of FD stent was designed and used to close the aneurysmal neck, as shown in Fig. 1. Simple 3D models were designed in which the parent artery diameter was 4 mm, the diameter of the

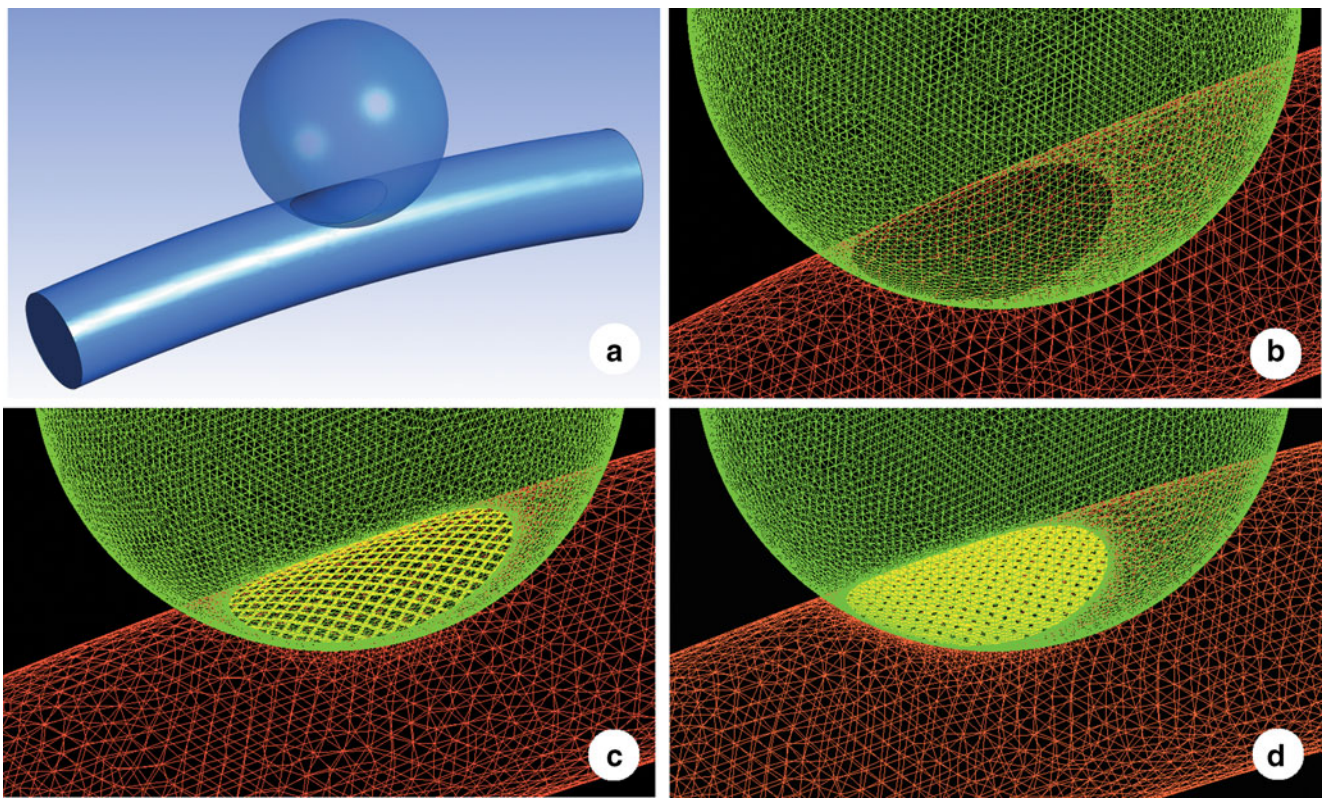

Fig. 1 **a** Schematic model of the unstructured tetrahedral grids representing the three saccular aneurysm models used in this study. **b Case A:** Saccular aneurysm without stent. **c Case B**: Saccular aneurysm after deployment of one flow-diverter stent. **d Case C**: Saccular aneurysm after deployment of two flow-diverter stents; stent struts are reduced 50% compared to case B

aneurysm 8 mm, and the diameter of the aneurysm neck 4 mm, as shown in Fig. 1a.

FD stents were designed similarly to pipeline FD devices; nearly 120 pores per inch were used in the stent design (Fig. 1c). The hole at the aneurysm neck is closed with a piece of pipeline stent that has approximately 120 pores per inch in case B. The area of each pore is nearly 0.02 mm^2. In case C, two FD stents were overlapped in such a way that the area of each pore of the final combined two stents was reduced to 50% of the single stent's pore size (Fig. 1d). Thus, the area of each pore is nearly 0.01 mm^2 in case C compared to 0.02 mm^2 in case B, as shown in Fig. 1d and c, respectively. This is quite similar to the real situation when a physician deploys two stents or even more within the aneurysm to overlap and narrow the stent struts.

Several computational grids were tested in this study to check the solution sensitivity, and ultimately the mesh chosen contained unstructured tetrahedral elements of 850,982, 1,261,931, and 1,503,637 for case A, B, and C, respectively (Fig. 1b, c and d).

Blood flow parameters and boundary conditions

The blood fluid was assumed to be Newtonian and incompressible, with a density of 1,060 kg/m^3 and a dynamic viscosity of 0.004 kg/m s. Blood was modeled to have a velocity $V = 0.8m/s$ at the inlet (left boundary in Fig. 1a). The blood flow was treated as steady laminar flow. A uniform flow condition at the inlet plane was applied. Vessel walls were assumed to be rigid, and no-slip boundary conditions were applied at the walls.

The governing equations for the blood flow are the continuity equation for mass conservation and the incompressible Navier-Stokes equations for momentum transport equations. These equations can be written in Cartesian form as follows:

$$\nabla \cdot \vec{u} = 0 \tag{1}$$

$$(\vec{u} \cdot \nabla)\vec{u} = -\frac{\nabla p}{\rho} + v\nabla^2\vec{u} \tag{2}$$

The governing equations for mass and momentum were discretized with a finite-volume method. The pressure was interpolated using the standard scheme, and the pressure-velocity coupling the SIMPLE (Semi-Implicit Methods for Pressure-Linked Equation) was used [19]. The residual absolute criteria were set to the value of 0.0001 for checking the convergence of the solution. The RANSE code Fluent was used in this study.

Results

The effect of the stent on the pressure distribution inside the aneurysm

The distribution of the pressure contours was studied at three different planes across the aneurysm, as described in Fig. 2: plane I at Y = −2 mm, plane II at Y = 0 (central plane), and plane III at Y = 2 mm across the aneurysm body for cases A, B, and C, as shown in Fig. 2.

Figure 3 shows the effect of using the FD stent on the pressure distribution inside and on the surface of the aneurysm. There is a noticeable increase in the values of the circumferential pressure distributed near the walls of the aneurysm at the three planes. The increase in the circumferential pressure distribution will increase the tension of the aneurysm surface, as can be noted from Fig. 3D1, D2, and D3.

Comparison among the previous three figures shows that the use of the flow diverter stent leads to spreading of relatively high pressure zones on the surface of the aneurysm. Pressure ranges from approximately 101,076 to $101{,}121\,Pa$ were affecting 100% of the surface of the aneurysm in case A; pressure of nearly 101,166 to 101,210 Pa affected the entire surface of the aneurysm in case B; and pressure of 101,272 to $101{,}359\,Pa$ affected the entire surface of the aneurysm in case C.

Figure 4a and b gives the values of the pressure at the three different planes and on the surface of the aneurysm for cases A, B, and C. The pressure values were calculated using the facet average formula (Eq. 3). The last graphs show that the use of an FD stent led to a noticeable increase in the values of the pressure at different planes. This pressure increase inside the aneurysm and on its surface was aggravated when the area of each pore had been

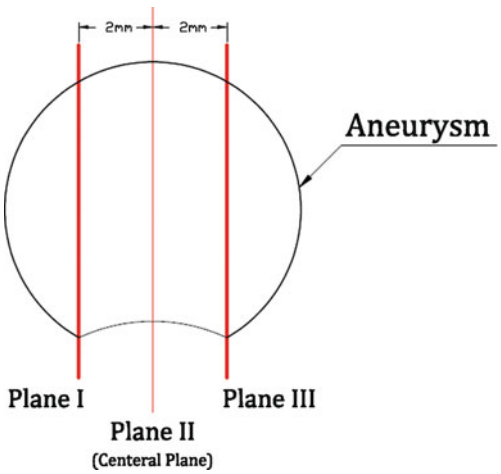

Fig. 2 Location of different longitudinal planes across the aneurysm (central plane at Y = 0)

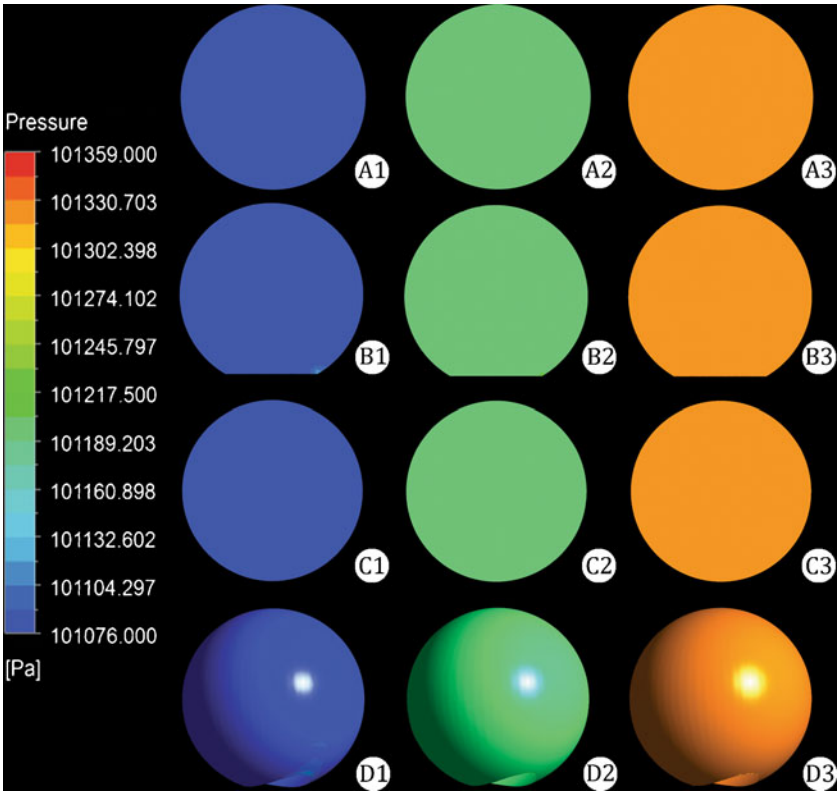

Fig. 3 Pressure distribution at the different longitudinal planes (plane I = A1, A2, A3; plane II = B1, B2, B3; plane III = C1, C2, C3). Figures A1, B1, C1, and D1 represent aneurysm pressure values before stent deployment. Figures A2, B2, C2, and D2 represent aneurysm pressure values after deployment of one stent. Figures A3, B3, C3, and D3 represent aneurysm pressure values after deployment of two stents. Note the progressive increase of intra-aneurysmal pressure [Pa] in the three planes in the non-stent situation; after deployment of one stent and of two stents: plane I: A3 > A2 > A1; plane II: B3 > B2 > B1; plane III: C3 > C2 > C1. Note the increase of the surface pressure of the aneurysm after deployment of one stent then of two stents: D3 > D2 > D1

reduced to 50% of its original area, as in case C. In conclusion, the above-mentioned results give a direct indication of the extent to which the surface of the aneurysm becomes tenser after the use of one FD stent or tenser with two stents.

$$\frac{\sum_{i=1}^{n} \phi_i}{n} \tag{3}$$

The effect of the stent on the velocity distribution inside the aneurysm

Figure 5 shows that the use of the FD stent leads to a reduction in the flow velocity inside the aneurysm. The FD stent dampened the region of high flow velocity at the base of the aneurysm and near the inflow zone (Fig. 5A1, A2, and A3). This effect translated into fluid-induced wall shear stress that also showed a reduction of its values at the aneurysmal inflow zone after FD stent deployment, as shown in (Fig. 5B1, B2, and B3). Such effects are considered to be the beneficial effects of stent deployment on aneurismal flow pattern. The deployment of a second FD stent will enhance this beneficial effect, further decreasing both the aneurysmal flow velocity and fluid-induced wall shear stress, as shown in Fig. 5.

Discussion

Flow diversion is undoubtedly a major advance in the treatment of cerebral aneurysms. Numerous impressive outcomes have been demonstrated for high-risk aneurysms for which there was no good treatment before the introduction of flow-diversion therapy. Currently, flow-diversion therapy seems to be best suited for aneurysms that are not amenable to coil therapy or surgical clipping, or that are likely to recur following coil therapy [6, 7, 10, 13, 15]. This is due to the impressive definite endoluminal reconstruction of the parent artery with a level of procedural safety analogous to that reported for the conventional coil-based endosaccular embolization of complex intracranial aneurysms. In addition, the high rate of complete aneurysm occlusion exceeds that of the traditionally reported series of

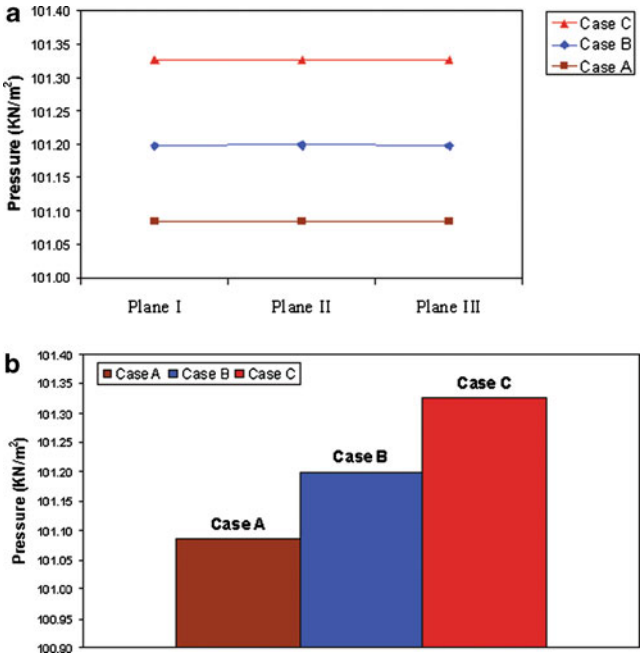

Fig. 4 Line and bar chart diagrams (**a**, **b**). Graph **A** demonstrates the increase of the pressure values in the situation of two stents compared to one stent and no stent situations at the three planes for case A, B, and C. Graph B shows the increase of the aneurysm surface pressure after the use of two FD stents compared to one stent and a non-stent situation

patients treated with conventional coil-based endosaccular embolization [4, 13, 14].

Several encouraging trials using FD stents have been reported in the literature; the Budapest experience [15] reported the treatment of 19 wide-neck aneurysms: 10 by implantation of an FD alone and 9 by a combination of FD and coils. Angiographic and clinical results were recorded immediately and at 6 months following treatment. Immediate angiographic occlusion was achieved in 4 and flow reduction in another 15 aneurysms. Angiography at 6 months demonstrated complete occlusion in 17 and partial filling in 1 of 18 patients. There was no difference in the results between coil-packed and unpacked aneurysms in their study. Using follow-up cross-sectional imaging, all giant aneurysms treated with FD alone were demonstrated to have involuted by 6 months. No post-procedure rupture of aneurysms occurred in their series.

Nelson et al. [13] reported the treatment of 31 intracranial aneurysms at different locations. FD placement was technically successful in 30 of 31 patients. Most aneurysms were treated with either one or two FDs. No post-procedure rupture of aneurysms occurred in their series. Lylyk et al. [10] reported their experiences in treating 63 intracranial aneurysms with the FD. Small, large, and giant wide-necked aneurysms were included. A total of 72 FDs were used. Treatment was achieved with a single PED in 44 aneurysms, with 2 overlapping PEDs in 17 aneurysms and with 3 overlapping PEDs in 2 aneurysms. Complete angiographic occlusion was achieved in 56%, 93%, and 95% of aneurysms at 3, 6, and 12 months, respectively. No major complications (stroke or death) were encountered during the study period.

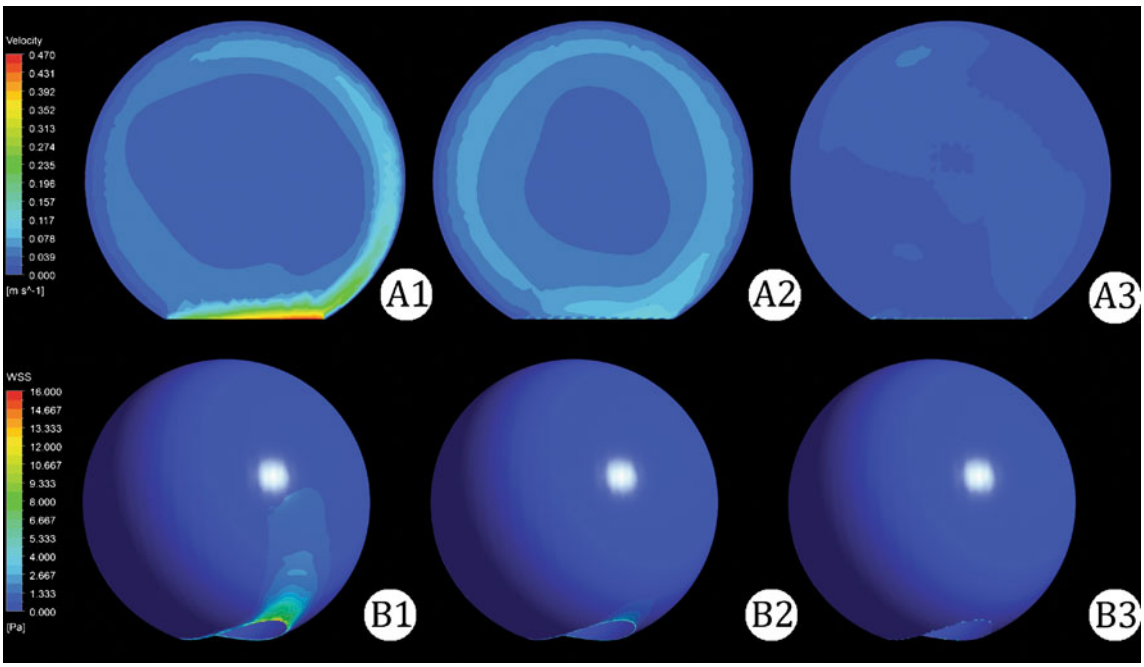

Fig. 5 Velocity contours (m/s) (A1, A2, A3). Wall shear stresses [Pa] (B1, B2, B3). Figures A1 and B1 represent values before stent deployment. Figures A2 and B2 represent values after deployment of one stent. Figures A3 and B3) represent values after deployment of two stents. Note the decrease of velocity contours and wall shear stress values after stent deployment (A3 < A2 < A1, B3 < B2 < B1)

Although the above three trials and studies are very encouraging, Turowski et al. [18] reported early fatal hemorrhage after endovascular treatment of a large paraopthalmic aneurysm with a flow-diverter (SILK) stent in a 69-year-old woman presenting with short-lasting recent episodes of visual impairment.

Kulcsar et al. [8] reported 13 cases of delayed postprocedural aneurysm rupture. There were ten internal carotid and three basilar artery aneurysms. A single FD was used for all saccular aneurysms, while fusiform lesions were treated by using multiple devices. Ten patients developed early aneurysm rupture after FD treatment (range, 2–48 days); in three patients, rupture occurred 3–5 months after treatment. In all cases, most of the aneurysm cavity was thrombosed before rupture.

This simulation study, although it has its limitations, emphasizes the increase of intra-aneurysmal pressure after single stent deployment. In many cases, FD stents do not immediately exclude the aneurysm mechanically from the circulation upon their deployment, but they rely on the hemodynamic environment created to initiate thrombosis and ultimately seal the aneurysm. This process takes time, so the immediate elimination of the aneurysm cannot be expected, unlike the mechanical elimination with coils. Until the healing of the aneurysm has been completed, the aneurysm wall is subject to the stresses and strains imposed by the pulsatile arterial circulation with a higher intra-aneurysmal pressure situation imposed by the FD stent. The reduction of blood flow does not equate to a reduction of the pressures experienced by the aneurysm wall, but to an increase, leaving a potentially dangerous time during which the weak wall may be broken by the sudden new hemodynamic changes represented by high intra-aneurysmal pressures. The present study raises concern about a potential period when aneurysm wall tensions are increased after placement of a flow diverter before the process of thrombosis occurs. In that period, the existence of intra-aneurysmal coils to strengthen the aneurysm wall may be important.

In all the cases reported by the Kulscar group [8], they implemented one stent in their work probably because of the very expensive stent costs or because physicians were used to depending on spontaneous postoperative aneurysmal thrombosis on future follow-up, as previously reported in the above studies [10, 13, 15]. They also reported that the inflow jet identified before device implantation was still present and clearly identifiable after device implantation in 11 cases.

The present study implemented the use of an ideal model of a small aneurysm on uniform arteries with a gentle curve. Aneurysms with this ideal shape usually do not rupture. The present aneurysm model was not also subjected to the usual hemodynamic stresses created because of the geometry of the parent artery, such as location at the bifurcation or at a large curvature. The present study aimed to examine the effect of deploying one or more FD stents on the fluid dynamics of an ideal aneurysm, trying to omit all other variables that could significantly influence the hemodynamic flow.

It seems that deployment of only one stent leaving a persistent flow jet inside the aneurysm at the end of the procedure is a dangerous situation with the 'creation of a tenser aneurysm.' This could help us to explain the rupture events in the above-mentioned cases [8]. This situation is probably not constant in all aneurysms, as some of them may get complete arrest of the inflow after one stent deployment, leaving the aneurysm in a probably safe situation after the procedure. Deployment of another stent will further increase the intra-aneurysmal pressure if the inflow jet still exists, even if it is slow, as shown in Figs. 3 and 5. Probably the safest situation for the physician is to continue with the deployment of several FD stents until the inflow jet disappears completely during the procedure, leaving the aneurysm "flow free."

Although the deployment of several FD stents has been used in the clinical series mentioned before, and although it looks computationally feasible, it is not always applicable in reality. In case of the existence of important side branches, such as the anterior choroidal artery, basilar artery perforators, SCA, and AICA, the deployment of several stents may not always be applicable. Careful selection of the treatment modality in combination with coils should be kept in mind to weigh the risks to the patient against the benefits. Coil deployment against the inflow zone or the ruptured area may decrease the risk of postoperative rupture. In this situation, CFD studies to identify the ruptured aneurysmal zone in a patient-specific case-by-case computational approach would be very helpful. We physicians should also be worried about the increase in pressure symptoms after stent deployment, such as the emergence of third nerve palsy after treating non-ruptured posterior communicating arteries with an FD stent (personal experience).

The peculiar increase of the intra-aneurysmal pressure can be explained with the aid of Bernoulli's equation (Eq. 4) [12, 20], which is a very powerful tool in fluid mechanics. Bernoulli's equation describes the relationship among pressure (p), velocity (V), and elevation (z) along a streamline in a fluid flow. For many real cases where the conditions required for satisfying Bernoulli's equation approximately exist, the equation gives very good results [20].

$$p + \frac{1}{2}\rho V^2 + \rho g z = \text{constant along streamline} \tag{4}$$

If the assumptions of Bernoulli's equation are valid, Eq. 4 can be applied along the 3D streamline ABC that

passes through points 1 and 2 (one point is in the artery, and the other one is inside the aneurysm), as shown in Fig. 6.

$$p_1 + \frac{1}{2}\rho V_1^2 + \rho g z_1 = p_2 + \frac{1}{2}\rho V_2^2 + \rho g z_2 \quad (5)$$

Where, $z_1 \approx z_2$ due to the small distance between points 1 and 2. Therefore,

$$p_1 + \frac{1}{2}\rho V_1^2 = p_2 + \frac{1}{2}\rho V_2^2 \quad (6)$$

$$p_2 = \left(p_1 + \frac{1}{2}\rho V_1^2\right) - \frac{1}{2}\rho V_2^2 \quad (7)$$

The final equation states that at the same values of p_1 and V_1 at point 1 (for case A and case B the values of p_1 and V_1 at point 1 are the same), the pressure at point 2, p_2 will be increased with the decrease of the velocity at point 2, V_2, and vice versa. This principal can be applied directly to the current case to explain the effect of the FD stent on the pressure inside the aneurysm. The existence of the flow-diverter stent will cause a reduction in the blood flow velocity inside the aneurysm, as shown before; hence

$$V_2(\text{before stent}) > V_2(\text{after stent}) \quad (8)$$

According to Eq. 7 and the inequality in (8), this will lead directly to an increase in the value of the pressure p_2 inside the aneurysm and near its surface as the value of V_2 decreases. Finally, the aneurysm becomes tenser as a direct effect of the stent deployment on the blood flow.

Cebral et al. [2] used a computational fluid dynamics model to generate results that suggest that FDs, in selected cases, may induce dramatic elevations of intra-aneurysmal pressure leading to post-procedural rupture. They present seven aneurysms, three with postprocedural rupture and four that were treated successfully. The selected aneurysms and arterial segments, along with assumptions about flow through the segments, constant pressure at the outlet of the segments, and rigid arterial walls, were evaluated within a CFD model. Using this model, their calculations showed

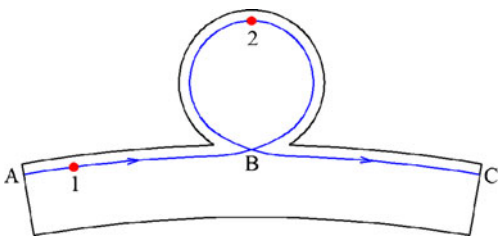

Fig. 6 Streamline used to explain Bernoulli's equation. The intersection at point B is an apparent intersection due to the projection, and there is no intersection in reality

that all three aneurysms that went on to rupture after FD demonstrated severe increases in intra-aneurysmal pressure (20 mmHg) after treatment, whereas those aneurysms that did not rupture after FD did not exhibit such dramatic pressure rises (3 mmHg). The present study agrees in principal with Cebral et al. in terms of the noticeable increase of intra-aneurysmal pressure after FD stent deployment. However, the present study cannot lead to recommending any quantitative measurements of pressures at the present time, even if we are studying patient-specific models. Cebral et al. compared the aneurysm geometries of three post-treatment ruptured narrow-necked giant aneurysms, whose necks were located on a pronounced curvature, with another four unruptured wide-necked aneurysms, three of which were small (less than 10 mm), and their necks were located at gentler curvatures. This comparison is not fair considering their mentioned study limitations, such as the absence of elastic wall criteria (solid wall boundary condition) and the lack of representations of patient-specific physiological pressure data.

In addition, FDs are meshed stents that change length and pore sizes, depending on the size of the vessel into which they are deployed. The operator can modify the porosity of these stents by varying the length of deployment and by using calculated overlaps at specific regions of the FD construct. The model of "whatever is ideal or patient-specific" for deploying one or two FDs so that the stent struts of one bisect the tines of the other is far from achievable in a real-life scenario, and the stent pore sizes can never be simulated like in reality because the resolution of angiography at the present time does not allow us to visualize the stent struts of the single or multiple stents, and the deployment mechanisms of current FDs are not precise enough for this. For these reasons, we cannot depend on any quantitative measurements of pressures at the present time when studying patient-specific models. Because of the above limitations, the present study has moved away from patient-specific aneurysm geometries to idealized geometries and FD models.

The current study also has several limitations common to many CFD hemodynamic analyses that should be considered when evaluating the results. These include the following: the assumption of rigid wall boundaries, Newtonian blood properties, and steady blood flow. Rigid wall boundaries may overestimate the pressure gradient values; however, comparing the relative increase of the pressure gradient among the three geometries may have potential value as an adverse effect on aneurysmal flow and should be kept in mind before conducting endovascular procedures. The steady blood flow simulation and the use of artificial aneurysm models have been utilized in this study to focus on the flow phenomena before and after deployment of the FD stents. The results and the analysis of the current study show that the existence of FD stents will cause a noticeable increase in the

aneurysm surface pressure comparing the three geometries, and this phenomenon will occur at any time during the cardiac cycle. Therefore, the use of the steady flow simulation in this study was satisfactory.

Conclusion

Aneurysms become tenser after the deployment of one flow-diverter stent and become tenser after the deployment of another stent until complete inflow jet arrest occurs. This principle should be kept in mind to choose which group of aneurysms is the best candidate for such a treatment strategy. Aneurysms presenting with rupture and mass effect may be safely excluded from this treatment modality unless used in combination with coils.

This CFD study recommends the safe deployment of several FD stents during endovascular procedures until the complete arrest of the blood flow occurs at the time of the procedure; otherwise, the aneurysm will be left dangerously tenser if a slow blood flow jet still exists inside it at the end of the endovascular treatment procedure.

Acknowledgment We acknowledge Mr. Mohamed Abdul-Aziz, engineer, for his substantial help with preparing the figures.

Conflicts of interest None.

References

1. Augsburger L, Farhat M, Reymond P, Fonck E, Kulcsar Z, Stergiopulos N, Rüfenacht DA (2009) Effect of flow diverter porosity on intraaneurysmal blood flow. Klin Neuroradiol 19:204–214
2. Cebral JR, Mut F, Raschi M, Scrivano E, Ceratto R, Lylyk P, Putman CM (2011) Aneurysm rupture following treatment with flow-diverting stents: computational hemodynamics analysis of treatment. AJNR Am J Neuroradiol 32(1):27–33
3. Doenitz C, Schebesch KM, Zoephel R, Brawanski A (2010) A mechanism for the rapid development of intracranial aneurysms: a case study. Neurosurgery 67:1213–1221
4. Ferns SP, Sprengers ME, van Rooij WJ, Rinkel GJ, van Rijn JC, Bipat S, Sluzewski M, Majoie CB (2009) Coiling of intracranial aneurysms: a systematic review on initial occlusion and reopening and retreatment rates. Stroke 40:e523–e529
5. Fiorella D, Albuquerque FC, Deshmukh VR, McDougall CG (2005) Usefulness of the Neuroform stent for the treatment of cerebral aneurysms: results at initial (3–6-mo) follow-up. Neurosurgery 56:1191–1201, discussion 1201–02
6. Fiorella D, Kelly ME, Albuquerque FC, Nelson PK (2009) Curative reconstruction of a giant midbasilar trunk aneurysm with the Pipeline embolization device. Neurosurgery 64:212–217, discussion 217
7. Fiorella D, Woo HH, Albuquerque FC, Nelson PK (2008) Definitive reconstruction of circumferential, fusiform intracranial aneurysms with the Pipeline embolization device. Neurosurgery 62:1115–1120, discussion 1120–21
8. Kulcsár Z, Houdart E, Bonafe A, Parker G, Millar J, Goddard AJ, Renowden S, Gál G, Turowski B, Mitchell K, Gray F, Rodriguez M, van den Berg R, Gruber A, Desal H, Wanke I, Rüfenacht DA (2011) Intra-aneurysmal thrombosis as a possible cause of delayed aneurysm rupture after flow-diversion treatment. AJNR Am J Neuroradiol 32(1):20–25
9. Lylyk P, Ferrario A, Pasbon B, Miranda C, Doroszuk G (2005) Buenos Aires experience with the Neuroform self-expanding stent for the treatment of intracranial aneurysms. J Neurosurg 102:235–241
10. Lylyk P, Miranda C, Ceratto R, Ferrario A, Scrivano E, Luna HR, Berez AL, Tran Q, Nelson PK, Fiorella D (2009) Curative endovascular reconstruction of cerebral aneurysms with the Pipeline embolization device: the Buenos Aires experience. Neurosurgery 64:632–642
11. Massoud TF, Turjman F, Ji C, Guglielmi G, Viñuela F, Robert J (1995) Endovascular treatment of fusiform aneurysms with stents and coils: technical feasibility in a swine model. AJNR Am J Neuroradiol 16:1953–1963
12. Munson BR, Young DF, Okiishi TH (2006) Fundamenals of fluid mechanics", Fifth Edition, Wiley, 2006
13. Nelson PK, Lylyk P, Szikora I, Wetzel SG, Wanke I, Fiorella D (2011) The Pipeline embolization device for the intracranial treatment of aneurysms trial. AJNR Am J Neuroradiol 32(1):34–40
14. Raymond J, Guilbert F, Weill A, Georganos SA, Juravsky L, Lambert A, Lamoureux J, Chagnon M, Roy D (2003) Long-term angiographic recurrences after selective endovascular treatment of aneurysms with detachable coils. Stroke 34:1398–1403
15. Szikora I, Berentei Z, Kulcsar Z, Marosfoi M, Vajda ZS, Lee W, Berez A, Nelson PK (2010) Treatment of intracranial aneurysms by functional reconstruction of the parent artery: the Budapest experience with the Pipeline embolization device. AJNR Am J Neuroradiol 31:1139–1147
16. Szikora I, Guterman LR, Wells KM, Hopkins LN (1994) Combined use of stents and coils to treat experimental wide-necked carotid aneurysms: preliminary results. AJNR Am J Neuroradiol 15:1091–1102
17. Turjman F, Massoud TF, Ji C, Guglielmi G, Viñuela F, Robert J (1994) Combined stent implantation and endosaccular coil placement for treatment of experimental wide-necked aneurysms: a feasibility study in swine. AJNR Am J Neuroradiol 15:1087–1090
18. Turowski B, Macht S, Kulcsar Z, Hänggi D, Stummer W (2010) Early fatal hemorrhage after endovascular cerebral aneurysm treatment with a flow diverter (Silk-Stent): do we need to rethink our concepts? Neuroradiology 53(1):37–41
19. Versteeg HK, Malalasekera W (1995) An Introduction to Computational Fluid Dynamics – The Finite Volume Method", Longman Group Ltd.
20. White FM, "Fluid Mechanics", Fourth Edition (1999) WCB/McGraw-Hill

Acta Neurochir (2011) 153:1641–1644
DOI 10.1007/s00701-011-1018-1

CLINICAL ARTICLE

Near-infrared indocyanine green videoangiography for assessment of carotid endarterectomy

Sei Haga · Shinji Nagata · Ai Uka · Yojiro Akagi · Yasuhiro Hamada · Tadahisa Shono

Received: 10 March 2011 / Accepted: 1 April 2011 / Published online: 17 April 2011

Abstract
Background Intraoperative fluorescence angiography with indocyanine green (ICG) as a tracer has recently been introduced as a novel technique for neurosurgery. We evaluated the feasibility and efficacy of near-infrared (NIR) indocyanine green (ICG) videoangiography for patients undergoing carotid endarterectomy (CEA).
Methods Sixty patients (7 females, 53 males; mean age, 71.8 years) undergoing CEA for severe stenosis of the internal carotid artery (ICA) were included. During CEA, microscope-integrated intraoperative NIR videoangiographic recording was performed before and after the excision of the plaque and closure of the ICA.
Results During the 60 CEA procedures, 60 consecutive ICG videoangiographic examinations were performed. All patients tolerated the intravenous injection of ICG well with no adverse effects. The videoangiographic study showed the blood stream of the ICA in all cases and the position of plaque in some cases.
Conclusion Microscope-based ICG videoangiography is simple, and provides reliable and rapid intraoperative assessment of CEA.

Keywords Angiography · Carotid endarterectomy · Indocyanine green · Fluorosence · Near-infrared

S. Haga (✉) · S. Nagata · A. Uka · Y. Akagi · Y. Hamada · T. Shono
Department of Neurosurgery, Clinical Research Institute, National Hospital Organization, Kyushu Medical Center, 1-8-1 Jigyohama, Chuo-ku, Fukuoka 810–8563, Japan
e-mail: sei.haga@kyumed.jp

Introduction

Microscope-integrated intraoperative near-infrared (NIR) indocyanine green (ICG) videoangiography has been used to visualize the blood stream in vessels in neurosurgical fields, and is particularly useful for observing the patency of bypass surgery or complete aneurysm clipping [3, 7]. However, there are few reports on its use in carotid endarterectomy (CEA) [1, 6]. The aim of this study was to evaluate whether ICG videoangiography is suitable for surgical procedures involving the extracranial internal carotid artery and to improve the safety of CEA.

Methods

Sixty consecutive patients (53 males, 7 females; age range, 59–88 years; mean age, 71.8 years) receiving CEA participated in the 18-month study at our institute (Table 1). All patients were collected prospectively and evaluated retrospectively to determine the feasibility and utility of NIR-ICG videoangiography. Written informed consent was obtained from all patients to perform intravenous ICG videoangiography before CEA.

During CEA, NIR-ICG videoangiographic recording was performed before and after the excision of the plaque and closure of the ICA. Indocyanine green (Diagnogreen®, Daichi-Sankyo, Tokyo, Japan) was administered intravenously as a bolus at 12.5 mg to give an approximate 0.25 mg/kg dose (25 mg dissolved in 5 ml of water). Following intravenous injection, ICG binds mainly to circulating globulins and remains intravascular. After binding to globulins it becomes an NIR fluorescent dye with an 805-nm absorption and an 835-nm emission peak.

Table 1 Characteristics of patients undergoing CEA

Gender	53 males	7 females
Age	59–88 years	Mean, 71.8 years
% stenosis of ICA (NASCET)	60–98%	Mean, 76%
ICG videoangiography		
Pre CEA	22 cases	
Detection of plaque	Good: 7 cases	Poor: 15 cases
Severe calcification on 3DCTA	6 cases	
Post CEA	60 cases	
Detection of blood stream	Good: 60 cases	Poor: 0 cases

Abbreviations: CEA, carotid endarterectomy; ICA, internal carotid artery; 3DCTA, three-dimensional computer tomographic angiography

At these wavelengths, absorption due to endogenous chromospheres is low. ICG is excreted by the liver and has a plasma half-life of 2–4 min. ICG fluorescence is induced when the dye enters the vessels in the operative field illuminated by NIR light. The fluorescence is specifically recorded by the NIR instrument (Infrared 800 module; Carl Zeiss Surgical GmbH, Oberkochen, Germany) integrated in the surgical microscope (OPMI Pentero; Carl Zeiss Surgical GmbH, Oberkochen, Germany).

Results

During the 60 CEA procedures, 60 consecutive ICG videoangiographic examinations were performed. Twenty-two videoangiographic examinations were performed before arteriotomy (Table 1). All patients tolerated the intravenous injection of ICG, and no side effects or allergic reactions were observed. Following ICG injection, blood flow within the ICA was rapidly visualized with a latency of 10–20 s followed by a subsequent contrast enhancement of the venous system. ICG videoangiography was characterized by high image quality and spatial resolution, which allowed the surgical team to judge the anatomical relationships and the blood stream (Fig. 1). In some cases, ICG videoangiography showed the exact location of stenosis before arteriotomy. Definitive lack of fluorescence was seen in 7 of 22 cases (Fig. 2; Table 1). Severe calcification of the plaque did not allow the exact location of the stenosis because of spontaneous fluorescence (Fig. 3a and b). At the distal end, ICA patency was seen with no stenosis in all cases.

At the end of the procedure the ICA was demonstrated to be patent on ICG videoangiography by homogenous enhancement following excision of the plaque (Fig. 1). The videoangiographic study could be repeated following clearance of the ICG. Repeated injections did not pose any problems with respect to patient safety and image quality. The ICG videoangiography also showed a sufficient blood stream after the closure of the artery using a Dacron patch (Hemashield ®, Meadox Medical, Oakland, NJ) (Fig. 3c, d).

ICG videoangiography proved to be an easy-to-use and practical procedure, adding no more than 5 min to the regular operation time. For each case, postoperative CT angiography was comparable to the data obtained from the perioperative videography with good patency of the ICA. In the 30 days following CEA, cerebrovascular and cardiovascular events were not observed.

Discussion

CEA is a safe and durable treatment that has been shown to prevent ipsilateral stroke [2]. Efficacy is achieved only if

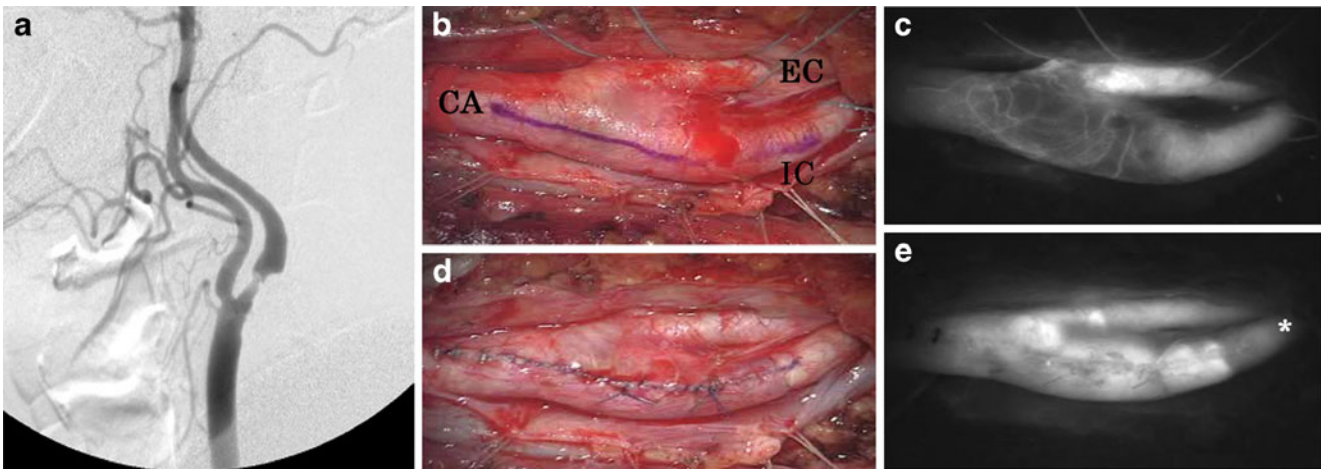

Fig. 1 Carotid endarterectomy (CEA) with ICG videoangiography. **a** Preoperative lateral digital subtraction angiography (DSA) shows IC stenosis (NASCET 81%). **b** Intraoperative photograph of CEA before arteriotomy. **c** ICG videoangiography before arteriotomy. Arrow shows the defect of signal as existence of plaque. **d** Intraoperative photograph of CEA after arteriotomy. **e** ICG videoangiography after arteriotomy. Asterisk shows the patency of the distal IC lumen

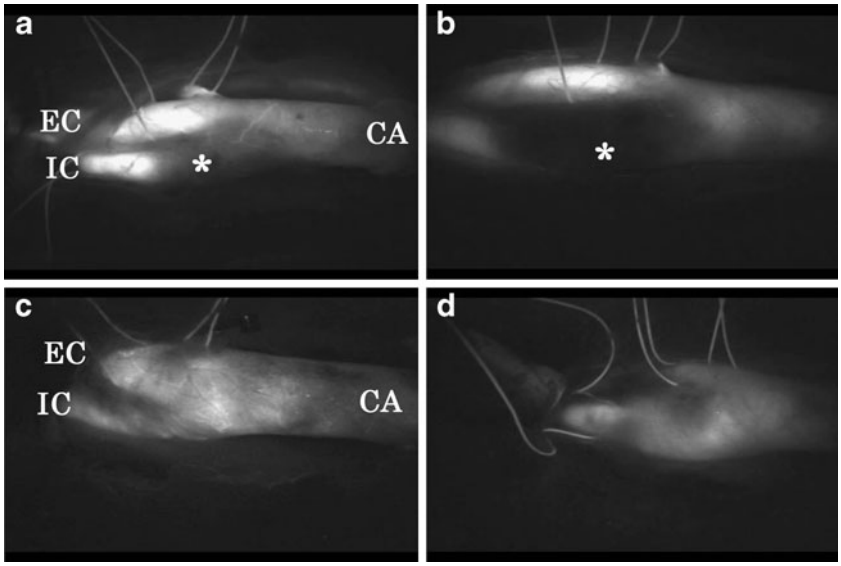

Fig. 2 Representative cases with preoperative ICG videoangiography. **a** and **b** Cases with a definitive lack of signals of plaque existence. Asterisk shows plaques. **c** and **d** Cases with signals present

surgical morbidity is sufficiently low. Given the fact that safe, effective treatment is available, safe surgical techniques are required. ICG videoangiography is a useful tool for EC-IC bypass surgery or the surgical clipping of intracranial aneurysms. It provides rapid high-quality online information on graft patency, or it can improve the rate of complete occlusion by decreasing the probability of inadvertently leaving a neck remnant [3, 7]. Nevertheless, there are a few reports on the application of ICG videoangiography during CEA [1, 6].

In the present study, ICG videoangiography provided a reliable intraoperative assessment of the blood stream and plaques during CEA. In some cases, ICG videoangiography showed the exact plaque location. Thus, ICG videoangiography represents an ideal high resolution imaging technique to determine the excision range of the plaque without distal embolism and to improve surgical results in CEA. Although there are some reports that ICG videoangiography could not show the ICA blood stream because of the thickness of the arterial wall or calcification [6], in those studies ICG was administered intravenously as a bolus at the minimum dose (approximately 2.5–5 mg). Using ICG at a 12.5 mg bolus (approximately 0.25 mg/kg), we were able to assess the ICA blood stream despite arteriosclerosis or calcification. In one case with severe calcification of the plaque, however, ICG videoangiography did not allow the exact location of the stenosis because of spontaneous fluorescence. Near-infrared light penetrates further into tissue than visible light, and as near-infrared light is scattered more by highly calcified tissues, spontaneous fluorescence can occur [4, 5].

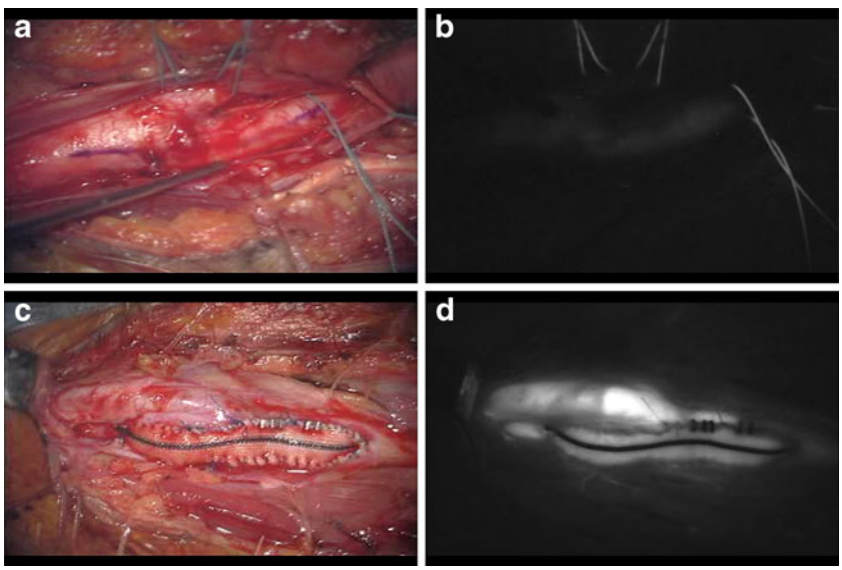

Fig. 3 **a** Intraoperative photograph of CEA with significant calcified plaque. **b** Videoangiography before injection of ICG. Spontaneous fluorescence is seen. **c** Intraoperative photograph of CEA with Dacron patch (Hemashield ®). **d** ICG videoangiography shows sufficient blood stream through the Dacron patch

Conclusions

ICG videoangiography is a useful tool for the intraoperative evaluation of CEA. It is easy to handle and provides rapid high-quality real-time information on the blood stream of the cervical ICA. Furthermore, ICG videoangiography allowed intraoperative evaluation of the blood stream and localization of the site of plaques, thus allowing for safe CEA surgery without distal embolism. Thus, ICG videoangiography is a suitable technique to improve technical and functional outcomes following CEA surgery.

Conflicts of interest None.

References

1. Kohno K, Uka A, Mori M, Haga S, Hamada Y, Nagata S, Yasaka M, Okada Y (2010) Usefulness of video angiography using indocyanine green for carotid endarterectomy (in Japanese). Nosinkeigeka-sokuho 20:328–332
2. Moore W, Barnett C, Beebe H, Bernstein EF, Brener BJ, Brott T, Caplan LR, Day A, Goldstone J, Hobson RW, Kempczinski RF, Matchar DB, Mayberg MR, Nicolaides AN, Norris JW, Ricotta JJ, Robertson JT, Rutherford RB, Thomas D, Toole JF, Trout HH, Wiebers DO (1995) Guidelines for carotid endarterectomy. Stroke 26:188–201
3. Raabe A, Nakaji P, Beck J, Kim LJ, Hsu FPK, Kamerman JD, Seifert V, Spetzler RF (2005) Prospective evaluation of surgical microscope integrated intraoperative near-infrared indocyanine green videoangiography during aneurysm surgery. J Neurosurg 103:982–989
4. Rolfe P (2000) In vivo near-infrared spectroscopy. Ann Rev Biomed Eng 2:715–754
5. Tanaka S, Kakio M, Yamakoshi K (2008) Non-destructive optical monitoring for calcification of tissue-engineered bone in vitro. J Biomed Sci Eng 3:332–342
6. Watanabe H, Ogami S, Hisakado Y (2009) Indocyanine green videoangiography in neurosurgical field (in Japanese). Nosinkeigeka-sokuho 37:104–108
7. Woitzik J, Horn P, Vajkoczy P, Schmiedek P (2005) Intraoperative control of extracranial intracranial bypass patency by near-infrared indocyanine green videoangiography. J Neurosurg 102:692–698

Comment

This is a novel and excellent contribution that will significantly enhance our technique for evaluating carotid reconstruction cases. The authors address two key technical questions that are crucial to obtaining excellent results in CEA: first, the distal extent of the atheromatous plaque, so that adequate distal exposure can always be assured, and second, the technical adequacy of the repair once the vessel has been closed, looking for residual stenosis or intimal flaps in the ICA or the CCA, or for ECA dissection or occlusion (which they do not discuss here).

In my own practice I use a combination of Doppler ausculation, digital palpation of the vessel, and angiographic landmarks to ascertain the distal extent of plaque, and I draw a blue line to mark the arteriotomy, just as these authors have done and illustrate. Following completed repair, always with a Hemashield patch in my practice, I again auscultate with the Doppler in all three branches of the arterial tree. I have not found it necessary to use completion angiography, or duplex ultrasound, to assure good results. But we are very careful to reopen and reassess any artery that sounds peculiar on the Doppler auscultation (1).

The use of ICG, if it is quick and reproducible, as these authors suggest, will change practice, including our own. We have tried ICG for CEA, but abandoned it as inadequate to visualize the lumen through the thick arterial wall. Probably we used too low a dose, as these authors point out. I can assure the readership that with this novel information, we will try the technique again next week.

Any improvement that makes CEA safer is a welcome advance and a benefit to the patient. I am pleased to see this most excellent report from Kyushu and recommend the technique enthusiastically to all carotid surgeons.

Christopher Loftus
Philadelphia, PA

1. Loftus CM: Carotid Artery Surgery: Principles and Technique. 2nd edition. New York, Informa Publishing 2006.

Acta Neurochir (2011) 153:1645–1648
DOI 10.1007/s00701-011-1035-0

TECHNICAL NOTE

Dissection of both frontal and parietal branches of the superficial temporal artery for bypass surgery through a single linear skin incision

Yoji Tamura · Atsushi Aoki · Yoshitaka Yamada · Naosuke Nonoguchi · Ryokichi Yagi · Adam Tucker · Toshihiko Kuroiwa

Received: 27 January 2011 / Accepted: 18 April 2011 / Published online: 8 May 2011

Abstract
Background Double superficial temporal artery (STA) to middle cerebral artery (MCA) bypass surgery has typically involved more than one linear incision. In this report, we demonstrate how the procedure can be performed through a single linear skin incision over the parietal branch of the STA.
Methods Initial dissection of the parietal branch and creation of a subcutaneous cavity along the frontal branch were performed using the conventional microscopic method. Detailed additional dissection and isolation of the frontal branch were accomplished with the aid of an endoscopic retractor.
Results This procedure was performed in five patients for harvesting of approximately 8- and 5-cm lengths of the parietal and frontal branches, respectively. The resultant lengths of the harvested vessels were sufficient for anastomotic revascularization of MCA recipient arteries in both the frontal and temporal lobes.
Conclusion This method can be safely performed with achievement of a less invasive dissection of the STA and an overall improved cosmetic outcome.

Keywords Bypass surgery · Superficial temporal artery · Frontal branch · Endoscope

Y. Tamura (✉) · A. Aoki · Y. Yamada · N. Nonoguchi · R. Yagi · A. Tucker · T. Kuroiwa
Department of Neurosurgery, Osaka Medical College,
2-7, Daigaku-machi,
Takatsuki City, Osaka 569–8686, Japan
e-mail: neu034@poh.osaka-med.ac.jp

Introduction

Superficial temporal artery (STA) to middle cerebral artery (MCA) bypass is an important cerebral revascularization surgical procedure, especially for salvage of the ischemic penumbra, i.e., "misery perfusion," in patients with cerebrovascular occlusive disease, including moyamoya disease [5, 7]. This standard bypass surgery varies according to which branch of the STA is used or what kind of skin incision is placed. The surgical method is determined by the size and location of the branch and the range of the ischemic penumbra. In this article, we present our strategy for dissection of both branches of the STA through a single linear skin incision over the parietal branch, without extending the incision anteriorly. A key feature of this arterial dissection procedure employs both the microscope and endoscope with an attached retractor.

Patient selection

Indications for STA-MCA bypass in cerebral ischemic patients was carefully decided according to the inclusion criteria of the Japanese Extracranial-Intracranial Bypass Trial [4, 5, 8]. From April 2007, five patients underwent double STA-MCA anastomosis with a single linear skin incision over the parietal branch of the STA (Table 1). All patients underwent the acetazolamide challenge test using single photon emission computed tomography for detecting stage II compromise in both the frontal and temporal lobes.

Table 1 Patient characteristics and length of the harvested frontal branch of STA

Patient	Age/sex	Diagnosis	Length of frontal STA (cm)
1	62/F	Moyamoya disease	5.5
2	56/M	Right ICA occlusion	5
3	59/M	Left MCA occlusion	4.8
4	70/M	Right ICA occlusion	4.5
5	72/F	Right MCA occlusion	4.6

STA: superficial temporal artery, ICA: internal carotid artery, MCA: middle cerebral artery

Surgical procedure

The surgical procedure is shown in Figs. 1, 2 and 3.

The patient was placed in the supine position. The neck was rotated to the contralateral side in order to place the surgical field at the highest point. Both branches of the STA were mapped by a portable Doppler device, and their running course was marked on the scalp. A strip of hair was shaved only along the planned linear incision over the parietal branch of the STA. After a single linear skin incision, a parietal branch length of approximately 8 cm was dissected from the surrounding galeal tissue down to the zygoma under the operating microscope. While the anterior scalp was elevated with a retractor, the subcutaneous tissue was separated from the galea along the frontal branch of the STA for the creation of adequate working space, similar to a pocket formation. In this space, a frontal branch length of 3 to 4 cm could be dissected by maneuvering the microscope along its optical axis. In the deep operative field, however, the endoscopic procedure is especially useful for dissecting the frontal branch by an additional 1 to 2 cm. A 4-mm, 0° rigid endoscope was attached to the endoscopic retractor (RX-1002, Keisei Medical Industrial Co., Ltd., Japan) and used to lift up the scalp. Endoscopic dissection was performed until a sufficiently long length of the frontal branch of the STA was harvested. Approximately 5 cm of the frontal branch of the STA was completely dissected, and its distal end was transected. The harvested parietal and frontal branches of the STA were anastamosed to the cortical branches of the MCA in the frontal and temporal lobes, respectively. The dissection time of the STA frontal branch was approximately 30 min, including the time for exchanging from microscope to endoscope. The suturing time of both of the STA branches was approximately 1 h. Each microscopic and endoscopic STA dissection procedure was performed with a standard bipolar device, scissors, and a sucker. By using this procedure through a linear skin incision, none of the patients experienced postoperative skin problems, such as necrosis or poor healing of the incision.

Discussion

In this article, we describe the safety and cosmetic efficacy of a double revascularization dissection of both the frontal and parietal branches of the STA using a single linear skin incision over the frontal branch. Previously, several skin incision types have been used for double STA-MCA anastomosis. In general, a linear skin incision has been placed over the parietal branch of the STA and extended anteriorly while the frontal branch of the STA is isolated

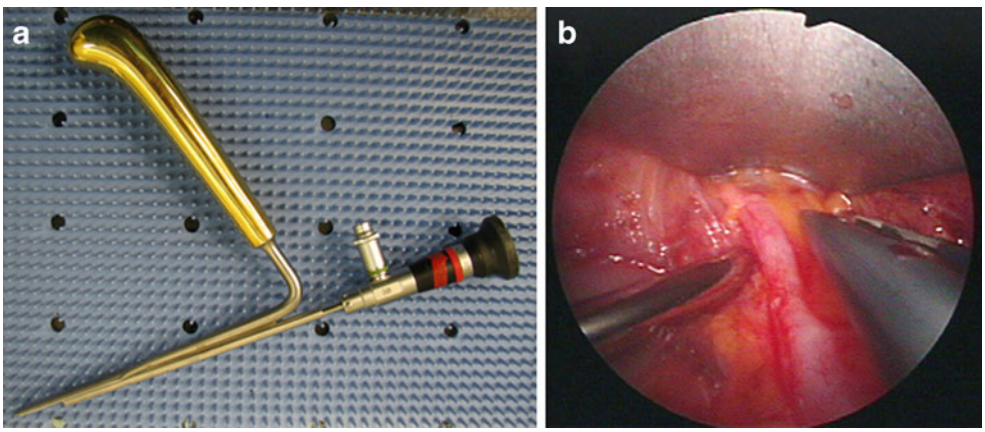

Fig. 1 **a** Endoscopic retractor; **b** endoscopic dissection of the frontal branch of the STA using a conventional bipolar device and sucker

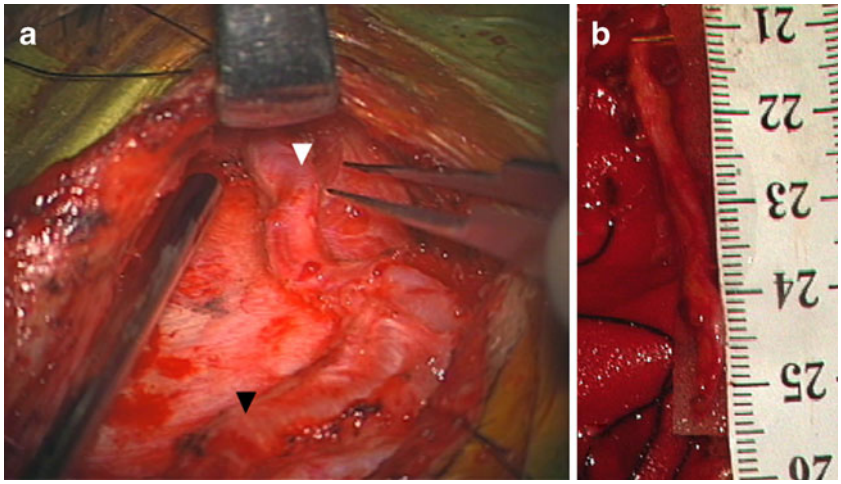

Fig. 2 **a** The scalp was elevated with a retractor, and the frontal branch of the STA (*white arrowhead*) was dissected under the microscope. *Black arrowhead* indicates the parietal branch of the STA. **b** The length of the harvested frontal branch of the STA was 5.5 cm long (case 1)

from a reflected skin flap. Another method involves a skin incision directly over both branches of the STA placed in a T-shaped fashion [3].

In contrast, we found it possible to isolate the frontal branch of the STA without arterial injury through a single linear skin incision. Kubo et al. reported the endoscopy-assisted harvesting of the frontal branch of the STA through a single skin incision, similar to our incision [6]. One drawback to this method, however, is the added time required to dissect the frontal branch of the STA for neurosurgeons inexperienced with endoscopic manipulation. Therefore, we modified this procedure by attempting to dissect the frontal branch of the STA with both microscope and endoscope. In order to shorten the operating time, microscopic dissection was used for most of the artery's length, and the endoscope was used for the remaining few centimeters. Although the harvested frontal branch of the STA was shorter than the parietal branch, it was long enough for complete anastomosis to MCA recipient vessels in the temporal lobe.

For this method, we used an endoscope with a retractor attachment. This tool is typically used for endoscopic dissection of muscles in the trunk or extremities. During the STA dissection procedure, the assistant must hold the retractor, and it is always necessary to advance the tip of the retractor to create the best optical space. The endoscopic dissection technique was slightly slower than standard microscopic dissection owing to more careful inspection. However, we did not spend a significant amount of time for the endoscopic operations, because the length of the STA frontal branch dissected using the endoscope was short.

In cardiovascular surgery, there have been several reports on utilizing the endoscope for harvesting donor vessels, e.g., the radial artery or saphenous vein, through minimal skin incisions [1, 2, 9]. These studies have claimed that the procedure involves a moderate learning curve, with experience in more than ten cases necessary before becoming comfortable with the endoscopic technique. With proficiency overall operation times were decreased [1].

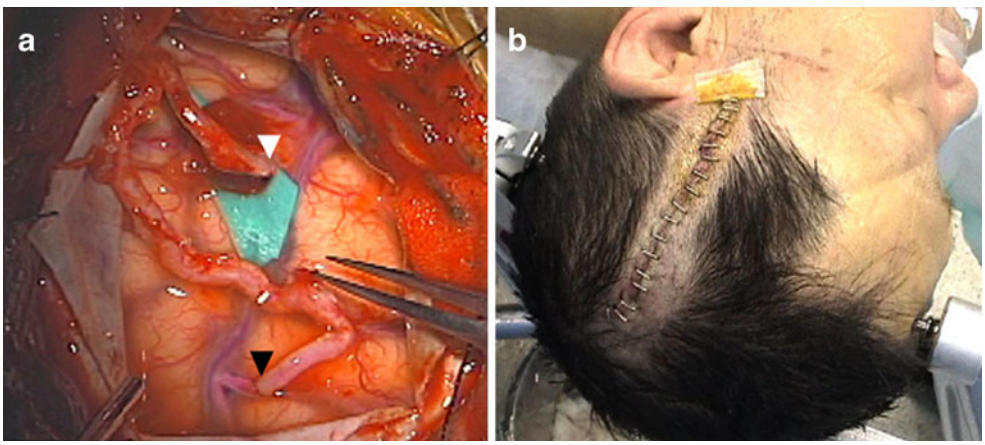

Fig. 3 **a** Both parietal (*black arrowhead*) and frontal (*white arrowhead*) branches of the STA were anastamosed to the cortical branches of the MCA in the frontal and temporal lobes, respectively. **b** The single linear skin incision over the parietal branch of the STA was closed with staples (case 3)

Likewise, in the future, it is anticipated that with greater application and repeated use of our technique, the distance of the arterial dissection will be extended and operation times shortened. Furthermore, we expect that the distal side of the parietal branch of the STA can be dissected with this method through an even shorter linear skin incision.

Conflicts of interest None.

References

1. Bleiziffer S, Libera P, Lange R (2006) Endoscopic radial artery harvesting through a single incision. Thorac Cardiovasc Surg 54 (3):208–209
2. Bonde P, Graham AN, MacGowan SW (2004) Endoscopic vein harvest: advantages and limitations. Ann Thorac Surg 77(6):2076–2082
3. Firlik AD, Yonas H (2003) Surgical procedures for cerebral revascularization. In: Batjer HH, Loftus CM (eds) Textbook of neurological surgery. Principle and practice. Lippincott Williams & Wilkins, Philadelphia, pp 2290–2296
4. JET Study Group (2002) Japanese EC-IC bypass trial (JET study): study design and interim analysis. Surg Cereb Stroke 30:97–100, Jpn
5. Jinnouchi J, Toyoda K, Inoue T, Fujimoto S, Gotoh S, Yasumori K, Ibayashi S, Iida M, Okada Y (2006) Changes in brain volume 2 years after extracranial-intracranial bypass surgery: a preliminary subanalysis of the Japanese EC-IC trial. Cerebrovasc Dis 22(2–3):177–182
6. Kubo S, Takimoto H, Yoshimine T (2003) Endoscopically assisted harvesting of the superficial temporal artery: technical note. Neurosurgery 52(4):982–984
7. Mesiwala AH, Sviri G, Fatemi N, Britz GW, Newell DW (2008) Long-term outcome of superficial temporal artery-middle cerebral artery bypass for patients with moyamoya disease in the US. Neurosurg Focus 24(2):E15
8. Mizumura S, Nakagawara J, Takahashi M, Kumita S, Cho K, Nakajo H, Toba M, Kumazaki T (2004) Three-dimensional display in staging hemodynamic brain ischemia for JET study: objective evaluation using SEE analysis and 3D-SSP display. Ann Nucl Med 18(1):13–21
9. Schurr UP, Lachat ML, Reuthebuch O, Kadner A, Mäder M, Seiffert B, Hoerstrup SP, Zünd G, Genoni M, Turina MI (2002) Endoscopic saphenous vein harvesting for CABG—a randomized, prospective trial. Thorac Cardiovasc Surg 50(3):160–163

Comment

Within the last quarter of a century or so, all studies have failed to show that STA-MCA bypasses are superior to pharmaceutical therapy in preventing ischemic events in patients with TIA or strokes. However, there is still an increasing role for EC-IC bypasses in selected patients with otherwise untreatable aneurysms, mainly when sacrifice of the MCA or ICA is necessary. The simpler the method, the better the results may be as there are fewer steps with which to have potential problems. Therefore, the enthusiasm for performing high-flow bypasses with often complicated methods has decreased and has turned to standard STA-MCA bypasses, which, in fact, often are enough for the patients. As endoscopic techniques are developing it is natural also to apply them successfully in bypasses, as the authors show. With experience, the procedure is not so time consuming, especially when combined with use of the operating microscope. The cosmetic results are better with shorter incisions, and perhaps there is also less risk of poor healing of the incision itself as all branches, also those feeding the skin, are harvested. We still need to develop even simpler techniques, especially for high-flow bypasses that can be performed quickly and safely even under local anesthesia in patients who are often sick and compromised in many ways.

Mika Niemelä
Juha Hernesniemi
Helsinki, Finland

Acta Neurochir (2011) 153:1649–1655
DOI 10.1007/s00701-011-1070-x

CASE REPORT

Bypass of the maxillary to proximal middle cerebral artery or proximal posterior cerebral artery with radial artery graft

Xiang'en Shi · Hai Qian · K I Singh K.C. · Yongli Zhang · Zhongqing Zhou · Yuming Sun

Received: 29 January 2011 / Accepted: 3 June 2011 / Published online: 18 June 2011

Abstract The authors report three cases of radial artery (RA) graft bypass from the maxillary artery (MA) to either the middle cerebral artery (MCA) or the posterior cerebral artery (PCA). The first two cases presented with the features of basal ganglion ischemia, and magnetic resonance imaging (MRI) revealed left and right basal ganglion ischemia respectively, whereas angiogram showed MCA occlusion. Computed tomography angiography (CTA) of the third case, who presented with headache and dysphasia, showed a giant basilar artery aneurysm with an absence of the left posterior communicating artery (PComA). The first two cases underwent MA-MCA graft bypass and the third case underwent MA-posterior cerebral artery (PCA) RA graft bypass, followed by clipping of the left dominance vertebral artery and a sub-occipital decompressive craniotomy. Postoperative angiogram disclosed patent RA graft and refilling of the ischemic segment. Follow-up at 7–9 months showed marked clinical improvement in all cases. To our knowledge, MA bypass has not been performed clinically till the date and this method may be a safe, effective and new surgical technique for the extracranial-intracranial (EC-IC) bypass surgery.

Keywords Maxillary artery bypass · High-flow bypass · Ischemic stroke · Radial artery graft

X. Shi (✉) · H. Qian · Y. Zhang · Z. Zhou · Y. Sun
Department of Neurosurgery, Beijing Sanbo Brain Hospital,
No. 50 Yikesong Rd, Haidian District Beijing 100093, China
e-mail: shixen@sina.com

X. Shi
Department of Neurosurgery, Affiliated Fuxing Hospital,
The Capital University of Medical Sciences,
Beijing 100038, China

K. I. S. K.C.
Department of Neurosurgery, 1st Affiliated Hospital,
Liaoning Medical University,
Jinzhou, Liaoning 121000, China

Introduction

The external carotid artery (ECA), internal carotid artery (ICA), and superficial temporal artery (STA) are the common donor vessels in extracranial-intracranial (EC-IC) bypass surgery. The authors report three cases of the radial artery (RA) graft bypass from the maxillary artery (MA) to either the middle cerebral artery (MCA) or the proximal posterior cerebral artery (PCA). To the authors' knowledge, MA-MCA/PCA bypass with an RA graft has not been reported for cerebral disorders in clinical practice.

EC-IC bypass procedures are indicated for selective cases with ischemic stroke or intracranial giant aneurysms. ECA, ICA and STA are used as the donor vessels in EC-IC bypass surgery. However, either the long graft from the proximal ECA/ICA to the MCA or the small diameter of the graft limited the advantages of the bypass surgery. We described a new surgical technique for the EC-IC bypass surgery.

Case reports

Case 1

History and examination A 36-year-old right-handed man was admitted to our department with a 2-month history of right-side weakness and slurred speech. Neurological examination revealed mixed aphasia and right central facial palsy. The muscle strength was grade 3 on the right side and grade 5 on the left side. Pulse at the RA was absent. Diffusion-weighted imaging (DWI) revealed ischemia on the left basal ganglion area (Fig. 1 *left*). Angiogram showed occlusion of M1 segment of left MCA (Fig. 1 *right*).

Operation The patient underwent a left pterional craniotomy with removal of the ipsilateral zygomatic arch to facilitate downward retraction of the temporal muscle. The

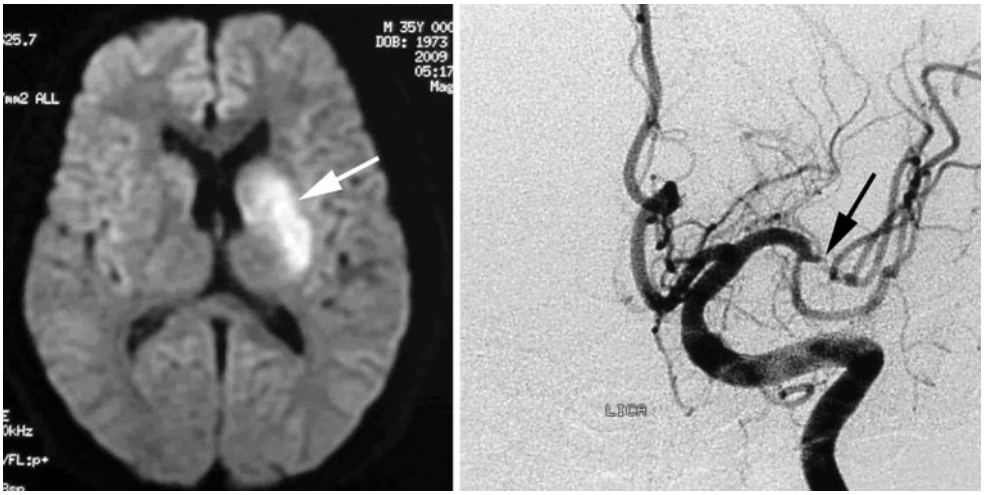

Fig. 1 *Left*: Preoperative DWI showing the ischemia at the left basal ganglia (*white arrow*). *Right*: Left ICA angiogram (anteroposterior view) of the same patient demonstrating occlusion site at the distal M1 (*black arrow*)

sylvian fissure was widely split. A pale and pulseless M1 segment was visualized, dividing into three branches (frontal, temporal-occipital and parietal, Fig. 2). The M2 segment of the MCA consisted of these branches. After exposing the pterygopalatine fossa, the MA could be dissected between the neck of the mandible and the sphenomandibular ligament, which was superficial to the lower head of the lateral pterygoid. Deep temporal arteries, the infraorbital artery, and distal MA were cut after being ligated. The diameter of the MA trunk was about 2.5 mm. A 7-cm RA graft was harvested from the left forearm. An end to end anastomosis was performed between the proximal RA graft and the proximal MA with 9–0 nylon suture, then the distal end of the RA graft was anastomosed to the side of the temporal-occipital branch of the MCA. After the temporary clips were removed, there appeared to be competitive flow at all the branches of the M2 segment (Fig. 3, right).

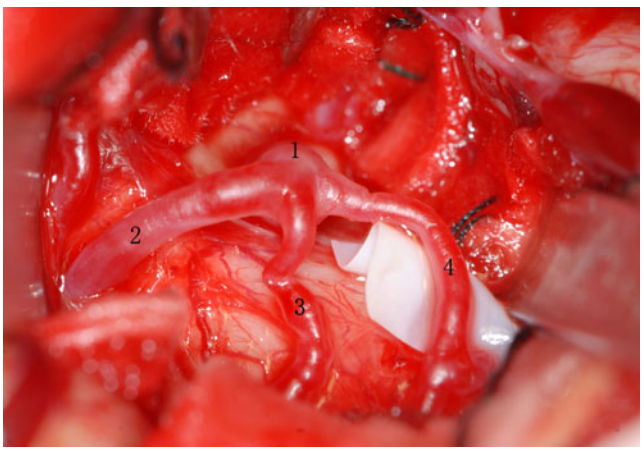

Fig. 2 Intraoperative view of the MCA bifurcation showing sclerosed distal M1 segment (*1*). The frontal branch (*4*), temporal-occipital branch (*2*) and parietal branch (*3*), which are reduced in diameter

Postoperative course The postoperative course was uneventful. After the first week the patient began to utter few words. Two weeks later an angiogram was done which revealed refilling of the artery above the occlusion site (Fig. 4). One month later the patient could speak clearly but slowly and the muscle power of the right side improved to grade 4. At the 9-month follow-up the patient had improved significantly and was able to return to his job.

Case 2

History and examination A 47-year-old right-handed man was referred to our department with the history of left-sided weakness with cognitive dysfunction for 1-month. Neurological examination revealed abnormal attention, memory, and calculations. Power on the left leg was grade 4. MRI showed ischemia on the right basal ganglion (Fig. 5). Angiogram showed right proximal MCA occlusion (Fig. 6).

Operation The patient underwent right pterional craniotomy with partial removal of ipsilateral zygomatic arch. The sylvian fissure was opened widely, exposing the M1 and M2 segments of the MCA, and C1 and C2 segments of the ICA. Atherosclerotic plaques were found on the proximal M1 segment, whereas the distal M1 appeared normal with a diameter of 4 mm. The MA was dissected in the pterygopalatine fossa in the same way as in case 1. A 7-cm RA graft was harvested from the right forearm. The proximal end of the RA graft was anastomosed to the proximal end of the MA with 9–0 nylon, and the distal end of the RA graft was anastomosed to the side of the distal M1. A good amount of intraoperative blood from the MA was observed after the anastomosis was completed.

Postoperative course Postoperative day 1 CTA revealed the partial visualization of patent RA graft and the left MCA

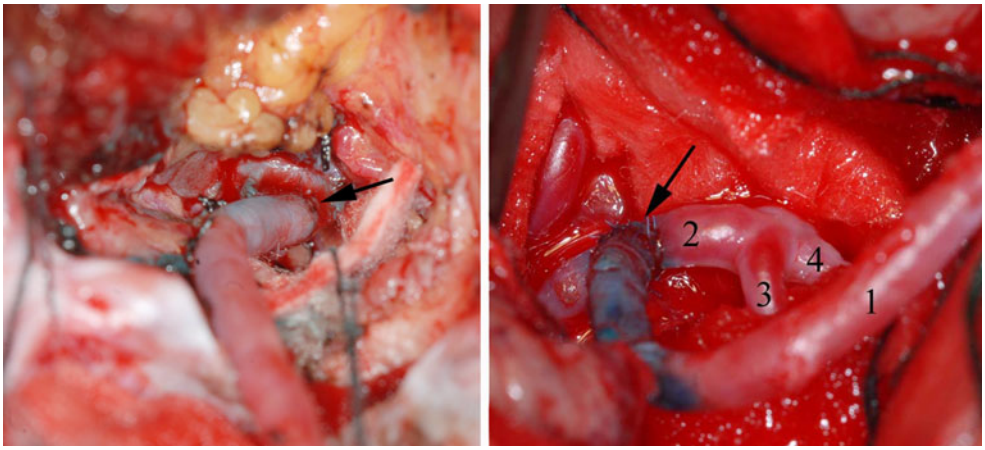

Fig. 3 *Left*: Intraoperative view in pterygopalatine fossa after RA graft being anastomosed to the MA. *Right*: MCA bifurcation after the distal end of RA being anastomosed to the side of the MCA; *1* the RA graft, *2* the temporal-occipital branch of M2, *3* the parietal branch of M2, *4* the frontal branch of M2

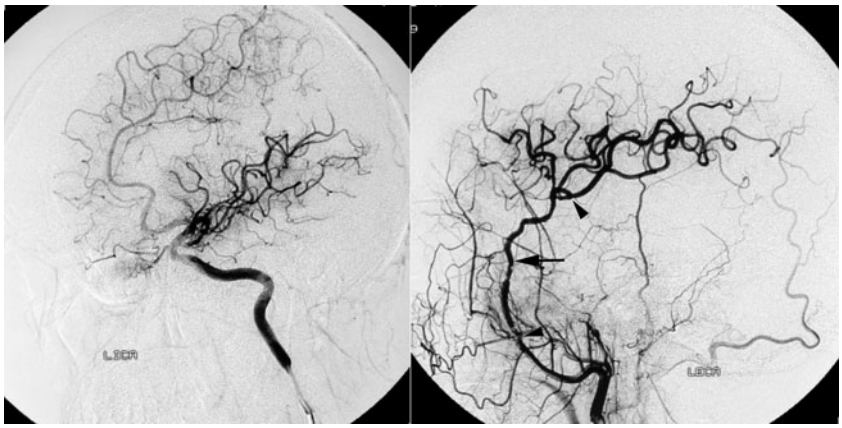

Fig. 4 Preoperative (*left*) and postoperative (*right*) angiogram showing the increasing MCA blood supply. The arterial segment *in between the two arrows* is the RA graft and *each arrow* shows the proximal and distal anastomotic site

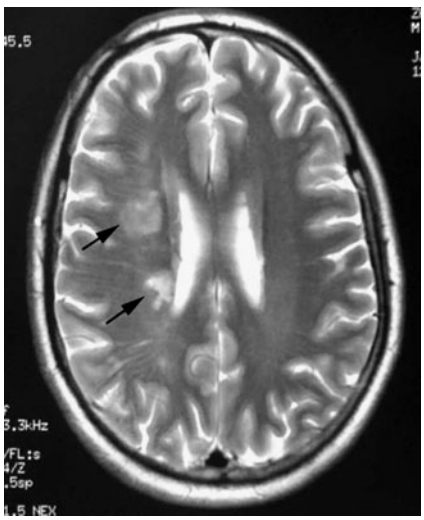

Fig. 5 Preoperative T2-weighted MRI; the *black arrows* show the ischemic site at the right basal ganglion region

(Fig. 7). Two weeks later, the cognitive dysfunction improved but the power on left lower limb remained unchanged. Angiogram revealed the patent RA graft with refilling of the artery at the MCA territory (Fig. 8). At the 9-month follow-up, the patient showed marked improvement, except for mild weakness of the left lower limb.

Case 3

History and examination A 46-year-old right-handed woman presented with headache for 3 years, and dysphasia and dyspnoea on lying, bowing and even on turning her head for 4 months. Neurological examination revealed weak rapid alternating movement and point-to-point movement on the right upper limb and had positive Romberg sign. CTA showed a giant basilar trunk aneurysm with absence of the left PComA (Fig. 9).

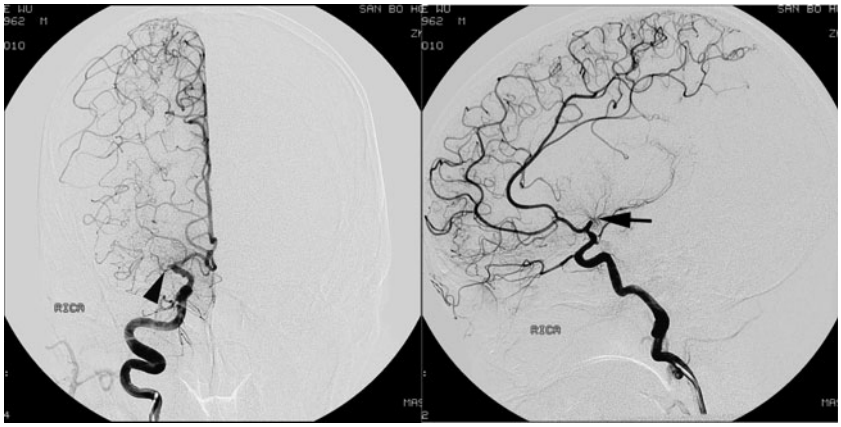

Fig. 6 *Left*: Preoperative anteroposterior view of left ICA angiogram showing the absence of MCA. *Right*: Lateral view. Both of the *arrows* show the occlusion site

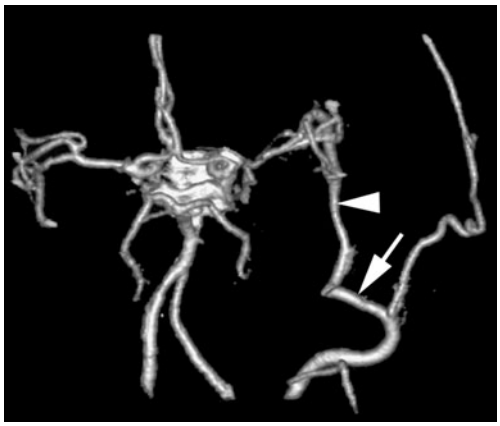

Fig. 7 Postoperative three-dimensional (3D) computed tomography angiography (CTA) revealing the patency of the RA graft (*white arrowhead*). Proximal MA (*white arrow*); MCA could be partially visualized

Operation A combination of left pterional and far lateral transcondyar approach were carried out with partial removal of the ipsilateral zygomatic arch. A 13-cm RA graft was harvested from the right forearm. The ambient cistern was exposed elevating the temporal base. The tentorial edge was cut and the posterior clinoid process was drilled, enlarging the operative field.

The proximal end of the RA graft was anastomosed to the proximal end of the MA with 9–0 nylon, and the distal end of the RA graft was anastomosed to the side of the P2. A good amount of blood flow into the P2 segment was observed when the temporary clips were removed after the bypass was completed. The vertebral artery proximal to the aneurysm distal to the posterior inferior cerebellar artery (PICA) was clipped, creating a reversal blood flow to the aneurysmal segment, so that a small channel containing the origin of the perforating arteries would obtain enough

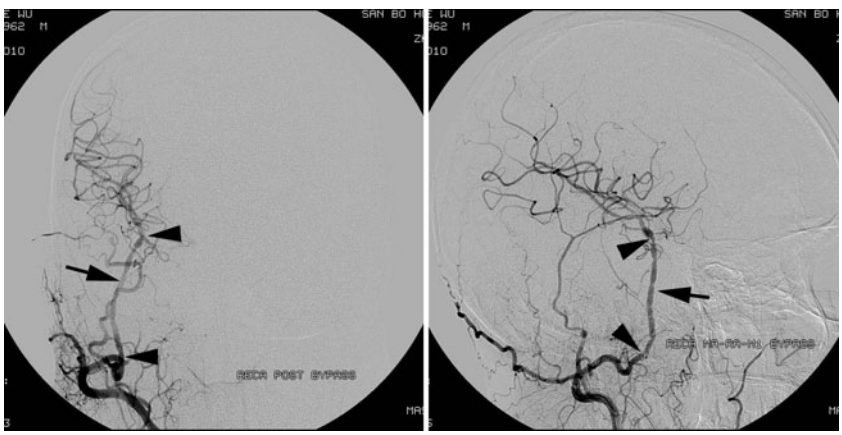

Fig. 8 Postoperative angiogram showing the blood supply of the right MCA. Anteroposterior view (*left*) and lateral view (*right*) of the right ECA angiogram showing the patency of the graft (*arrows*) with sufficient blood flow in the right MCA. *Arrowheads* showing the proximal and distal anastomosis sites

Fig. 9 Preoperative MRA revealing the giant basilar aneurysm. The basilar artery was enlarged except the upper third of it and the left PICA was absent

reverse blood flow from the distal bypass. The suboccipital decompression was performed to release the mass effect due to giant aneurysm.

Postoperative course The postoperative course was uneventful. On postoperative day 1, the patient could lie down and move her head. The postoperative CTA showed the patent RA graft (Fig. 10), though the aneurysm was still visualized. At the 7-month follow-up, the patient had no headache or dyspnea, but choked on liquids occasionally.

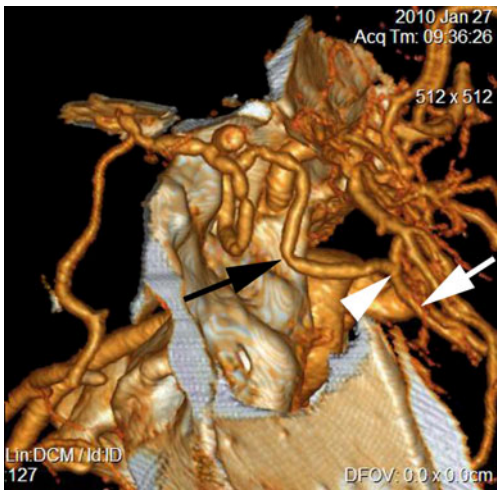

Fig. 10 Postoperative 3D-CTA showing the patent RA graft (*black arrow*); P2 segment of the PCA *white arrow*; distal anastomotic site *white arrowhead*

Discussion

EC-IC bypass for the treatment of ischemic cerebrovascular disease was pioneered by Yasargil in 1967 [21]. However, a multi-institutional, randomized, controlled, clinical trial published in 1985 caused EC-IC bypass to lose favor as an option for the treatment of ischemic stroke [18]. Depending on the extent of blood flow augmentation, the choice of graft bypass was described as the low flow graft (15–25 ml/min) of the superficial temporal arteries or the occipital artery, moderate flow graft (40–70 ml/min) of the RA, and high flow graft (70-140 ml/min) of the greater saphenous vein (SV) [8]. The STA-MCA bypass was a relatively low-flow bypass (15–25 ml/min) compared with ECA-MCA or ICA-MCA bypass, which may reduce the effect of the EC-IC bypass surgery [2, 5]. At the same time, the small diameter of the conduit led to a lower long-term patency rate. On the other hand, a high-flow EC-IC bypass was used as a surgical strategy to treat an ischemic stroke or intracranial giant aneurysm [7, 13, 16]. The ECA or ICA were the common donor vessels, but the longer graft (15–20 cm) has some disadvantages in bypass surgery, such as

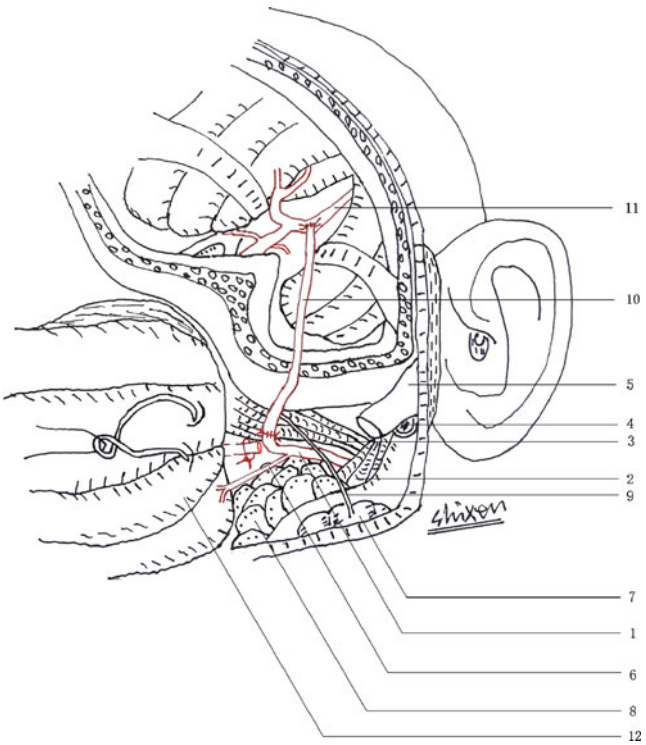

Fig. 11 Schematic drawing of the frontotemporal craniotomy with the resection of the ipsilateral zygomatic arch. Illustrating the internal MA course in the pterygopalatine fossa after reflecting the temporalis muscle anteriorly. *1* Internal MA, *2* inferior belly of the lateral pterygoid muscle, *3* superior belly of the lateral pterygoid muscle; *4* mandibular condyle, *5* zygomatic root, *6* deep temporal artery, *7* masseter muscle, *8* fat tissue of the deep temporal space, *9* masseteric nerve, *10* RA graft, *11* M2 segment of MCA, *12* temporalis muscle

more difficult graft harvesting and uncertain patency rate [10, 14]. On the basis of anatomy research, we performed MA-to-MCA or MA-to-PCA surgery in patients with MCA occlusion or giant vertebral aneurysm. The anatomical location of the MA, being inferior to the zygoma in the pterygopalatine fossa, which is accessible within the craniotomy field, made the bypass surgery easier. Moreover, the diameter of the MA is 2.6+−3 mm, whereas the diameter of the STA is 2.2 mm, thus providing comparatively higher blood flow to the STA [19]. Pterional craniotomy was extended, removing the ipsilateral zygomatic arch and reflecting the temporal muscle anterior-inferiorly. The deep temporal artery was identified in the fat pad and was followed inferiorly, reaching the MA at the inter-muscular space between superior and inferior belly of the lateral pterygoid muscle, then the artery was dissected towards the origin of the lateral pterigoid muscle. After exposing about 2 cm, the artery was ligated at the distal end with a suture, while clipped with a temporary clip at the proximal end, and the artery was cut, securing the donor end; finally, an end-to-end anastomosis with RA graft was done (Fig. 11). The neural structures pass just below the MA, which favors the prevention of neural damage [1].

In the high-flow EC-IC bypass surgery, the SVor RA is usually chosen to be the graft donor. The SV is easily harvested, and can provide plenty of length and adequate blood flow (70–140 ml/ min) [11]. However, the tunica media of the venous wall is thinner than the arterial wall, which leads to a higher possibility of aneurysmal dilatation, turbulent flow, and occlusion. The long-term patency rate of venous grafts was lower in about 60-70% [6, 12, 15]. The RA is another option for preferred donor graft, since it is physiologically equipped to convey arterial flow and it can be matched to a recipient vessel of the M2 branch. An RA graft about 18–20 cm long is usually required if an EC-IC bypass is performed. Theoretically, the longer the RA graft, the higher the occurrence of RA spasm, resulting in reduction in the blood flow and the possibility of occlusion. A shorter RA graft should have fewer spasms.

The MA has been considered to be a donor vessel since 2001 [9]. Some authors tried to investigate the use of an RA graft for bypass of the MA to the MCA or PCA [3, 4, 19, 20]. The MA is described in three parts according to its course: mandibular, pterygoid and pterygopalatine. The pterygoid section ascends obliquely forward, medial to the temporalis muscle, and in 60% of cases is superficial to the lower head of the lateral pterygoid [17]. The deep temporal artery branch of the MA lies superficial to the lateral pterygoid muscle, which is a landmark of the pterygoid segment and will aid in selecting the anastomosis site. The advantages of MA-to-MCA are that it has a higher blood flow than the STA-to-MCA, it is a shorter distance for the bypass, and does not need for cervical exposure. The disadvantage of the MA-to-MCA is that it is more difficult to expose the MA, by having to go into the pterygopalatine fossa, deep to the zygomatic arch.

Despite being beginners to MA-to-MCA or MA-to-PCA bypass surgery, we treated three patients with ischemic stroke or intracranial giant aneurysm with good results clinically, which also worked as a new bypass technique on the basis of anatomical research. As beginners with only a few cases, it is a pity that we could not add physiologic/metabolic endpoint data, such as PET-OEF, at present, but we will definitely advance our experience and provide the data in the near future with more successful cases. This bypass provides sufficient blood flow with a shorter graft. It may be a safe and effective technique for the treatment of selective cases of ischemic stroke or intracranial giant aneurysms.

Conflicts of interest None.

References

1. Rhoton AL Jr (2003) Rhoton's Cranial anatomy and surgical approaches, vol 53. Lippincott, Williams & Wilkins, Philadelphia, pp 665–666
2. Al-Mefty O, Khalil N, Elwany MN, Smith RR (1990) Shunt for bypass graft of the cavernous carotid artery: an anatomical and technical study. Neurosurgery 27:721–727, discussion 727–8
3. Arbag H, Ustun ME, Buyukmumcu M, Cicekcibasi AE, Ulku CH (2005) A modified technique to bypass the maxillary artery to supraclinoid internal carotid artery by using radial artery graft: an anatomical study. J Laryngol Otol 119:519–523
4. Buyukmumcu M, Ustun ME, Seker M, Karabulut AK, Uysal YY (2003) Maxillary-to-petrous internal carotid artery bypass: an anatomical feasibility study. Surg Radiol Anat 25:368–371
5. Diaz FG, Ausman JI, Pearce JE (1982) Ischemic complications after combined internal carotid artery occlusion and extracranial-intracranial anastomosis. Neurosurgery 10:563–570
6. Diaz FG, Pearce J, Ausman JI (1985) Complications of cerebral revascularization with autogenous vein grafts. Neurosurgery 17:271–276
7. Hanel RA, Spetzler RF (2008) Surgical treatment of complex intracranial aneurysms. Neurosurgery 62:1289–1297, discussion 1297–9
8. Mura J, Malogo-Tavares W, Figueiredo EG (2010) Basic aspects of high flow extracranial–intracranial bypass: part I. Contemp Neurosurg 32(4):1–4
9. Karabulut AK, Ustun ME, Uysal II, Salbacak A (2001) Saphenous vein graft for bypass of the maxillary to supraclinoid internal carotid artery: An anatomical short study. Ann Vasc Surg 15:548–552
10. Little JR, Furlan AJ, Bryerton B (1983) Short vein grafts for cerebral revascularization. J Neurosurg 59:384–388
11. Liu JK, Kan P, Karwande SV, Couldwell WT (2003) Conduits for cerebrovascular bypass and lessons learned from the cardiovascular experience. Neurosurg Focus 14:e3
12. Regli L, Piepgras DG, Hansen KK (1995) Late patency of long saphenous vein bypass grafts to the anterior and posterior cerebral circulation. J Neurosurg 83:806–811

13. Sekhar LN, Kalavakonda C (2002) Cerebral revascularization for aneurysms and tumors. Neurosurgery 50:321–331
14. Sekhar LN, Schramm VL Jr, Jones NF, Yonas H, Horton J, Latchaw RE (1986) Operative exposure and management of the petrous and upper cervical internal carotid artery. Neurosurgery 19:967–982
15. Sen C, Sekhar LN (1992) Direct vein graft reconstruction of the cavernous, petrous, and upper cervical internal carotid artery: lessons learned from 30 cases. Neurosurgery 30:732–742, discussion 742–3
16. Sundt TM Jr, Piepgras DG, Fode NC, Meyer FB (1991) Giant intracranial aneurysms. Clin Neurosurg 37:116–154
17. Standring S (2008) Gray's Anatomy. Elsevier, Churchill Livingstone, London
18. The EC/IC bypass study group (1985) Failure of extracranial-intracranial arterial bypass to reduce the risk of ischemic stroke. Results of an international randomized trial. N Engl J Med 313:1191–1200
19. Ulku CH, Ustun ME, Buyukmumcu M, Cicekcibasi AE, Ziylan T (2004) Radial artery graft for bypass of the maxillary to proximal posterior cerebral artery: an anatomical and technical study. Acta Otolaryngol 124:858–862
20. Ustun ME, Buyukmumcu M, Ulku CH, Cicekcibasi AE, Arbag H (2004) Radial artery graft for bypass of the maxillary to proximal middle cerebral artery: an anatomic and technical study. Neurosurgery 54:667–670, discussion 670–1
21. Yasargil MG (1969) Anastomosis between the superficial temporal artery and a branch of the middle cerebral artery. In: Yasargil MG (ed) Microsurgery applied to neurosurgery. Thieme, Stuttgart, pp 105–115

Comment

This is essentially an expanded report of three cases where MA to MCA or PCA artery bypass was performed with an RA short-segment interposition graft. The indications were MCA occlusion and stroke in the first two cases and fusiform VA-BA aneurysm in the third. The authors have confirmed patency with either CTA or DSA in all cases, and describe favorable clinical endpoints in what were, admittedly, three quite impaired patients. They did not obtain preoperative or postoperative assessments of cerebral perfusion. This is a pity, because most contemporary bypass reports now show physiologic and imaging endpoints (beyond merely patency) as well as clinical ones, and these data would certainly have enhanced their report.

The method is clever and novel, with tangible advantages. The MA should be accessible within a craniotomy field, in the pterygopalatine fossa (where most of us have probably encountered it inadvertently, rather than by design). The RA graft, at least in the MCA circulation, can be short, enhancing patency rates. The microsurgical techniques are routine and straightforward.

This paper has value as yet another clever trick to deliver extracranial circulation flow to the brain, for specific clinical problems. The authors should go forward now to expand upon their experience and add physiologic/metabolic endpoint data, such as PET-OEF could provide, if they are to further advance our ability to treat stroke by surgical means.

Christopher Miranda Loftus
Philadelphia, USA

Acta Neurochir (2011) 153:1657–1661
DOI 10.1007/s00701-011-1025-2

CASE REPORT

Angiogenic and inflammatory factor expressions in cutaneomeningospinal angiomatosis (Cobb's syndrome): case report

Peng Gao · Hongqi Zhang · Feng Ling

Received: 6 January 2011 / Accepted: 6 April 2011 / Published online: 26 April 2011

Abstract We report on a case of cervical cutaneomeningospinal angiomatosis (Cobb's syndrome), a rare somatic disorder, characterized by vascular abnormalities of the spinal cord, with a triad of associated vascular skin, muscle, bone, and dura involvement at the same somite. This case follows an 18-year-old male patient presenting with left extremity weakness and back cervical pain. Magnetic resonance imaging (MRI) revealed a spinal cord arteriovenous malformation (AVM) at the C3-C5 level. Cobb's syndrome was diagnosed by coexistence of cutaneous naevi in a dermatomal pattern and neurological signs of a spinal cord lesion together with cervical MRI and angiography. The patient underwent a combination of staged endovascular embolization and microsurgical resection. Multiple biopsies of the mass including the skin, muscle, dura, and spinal cord at the same somite revealed that the lesions had a similar pathology. Post-operative immunohistochemical characterizations on specimen included CD31, smooth muscle actin (SMA), vascular endothelial growth factor (VEGF), and matrix metalloproteinase (MMP-9). The unique associations of somatic and spinal cord lesion as well as angiogenic and inflammatory factor expressions in all specimens are reported.

Keywords Cobb's syndrome · Angiogenesis · Inflammation

Introduction

Cutaneomeningospinal angiomatosis, or Cobb's syndrome, was first described in 1895, and reported by Cobb [4] in 1915, who described the syndrome of a somatic angiomatosis with segmental involvement of the skin, subcutaneous tissue, vertebral column, dura and spinal cord. To date, no more than 100 reports of Cobb's syndrome exist in the literature [1, 2, 4, 5, 7, 8, 10, 11, 13, 14]. Spinal cord angiomatosis has been even rarely characterized by immunohistochemistry [6]. Here, we report a case describing the angiogenic factor and inflammatory expressions of the angiomatosis lesions that Cobb involved at the same somite, and examined their homological correlation.

P. Gao · H. Zhang · F. Ling (✉)
Department of Neurosurgery, Xuanwu Hospital,
Capital University of Medical Sciences,
45 Changchun Street, Xicheng District,
Beijing 100053, China
e-mail: lingfengdoc@yahoo.com.cn

Case description

An 18-year-old male patient was admitted for progressive left extremity weakness and neck pain. Neurological examination showed decreased muscle strength of left lower extremity (4+/5). Bladder or bowel function was normal. No familial history was observed. Cervical MRI demonstrated lesions within the spinal cord parenchyma, and multiple flow void signals along the dorsal interface (Fig. 1). Angiogram analysis showed an arteriovenous malformation (AVM) at the C3-C5 segment, involving the spinal cord and associated paravertebral tissues at the same level. The AVM feeders, including intra-spinal and paravertebral tissues, arose from bilateral vertebral artery (VA), bilateral costocervical trunk (CCT), and right thyrocervical trunk (TCT). For the spinal cord AVM: PSA (posterior spinal artery), fed mainly by L-VA, was followed with aneurysm-like structure within the spinal cord parenchyma; ASA derived from R-VA and R-TCT. Paravertebral soft tissues were mainly fed by bilateral CCT and right TCT (Fig. 2).

A multidisciplinary approach to the patient's care was undertaken, including staged embolization and microsurgical resection. Endovascular embolization was performed with GLUBRAN (GLUBRAN 2 acrylic glue) via bilateral CCT

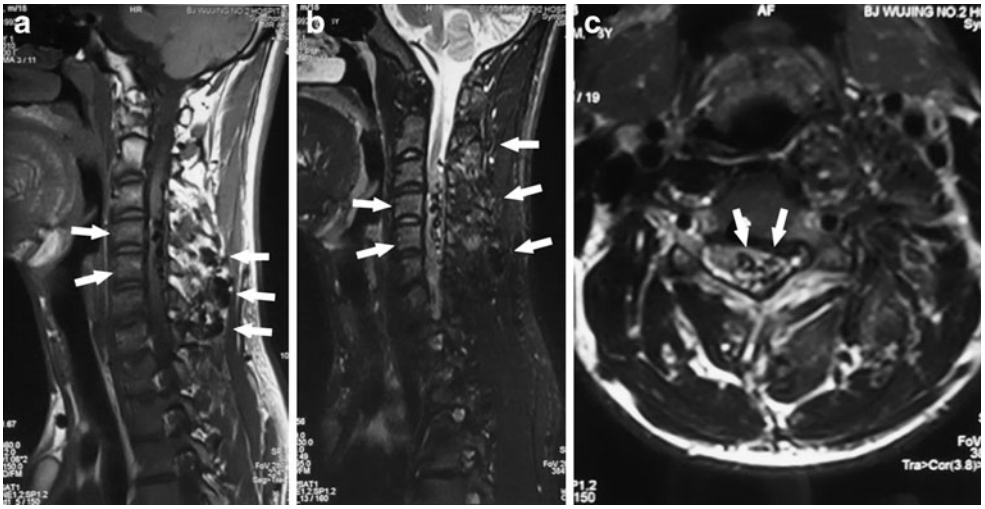

Fig. 1 MRI delineates the cervical spinal cord. Note the flow void signals mass occupying the spinal cord and paravertebral lesions (*white arrow*). **a** Sagittal T1-weighted image. **b** Sagittal T2-weighted image. **c** Axial view

and right TCT route (Fig. 2). Systemic heparinization was administrated after a 5-F sheath was introduced into the right femoral artery. A Marathon™ microcatheter (ev3, Irvine, CA, USA) over a SilverSpeed 0.010-in microguidewire was advanced at the bilateral CCT and right TCT, respectively. Stepwise superselective angiography was performed to ensure that the para-vertebral branches made no contributing flow for the spinal cord AVM. An appropriate mixture of glue was used (GLUBRAN glue in 20%). Feeding flow was decreased significantly, and nidus was not remarkably opacified. The patient was scheduled for microsurgical resection 24 h after embolization. Vigorous bleeding was encountered during the surgery from skin incision to laminectomy. The extradural-intradural AVMs corresponded with metameric lesions, which involved the soft tissue, spinal canal, spinal cord, spinal canal, and nerve root along an entire spinal level. Intra-operative findings showed that the dura, rich with blood supply, was grossly thickened by infiltration of tiny vessels (Fig. 3a). Dilated arterialized venous plexus was located between subarachnoid and pia mater, and moved along the dorsal interface of the spinal cord (Fig. 3b). PSA as the main feeder along the nerve root sleeve was dissected and applied with temporary block to provide for flow control and minimize hemorrhage. Non-stick bipolar cauterization and microscissors were used to interrupt the nidus angioarchitecture. The nidus beneath the pia mater was then resected (Fig. 4). During the operation, multiple biopsies of the skin, muscle (paravertebral muscle),

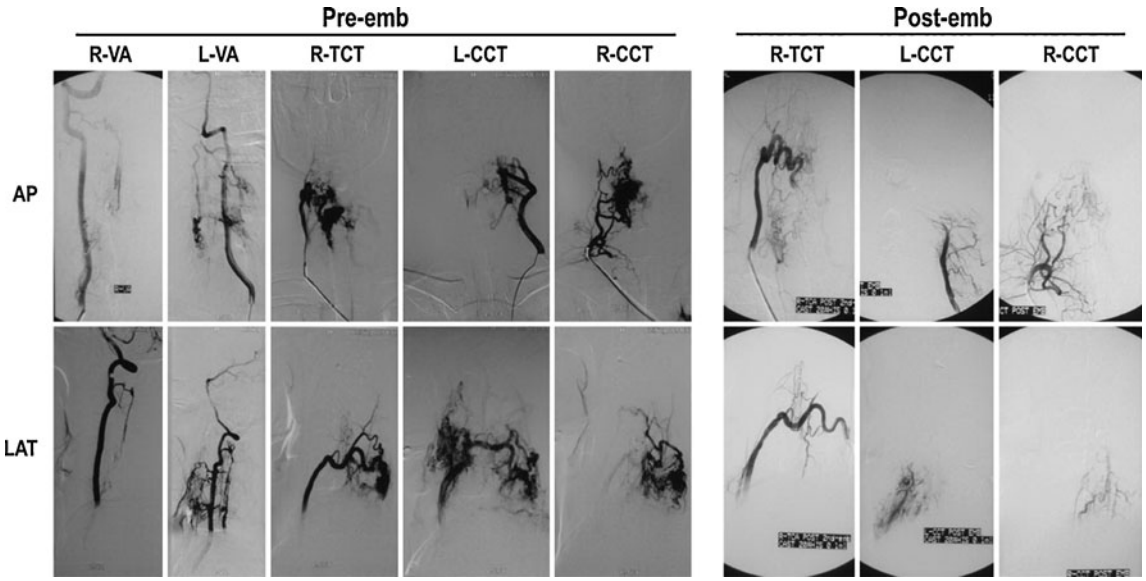

Fig. 2 Superselective angiography and endovascular embolization. *Left column*: angiography for bilateral VA, CCT and TCT; *right column*: post-emb angiography; the embolization was performed via the following feeders: R-CCT, L-CCT, and R-TCT, respectively. The feeding flow was decreased significantly, and nidus was not remarkably opacified. *AP* anterior-posterior view; *LAT* lateral view; *Pre-emb* pre-embolization; *Post-emb* post-embolization; *R* right; *L* left; *VA* vertebral artery; *CCT* costocervical trunk; *TCT* thyrocervical trunk

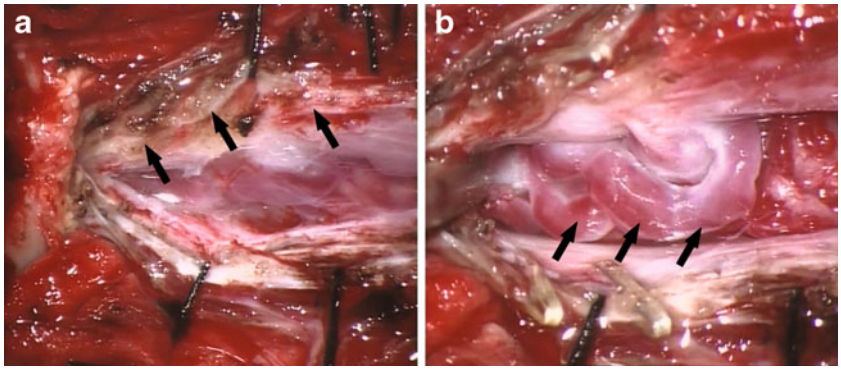

Fig. 3 Intra-operative finding. The dura was grossly thickened (*arrow*, **a**), and an arterialized tortuous vein coursed beneath the subarachnoid space along the dorsal interface of the spinal cord (*arrow*, **b**)

dura, and spinal cord at the same somite were performed. SEM (somatosensory evoked potential), MEP (motor evoked potential), and sphincter electromyography were stable throughout the procedure. Postoperatively, physical examination revealed no neurologic deficit, and the patient resumed independent ambulation. The patient has been followed-up for 7 months. Cervical MRI showed multiple flow void signals in the spinal cord and paravertebral lesions disappeared (Fig. 5). Angiography demonstrated that the feeding flow for paravertebral tissues was decreased significantly, and no nidus could be remarkably identified within the spinal cord (Fig. 6).

We used immunocytochemistry to characterize the tissues. Tissues from the same somite (skin, muscle, dura, and spinal cord) were embedded in paraffin and cut at a thickness of 10 μm. Sections were stained with the following markers, including CD31, SMA, VEGF, and MMP-9. As shown in Fig. 4, AVM-like structures were identified in skin, dura, muscle, and spinal cord (H&E staining). CD31- and SMA-positive signals were present in

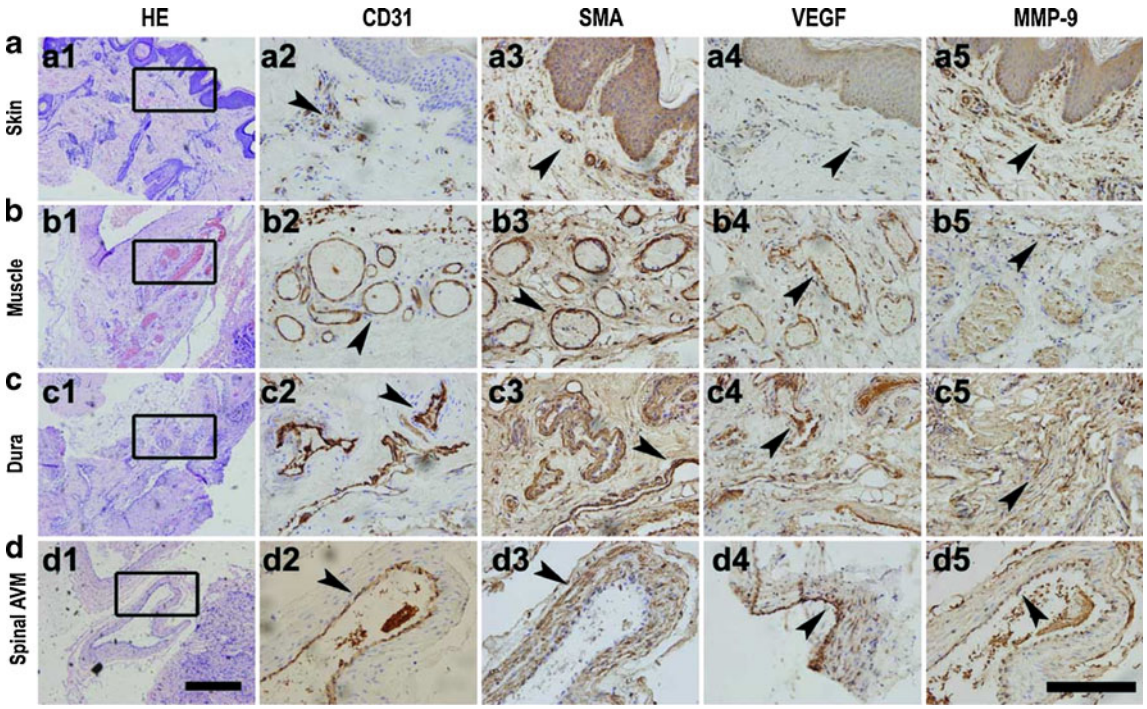

Fig. 4 Panels **a**, **b**, **c**, and **d** represent the AVM-like tissue from skin, muscle, dura, and spinal cord tissues, respectively. H&E staining (*left column*) shows the nidus of the AVM-like structure (*a1-d1*). Tissues were stained with CD31, SMA, VEGF, and MMP-9, respectively. All the marker stainings are a higher magnification of the boxed area from the H&E staining, respectively. For panels **a**–**d**, CD31, SMA, VEGF, and MMP-9-positive signals were all observed in all tissue nidus (*brown color* indicated by *arrows*). CD31-positive staining was specifically found in the lumen of the vessel (*a2-d2*). SMA markers were mainly found within the vessel wall in skin, muscle, dura, and spinal cord (*a3-d3*). VEGF can be found either on the surface of the lumen or in the vessel wall of the AVM-like nidus or in the parenchymal tissues adjacent to the vascular wall (*a4-d4*). MMP-9-positive signals can be mainly found in the lumen of the vessel wall (*a5-d5*), and occasionally in the parenchyma (*c5*). Sections were counterstained with hematoxylin to show blue nuclei. *Scale bar* for H&E, 500 μm; for CD31, SMA, VEGF, and MMP-9 staining, 100 μm

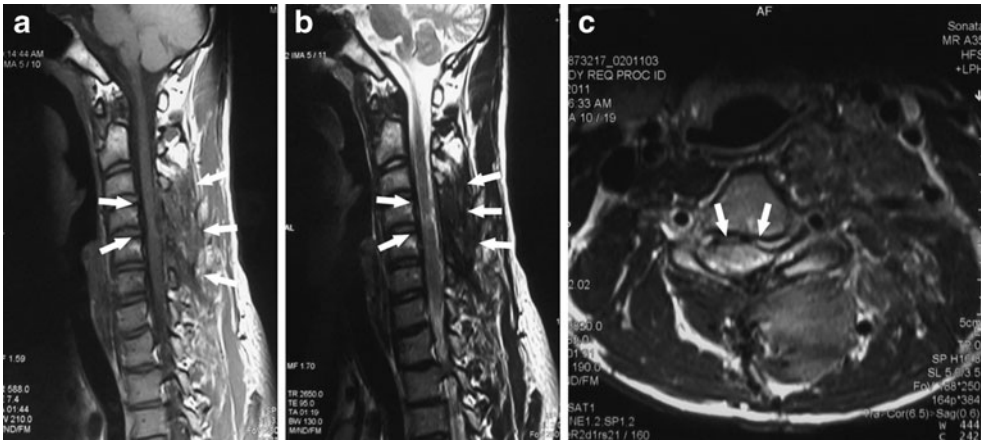

Fig. 5 MRI 6 months after microsurgical resection. Note the flow void signals inside the spinal cord and paravertebral lesions disappeared (*white arrow*). **a** Sagittal T1-weighted image. **b** Sagittal T2-weighted image. **c** Axial view

all tissues, which confirmed blood vessel in nature. Furthermore, these tissues were characteristics of angiogenesis and inflammation. VEGF and MMP-9 were highly expressed within the lesions. VEGF signals were found on the surface of the lumen, within the vessel wall, or in parenchymal tissues adjacent to the vascular wall. MMP-9-positive signals can be mainly found in the lumen of the vessel wall, and occasionally in the parenchyma.

Discussion

Histological characterization of Cobb's syndrome is rarely reported. We report the first description of tissues removed from the same somite during microsurgical resection. Using immunohistochemical analysis in paraffin-embedded samples, this case demonstrated that similar AVM-like structures could be found in tissues within one segment. Angiogenic and inflammatory factors were significantly increased not only in the spinal cord but also in the dura, muscle, and skin, suggesting that these AVM-like structures were of angiogenesis and inflammation.

Cobb's syndrome manifests as the coexistence of cutaneous naevi in a dermatomal pattern and neurological signs of a spinal cord lesion [1]. This is based on the fact that the embryologic origin of the blood supply to the vertebrae and spinal cord derives from the segmental dorsal arteries. Our data corresponds well to a common metameric origin of AVM vessels that create the cutaneomeningospinal angiomas of Cobb's syndrome [12].

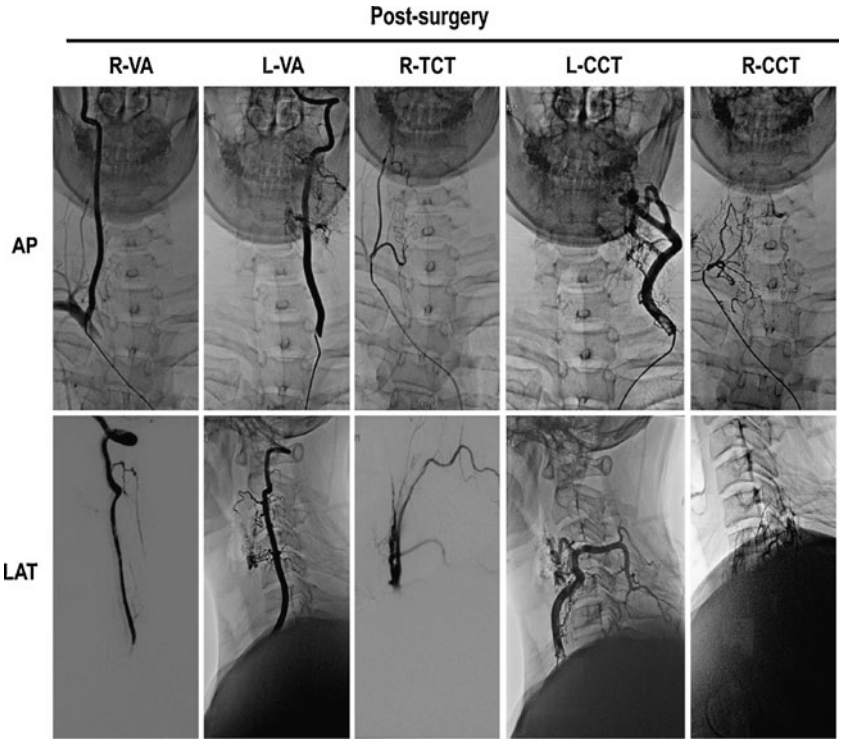

Fig. 6 Superselective angiography 6 months after microsurgical resection. The feeding flow for paravertebral tissues was decreased significantly. No nidus could be remarkably identified within the spinal canal and spinal cord. *AP* anterior-posterior view; *LAT* lateral view; *R* right; *L* left; *VA* vertebral artery; *CCT* costocervical trunk; *TCT* thyrocervical trunk

Not all lesions of Cobb's syndrome can be cured anatomically [10]. Surgery and embolization, or a combination of the two, are the current candidates for treatment. However, AVMs associated with Cobb's syndrome are formidable and treacherous lesions, and are primarily treated with endovascular embolization; surgery is reserved [9]. For this case, microsurgery was attributed to the following reasons: blood flow, particularly those for extradural paravertebral tissues fed by bilateral CCT and right TCT have been significantly decreased by embolization prior to resection, so the risk of life-threatening bleeding during surgery can be minimized; the intradural AVM nidus was mainly fed by PSA, and a posterior approach can provide flow control, make the surgery accessible and biopsy feasible. This surgery was aimed at improving the neurological function by resection of the spinal cord lesions, so the paravertebral and soft lesions were not essentially treated.

These AVM-like structures in Cobb's syndrome seemed to share the similar characterization of brain and spinal cord AVM. First, it manifested as complexes of tortuous, tangled vessels, representing fistulous shunt. Furthermore, our histopathological evidence demonstrated unstable blood vessels, active angiogenesis, and inflammation in AVM-like lesions, which is consistent with the previous report for brain [3] and spinal cord AVM [6]. These factors, including VEGF and MMP-9, mainly resided in the vessel wall or lumen. It may mediate pathological vascular remodeling and impact the clinical course of Cobb's syndrome. Angiogenesis and inflammation may be a contributory cause of Cobb's syndrome pathogenesis or progression linking cytokine genotype with clinical course, such as rupture and bleeding.

Acknowledgements None.

Conflicts of interest None.

Financial disclosure We have no conflicts of interest to disclose.

Grant information / other acknowledgements This study was supported by National Natural Science Foundation of China (81070927)

References

1. Baraitser P, Shieff C (1990) Cutaneomeningo-spinal angiomatosis: the syndrome of Cobb. A case report. Neuropediatrics 21:160–161
2. Brant AJ, James HE, Tung H (1999) Cutaneomeningospinal angiomatosis (Cobb syndrome) with tethered cord. Pediatr Neurosurg 30:93–95
3. Chen Y, Zhu W, Bollen AW, Lawton MT, Barbaro NM, Dowd CF, Hashimoto T, Yang GY, Young WL (2008) Evidence of inflammatory cell involvement in brain arteriovenous malformations. Neurosurgery 62:1340–1349, discussion 1349-1350
4. Cobb S (1915) Haemangioma of the spinal cord: associated with skin naevi of the same metamere. Ann Surg 62:641–649
5. Fukutake T, Kawamura M, Moroo I, Asahina M, Hirayama K (1991) Cobb syndrome and Klippel-Trenaunay-Weber syndrome. Rinsho Shinkeigaku 31:275–279
6. Gao P, Chen Y, Lawton MT, Barbaro NM, Yang GY, Su H, Ling F, Young WL (2010) Evidence of endothelial progenitor cells in the human brain and spinal cord arteriovenous malformations. Neurosurgery 67:1029–1035
7. Gordon-Firing S, Purriel JA, Pereyra D, Brodbek I (1981) Report of a new case of Cobb syndrome. Meningo-spinal cutaneous angiomatosis. Acta Neurol Latinoam 27:99–111
8. Jessen RT, Thompson S, Smith EB (1977) Cobb syndrome. Arch Dermatol 113:1587–1590
9. Kim LJ, Spetzler RF (2006) Classification and surgical management of spinal arteriovenous lesions: arteriovenous fistulae and arteriovenous malformations. Neurosurgery 59:S195–S201, discussion S193-113
10. Liang CH, Zhang HQ, Zhi XL, Zhang P, Li M, Ling F (2010) Treatment of cutaneous vertebral medullary angiomatosis. Zhonghua Yi Xue Za Zhi 90:882–885
11. Miyatake S, Kikuchi H, Koide T, Yamagata S, Nagata I, Minami S, Asato R (1990) Cobb's syndrome and its treatment with embolization. Case report. J Neurosurg 72:497–499
12. Rodesch G, Hurth M, Alvarez H, Ducot B, Tadie M, Lasjaunias P (2004) Angio-architecture of spinal cord arteriovenous shunts at presentation. Clinical correlations in adults and children. The Bicetre experience on 155 consecutive patients seen between 1981-1999. Acta Neurochir Wien 146:217–226, discussion 226-217
13. Shim JH, Lee DW, Cho BK (1996) A case of Cobb syndrome associated with lymphangioma circumscriptum. Dermatology 193:45–47
14. Wang GB, Xu L, Zhao B, Cai SF, Shi H, Li HH, Qu L (2005) Medical imaging findings in Cobb syndrome: two case reports. Chin Med J Engl 118:1050–1053

Acta Neurochir (2011) 153:1669–1675
DOI 10.1007/s00701-011-1049-7

EXPERIMENTAL RESEARCH

Continuous intrathecal glyceryl trinitrate prevents delayed cerebral vasospasm in the single-SAH rabbit model in vivo

Ali Reza Fathi · Serge Marbacher · Thilo Graupner · Felix Wehrli · Stephan M. Jakob · Gerhard Schroth · Javier Fandino

Received: 7 December 2010 / Accepted: 6 May 2011 / Published online: 14 June 2011

Abstract
Background Delayed cerebral vasospasm after aneurysmal subarachnoid hemorrhage (SAH) is a major cause of high morbidity and mortality. The reduced availability of nitric oxide (NO) in blood and cerebrospinal fluid (CSF) is well established as a key mechanism of vasospasm. Systemic administration of glyceryl trinitrate (GTN), an NO donor also known as nitroglycerin, has failed to be established in clinical settings to prevent vasospasm because of its adverse effects, particularly hypotension. The purpose of this study was to analyze the effect of intrathecally administered GTN on vasospasm after experimental SAH in the rabbit basilar artery.
Methods A single-hemorrhage model of SAH in rabbits was used to induce vasospasm. GTN (0.5 mg/ml) or saline was infused via a subcutaneous implanted osmotic pump with continuous drug release into the cerebellomedullary cistern over 5 days. The degree of vasospasm in the basilar artery was recorded with angiography on day 5 after SAH and was compared to baseline angiography on day 0.
Findings Significant reduction of basilar artery diameter was observed in the SAH group with saline infusion compared to sham-operated animals. Intrathecally administered GTN had no effect on the vessel diameter in sham-operated animals, whereas it significantly prevented vasospasm in the SAH group. Intrathecal GTN infusion did not affect arterial blood pressure.
Conclusions Prophylactic, continuous intrathecal administration of GTN prevents vasospasm of the basilar artery in the rabbit SAH model. No toxic effects could be demonstrated in this study. The clinical safety and feasibility of this strategy need to be further investigated.

Keywords Subarachnoid hemorrhage · Cerebral vasospasm · Delayed ischemic neurological deficits · Nitroglycerin · Nitric oxide donors

A. R. Fathi · S. Marbacher · T. Graupner · F. Wehrli · S. M. Jakob · J. Fandino
Cerebrovascular Research Group, Department of Intensive Care Medicine, University of Berne,
Berne, Switzerland

A. R. Fathi (✉) · S. Marbacher · J. Fandino
Department of Neurosurgery, Kantonsspital Aarau,
Tellstrasse,
5001, Aarau, Switzerland
e-mail: ar.fathi@gmx.net

G. Schroth
Institute of Diagnostic and Interventional Neuroradiology,
University Hospital Inselspital Bern,
Bern, Switzerland

T. Graupner · F. Wehrli
Department of Neurosurgery, University Hospital Inselspital Bern,
Bern, Switzerland

Introduction

Aneurysmal subarachnoid hemorrhage (aSAH) occurs in ~15/100,000 persons each year. Delayed ischemic neurological deficit (DIND) develops within 14 days after aSAH and remains the major cause of unfavorable outcome in 25–30% of these patients [8, 9]. The underlying causes of DIND are multifactorial. Nevertheless, arterial narrowing in the time course of DIND, also known as delayed cerebral vasospasm, is a major cause of territorial and/or lacunar brain infarctions [7].

Vasospasm itself underlies a number of different pathophysiological factors. A key factor is the reduced intraar-

terial [16] and cerebrospinal fluid (CSF) [20, 35] concentrations of nitric oxide (NO) as an endothelial-derived relaxing factor (EDRF) after SAH. The pathophysiological mechanisms are mainly the dysfunction of the NO-producing enzyme nitric oxide synthase (NOS) and scavenging of NO due to the presence of deoxyhemoglobin and its high affinity for NO [6]. Based on these facts, classic NO donors [sodium nitroprusside and glyceryl trinitrate (GTN)] have been administered in several experimental settings since the early 1970s [21] in order to enhance NO concentrations and dilate spastic vessels.

Sodium nitroprusside is the most frequently used of these substances, and has been administered intrathecally in several human studies in order to bypass the side effects of systemic administration, such as hemodynamic hypotension and development of tolerance [24, 31]. Despite positive effects on vessel diameter, its routine clinical application has been limited by side effects, such as nausea and vomiting, cardiac arrhythmia, and intracranial hypertension. GTN has been shown to dilate cerebral vessels after experimental SAH and in the clinical setting by intravenous, intraarterial or transdermal administration. In three clinical studies, side effects similar to those seen with sodium nitroprusside developed after systemic administration of the drug (intravenous and transdermal) and therefore limited its use for treatment of vasospasm [13, 26, 29]. Intrathecal administration of GTN has not been tested in clinical studies as of yet.

In a previous study we used intrathecal GTN infusion as a control to the nimodipine infusion group [14]. Despite promising results, this study has been criticized because of remarkable vasospasm in the control group and lack of sham-operated control. More recently, Pluta et al. published a study in primates questioning the effect of intrathecally administered drugs [19]. Consequently, the present study was specifically designed to elucidate the effects of continuous intrathecal GTN on prevention of SAH-induced cerebral vasospasm in an optimized study protocol compared to a sham-operated control.

Methods

The study was performed in accordance with the National Institutes of Health guidelines for the care and use of experimental animals, and with the approval of the Animal Care Committee of the Canton of Bern, Switzerland (approval no. 63/03).

Study design

Forty-six adult male New Zealand White rabbits weighing 3–5 kg were randomly assigned to four experimental groups (6 animals excluded): group 1: sham operation with saline infusion (n=10); group 2: sham operation with continuous GTN infusion (n=10); group 3: SAH with saline infusion (n=10); group 4: SAH with continuous GTN infusion (n=10). All surgical procedures were performed under sterile conditions.

Anesthesia, monitoring, and euthanasia

Induction of general anesthesia was performed by intramuscular administration of ketamine (30 mg/kg) (Ketalar® 50 mg/ml, Pfizer AG, Zurich, Switzerland) and xylazine (6 mg/kg) (Xylapan® 20 mg/mL, Vétoquinol AG, Bern, Switzerland). During surgery, pain evaluation was performed periodically by toe-pinch. Postoperative pain relief was managed by subcutaneous administration of buprenorphine (0.1–0.2 mg/kg; Temgesic® 0.3 mg/ml, Essex Chemie AG, Lucerne, Switzerland) for up to 36 h after SAH. The animals were killed on day 5 post-SAH induction by intraarterial bolus injection of sodium thiopental (40 mg/kg) (Pentothal®, Ospedalia AG, Hünenberg, Switzerland), the same anesthetic used for angiography.

Heart rate and blood pressure were monitored throughout the digital subtraction angiography (DSA) on day 0 and day 5 after experimental SAH. Intravascular pressures and heart rate were measured with a Camino® Multi-Parameter Monitor (Integra™, Plainsboro, NJ). On the same days, arterial blood gas status was analyzed from collected arterial blood samples in order to monitor oxygenation parameters (ABL 725, Radiometer, Copenhagen, Denmark). The animals underwent daily clinical observation.

Angiography

After induction of general anesthesia by intramuscular administration of ketamine (30 mg/kg) and xylazine (6 mg/kg), DSA was performed on day 0 and day 5, as reported previously.[15]. In brief, the rabbit's left (day 0) or right (day 5) subclavian artery was microsurgically exposed and cannulated using a 5.5-French pediatric three-lumen central venous catheter (Arrow Int. Inc., Reading, PA). Subsequently, images of the vertebro-basilar system were obtained by rapid sequential DSA using intraarterial bolus injections of non-ionic iopamidol (0.6 ml/kg; Iopamiro® 300 mg/ml, Bracco, Milan, Italy) as contrast agent. The average diameter of the basilar artery (BA) was digitally calculated in μm using the automatic measurement tool of the ImagePro Discovery® analysis software (Media Cybernetics, Bethesda, MD). Measurements were performed by three blinded investigators, and mean values were used for statistical analysis.

Cerebral vasospasm model

Following baseline DSA on day 0, the atlanto-occipital membrane was microscopically exposed, and a 25-gauge needle was inserted into the cerebromedullary cistern. After relief of 1.0 mL of CSF, an equal amount of nonheparinized autologous arterial blood (saline in sham group) was injected into the cistern under microscopic view [3]. The rabbits were kept positioned at a 65° angle, head-down, for 10 min in order to allow blood dissemination throughout the subarachnoidal space.

Implantation of miniosmotic pump

A miniosmotic pump (0.5 μl/h, model 1007D, Alzet Osmotic Pumps, Durect, Cupertino, CA) containing either 0.5 mg/ml of GTN solution (pH 7.35; Perlinganit, Schwarz Pharma, Münchenstein, Switzerland) or sodium chloride (NaCl) was implanted subcutaneously. This pump model ensures a drug release over 7 days. The dose of GTN was derived from studies with sodium nitroprusside administration in humans in which up to 8 mg/24 h was used for prophylaxis against vasospasm [30, 31]. Pumps, associated tubing, and drugs were protected from light at all times. A silicone catheter (STH-C040, Connectors Verbindungstechnik, Tagelswangen, Switzerland) was connected to the pump and inserted under microscopic view at least 1 mm through the atlanto-occipital membrane into the subarachnoid space. The tube insertion site was sealed by a muscle patch and fixed by several stitches. The midline spinal muscle incision was closed in two layers. Finally, the wounds were superficially irrigated with neomycin sulfate (Research Organics, Cleveland, OH) for infection prophylaxis.

Statistical methods

Values were expressed as a mean in each group±SEM (n= number of animals). Statistical significance between two means and multiple means was determined by parametric one-way ANOVA and Bonferroni's multiple comparisons post-testing, respectively. Statistical significance was considered if the P value was less than 0.05 ($p<0.05$) in the context of 95% confidence intervals of the differences examined (95% CI of difference).

Results

Physiological data

Mean arterial blood pressure (mean 73±12.64 mmHg) and heart rate (mean 165.5±5.9) were not significantly different among the study groups ($p>0.05$). Blood gas analysis showed no significant difference for pCO_2 (mean 43.79± 5.50 mmHg, $p>0.05$), pO_2 (mean 77.8±10.4 mmHg, $p>0.05$), or pH (mean 7.37±0.1, $p>0.05$) (Table 1).

Morbidity, mortality, and neurological status

Five rabbits had to be euthanized before completion of the studies because of poor clinical conditions and were excluded from analysis. Three of them had permanent paralysis of the lower extremities after SAH induction, while two other animals had loss of appetite and deteriorated in general condition. Clinical daily follow-up of the remaining animals was uneventful up to day 5. Gross pathological evaluation revealed no signs of infection. All of the implanted pump devices were precisely placed 1–2 mm beneath the atlanto-occipital membrane.

Angiographic measurements

A total of 80 angiograms of the basilar artery were analyzed. There were no significant differences in the intra- and interobserver analyses ($p>0.05$). Baseline vessel diameter on day 0 did not significantly differ among the six experimental groups. Basilar artery diameter changes in sham-operated animals were not significantly different between saline (4.57±3.6%) and GTN (8.8±5.1%) groups ($p>0.05$). In the SAH group with saline infusion, basilar artery diameter was significantly reduced (16.2±2.8%) on day 5 compared to baseline values ($p<0.05$). The BA

Table 1 Physiological data of the animals during final angiogram

	Sham/NaCl	Sham/GTN	SAH/NaCl	SAH/GTN
MABP (mmHg)	72.8±4.3	73.5±2.1	74.2±2.4	70.9±2.6
Heart Rate	159±6	163±4.8	168±5.4	172±7.5
pO_2 (mmHg)	79.4±14.1	80.5±14.4	76.1±7.1	75.3±5.9
pCO_2 (mmHg)	44.6±1.1	43.8±2.3	41.5±3.5	44.7±2.2
pH	7.4±0.01	7.36±0.02	7.37±0.02	7.36±0.02

There is no significant difference for each parameter between the groups. NaCl: sodium chloride, GTN: glyceryl trinitrate, SAH: subarachnoid hemorrhage, MABP: mean arterial blood pressure. Values are mean ± standard error of mean

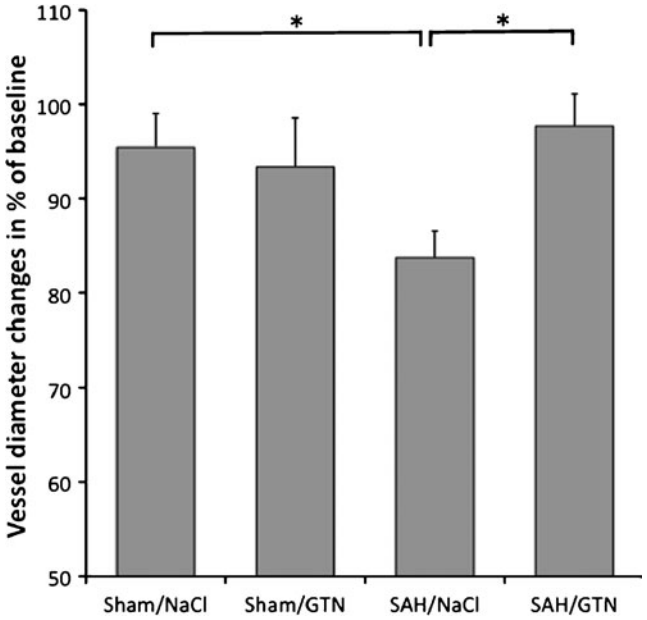

Fig. 1 Relative changes of basilar artery diameter compared to baseline angiograms. Glyceryl trinitrate (GTN) has no significant effect on the basilar artery in sham-operated animals. Subarachnoid hemorrhage (SAH) induces significant vasospasm in the basilar artery, while GTN prevents vasospasm (*$p<0.05$)

diameter after SAH and continuous GTN showed significant prevention of the vessel constriction and was reduced by only 2.29±3.4% ($p<0.05$; Fig. 1).

Discussion

This study confirms that intrathecal continuous infusion of GTN prevents delayed cerebral vasospasm of the rabbit basilar artery after SAH.

Nitric oxide donors have been proven to be effective for reversal and prevention of vasospasm in experimental and clinical trials for almost 4 decades [1, 21]. However, routine clinical application has been limited because of systemic side effects. Intravenous and transdermal GTN have been tested in three clinical trials showing dilative effects on vessel diameter (Table 2) [13, 26, 29]. However, further clinical evaluation was abandoned because of systemic side effects. Although several animal studies have shown a beneficial effect of GTN (Table 3), the effect of intrathecal GTN administration with the intention of bypassing these side effects has not been conclusively investigated. In a previous study with intrathecal nimodipine and GTN, we have shown the feasibility of intrathecal administration of GTN [14]. The present study confirms that intrathecal administration of GTN is safe and prevents vasospasm at lower dosage over 5 days of infusion in a rabbit model.

The clinical status and the arterial blood pressure at day 5 did not indicate a drop in blood pressure compared to day 0. Since pH and pO_2 can alter pCO_2 and thus influence cerebral autoregulation and vessel diameter [4], we excluded the effect of these parameters by maintaining comparable values in all study groups. However, we did not measure the concentration of the NO metabolome in CSF and in blood for correlation studies with clinical data.

Another limitation of the systemic application of GTN as prescribed for long-term use in angina pectoris treatment is the development of drug tolerance [10]. Since the vasodilatory effect is present after 5 days of continuous infusion, we conclude that there is no drug tolerance in this short period of treatment. Considering that peak vasospasm after SAH occurs between days 3 and 14, we do not expect tolerance to develop during short-term treatment in SAH patients receiving GTN.

Pluta et al. investigated the extent of intrathecal drug distribution around the middle cerebral artery in the primate model of SAH and expressed concern about sufficient drug penetration through the blood clot to the artery [19]. However, the present study, like others with sodium nitroprusside, has demonstrated that this limitation does not apply to NO donors since the vasoactive effect remains unaffected by the presence of the blood clot. The main

Table 2 Clinical studies with nitroglycerin

Author	Year	Journal	Administration route	Assessment method	Results	Comments
Tanaka	2001	Acta Neurochirurgica	Intravenous	Neurological outcome	DIND 24% in nitroglycerin group vs. 60% in Fasudil group alone	25 patients in combination with Fasudil
Lesley	2003	American Journal of Neurorad	Transdermal	Arteriogram	Improvement of CVS signs in all patients (no outcome data)	5 patients, technical note
Reinert	2004	Neurological Research	Transdermal	TCD and CT perfusion	TCD velocity significantly decreased in nitroglycerin group	9 patients, 8 controls

None of the human studies tested intrathecal administration of nitroglycerin

TCD: Transcranial Doppler

Table 3 Experimental studies with nitroglycerin

Author	Year	Journal	Animal type	In vivo/ex vivo	Administration route	Assessment method
Poletti	1972	Surg Forum	Dog	In vivo	Local perivascular	In vivo visualization
Kistler	1979	Stroke	Dog	In vivo	Intravenous	Arteriogram
Shimizu	1980	Stroke	Dog	Ex vivo	Local perivascular	Ex vivo analysis
Frazee	1981	J Neurosurg	Primate	In vivo	Intravenous	Arteriogram
VonEssen	1981	Stroke	Dog	In vivo	Intravenous	CBF and ICP
Kistler	1982	Arch Neurolo	Primate	In vivo	Intravenous and intraarterial	Arteriogram
Liszczak	1983	J Neurosurg	Dog	In vivo	Intravenous	Arteriogram
Kanamaru	1989	J Neurosurg	Primate	In vivo	Local perivascular	Ex vivo analysis
Nakao	1996	Stroke	Primate	In vivo	Intravenous	Arteriogram
Thomas	1997	Neurosurgery	Rabbit	In vivo	Local perivascular	In vivo visualization
Ito	2000	J Cardiovasc Pharmacol	Rabbit	In vivo	Transdermal	Arteriogram
Tanaka	2001	Neurol Med Chir (Tokyo)	Dog	Ex vivo	Local perivascular	Ex vivo analysis
Marbacher	2008	Intensive Care Medicine	Rabbit	In vivo	Intrathecal	Arteriogram

TCD: Transcranial Doppler, CBF: Cerebral blood flow, ICP: Intracranial pressure

reason for this might be that the viscosity of Evans blue (in Pluta's study) [19] is not comparable to the viscosity of nitric oxide donors, and moreover, once NO is released from GTN, it has very high tissue permeability and diffuses freely across membranes.

Another concern with intrathecal administration of drugs is catheter infections resulting in meningitis and ventriculitis. Infection risk might be reduced by implanting antibiotic-impregnated catheters [28]. Moreover, the intrathecal route might become more accessible since studies with intrathecal rTPA, cisternal washing, and lumbar CSF drainage may be more applicable in combination with NO donors and similar drugs that are more feasibly administered this way [11].

Intrathecal sodium nitroprusside, a different class of NO donor, is the only NO donor that has been tested intrathecally in clinical studies after SAH, and has also been proven to dilate constricted vessels (Table 4) [1, 12, 17, 18, 23, 24, 30, 31, 33]. However, systemic side effects, especially cyanide poisoning [25], have limited further use of this drug. Since GTN has different mechanisms of NO release than sodium nitroprusside, distinct patterns of adverse effects are expected. However, this has yet to been confirmed and evaluated in clinical studies.

Our study confirms the important role of NO in the pathophysiology of vasospasm, as reported with other classes of NO donors in experimental settings. Among them, NONOates represent a distinct class of NO donors

Table 4 Clinical studies with Sodium nitroprusside as an NO donor and intrathecal application

Author	Year	Journal	Results	Assessment method	Comments
Thomas	1999	Neurosurgery	Reversal, all 3 patients with good outcome	Arteriogram and TCD	3 patients
Thomas	1999	Stroke	Reversal in 6/15 patients	Arteriogram and TCD	15 patients
Vajkoczy	2000	Stroke	Reversal of CVS	CPP, brain O_2 saturation	Case report
Raabe	2002	JNNP	Reversal of CVS	Brain O_2 saturation	Case report
Raabe	2002	Neurosurgery	1 patient with angiographic reversal, no difference in outcome between treated and untreated patients	Arteriogram and brain O_2 saturation	13 patients
Kumar	2003	Neurol India	Reversal, good outcome in 6/10	Arteriogram and TCD	10 patients
Pathak	2003	Br J Neurosurg	Prevention and reversal, good outcome in 5/8 patients	TCD	8 patients
Pachl	2005	Acta Neurochirurgica	Prevention in 13/17	TCD, GCS	16 patients, inhomogeneous study design
Agrawal	2009	Minim Invas Neurosurg	Reversal, good outcome in 7/10	TCD	10 patients

TCD: Transcranial Doppler, CPP: Cerebral perfusion pressure, GCS: Glasgow Coma Scale

that have been tested intrathecally in animal studies using polymer pellets [2, 22, 32, 34]. Other than one study in primates [2], all other studies with NONOates have shown significant vessel dilation. One drawback with NONOates is that they have been shown to open the blood-brain barrier at higher doses und thus provoke brain infarction and toxicity [5]. Other classes of NO donors that have been tested in experimental settings are S-nitrosothiols and sodium nitrite [20, 27]. Preliminary results are very promising, but the therapeutic value has yet to be confirmed.

Despite certain limitations of the single-hemorrhage rabbit model of SAH, it provides a reliable screening method to evaluate the therapeutic potential of various drugs. This applies particularly to the vast array of nitric oxide donors and the need to investigate doses and administration routes. This study serves as a *proof of concept* for development of new treatment strategies such as intrathecal delivery of NO donors. It is of utmost importance to consider the multifactorial course of the disease, and thus to consider the therapeutic aspects as multidirectional as well. This includes the neuroprotective effect of nimodipine, optimized clinical management, NO donors, and anti-inflammatory therapeutics. In this multidirectional treatment approach one goal should be the reduction of individual drug dosages in order to minimize side effects.

Many patients are referred several days after SAH and may present with clinical and angiographic signs of vasospasm. Whether intrathecal GTN can reverse established vasospasm in this specific patient group remains unclear. Thus, addition studies are warranted to address the effect of intrathecal NO not only for prevention but also for reversal of vasospasm.

Conclusion

Intrathecal administration of the NO donor GTN attenuates vasospasm in the rabbit single-hemorrhage SAH model. Further experimental and clinical evaluation of different classes of NO donors is necessary in order to ascertain the best source and administration route of NO and to optimize its therapeutic potential.

Conflicts of interest None.

References

1. Agrawal A, Patir R, Kato Y, Chopra S, Sano H, Kanno T (2009) Role of intraventricular sodium nitroprusside in vasospasm secondary to aneurysmal subarachnoid haemorrhage: a 5-year prospective study with review of the literature. Minim Invasive Neurosurg 52:5–8
2. Aihara Y, Jahromi BS, Yassari R, Sayama T, Macdonald RL (2003) Effects of a nitric oxide donor on and correlation of changes in cyclic nucleotide levels with experimental vasospasm. Neurosurgery 52:661–667, discussion 666–667
3. Fandino J, Sherman JD, Zuccarello M, Rapoport RM (2003) Cocaine-induced endothelin-1-dependent spasm in rabbit basilar artery in vivo. J Cardiovasc Pharmacol 41:158–161
4. Faraci FM, Breese KR, Heistad DD (1994) Cerebral vasodilation during hypercapnia. Role of glibenclamide-sensitive potassium channels and nitric oxide. Stroke 25:1679–1683
5. Gabikian P, Clatterbuck RE, Eberhart CG, Tyler BM, Tierney TS, Tamargo RJ (2002) Prevention of experimental cerebral vasospasm by intracranial delivery of a nitric oxide donor from a controlled-release polymer: toxicity and efficacy studies in rabbits and rats. Stroke 33:2681–2686
6. Gow AJ, Stamler JS (1998) Reactions between nitric oxide and haemoglobin under physiological conditions. Nature 391:169–173
7. Hansen-Schwartz J, Vajkoczy P, Macdonald RL, Pluta RM, Zhang JH (2007) Cerebral vasospasm: looking beyond vasoconstriction. Trends Pharmacol Sci 28:252–256
8. Hop JW, Rinkel GJ, Algra A, van Gijn J (1997) Case-fatality rates and functional outcome after subarachnoid hemorrhage: a systematic review. Stroke 28:660–664
9. Kassell NF, Torner JC (1984) The International Cooperative Study on Timing of Aneurysm Surgery–an update. Stroke 15:566–570
10. Klemenska E, Beresewicz A (2009) Bioactivation of organic nitrates and the mechanism of nitrate tolerance. Cardiol J 16:11–19
11. Klimo P Jr, Kestle JR, MacDonald JD, Schmidt RH (2004) Marked reduction of cerebral vasospasm with lumbar drainage of cerebrospinal fluid after subarachnoid hemorrhage. J Neurosurg 100:215–224
12. Kumar R, Pathak A, Mathuriya SN, Khandelwal N (2003) Intraventricular sodium nitroprusside therapy: a future promise for refractory subarachnoid hemorrhage-induced vasospasm. Neurol India 51:197–202
13. Lesley WS, Lazo A, Chaloupka JC, Weigele JB (2003) Successful treatment of cerebral vasospasm by use of transdermal nitroglycerin ointment (Nitropaste). AJNR Am J Neuroradiol 24:1234–1236
14. Marbacher S, Neuschmelting V, Graupner T, Jakob SM, Fandino J (2008) Prevention of delayed cerebral vasospasm by continuous intrathecal infusion of glyceroltrinitrate and nimodipine in the rabbit model in vivo. Intensive Care Med 34:932–938
15. Neuschmelting V, Fathi AR, Hidalgo Staub ET, Marbacher S, Schroth G, Takala J, Jakob SM, Fandino J (2009) Norepinephrine-induced hypertension dilates vasospastic basilar artery after subarachnoid haemorrhage in rabbits. Acta Neurochir (Wien) 151:487–493
16. Neuschmelting V, Marbacher S, Fathi AR, Jakob SM, Fandino J (2009) Elevated level of endothelin-1 in cerebrospinal fluid and lack of nitric oxide in basilar arterial plasma associated with cerebral vasospasm after subarachnoid haemorrhage in rabbits. Acta Neurochir (Wien) 151:795–801, discussion 801–792
17. Pachl J, Haninec P, Tencer T, Mizner P, Houst'ava L, Tomas R, Waldauf P (2005) The effect of subarachnoid sodium nitroprusside on the prevention of vasospasm in subarachnoid haemorrhage. Acta Neurochir Suppl 95:141–145
18. Pathak A, Mathuriya SN, Khandelwal N, Verma K (2003) Intermittent low dose intrathecal sodium nitroprusside therapy for treatment of symptomatic aneurysmal SAH-induced vasospasm. Br J Neurosurg 17:306–310
19. Pluta RM, Butman JA, Schatlo B, Johnson DL, Oldfield EH (2009) Subarachnoid hemorrhage and the distribution of drugs delivered into the cerebrospinal fluid. J Neurosurg

20. Pluta RM, Dejam A, Grimes G, Gladwin MT, Oldfield EH (2005) Nitrite infusions to prevent delayed cerebral vasospasm in a primate model of subarachnoid hemorrhage. JAMA 293:1477–1484
21. Poletti CE, Wepsic JG, Sweet WH (1972) Middle cerebral arterial spasm from subarachnoid blood: spasmolysis with topical use of nitroglycerin. Surg Forum 23:449–450
22. Pradilla G, Thai QA, Legnani FG, Hsu W, Kretzer RM, Wang PP, Tamargo RJ (2004) Delayed intracranial delivery of a nitric oxide donor from a controlled-release polymer prevents experimental cerebral vasospasm in rabbits. Neurosurgery 55:1393–1399, discussion 1399–1400
23. Raabe A, Vatter H, Zimmermann M, Seifert V (2002) Reversal of tissue hypoxia by a single intraventricular dose of sodium nitroprusside in a patient with severe medically refractory cerebral vasospasm after subarachnoid haemorrhage. J Neurol Neurosurg Psychiatry 72:123–124
24. Raabe A, Zimmermann M, Setzer M, Vatter H, Berkefeld J, Seifert V (2002) Effect of intraventricular sodium nitroprusside on cerebral hemodynamics and oxygenation in poor-grade aneurysm patients with severe, medically refractory vasospasm. Neurosurgery 50:1006–1013, discussion 1013–1004
25. Ram Z, Spiegelman R, Findler G, Hadani M (1989) Delayed postoperative neurological deterioration from prolonged sodium nitroprusside administration. Case report. J Neurosurg 71:605–607
26. Reinert M, Wiest R, Barth L, Andres R, Ozdoba C, Seiler R (2004) Transdermal nitroglycerin in patients with subarachnoid hemorrhage. Neurol Res 26:435–439
27. Sehba FA, Ding WH, Chereshnev I, Bederson JB (1999) Effects of S-nitrosoglutathione on acute vasoconstriction and glutamate release after subarachnoid hemorrhage. Stroke 30:1955–1961
28. Sloffer CA, Augspurger L, Wagenbach A, Lanzino G (2005) Antimicrobial-impregnated external ventricular catheters: does the very low infection rate observed in clinical trials apply to daily clinical practice? Neurosurgery 56:1041–1044, discussion 1041–1044
29. Tanaka Y, Masuzawa T, Saito M, Yamada T, Ebihara A, Iwasa H, Mori S (2001) Combined administration of Fasudil hydrochloride and nitroglycerin for treatment of cerebral vasospasm. Acta Neurochir Suppl 77:205–207
30. Thomas JE, Rosenwasser RH (1999) Reversal of severe cerebral vasospasm in three patients after aneurysmal subarachnoid hemorrhage: initial observations regarding the use of intraventricular sodium nitroprusside in humans. Neurosurgery 44:48–57, discussion 57–48
31. Thomas JE, Rosenwasser RH, Armonda RA, Harrop J, Mitchell W, Galaria I (1999) Safety of intrathecal sodium nitroprusside for the treatment and prevention of refractory cerebral vasospasm and ischemia in humans. Stroke 30:1409–1416
32. Tierney TS, Clatterbuck RE, Lawson C, Thai QA, Rhines LD, Tamargo RJ (2001) Prevention and reversal of experimental posthemorrhagic vasospasm by the periadventitial administration of nitric oxide from a controlled-release polymer. Neurosurgery 49:945–951, discussion 951–943
33. Vajkoczy P, Hubner U, Horn P, Bauhuf C, Thome C, Schilling L, Schmiedek P, Quintel M, Thomas JE (2000) Intrathecal sodium nitroprusside improves cerebral blood flow and oxygenation in refractory cerebral vasospasm and ischemia in humans. Stroke 31:1195–1197
34. Wolf EW, Banerjee A, Soble-Smith J, Dohan FC Jr, White RP, Robertson JT (1998) Reversal of cerebral vasospasm using an intrathecally administered nitric oxide donor. J Neurosurg 89:279–288
35. Woszczyk A, Deinsberger W, Boker DK (2003) Nitric oxide metabolites in cisternal CSF correlate with cerebral vasospasm in patients with a subarachnoid haemorrhage. Acta Neurochir (Wien) 145:257–263, discussion 263–254

Comment

In the present report, the authors have studied the effects of intrathecal administration of the NO donor glyceryl trinitrate using a single-hemorrhage model in the rabbit. GTN is shown to reduce the SAH-associated vasoconstriction of the basilar artery by approximately 10% during a 5-day infusion protocol using osmotic mini pumps. The results are statistically significant but seem to be not too impressive with respect to clinical relevance, especially in light of the drawbacks of the single-hemorrhage model in the rabbit. On the other hand, this study may serve as a proof of concept for further development of strategies that aim at local delivery of NO donors to the basal cisterns. We strongly believe that the recent, disappointing results with the systemic administration of vasoactive drugs in order to prevent cerebral vasospasm underline the necessity of promoting alternative routes of drug administration, especially directly to the affected blood vessels. This can be achieved by using continuous infusion techniques or the use of slow-release formulations. For the future, this certainly is the most promising concept for achieving an optimal vasodilatory effect at the vessels and, at the same time, avoiding systemic side effects that might counteract the beneficial effect of the drug.

Peter Vajkoczy
Berlin, Germany

This paper explores the use of nitiric oxide donors in the intrathecal space for the treatment of subarachnoid hemorrhage. The topic itself is not new. Intrathecal pumps and intrathecal polymers delivering nitric oxide agents directly to the subarachnoid space have been tested in trials over the last several years, mostly with encouraging reductions in pathological markers of vasospasm. In the vein of these past studies, the authors have demonstrated that glyceryl trinitrate, a compound previously abandoned as a systemic therapy for vasospasm, may have genuine therapeutic value as an intrathecal agent. They demonstrate that intrathecal delivery of this nitric oxide donor does not produce the same prohibitive hypotension noted in systemic administration. While they also demonstrate that basilar artery diameter reduction was less with the experimental arm, it would be interesting to know whether delayed administration of this drug would produce similar results. Few patients, after all, could have intrathecal administration of a drug immediately with their aneurismal rupture. The concept is clever and promising, and we hope to learn more from this group.

Markus J. Bookland
Christopher Loftus
Philadelphia, PA

Acta Neurochir (2011) 153:1677–1685
DOI 10.1007/s00701-011-1016-3

CLINICAL ARTICLE

The clinical features and surgical outcomes of patients with intramedullary spinal cord cavernous malformations

Gwi Hyun Choi · Keung Nyun Kim · Sarah Lee · Gyu Yeul Ji · Jae Keun Oh · Tae Yup Kim · Do Heum Yoon · Yoon Ha · Seong Yi · Hyunchul Shin

Received: 16 November 2010 / Accepted: 1 April 2011 / Published online: 2 July 2011

Abstract
Background Cavernous malformations (CMs) are not uncommon, but most of them are found to be located intracranially. Intramedullary CMs are rare, accounting for only 3–5% of identified total central nervous system lesions. The natural history of intramedullary CMs and their clinical features, including the risk of hemorrhage from a large series, still remains unclear and needs to be elucidated. We review our experience with surgically treated patients with intramedullary CMs and discuss the clinical features and surgical outcomes.
Methods Between March 2004 and March 2010, a total of 21 patients with intramedullary spinal cord CMs were surgically treated in a single institution. Data from 21 patients were retrospectively analyzed.
Results There were 13 females and 8 males ranging in age from 10 to 70 years (mean age 39.3 years). All patients harbored single symptomatic CM of the nervous system, and multiple lesions were not found. The annual retrospective hemorrhage rate was 2.18% per patient/year. All but one CM were completely resected, and the average follow-up period was 22.1 months (1–73 months). Ten of the 21 patients experienced an improvement in neurological state, 9 patients remained unchanged, and 2 patients experienced worsening of their conditions.
Conclusions Symptomatic intramedullary CMs should be surgically removed to avoid further neurological deterioration. Though there are some limitations due to the retrospective nature of this study and its small number of patients, the prognosis was found to be related to the preoperative neurological state and to the type of symptom presentation.

Keywords Cavernous malformations · Spinal cord · Intramedullary · Prognostic factors

This study was presented as a digital poster at the 2010 annual meeting of the Congress of Neurological Surgeons, San Francisco, CA

G. H. Choi · K. N. Kim · G. Y. Ji · J. K. Oh · T. Y. Kim · D. H. Yoon · Y. Ha · S. Yi
Department of Neurosurgery, College of Medicine, Yonsei University, Seoul, Korea

S. Lee
Department of Pathology, College of Medicine, Yonsei University, Seoul, Korea

H. Shin
Department of Neurosurgery, College of Medicine, Sungkyunkwan University, Seoul, Korea

H. Shin (✉)
Department of Neurosurgery, Kangbuk Samsung Hospital, Sungkyunkwan University, School of Medicine, Seoul 110–746, South Korea
e-mail: nsdrshin@gmail.com

Introduction

Cavernous malformations (CMs) are angiographically occult vascular malformations that can arise in any part of the central nervous system. Two large retrospective reviews found an overall incidence rate of 0.4-0.5% in the general populations [6, 20]. They are not uncommon, but most are found in intracranial locations, especially in supratentorial compartments [3]. Intramedullary CMs are rare, accounting for only 3–5% of the total identified CNS lesions [5, 9, 10, 12, 15, 22].

There are many reports regarding the natural history and surgical outcomes of intramedullary CMs. However, most of these are case series with a small number of patients, and few authors have presented a series of more than ten cases [4, 13]. The natural history of intramedullary CMs and their potential risk of hemorrhage from a large series remain unclear and should be elucidated. In this study, we retrospectively review a series of 21 patients with surgically treated intramedullary CMs in a single institution and discuss their clinical features, potential risks of hemorrhage, surgical outcomes and prognostic factors.

Methods and materials

Patient population

Between March 2004 and March 2010, a total of 618 patients with spinal cord tumors were surgically treated in our institution. Among them, 21 patients harbored histologically proven intramedullary spinal cord CMs, and their charts were reviewed retrospectively. All patients had single symptomatic CMs of the nervous system, and multiple lesions were not found. There were 13 female and 8 male patients ranging in age from 10 to 70 years (mean age 39.3 years). Our criteria for hemorrhage were sudden onset of neurological symptoms and corresponding manifestation of neurological deficits. The annual retrospective hemorrhage rate was calculated using the following formula.

Hemorrhage rate = the number of hemorrhagic events/ summation of patient age in years

The patients' pre- and postoperative neurological states were classified according to the modified McCormick scale (MMCS) [17](Table 1). We identified some common features of symptom presentation among patients with CMs and classified the patients into the following three groups:

(1) A: acute onset of symptoms
(2) C: chronic progressive myelopathy
(3) M: acute neurological decline from various sequelae by previous attack

Radiological study

The preoperative radiological investigation included plain films and magnetic resonance imaging (MRI) in all cases. Postoperative MRI was performed in selected cases with the patient's consent during follow-up.

Surgery

Patients were placed prone, and additional three-point skull fixation was used for lesions above the upper thoracic level. The operative approach was made through a conventional laminectomy in the early days of surgery and through laminoplastic laminotomy. The surgery was performed under standard microsurgical conditions with intraoperative monitoring of somatosensory-evoked potentials (SSEP) to minimize the risk of neurological injury. After the opening of the dura over the location of the lesion as defined by MRI, the myelotomy was performed, and the lesion was removed along the gliotic plane surrounding the malformation.

Follow-up

Patient follow-up was performed via an outpatient department clinic or by telephone interviews. The average follow-up period was 22.1 months (1–73 months).

Statistical analysis

Statistical analysis was carried out using the Kruskal-Wallis and Mann-Whitney tests with SPSS (Statistical Package for Social Science) for Windows Release 14.0 to analyze the differences in outcomes. A p value of less than 0.05 was considered statistically significant.

Illustrative cases

Case 11

This 45-year-old female presented with a tingling sensation and numbness of the left lower extremity for 2 months. A

Table 1 Modified McCormick scale for functional classification of patients with CMs

Grade	Definition
1	Neurologically intact, ambulates normally, may have minimal dysesthesia
2	Mild motor or sensory deficit, maintains functional independence
3	Moderate deficit, limitation of function, independent with external aid
4	Severe motor or sensory deficit, dependent with external aid
5	Paraplegia or quadriplegia

neurological examination revealed no deficit except numbness of the left lower extremity. The MR images of her thoracic spine showed a 9-mm-sized intramedullary lesion with mixed signal intensity on T1- and T2-weighted sequences. A dark signal intensity rim on T2-weighted images, suggestive of a hemosiderin ring, was also observed. The preoperative diagnosis was intramedullary CM, and she underwent an operation through a T2 laminoplastic laminotomy. After the opening of the dura, the lesion was identified directly on the surface of the spinal cord and was completely excised along the gliotic plane. The histopathological findings were consistent with CM. She complained of brief postoperative aggravation of the tingling sensation in the left lower extremity, but at her last follow-up 26 months postoperation, there was only mild numbness in the extremity. The postoperative MR images showed complete resection of the lesion (Fig. 1).

Case 12

This 43-year-old male presented with pain and paresthesia in both hands for 6 months. Upon neurological examination, he was found to be quadriparetic with grade 4 motor strength in all his extremities. The MR images showed a 15-mm-sized mixed signal intensity lesion at the cervicomedullary junction on the T1- and T2-weighted images. Mild to moderate and heterogenous enhancement was observed after administration of gadolinium. Total laminectomy of C1 and C2, and an additional suboccipital craniectomy were performed, and the lesion was completely excised. The histopathological examination revealed a diagnosis of CM. No remnant of the tumor was identified on postoperative MR images performed 9 months after the operation. At the last follow-up, the objective muscle strength was the same as in the preoperative state, but he described a worsening of subjective weakness (Fig. 2).

Case 16 (Fig. 3)

This 24-year-old female presented with a sudden-onset tingling sensation in her right hand and quadriparesis for 4 days. She had no significant medical or trauma history. The neurological examination revealed grade 2 to 3 quadriparesis. The initial MR images of her cervical spine showed hematomyelia accompanied by severe cord swelling. After conservative care for 3 weeks, repeated MR images were obtained and revealed resolved cord swelling and a dark intensity rim on T2- weighted images at the center of the hematoma. She underwent an operation through C4, C5, C6 laminoplastic laminotomy. The

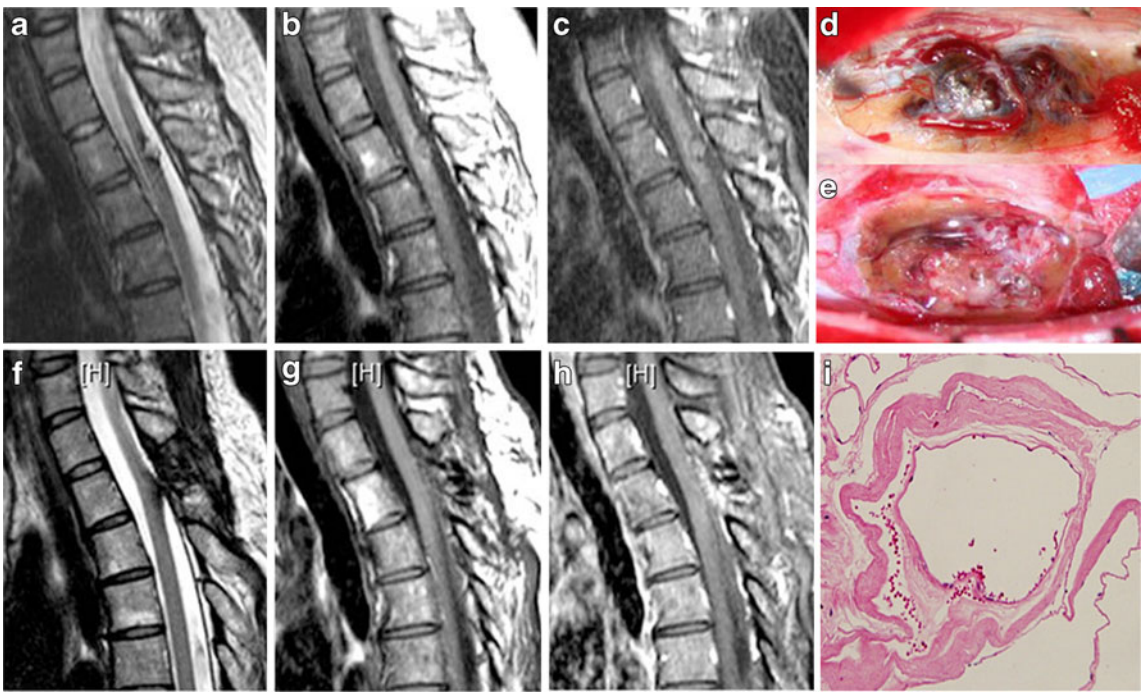

Fig. 1 Case 11. CM located at T2 level. **a-c** Preoperative MRI. **d**, **e** Intraoperative photographs. **f-h** Postoperative MRI. **i** Pathological image. **a** Sagittal T2-weighted image showing the intramedullary lesion with hemosiderin ring. **b** Sagittal T1-weighted image demonstrating mixed signal intensity inside the lesion. **c** Sagittal contrast-enhanced T1-weighted image revealing poor enhancement of the lesion. **d**, **e** Operative photographs showing complete removal of the lesion. **f**, **g**, **h** Postoperative MRI showed no remnant. **i** Pathological image showing large, dilated, blood-filled vessels lined with a single layer of flattened endothelial cells with no intervening parenchyma. Hematoxylin and eosin, ×100

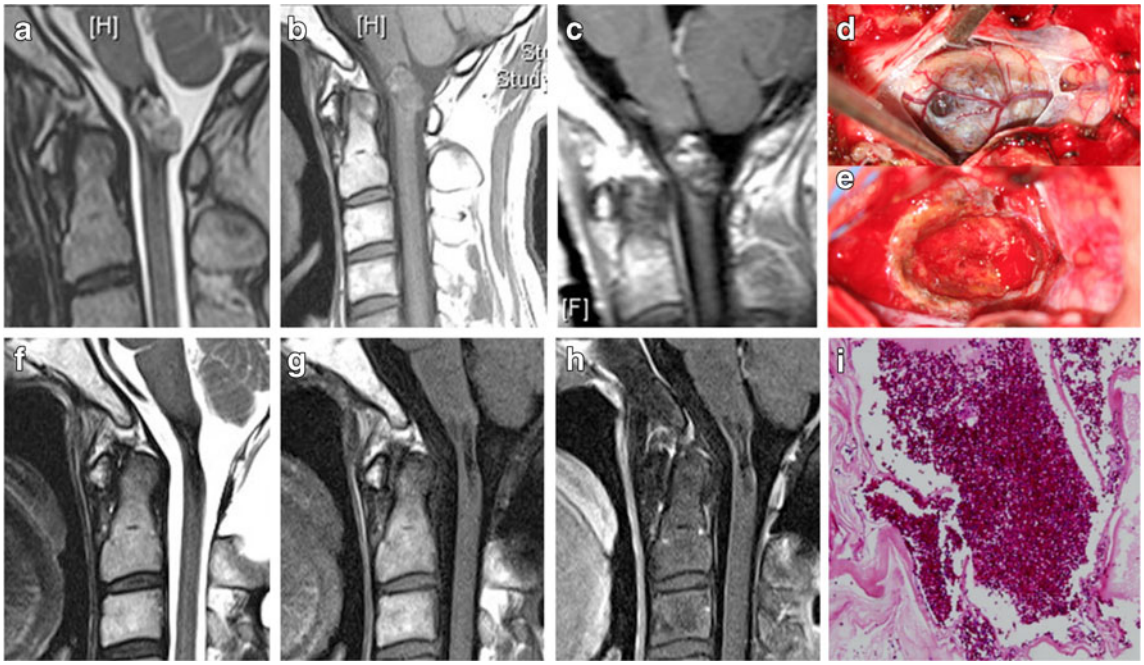

Fig. 2 Case 12. CM located at the cervicomedullary junction. **a-c** Preoperative MRI. **d**, **e** Intraoperative photographs. **f-h** Postoperative MRI. **i** Pathological image. **a**, **b**, **c** Preoperative MRI showing the irregularly shaped, sharply defined and poorly enhanced intramedullary lesion with hemosiderin ring. **d**, **e** Operative photographs showing abnormal dilated vessels and grayish discoloration of the pial surface. **f**, **g**, **h** Postoperative MRI showing no remnant. **i** Pathological image compatible with diagnosis of CM. Hematoxylin and eosin, ×40

postoperative diagnosis of CM was histopathologically confirmed. Her neurological state remained unchanged immediately postoperation, but it improved to grade 4 of muscle strength at 13 months postoperation.

Results

Clinical presentation and radiological findings

The clinical data of the patients with cavernous malformations are listed in Table 2. We observed a total of 18 hemorrhagic episodes in 826 patient-years of life. Namely, there were eight patients who had one hemorrhagic episode and five patients who had two hemorrhagic episodes. Assuming that these patients were harboring cavernous malformation already at birth, the retrospective hemorrhage rate would be 2.18% per lesion and year. The most common presenting symptom was motor deficit. According to the aforementioned classification of symptom presentation, eight patients were categorized as type A, eight patients as type B, and five patients as type M. The level of the lesion was cervical in nine patients, thoracic in nine patients, lumbar in one patient, cervicomedullary junction in one patient, and thoracolumbar junction in one patient. The mean size of the lesion was 11.7 mm (4.93–26.74 mm). The location of the lesion within the spinal cord was central in 11 patients and lateral in 10 (Table 3).

Surgical procedures and findings

For the surgical approach, ten patients underwent conventional laminectomy and one patient underwent an additional suboccipital craniectomy. Nine patients underwent laminoplastic laminotomy, and the remaining patient (case 17) underwent a second operation; the first operation was 13 years prior through laminectomy at another hospital. After bony removal and the opening of the dura, the lesion itself or bluish discoloration of the pial surface were easily found in most of the patients. The myelotomy was performed over this area using the operating microscope. Cavernous angiomas generally have a gliotic plane separating the lesion from normal spinal cord, and the complete resection from the center to periphery was possible in all except one patient. Complete resection was also confirmed in 14 patients with postoperative MRI, but the remaining 7 patients refused postoperative MRI for personal reasons. Intraoperative SSEP monitoring showed no significant change during the operation in all patients. We observed no major complications related to the surgical procedures.

Surgical outcomes and prognostic factors

Postoperatively, there were eight patients with MMCS 1, seven patients with MMCS 2, five patients with MMCS 3, and one patient with MMCS 4, respectively (Table 4). Seven patients experienced improvement of the neurological state

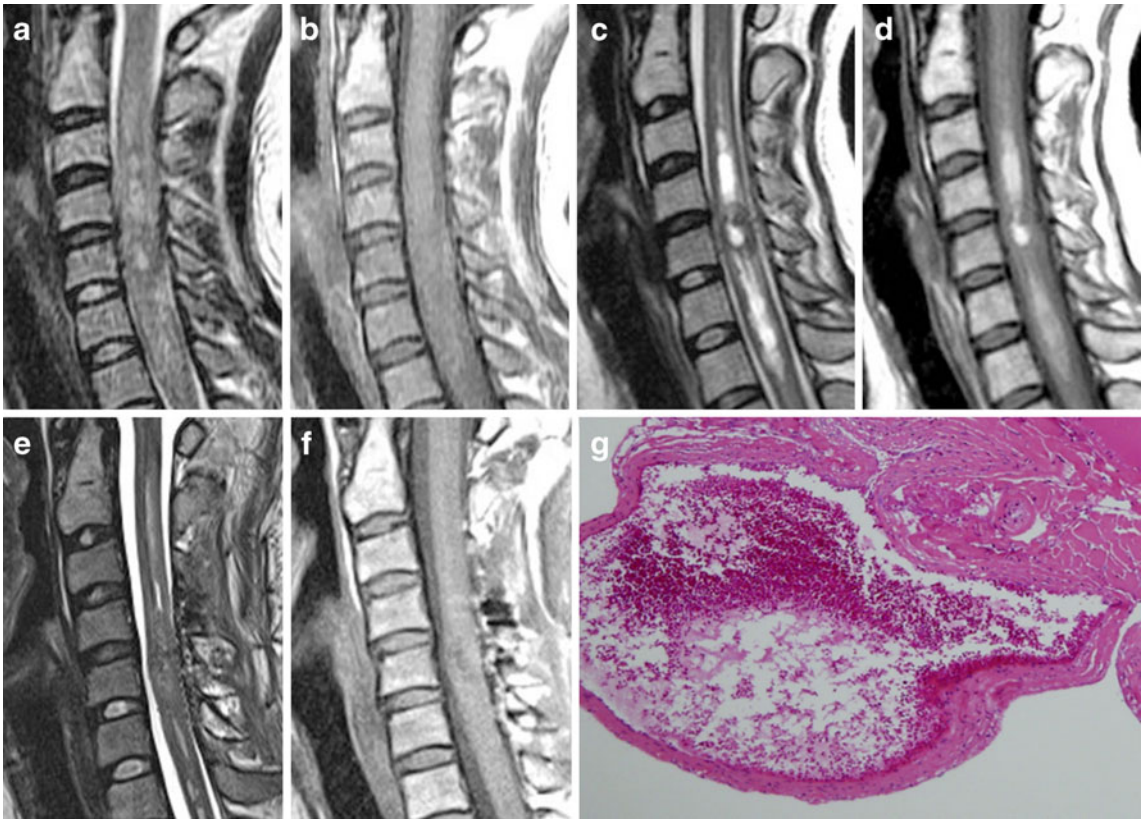

Fig. 3 Case 16. CM located at the C5 level. **a**, **b** Initial MRI. **c**, **d** MRI 3 weeks after admission. **e**, **f** Postoperative MRI. **g** Pathological image. **h**, **i** Postoperative plain X ray. **a**, **b** Initial MRI showing hematomyelia accompanied by severe cord swelling. **c**, **d** MRI 3 weeks after the initial MRI demonstrating resolved cord swelling and dark intensity rim on T2-weighted images at the center of the hematoma. **e**, **f** Postoperative MRI showing complete removal of the lesion and some residual hematoma inside the spinal cord. **g** Pathological image compatible with diagnosis of CM. Hematoxylin and eosin, ×40

on the MMCS over their preoperative status, and 11 patients' status remained unchanged. There were three patients who experienced postoperative worsening of their neurological state (case 5, 13, 19). One of them (case 5) recovered preoperative motor strength at the last follow-up evaluation, but the remaining two showed persistent neurological deterioration.

Case 7, the only patient whose lesion was subtotally resected, experienced arm pain and additional subjective weakness 5 months after the operation. We thought the extent of the previous surgical resection was complete, but re-bleeding of the lesion at the same level was observed on the follow-up MRI taken at the other hospital. The second operation was not performed because of the patient's his concerns related to surgical morbidity of the revision.

At the long-term follow-up evaluation, satisfying (improved and unchanged) results were seen in 19 of 21 patients (91%) (Table 3). The preoperative neurological state and type of symptom presentation were significant prognostic factors related to long-term surgical outcomes. That is, patients with a good preoperative neurological state (p=0.034) and presenting with type A or C symptoms rather than M were more likely to yield good postoperative neurological outcomes (p=0.024) (Tables 4, 5). The location of the lesion within the spinal cord is an important factor for practical surgical resection of the lesion. A lesion deeply embedded in the cross section of the cord with no pial contact can be more risky than superficial or dorsally exophytic lesions. However, this factor did not show statistically significant correlation with the postoperative outcome. Any other factors including age, sex, level of lesion, lesion size, duration of symptoms and number of hemorrhagic episodes did not correlate with the postoperative neurological outcome with statistical significance.

Discussion

Although CMs can be found at all locations within the central nervous system, most of them are found in the intracranial region, and an intramedullary spinal location is relatively rare, accounting for only 3–5% of the total identified CNS lesions [5, 9, 10, 12, 15, 22]. They are a type of vascular malformation composed of abnormal,

Table 2 The clinical characteristics of patients with CMs

Case no.	Age (years)	Sex	Level	Symptoms	Duration (mos)	No. of hemorrhages	Symptom type	Size (mm)	Location	Op. method	Resection	MMCS			F/u
												Preop	Postop	Last	(mos)
1	35	M	C2	Lt hemiparesis, sensory change	2	1	A	9.6	Lt, D	Laminectomy	Total	3	2	2	73
2	32	F	T7	Paraparesis, voiding and defecation difficulty	1	1	A	9.2	C	Laminectomy	Total	4	4	2	61
3	10	F	C6/7	Back pain, gait disturbance. Lt hand pain	0.1	1	A	19.54	C	Laminectomy	Total	2	2	1	60.5
4	70	F	T6/7	Both leg pain, paraparesis	24	2	M	9.88	Rt	Laminectomy	Total	3	3	3	60
5	69	M	T5	Paraparesis, both leg pain, hypoesthesia below T4	36	2	M	12.02	C	Laminectomy	Total	2	3	2	55
6	17	F	L1	Lt leg pain, paraparesis, voiding and defecation difficulty	0.5	2	M	15.81	C	Laminectomy	Total	3	3	2	54
7	29	M	C3-4	Rt arm pain. Lt arm and leg numbness	96	2	C	26.74	C, D	Laminotomy	Subtotal	1	1	1	52
8	37	F	T3	Paraparesis. Lt leg sensory change	14	1	C	6.35	Rt	Hemilaminectomy	Total	3	2	2	50
9	33	F	C5/6	Lt arm tingling, sensory change, gait disturbance	60	1	C	11.43	Lt, D	Laminotomy	Total	2	2	2	43
10	27	F	T11	Paraplegia, leg pain, sole tingling sense	24	2	M	11.61	C	Laminectomy	Total	5	3	2	40
11	45	F	T2	Lt leg numbness, tingling sense	2	1	C	9.01	C	Laminotomy	Total	1	1	1	26
12	43	M	C-M junction	Hand paresthesia and pain	6	1	C	15.47	C	Laminectomy craniectomy	Total	2	2	2	25
13	33	M	C4/5	Lt hand and hemibody tingling sense. Lt arm pain	4	1	C	7.21	C	Laminectomy	Total	1	2	2	20
14	26	F	T12/L1	Paraparesis. Rt foot tingling sense	19	1	A	6.95	C	Laminectomy	Total	1	1	1	13
15	49	M	C5	Lt hand weakness. Rt hand numbness	1	1	A	7.65	Lt	Laminotomy	Total	3	1	1	12
16	24	F	C5	Quadriparesis	0.1	1	A	14.64	Rt	Laminotomy	Total	4	2	2	17
17	59	F	C2	Quadriparesis	312	1	A	16.61	Rt	No(Revision)	Total	2	1	1	12
18	57	F	T2/3	Sensory change below T6, subjective paraparesis	24	1	C	11.62	Rt	Laminotomy	Total	2	1	1	12
19	40	M	T9	Paraparesis, unrinary urgency	46	2	M	12.4	Rt	Laminotomy	Total	2	3	3	6
20	56	F	C4	Lt arm pain	36	1	C	4.93	Lt	Laminotomy	Total	1	1	1	5
21	35	M	T11	Lt butock, inguinal area pain, voiding difficulty	2	1	A	10.85	C	Laminotomy	Total	1	1	1	1

*No = number; mos = months; C-M = cervicomedullary; Lt = left; Rt = right; Op = operation; F/u = follow-up; D = dorsal; C = central; A = acute onset of symptoms; C = chronic progressive myelopathy; M = acute neurological decline from various sequelae by previous attack

Table 3 Summary of characteristics of patients with intramedullary CMs

Variables	
Mean age	38.4 (10–70) years
M:F	8:13
Mean symptom duration	37.0 (0.1–312) months
Symptom type	
A	8
C	8
M	5
Level	
Cervical	9
Thoracic	9
Lumbar	1
Cervicomedullary junction	1
Thoracolumbar junction	1
Number of hemorrhages	
1	15
2	6
Mean size of lesion	11.7 (4.93–26.74) mm
Long-term outcome	
Improved	10 (48%)
Unchanged	9 (43%)
Worsen	2 (10%)

dilated, thin-walled vascular sinusoidal channels [8]. Typically, no brain parenchyma intervenes between these vascular channels [14, 19]. There is often gliotic and hemosiderin-stained neural tissue parenchyma around the lesion, and small low-flow feeding arteries and draining veins can also be found [14, 15].

Because of the paucity of large case series studies of this lesion, it is difficult to establish the epidemiological features of cavernous malformations. These lesions have a slightly higher incidence in women and a peak age presentation in the 4th decade [16, 18, 24]. The findings of our case series were concordant with these observations. However, the site of development showed equal distribution of cervical and thoracic locations, unlike previous reports that documented thoracic predilection [18, 24].

Assuming the lesion was already present at birth, the calculated retrospective annual hemorrhage rate was 2.18% per person and year, similar to previous reports (1.4–4.5%) [10, 21, 24]. But this would be the rate for symptomatic cases, and the hemorrhage rate of patients including asymptomatic patients was hard to estimate with this case series.

Magnetic resonance imaging is the imaging modality of choice for diagnosing cavernous malformations. Actually, most cases of cavernous malformations were reported after the introduction of MRI because these lesions are angiographically occult and difficult to diagnose with conventional tomography and myelography. A typical finding includes a peripheral hypointense ring of hemosiderin on the T2-weighted images. The central core of the lesion shows mixed heterogenous signal intensity on both T1- and T2-weighted images, with little contrast enhancement [1, 2, 18, 24].

The symptom presentation of patients with CMs may be acute or slowly progressive. Acute neurological deterioration occurs in cases with significant bleeding within the spinal cord, and slow progressive deterioration is related to multiple repeated microhemorrhages, subsequent thrombosis, hyalinization and possible enlargement of the malformation [23].

Ogilvy et al. [18] previously reported four types of clinical presentation in patients with CMs.

(1) Discrete episodes of neurological decline with varying degrees of recovery between episodes
(2) Slow progressive myelopathy
(3) Rapid decline after acute onset of symptoms
(4) Gradual decline after acute onset of symptoms

In our case series, we observed three common patterns of symptom presentation that were closely related to the prognosis of the patients. In symptomatic patients with

Table 4 Preoperative neurological status and postoperative outcome (MMCS)

Preop. grade	Long-term outcome					Total
	1	2	3	4	5	
1	5	1	0	0	0	6
2	3	3	1	0	0	7
3	1	3	1	0	0	5
4	0	2	0	0	0	2
5	0	1	0	0	0	1
Total	9	10	2	0	0	21

P=0.034

Table 5 Type of symptom presentation and postoperative outcome (MMCS)

Type of symptom	Long-term outcome					Total
	1	2	3	4	5	
A	5	3	0	0	0	8
C	4	4	0	0	0	8
M	0	3	2	0	0	5
Total	9	10	2	0	0	21

P=0.024

cavernous malformations, complete surgical removal of the lesion is the only method of stopping its progression, reducing further neurological deterioration. The rate of re-bleeding is unknown, but given the significant risk related to further neurological deterioration and low surgical morbidity, surgery should be the mainstay treatment, especially in symptomatic patients. Our results that patients with type M symptom presentation (acute neurological decline from pre-existing sequelae) show poor surgical outcome support this also. Furthermore, spinal CMs can cause more aggressive clinical symptoms and signs compared to their brain counterpart because of the spinal cord's lower degree of tolerance for mass lesions [7, 11]. However, there are some controversies regarding the treatment of asymptomatic patients. In such cases, we generally recommend close follow-up of patients using serial MRI rather than immediate surgery.

Perilesional edema or a significant mass effect is not a common finding in patients with intramedullary CMs. One of our cases (no. 16) showed severe cord swelling accompanied by hematomyelia on the initial MRI. In such cases, the timing of surgery is something to consider. Immediate operation of these lesions could be harmful for an already stressed spinal cord. As long as the neurological state of the patient is not declining, postponing the surgery for several weeks will be helpful for resolving the hematoma, diminishing cord swelling and, as a result, creating a discrete border on the lesion itself.

Ethical standards All human studies were approved by the appropriate ethics committee and have therefore been performed in accordance with the ethical standards laid down in the 1964 Declaration of Helsinki. All persons gave their informed consent prior to inclusion in this study.

Conflicts of interest None.

References

1. Abid R, Carlier R, Idir AB, David P, Hurth M, Doyon D (1993) Brain and spinal cord cavernoma. Value of MRI and review of the literature. Apropos of a case. J Radiol 74:563–567
2. Barnwell SL, Dowd CF, Davis RL, Edwards MS, Gutin PH, Wilson CB (1990) Cryptic vascular malformations of the spinal cord: diagnosis by magnetic resonance imaging and outcome of surgery. J Neurosurg 72:403–407
3. Bertalanffy H, Benes L, Miyazawa T, Alberti O, Siegel AM, Sure U (2002) Cerebral cavernomas in the adult. Review of the literature and analysis of 72 surgically treated patients. Neurosurg Rev 25:1–53
4. Bian LG, Bertalanffy H, Sun QF, Shen JK (2009) Intramedullary cavernous malformations: clinical features and surgical technique via hemilaminectomy. Clin Neurol Neurosurg 111:511–517
5. Bucciero A, Del Basso de Caro M, Carangelo B, Vizioli L (1994) Intramedullary cavernoma: a case report and review of the literature. Acta Neurol (Napoli) 16:162–169
6. Del Curling O Jr, Kelly DL Jr, Elster AD, Craven TE (1991) An analysis of the natural history of cavernous angiomas. J Neurosurg 75:702–708
7. Deutsch H, Jallo GI, Faktorovich A, Epstein F (2000) Spinal intramedullary cavernoma: clinical presentation and surgical outcome. J Neurosurg 93:65–70
8. Duke BJ, Levy AS, Lillehei KO (1998) Cavernous angiomas of the cauda equina: case report and review of the literature. Surg Neurol 50:442–445
9. Furuya K, Sasaki T, Suzuki I, Kim P, Saito N, Kirino T (1996) Intramedullary angiographically occult vascular malformations of the spinal cord. Neurosurgery 39:1123–1130
10. Ghogawala Z, Ogilvy CS (1999) Intramedullary cavernous malformations of the spinal cord. Neurosurg Clin N Am 10:101–111
11. Gordon CR, Crockard HA, Symon L (1995) Surgical management of spinal cord cavernoma. Br J Neurosurg 9:459–464
12. Harrison MJ, Eisenberg MB, Ullman JS, Oppenheim JS, Camins MB, Post KD (1995) Symptomatic cavernous malformations affecting the spine and spinal cord. Neurosurgery 37:195–204
13. Jallo GI, Freed D, Zareck M, Epstein F, Kothbauer KF (2006) Clinical presentation and optimal management for intramedullary cavernous malformations. Neurosurg Focus 21:e10
14. Jellinger K (1986) Vascular malformations of the central nervous system: a morphological overview. Neurosurg Rev 9:177–216
15. Lunardi P, Acqui M, Ferrante L, Fortuna A (1994) The role of intraoperative ultrasound imaging in the surgical removal of intramedullary cavernous angiomas. Neurosurgery 34:520–523
16. McCormick PC, Michelsen WJ, Post KD, Carmel PW, Stein BM (1988) Cavernous malformations of the spinal cord. Neurosurgery 23:459–463
17. McCormick PC, Torres R, Post KD, Stein BM (1990) Intramedullary ependymoma of the spinal cord. J Neurosurg 72:523–532
18. Ogilvy CS, Louis DN, Ojemann RG (1992) Intramedullary cavernous angiomas of the spinal cord: clinical presentation, pathological features, and surgical management. Neurosurgery 31:219–229
19. Rigamonti D, Drayer BP, Johnson PC, Hadley MN, Zabramski J, Spetzler RF (1987) The MRI appearance of cavernous malformations (angiomas). J Neurosurg 67:518–524
20. Robinson JR, Awad IA, Little JR (1991) Natural history of the cavernous angioma. J Neurosurg 75:709–714
21. Sandalcioglu IE, Wiedemayer H, Gasser T, Asgari S, Engelhorn T, Stolke D (2003) Intramedullary spinal cord cavernous malformations: clinical features and risk of hemorrhage. Neurosurg Rev 26:253–256
22. Stone JL, Lichtor T, Ruge JR (1995) Cavernous angioma of the upper cervical spinal cord. A case report. Spine Phila Pa 1976 20:1205–1207
23. Sure U, Freman S, Bozinov O, Benes L, Siegel AM, Bertalanffy H (2005) Biological activity of adult cavernous malformations: a study of 56 patients. J Neurosurg 102:342–347
24. Zevgaridis D, Medele RJ, Hamburger C, Steiger HJ, Reulen HJ (1999) Cavernous haemangiomas of the spinal cord. A review of 117 cases. Acta Neurochir (Wien) 141:237–245

Comment

There are not many series with this number of operated CMs of the spinal cord (SCCMs). The authors should be commended for presenting their results. It is interesting to note that no statistically powered positive correlation could be found between the number of hemorrhagic episodes and the postoperative outcome. The authors suggest that this unexpected effect may be due to the fact that not all hemorrhagic episodes carry the same clinical burden for the patient. This judgment is logical and likely correct. The larger the numbers of the clinical series, the better this assumption can be tested, because the more diluted the effect of each single hemorrhage is. Type M clinical evolution is in my opinion not optimally phrased. These are patients whose neurological deficit is built on a previous insult to the cord, therefore not starting from a clinically intact baseline. Preoperative MRIs were obtained for all patients but not postoperative ones. This is not irrelevant! In fact, the authors recommend surgery for SCCMs because it is a curative treatment, which will therefore eradicate the chance of future hemorrhages. However, as was proven with the SCCM in the series, which re-bled despite the fact that the authors were convinced they had it completely resected, the surgeon's estimation of resection needs to be demonstrated on postoperative MRI. It is also of note that three patients were left clinically worse after surgery, but that no significant SSEP changes could be detected during their surgery compared to all the others who experienced no increased deficit.

Manuel Cunha e Sa
Almada, Portugal

Acta Neurochir (2011) 153:1687–1694
DOI 10.1007/s00701-011-1002-9

CLINICAL ARTICLE

Genu of corpus callosum in diffuse axonal injury induces a worse 1-year outcome in patients with traumatic brain injury

Hidetoshi Matsukawa · Masaki Shinoda · Motoharu Fujii · Osamu Takahashi · Daisuke Yamamoto · Atsushi Murakata · Ryoichi Ishikawa

Received: 1 December 2010 / Accepted: 17 March 2011 / Published online: 9 April 2011

Abstract
Background Previous studies have shown a relationship between diffuse axonal injury (DAI) and unfavorable clinical outcome in patients with traumatic brain injury (TBI), but it remains unclear whether the type of DAI lesion influences outcome after TBI. The aim of the present study was to investigate whether 1-year outcome after TBI differed between patients with different types of lesions.
Methods A retrospective, single-institution study involving 261 patients with TBI was carried out between April 2003 and December 2009. Outcome was measured using the Glasgow Outcome Scale (GOS) 1 year after TBI. DAI lesions occurred in the lobar region, corpus callosum (CC), and brainstem. CC lesions were subdivided into three types: genu, body, and splenium. Univariate and multivariate logistic regression analyses were performed to evaluate the relationships between clinical characteristics and outcome for each type of DAI lesion and each type of CC lesion in patients with TBI.
Findings Sixty-nine patients had DAI lesions: 34 in the lobar region, 30 in the CC, and five in the brainstem. Of the 30 patients with CC lesions, ten each were found in the genu, body, and splenium. Each DAI, CC, and genu lesion was significantly associated with unfavorable outcome 1 year after TBI by multivariate analysis using variables that were significantly associated with unfavorable outcome as determined by univariate analysis after adjustment for age.
Conclusions CC lesions, especially those in the genu, were related to unfavorable 1-year outcome in patients with TBI.

Keywords Corpus callosum · Diffuse axonal injury · Genu · Traumatic brain injury

H. Matsukawa (✉) · M. Shinoda · M. Fujii · D. Yamamoto · A. Murakata · R. Ishikawa
Department of Neurosurgery, St. Luke's International Hospital,
9–1 Akashi-cho, Chuo-ku,
Tokyo 104-8560, Japan
e-mail: mahide@luke.or.jp

O. Takahashi
Department of Clinical Epidemiology,
St. Luke's International Hospital,
9–1 Akashi-cho, Chuo-ku,
Tokyo 104-8560, Japan

Introduction

Traumatic brain injury (TBI) is characterized as either focal or diffuse. Diffuse injury mainly consists of diffuse axonal injury (DAI), which may be an important cause of poor clinical outcome in patients with TBI [19]. DAI is considered to be associated with post-traumatic impairment in cognitive and multi-task execution due to neural network disruption in the brain [6, 20, 26]. Three types of DAI lesions have been identified based on neuropathological examination and magnetic resonance imaging (MRI): those in the lobar white matter, the corpus callosum (CC), and the brainstem [1, 8, 10]. The presence of lesions and the severity of DAI is thought to be related to many factors [2, 25, 32].

The CC is the second most common area involved in DAI (21–47% of DAI lesions)[10, 12]. The CC is the main tract connecting the hemispheres and forms the largest commissural white matter bundle in the brain, with some 200 million axons. CC lesions are of serious concern in TBI owing to the structural role of the CC in the inter-hemispheric transfer of auditory, visual, sensory, and motor information that is relevant to multiple cognitive processes [13]. In addition, the CC is considered to be particularly vulnerable to TBI due to its unique location and composition [13].

The CC mainly consists of three regions: the genu contains fibers connecting the bilateral prefrontal cortices; the body primarily contains crossing fibers for the motor, somatosensory, and auditory cortices; and the splenium carries fibers mainly to the temporal, parietal, and occipital lobes [31, 33]. One study showed that the genu of the CC was primarily affected in mild TBI [27], whereas other studies showed that the posterior region of the CC was affected in TBI [2, 10, 11, 24]. Although several studies have investigated CC lesions in patients with DAI [16, 22], the influence of CC lesions on clinical outcome, and whether or not the vulnerability of each region of the CC to trauma is different, remain unclear.

Indeed, the influence on outcome of types of DAI lesions in general is not well understood. With such background, the aim of the present study was to confirm whether type of DAI lesion, and specifically CC lesions, were related to clinical outcome 1 year after patients had experienced TBI.

Methods and materials

A total of 334 patients with TBI were admitted to the Neurosurgery Department at St. Luke's International Hospital in Tokyo, Japan, between April 2003 and August 2009, MRI was performed within 2 weeks of injury. These results were reviewed retrospectively.

The collected variables were as follows: vital signs (blood pressure, heart rate, and respiratory rate), Glasgow Coma Scale (GCS) on admission, pupillary abnormality (anisocoria, loss of light reflex, or pupil dilation), Injury Severity Score (ISS; calculated as the sum of the squares of the largest Abbreviated Injury Scale severity value from each of the three most severely injured body regions) [3], radiological findings (skull fracture, intraventricular bleeding, cerebral contusion, traumatic subarachnoid hemorrhage, acute epidural hematoma, and acute subdural hematoma) diagnosed on computed tomography (CT), emergency surgery (within 24 h from injury), and laboratory data (alcohol level, platelet count, and markers of blood coagulation). Severe head injury was defined as a GCS score of less than or equal to 8. Head injury sites were classified as frontal, temporal, occipital, or parietal, as judged by localization of subcutaneous hematoma, skull fractures, damage caused by a helmet if wearing one, and information from the patient or bystanders at the time of injury. Information about past medical history and medication use were also obtained. Clinical outcome was measured by the Glasgow Outcome Scale (GOS) [17] 1 year after TBI, either by telephone or during a physical examination for those patients who were able to visit the hospital. GOS score was separated into either 'favorable' (moderate disability or good recovery) or 'unfavorable' (dead, persistent vegetative state, or severe disability) outcome.

MRI was performed to diagnose DAI lesions on a 1.5-T Signa Exice or Intera (GE Medical Systems, Milwaukee, WI or Philips, New York, NY) using the following different scanning methods: sagittal turbo spin-echo T2-weighted imaging; axial T2*-weighted gradient-echo imaging; axial and sagittal T2-weighted fluid attenuated inversion recovery (FLAIR) imaging; and axial diffusion-weighted imaging. Patients with hemorrhagic lesions on T2*-weighted gradient-echo imaging in different white matter regions of the brain were considered to have hemorrhagic DAI [30]. White matter abnormalities detected on FLAIR imaging with no demonstrable hemorrhage on T2*GRE other than at the site of contusion were considered to be non-hemorrhagic DAI [30]. Patients with contusion on CT but no other demonstrable white matter abnormality on T2*-weighted gradient-echo imaging or FLAIR imaging were defined as having no DAI.

DAI lesions were classified into three types: those that occurred in the lobar white matter, in the CC, or in the bilateral dorsolateral quadrants of the midbrain and upper pons [10]. In addition, the CC lesions were subdivided into three lesions: those involving the genu, the body, or the splenium.

Patient recruitment and exclusion criteria were as follows (see Fig. 1): receiving antithrombotics containing oral antiplatelets and anticoagulants; presence of non-traumatic intracranial lesions involving primary or metastatic brain tumor, Parkinson's disease, cerebral infarction, or senile dementia of Alzheimer's type; presence of multiple DAI lesions, defined as more than two DAI lesions, intoxication due to chronic alcohol abuse or drug abuse; psychiatric disease, specifically schizophrenia or personality disorder; and hematological disorder, specifically hemophilia or myelodysplastic syndrome. After exclusion, data from 261 patients with and without DAI were analyzed in the present study.

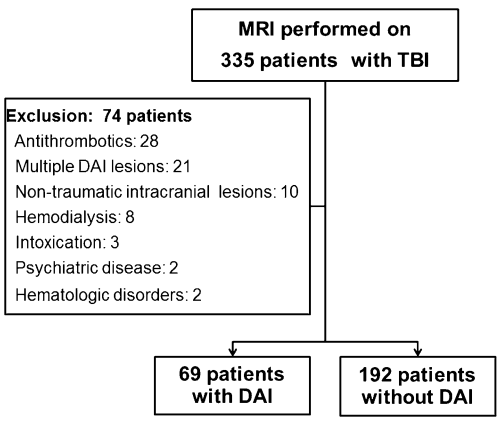

Fig. 1 Exclusion criteria. *TBI* traumatic brain injury, *DAI* diffuse axonal injury

Statistical analysis was performed using JMP 8.0 (SAS, Cary, NC, USA). The normality of the data was evaluated using the Shapiro-Wilks test. Variables were expressed as mean (± standard deviation), median (inter-quartile range: 25th percentile to 75th percentile), or number of patients (%), as appropriate. Normally distributed variables were compared using Student's *t*-test and non-normally distributed variables were compared using the Mann-Whitney *U*-test. Multivariate logistic regression analysis was performed using variables that were significantly associated with unfavorable outcome, as determined by univariate analysis, to confirm that CC lesions had an influence on outcome 1 year after TBI. Differences were considered significant at $p<0.05$.

The study protocol was approved by the ethics committee of our hospital.

Results

Of 261 patients, 69 were diagnosed with DAI. Brain CT was performed in all patients who underwent MRI.

The clinical characteristics of all 261 patients with either favorable or unfavorable outcome are shown in Table 1. A significantly higher proportion of patients with unfavorable outcome had severe head injury, pupillary abnormality, intraventricular bleeding, and DAI compared with those with favorable outcome. Patients with unfavorable outcome

Table 1 Clinical characteristics of patients with favorable or unfavorable outcome 1 year after TBI among patients who underwent MRI

	Total (n=261)	Favorable (n=242)	Unfavorable (n=19)	Univariate p value	Multivariate p value
Baseline characteristics					
Mean age in yrs (±SD)	48 (21)	47 (21)	56 (20)		
Male	210 (80)	193 (79)	17 (89)		
Median GCS (IQR)	13 (12–15)	13 (13–15)	7.8 (4–12)		
Severe head injury (GCS≤8)[a]	34 (13)	23 (10)	11 (58)	<0.0001	0.0057
Pupillary abnormality	15 (5.8)	10 (4.1)	5 (26)	<0.0001	
Median ISS (IQR)	15 (11–20)	15 (11–18)	24 (18–29)	<0.0001	
Subcutaneous hematoma	211 (81)	194 (81)	17 (89)		
Median serum ethanol, mg/dl (IQR)	68 (0–151)	70 (0–154)	35 (0–68)		
Head injury site					
Frontal	55 (21)	54 (22)	1 (5.2)		
Temporal	41 (16)	38 (16)	3 (16)		
Occipital	69 (26)	62 (26)	7 (37)		
Parietal	51 (20)	46 (19)	5 (26)		
Unknown	45 (17)	42 (17)	3 (16)		
Mechanism of injury					
Fall injury	158 (61)	148 (61)	10 (53)		
Traffic accident	95 (36)	86 (36)	9 (50)		
Sport	7 (2.7)	0	7 (2.9)		
Radiological findings					
Skull fracture	137 (52)	126 (53)	11 (58)		
IVB	13 (4.9)	9 (3.7)	4 (21)	0.0095	
Cerebral contusion	96 (37)	85 (35)	11 (58)		
tSAH	138 (53)	126 (52)	12 (63)		
AEDH	41 (16)	38 (16)	3 (17)		
ASDH	84 (32)	75 (31)	9 (47)		
DAI[a]	69 (26)	56 (23)	13 (68)	<0.0001	0.0198
Hematoma evacuation	18 (6.9)	15 (6.2)	3 (16)		

Data expressed as number of patients (%), unless otherwise indicated. IQR=25th percentile to 75th percentile

TBI traumatic brain injury, *MRI* magnetic resonance imaging, *SD* standard deviation, *GCS* Glasgow Coma Scale, *IQR* inter-quartile range, *ISS* injury severity score, *IVB* intraventricular bleeding, *tSAH* traumatic subarachnoid hemorrhage, *AEDH* acute epidural hematoma, *ASDH* acute subdural hematoma, *DAI* diffuse axonal injury

[a] Variables related to unfavorable outcome 1 year after TBI

also had a higher ISS as determined by univariate analysis. After multivariate logistic regression analysis using variables that were found by univariate analysis to be significantly related to unfavorable outcome, a higher proportion of patients with unfavorable outcome after TBI had severe head injury and DAI than patients with favorable outcome.

Table 2 shows the outcome of patients with DAI in relation to each lesion as determined by GOS score. It was found that CC lesions, especially lesions of the genu, were related to unfavorable outcome. The clinical characteristics of the 69 patients with DAI are shown in Table 3. Significantly higher proportions of severe head injury, pupillary abnormality, and contusion on CT were seen in patients with unfavorable outcome than those with favorable outcome. The ISS of patients with unfavorable outcome was also significantly higher. After multilogistic regression analysis using variables that were determined by univariate analysis to be significantly related to unfavorable outcome, a higher proportion of patients with DAI and unfavorable outcome had cerebral contusion on CT and CC lesions. The clinical characteristics of 30 patients with CC lesions are shown in Table 4. A significantly higher proportion of severe head injury was seen in patients with unfavorable outcome compared with those with favorable outcome. Patients with unfavorable outcome also had a higher ISS. Following multilogistic regression analysis using variables determined by univariate analysis to be significantly related to unfavorable outcome, significantly higher proportions of lesions in the genu of the CC were found in patients with unfavorable outcome.

There were no significant differences in the proportions of head injury site, mechanism of injury, and hematoma evacuation between the two groups. Similarly, laboratory data did not significantly differ between the two groups.

Discussion

In the present study, significantly more patients with DAI had unfavorable outcome than patients without DAI 1 year after TBI. This result is in good agreement with previous studies [6, 19, 20, 26]. Furthermore, among the patients with DAI, those with CC lesions, especially in the genu, had unfavorable outcome 1 year after TBI compared with patients without CC lesions. To our knowledge, the present study is the first 1-year observational study to investigate the relationship between the presence of different types of DAI lesions, and specifically different CC lesions, and outcome in patients with TBI. Severe head injury was found to be significantly associated with unfavorable outcome in patients with DAI, CC, and genu lesions. These results concur with the findings of a previous study on TBI [29].

The CC is thought to serve several key roles in motor control: namely, transfer of lateralized information (i.e. verbal input from the left hemisphere) to the opposite hemisphere to guide unilateral movement, transfer of information to coordinate bilateral movements, and transfer of information to inhibit contralateral movement during a unilateral motor activity [9]. CC lesions are thought to be a marker of the severity of diffuse TBI [5, 18]. One neurosurgical operative study showed that the middle portion of the genu was related to both simple bimanual coordination, such as that assessed using the Purdue Pegboard test, and a complex task involving asynchronous movements of the hands, as assessed by Preilowski's test [7]. Furthermore, it also showed that the anterior portion of the genu was related to bimanual asynchronous motor coordination, planning, and mental flexibility, as assessed by Thurstone's unimanual and bimanual performance test [7]. Therefore, traumatic lesions of the genu may also be associated with such dysfunctions.

White matter integrity in the genu—but not in the splenium or body—is an important marker of gait in the elderly [4, 14, 21], and the anterior part of the CC (rostrum, genu, and rostral body) is involved in bilateral motor coordination and in transfer of visuomotor tasks [23]. This clinicoanatomic correlation is consistent with the concept of the importance of integrated frontal executive function for the maintenance of gait and balance [15]. The loss of volume of the genu was found to be most significantly

Table 2 Outcome 1-year after injury in relation to lesions of diffuse axonal injury

GOS	Total	Lobar	Corpus callosum				Brainstem
			Total	Genu	Body	Splenium	
Favorable	55 (80)	32 (95)	20 (67)	2 (20)	9 (90)	9 (90)	4 (80)
Good	38 (55)	25 (74)	12 (40)	1 (10)	6 (60)	5 (50)	3 (60)
Moderate	17 (25)	7 (21)	8 (27)	1 (10)	3 (30)	4 (40)	1 (20)
Unfavorable	14 (20)	2 (5)	10 (33)[a]	8 (80)[a]	1 (10)	1 (10)	1 (20)
Severe	10 (14)	2 (5)	7 (23)	5 (50)	1 (10)	1 (10)	0
Vegetative	4 (6)	0	3 (10)	3 (30)	0	0	1 (20)
Total	69	34		10	10	10	5

Data expressed as number of patients (%)

GOS Glasgow Outcome Scale. No patients with lesions of diffuse axonal injury died

[a] Lesions related to unfavorable outcome

Table 3 Clinical characteristics of patients with favorable or unfavorable outcome 1 year after TBI among patients with DAI

	Total (n=69)	Favorable (n=56)	Unfavorable (n=13)	Univariate p value	Multivariate p value
Baseline characteristics					
Mean age in yrs (±SD)	45 (19)	43 (18)	53 (23)		
Male	59 (86)	48 (86)	1 (85)		
Median GCS (IQR)	11 (9–14)	12 (9–15)	8.1 (3.5–13)		
Severe head injury (GCS≤8)	16 (23)	9 (16)	7 (58)	0.0017	
Pupillary abnormality	9 (13)	5 (8.9)	4 (33)	0.0236	
Median ISS (IQR)	19 (11–26)	17 (11–25)	25 (18–29)	0.0038	
Subcutaneous hematoma	57 (83)	46 (82)	11 (85)		
Median serum ethanol, mg/dl (IQR)	65 (0–90)	77 (0–186)	11 (0–0)		
Head injury site					
Frontal	12 (17)	11 (20)	1 (7.7)		
Temporal	10 (14)	8 (14)	2 (15)		
Occipital	15 (22)	11 (20)	4 (31)		
Parietal	17 (25)	14 (25)	3 (23)		
Unknown	15 (22)	12 (21)	3 (23)		
Mechanism of injury					
Fall injury	26 (38)	21 (38)	5 (38)		
Traffic accident	43 (62)	35 (63)	8 (62)		
Sport	0				
Radiological findings					
Skull fracture	39 (57)	31 (55)	8 (62)		
IVB	13 (19)	9 (16)	4 (31)		
Cerebral contusion[a]	31 (45)	21 (38)	10 (77)	0.0176	0.0403
tSAH	42 (61)	33 (59)	9 (69)		
AEDH	11 (16)	9 (16)	2 (15)		
ASDH	18 (26)	13 (23)	5 (38)		
Lesions of DAI					
Lobar white matter	34 (49)	32 (57)	2 (15)		
Corpus callosum[a]	30 (43)	20 (36)	10 (77)	0.0069	0.0236
Brainstem	5 (7)	4 (7.1)	1 (7.7)		
Hematoma evacuation	8 (12)	6 (11)	2 (15)		

Data expressed as number of patients (%), unless otherwise indicated. IQR=25th percentile to 75th percentile

TBI traumatic brain injury, *DAI* diffuse axonal injury, *SD* standard deviation, *GCS* Glasgow Coma Scale, *IQR* inter-quartile range, *ISS* injury severity score, *IVB* intraventricular bleeding, *tSAH* traumatic subarachnoid hemorrhage, *AEDH* acute epidural hematoma, *ASDH* acute subdural hematoma

[a] Variables related to unfavorable outcome 1 year after TBI

associated with gait difficulty [28], although the body and splenium were also smaller among patients with age-related white matter changes. The presence of lesions of the CC, especially of the genu, may be an important predictor for global cognitive impairment in patients with these changes [28, 35, 36]. Furthermore, one study showed that patients with vascular dementia had reduced axon density specific to the anterior CC [34]. Patients with unfavorable outcome were significantly older than those with favorable outcome in each of the three comparisons in the present study. This might be derived from the relationship between the above age-related lesions and global cognitive impairment. Thus, not only traumatic but also non-traumatic, age-related, lesions of the genu were associated with various critical dysfunctions.

Early detection of lesions of the genu among patients with TBI is important because clinical outcome may be improved by appropriate early medical management—that is, training of higher-order function and clinical strategies to support loss of various critical functions.

Table 4 Clinical characteristics of patients with good and poor outcome 1 year after TBI among patients with lesions in the corpus callosum

	Total (n=30)	Favorable (n=20)	Unfavorable (n=10)	Univariate p value	Multivariate p value
Baseline characteristics					
Mean age in yrs (±SD)	42 (19)	39 (17)	48 (24)		
Male	26 (87)	18 (90)	8 (80)		
Median GCS (IQR)	11 (8.5–14)	12 (10–15)	8.5 (3.8–13)		
Severe head injury (GCS≤8)	7 (23)	2 (10)	5 (50)	0.0146	
Pupil abnormalities	7 (24)	4 (20)	3 (30)		
Median ISS (IQR)	21 (14–27)	18 (11–25)	27 (18–32)	0.0228	
Subcutaneous hematoma	23 (77)	14 (70)	9 (90)		
Median serum ethanol, mg/dl (IQR)	29 (0–0)	40 (0–0)	6.8 (0–0)		
Head injury site					
Frontal	5 (17)	4 (20)	1 (10)		
Temporal	5 (17)	3 (15)	2 (20)		
Occipital	6 (20)	3 (15)	3 (30)		
Parietal	6 (20)	4 (20)	2 (20)		
Unknown	8 (27)	6 (30)	2 (20)		
Mechanism of injury					
Fall injury	9 (30)	6 (28)	3 (30)		
Traffic accident	23 (77)	16 (73)	7 (78)		
Sport	0				
Radiological findings					
Skull fracture	18 (60)	11 (55)	7 (70)		
IVB	7 (24)	3 (16)	4 (40)		
Cerebral contusion	17 (57)	9 (45)	8 (80)		
tSAH	19 (63)	12 (60)	7 (70)		
AEDH	2 (6.7)	1 (5.0)	1 (11)		
ASDH	10 (33)	5 (25)	5 (50)		
Lesions of corpus callosum injury					
Genu[a]	10 (33)	2 (10)	8 (80)	0.0002	0.0051
Body	10 (33)	9 (45)	1 (11)		
Splenium	10 (33)	9 (45)	1 (11)		
Hematoma evacuation	3 (10)	2 (10)	1 (11)		

Data expressed as number of patients (%), unless otherwise indicated. IQR=25th percentile to 75th percentile

TBI traumatic brain injury, *SD* standard deviation, *GCS* Glasgow Coma Scale, *IQR* inter-quartile range, *ISS* injury severity score, *IVB* intraventricular bleeding, *tSAH* traumatic subarachnoid hemorrhage, *AEDH* acute epidural hematoma, *ASDH* acute subdural hematoma

[a] Variables related to an unfavorable outcome 1 year after TBI

Some limitations of this study should be mentioned. The study was carried out at a single institution and was retrospective. There was likely to be some bias as patients who did not undergo MRI because of death in the acute phase or minor injuries might have had DAI and this may affect the present results. While premorbid intoxication and psychiatric disease might influence on the outcome, these patients were excluded from the present study and therefore they remain topics for future study.

Finally, the number of patients who participated in this study was small and this might have an influence on the reliably of the results. To further efforts toward improving the outcome of the patients with lesions of the CC, especially of the genu, after TBI, a large randomized clinical trial should be conducted for exclusion of these biases. Based on the findings of this study, lesions of the genu of the CC may indicate unfavorable outcome 1 year after TBI.

Acknowledgements This study was supported by a medical research grant on traffic accident from The General Insurance Association of Japan 2010.

Conflicts of interest None.

References

1. Adams J, Doyle D, Ford I, Gennarelli T, Graham D, McLellan D (1989) Diffuse axonal injury in head injury: definition, diagnosis and grading. Histopathology 15:49–59
2. Adams J, Graham D, Murray L, Scott G (1982) Diffuse axonal injury due to nonmissile head injury in humans: an analysis of 45 cases. Ann Neurol 12:557–563
3. Baker S, O'Neill B, Haddon W Jr, Long W (1974) The injury severity score: a method for describing patients with multiple injuries and evaluating emergency care. J Trauma 14:187–196
4. Bhadelia RA, Price LL, Tedesco KL, Scott T, Qiu WQ, Patz S, Folstein M, Rosenberg I, Caplan LR, Bergethon P (2009) Diffusion tensor imaging, white matter lesions, the corpus callosum, and gait in the elderly. Stroke 40:3816–3820
5. Bigler E (2001) Quantitative magnetic resonance imaging in traumatic brain injury. J Head Trauma Rehabil 16:117–134
6. Bruce J, Echemendia R (2003) Delayed-onset deficits in verbal encoding strategies among patients with mild traumatic brain injury. Neuropsychology 17:622–629
7. Caill S, Sauerwein H, Schiavetto A, Villemure J, Lassonde M (2005) Sensory and motor interhemispheric integration after section of different portions of the anterior corpus callosum in nonepileptic patients. Neurosurgery 57:50–59
8. Gallo A, Rovaris M, Riva R, Ghezzi A, Benedetti B, Martinelli V, Falini A, Comi G, Filippi M (2005) Diffusion-tensor magnetic resonance imaging detects normal-appearing white matter damage unrelated to short-term disease activity in patients at the earliest clinical stage of multiple sclerosis. Arch Neurol 62:803–808
9. Geffen G, Jones D, Geffen L (1994) Interhemispheric control of manual motor activity. Behav Brain Res 64:131–140
10. Gentry L (1994) Imaging of closed head injury. Radiology 191:1–17
11. Gentry L, Godersky J, Thompson B (1988) MR imaging of head trauma: review of the distribution and radiopathologic features of traumatic lesions. AJR Am J Roentgenol 150:663–672
12. Gentry L, Thompson B, Godersky J (1988) Trauma to the corpus callosum: MR features. AJNR Am J Neuroradiol 9:1129–1138
13. Gorrie C, Duflou J, Brown J, Gibson T, Waite P (2001) Extent and distribution of vascular brain injury in pediatric road fatalities. J Neurotrauma 18:849–860
14. Guttmann CR, Benson R, Warfield SK, Wei X, Anderson MC, Hall CB, Abu-Hasaballah K, Mugler JP 3rd, Wolfson L (2000) White matter abnormalities in mobility-impaired older persons. Neurology 54:1277–1283
15. Hausdorff J, Yogev G, Springer S, Simon E, Giladi N (2005) Walking is more like catching than tapping: gait in the elderly as a complex cognitive task. Exp Brain Res 164:541–548
16. Inglese M, Makani S, Johnson G, Cohen B, Silver J, Gonen O, Grossman R (2005) Diffuse axonal injury in mild traumatic brain injury: a diffusion tensor imaging study. J Neurosurg 103:298–303
17. Jennett B, Bond M (1975) Assessment of outcome after severe brain damage: a practical scale. Lancet 305:480–484
18. Levin H, Benavidez D, Verger-Maestre K, Perachio N, Song J, Mendelsohn D, Fletcher J (2000) Reduction of corpus callosum growth after severe traumatic brain injury in children. Neurology 54:647–653
19. Maas A, Stocchetti N, Bullock R (2008) Moderate and severe traumatic brain injury in adults. Lancet Neurol 7:728–741
20. Maxwell W, Povlishock J, Graham D (1997) A mechanistic analysis of nondisruptive axonal injury: a review. J Neurotrauma 14:419–440
21. Moretti M, Carlucci G, Di Carlo A, Fonda C, Prieto M, Mugnai S, Bracco L, Piccini C, Pracucci G, Inzitari D (2005) Corpus callosum atrophy is associated with gait disorders in patients with leukoaraiosis. Neurol Sci 26:61–66
22. Nakayama N, Okumura A, Shinoda J, Yasokawa Y, Miwa K, Yoshimura S, Iwama T (2006) Evidence for white matter disruption in traumatic brain injury without macroscopic lesions. J Neurol Neurosurg Psychiatry 77:850–855
23. Pandya DN, Karol EA, Heilbronn D (1971) The topographical distribution of interhemispheric projections in the corpus callosum of the rhesus monkey. Brain Res 32:31–43
24. Parizel P, Van Goethem J, Zsarlak, Maes M, Phillips C (2005) New developments in the neuroradiological diagnosis of craniocerebral trauma. Eur Radiol 15:569–581
25. Parizel P, Zsarlak, Van Goethem J, Van Den Hauwe L, Dillen C, Verlooy J, Cosyns P, De Schepper A (1998) Imaging findings in diffuse axonal injury after closed head trauma. Eur Radiol 8:960–965
26. Povlishock J, Katz D (2005) Update of neuropathology and neurological recovery after traumatic brain injury. J Head Trauma Rehabil 20:76–94
27. Rutgers DR, Fillard P, Paradot G, Tadie M, Lasjaunias P, Ducreux D (2008) Diffusion tensor imaging characteristics of the corpus callosum in mild, moderate, and severe traumatic brain injury. AJNR Am J Neuroradiol 29:1730–1735
28. Ryberg C, Rostrup E, Stegmann M, Barkhof F, Scheltens P, van Straaten E, Fazekas F, Schmidt R, Ferro J, Baezner H (2007) Clinical significance of corpus callosum atrophy in a mixed elderly population. Neurobiol Aging 28:955–963
29. Salazar A, Grafman J, Vance S, Weingartner H, Dillon J, Ludlow C (1986) Consciousness and amnesia after penetrating head injury: neurology and anatomy. Neurology 36:178–187
30. Scheid R, Preul C, Gruber O, Wiggins C, Von Cramon D (2003) Diffuse axonal injury associated with chronic traumatic brain injury: evidence from T2*-weighted gradient-echo imaging at 3 T. AJNR Am J Neuroradiol 24:1049–1056
31. Schmahmann J, Pandya D (2009) Fiber pathways of the brain. Oxford University Press, New York
32. Skandsen T, Kvistad KA, Solheim O, Strand IH, Folvik M, Vik A (2010) Prevalence and impact of diffuse axonal injury in patients with moderate and severe head injury: a cohort study of early magnetic resonance imaging findings and 1-year outcome. J Neurosurg 113:556–563
33. Witelson S (1989) Hand and sex differences in the isthmus and genu of the human corpus callosum: a postmortem morphological study. Brain 112:799–835
34. Yamanouchi H, Sugiura S, Shimada H (1990) Loss of nerve fibres in the corpus callosum of progressive subcortical vascular encephalopathy. J Neurol 237:39–41
35. Yamauchi H, Fukuyama H, Ogawa M, Ouchi Y, Kimura J (1994) Callosal atrophy in patients with lacunar infarction and extensive leukoaraiosis. An indicator of cognitive impairment. Stroke 25:1788–1793
36. Yamauchi H, Fukuyama H, Shio H (2000) Corpus callosum atrophy in patients with leukoaraiosis may indicate global cognitive impairment. Stroke 31:1515–1520

Comment

In this manuscript the authors investigate the relationship between diffuse axonal injury (DAI) and unfavorable clinical outcome in patients with traumatic brain injury (TBI). They report a retrospective study which included 261 patients with TBI, 69 of which with DAI lesions as diagnosed within 2 weeks from injury with MRI. DAI lesions were classified into three types: lobar white matter lesions, corpus callosum (CC) lesions, lesions in the dorsolateral quadrants of the midbrain and upper pons. Furthermore, lesions involving the CC were additionally subdivided into three types: genu, body or splenium lesions. The clinical outcome was measured using the Glasgow Outcome Scale (GOS).

Univariate and multivariate logistic regression analyses were performed to evaluate the relationships between clinical characteristics and outcome for each type of DAI lesion and CC lesion in patients with TBI. Results indicate that, one year after TBI, significantly more patients with DAI had unfavorable outcome than patients without DAI. Patients with CC lesions, especially in the genu had the most unfavorable outcome.

Methodology is sound and results are clearly presented and well discussed. This paper leaves these reviewers with some unanswered questions, possibly to be addressed by further studies enrolling larger cohorts of patients. One is the singular preponderant number of patients with single, anatomically well localized DAI lesions in this series. The other point, given the relative importance of the educational level which may modulate premorbid cognitive performance, is the lack of such data which should be included to guarantee that the center point of the manuscript is not a side effect result of premorbid differences.

Besides that, this is an interesting investigation adding valuable information to the prognostic process in severe TBI.

Domenico d'Avella
Giuseppe Sartori
Padova, Italy

Acta Neurochir (2011) 153:1695–1699
DOI 10.1007/s00701-011-1068-4

HOW I DO IT

How I do it: cervical lateral mass screw fixation

Enrico Tessitore · Yassine El-Hassani · Karl Schaller

Received: 21 April 2011 / Accepted: 2 June 2011 / Published online: 19 June 2011

Abstract
Background Cervical lateral mass screw fixation is indicated for the treatment of cervical subaxial C3-C7 lesions associated with instability.
Method The authors first describe the surgical anatomy of the subaxial cervical posterior approach. Then the Magerl technique is detailed. In particular, tricks to avoid complications are presented. The ideal screw entry point, direction, size and exit point are mentioned. A surgical video, artist's drawings and a radiological case report are included.
Conclusion The Magerl technique is a safe and effective lateral mass fixation technique. Respecting anatomical landmarks is crucial to avoid nerve root, vertebral artery and facet joint injury.

Keywords Cervical instability · Lateral mass · Screw placement · Magerl technique

Relevant surgical anatomy

A standard posterior cervical approach is performed to expose lateral masses. Three different muscular layers are crossed. The first one is the trapezius muscle, which originates from the external occipital protuberance, the medial nuchal line and the C7 to D12 spinous processes; the trapezius muscle also inserts onto the upper body of the scapula, acromion and the lateral aspect of the clavicle. The intermediate layer includes the splenius capitis and splenius cervicis. The sacrospinalis muscle group (semispinalis cervicis, semispinalis capitis, semispinalis medially, longissimus cervicis and longissimus capitis centrally, then the ciliocostalis laterally) and the transversospinalis muscle group (semispinalis muscle, multifidus muscle and rotator muscle) represent the third deepest layer [2, 13, 14, 16].

The facet joint is composed of articular processes, the facet capsular ligament and intervening fibro-cartilage. The lateral mass area is the part lateral to the lamina and between the inferior borders of the adjacent inferior facets. The mean superoinferior length of the lateral mass ranges between 11 mm at C3 and 15 mm at C7, and the mean mediolateral distance ranges from 12 to 13 mm at C3 through C7. The isthmus is the part of the bone between the superior and inferior facet joint, the equivalent of the more evident region in the lumbar region [3, 4, 10, 14].

The spinal nerve exits the spinal canal through the interpedicular foramen. Laterally, it divides into a larger ventral ramus and a smaller dorsal ramus. The ventral ramus of the cervical spinal nerve courses on the transverse process in the anterolateral direction to form the cervical and the brachial plexus [4]. The mean distance from the posterior center of the lateral mass and the projections of the spinal nerves is about 5.6 mm [5]. On the axial plane, the spinal nerve is situated anteromedially to the anterior aspect of the superior facet.

The V2 segment of the vertebral artery goes from the sixth to the second cervical transverse foramen. On the

Electronic supplementary material The online version of this article (doi:10.1007/s00701-011-1068-4) contains supplementary material, which is available to authorized users.

E. Tessitore (✉) · Y. El-Hassani · K. Schaller
Neurosurgical Unit, Faculty of Medicine,
Geneva University Medical Center,
Rue Gabrielle Perret-Gentil 4,
1211 Geneva 14, Switzerland
e-mail: tessenri@libero.it

axial plane, the vertebral artery lies in front of the lateral mass, but is separated by the spinal nerve. The vertebral artery is not at risk of injury as long as the screw is directed laterally to the sagittal plane [4].

Description of the technique

Posterior placement of lateral mass screws is a well-established and routine technique used in the fusion and stabilization of the subaxial cervical spine. The patient is placed in prone position with the chest elevated 15° to reduce venous bleeding and the neck in a neutral position to avoid fusion in rotation. The head is fixed into a three-pin Mayfield head-holder allowing strong immobilization during screw placement. The arc of Mayfield head holder should be perpendicular to the floor. The shoulders are stitched off with a tap in order to improve the visualization of the lower subaxial spine. Lateral fluoroscopy is performed to confirm the level.

After disinfection, a median skin incision is made. Muscular subperiosteal dissection is performed and self-retaining spreaders installed. The spinous processes, the laminae and the lateral masses are prepared. The lateral dissection is stopped as soon as the external border of the lateral mass is identified to avoid annoying bleeding [11, 12].

The lateral mass is considered to be split in four quadrants. A cross is marked with a monopolar coagulation, and the lateral mass center point is identified.

According to the Magerl technique [8], the entry point is 1 mm above and 1 mm medial to the center point (Fig. 1).

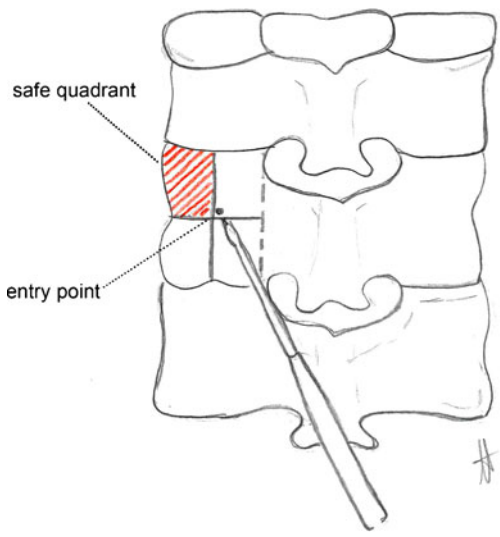

Fig. 1 Artist's drawing: the left lateral mass is identified; "the safe quadrant," the entry point and the drill direction are detailed. The drill is touching the spinous process of the vertebra below

A 2-mm high-speed drill is used to decorticate the bone at the entry point. Under fluoroscopic control, a manual 2.9-mm drill with an adjustable drill guide is then directed toward the so-called "safe quadrant," which is the supero-lateral one (Fig. 1). The direction is 20 to 30 degrees divergent from the midline (Fig. 2) and upwardly parallel to the superior facet joint (Fig. 3). A useful trick is to operate from the controlateral side and to touch the tip of the spinous process of the vertebra below with the drill (Fig. 1). The technical challenge is not to be too high, thus avoiding the facet joint, and also not to be too low, thus avoiding root injury. In this way, the tip of the screw at the exit point will be far enough from both the vertebral artery, which is more medial and anterior, and the exiting nerve root, which is more downward and anterior (Fig. 4). Normally both cortical bones of the lateral mass should be drilled in order to have better purchase. As demonstrated previously by Heller et al., bicortical purchase provides a greater pullout resistance for lateral mass screws with a gain of approximately 30% [6]. The breaching of the deep cortical bone can only be felt as a loss of resistance.

The surgeon can imagine the ventral perforation of the lateral mass on lateral fluoroscopy. The tip of the screw should never overpass the posterior fourth of the vertebral body [5].

Afterwards, a 3.5-mm tap is used, and a 4-mm-diameter polyaxial screw is inserted. The usual length is between 12 to 18 mm. The screws are then connected with rods. A head nut is then inserted and closed with a dynamometric tool.

Wound closure is accomplished by suturing the muscle layers in a multiple plan using resorbable stitches, and the skin is finally sutured.

Minimally invasive procedures through tubular retractors have also been described to achieve lateral mass fixation. In this way, muscular damage and postoperative pain can be drastically reduced [15].

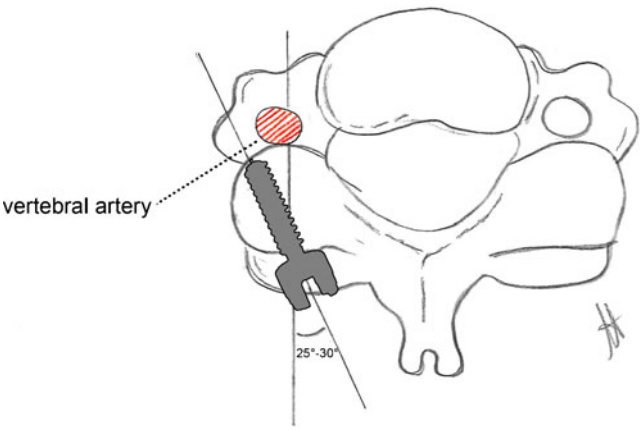

Fig. 2 Artist's drawing: axial view; the divergent direction of the screw is shown. The VA is more medial and anterior

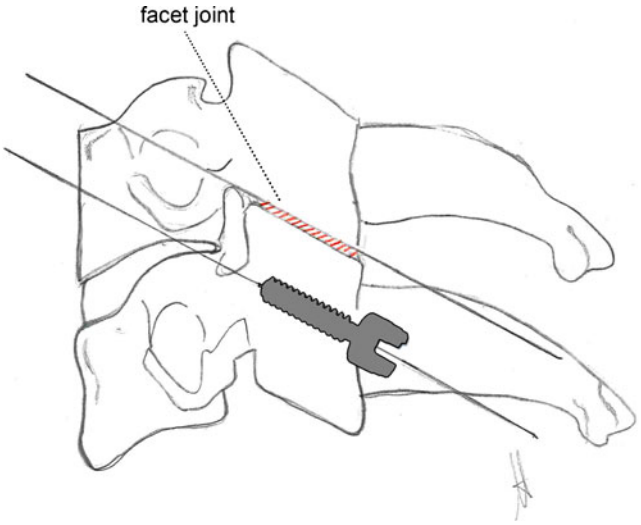

Fig. 3 Artist's drawing: lateral view; the screw trajectory is parallel to the superior facet joint

The C7 lateral mass is often too small and thin to accommodate a screw [1]. In those cases, the authors perform a pedicle screw technique. If the lateral mass is large enough, due to the obliquity of the screwing process, a skin incision should be carried out much lower than C7.

Indications

Lateral mass screw fixation is indicated for the treatment of cervical subaxial C3-C7 pathologies associated with instability. Main indications are:

1. Cervical stenosis with loss of lordosis or focal kyphosis
2. Cervical instability due to trauma, tumors or infections involving the posterior tension band
3. Cervical chronic instability due to degenerative lesions
4. Cervical deformity

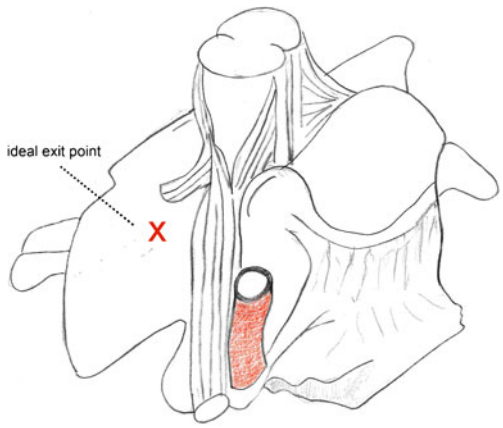

Fig. 4 Artist's drawing: oblique anterior view; the relationship among the screw exit point, the vertebral artery and the nerve root is shown

Limitations

This technique cannot be used in the following situations:

1. Fracture of the lateral mass.
   The presence of a lateral mass fracture is a contraindication to using this technique. In this case the surgeon should plan for an alternative cervical fixation technique (laminar hooks, laminar or pedicle screws). Cervical pedicle screw insertion is by far the stiffest technique for cervical fixation. This technique is considered difficult because of the pedicles' size and the proximity between the screw and the vertebral artery in its transverse foramen. This is why the use of neuronavigation systems is highly recommended [7]. The laminar hooks technique is dependent on the integrity of posterior elements and is not stiff enough in flexion and rotation. The laminar screws can be used as a rescue technique if the laminar thickness is large enough.
2. Relevant anterior column deficiency.
   Lateral mass screw fixation cannot be used alone for those cases in which the instability is mainly related to an anterior column deficiency. In this case an anterior complementary approach (cage/graft plus plating) should be added (Fig. 5a, b, c).
3. Previous posterior surgery affecting normal lateral mass integrity.
   Previous laminectomy with partial lateral mass resection can preclude the use of a lateral mass fixation. In such cases, the anatomical landmarks are distorted, and the bony surface may not be sufficient to accommodate a screw.

Furthermore, lateral mass screw fixation has been shown to be less stiff than the pedicle screw technique, with moderate resistance to withdrawal forces [9]. As a consequence, screwing a significant number of lateral masses is usually necessary to have good purchase.

How to avoid complications

1. Distorted anatomy:
   In elderly patients, the identification of the lateral mass anatomy and "safe quadrant" can be difficult because of the degenerative changes. Osteophytic spurs often cover the facet joints. In this case the surgeon should "create" the anatomy by resecting the spurs and by flattening the lateral mass with a high-speed drill.
2. Vertebral artery:
   If the screw is too long or the trajectory wrong, the vertebral artery can be damaged at its V2 segment. In order to avoid the artery, a good divergent direction

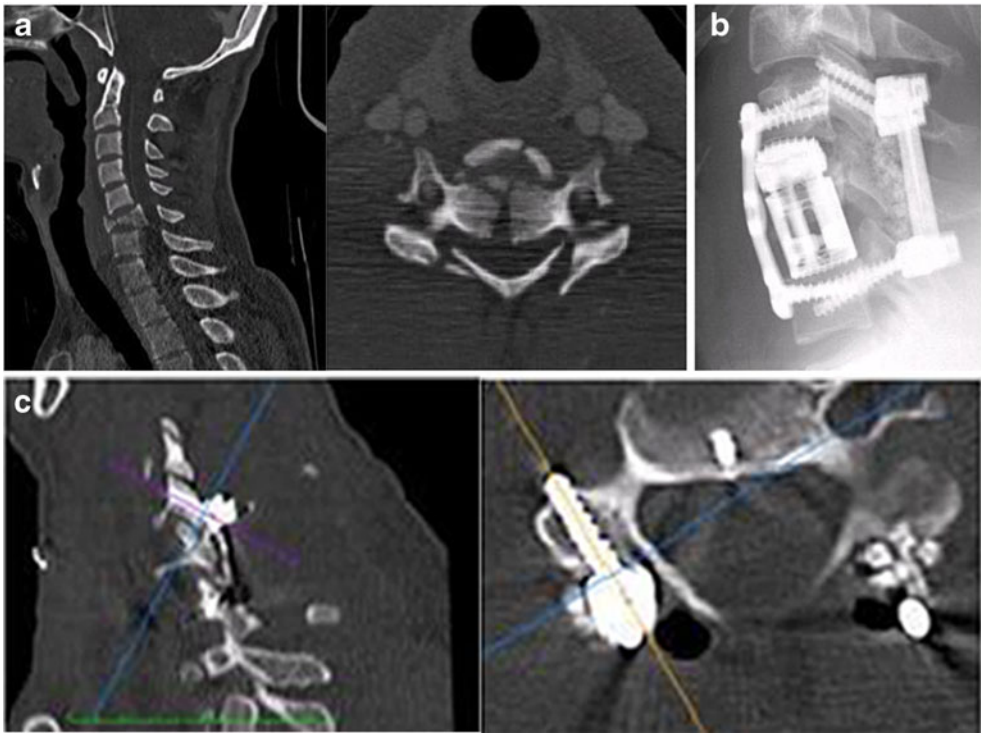

Fig. 5 Illustrative case (see video). **a** Preoperative CT scan showing a C6 burst fracture. **b** Postoperative x-ray showing screw placement and anterior stabilization. The inferior screws are C7 pedicle screws. **c** Postoperative CT on lateral and axial view showing screw placement

should be kept (about 25°) and the correct screw length chosen. If strong suspicion of VA damage exists, the surgeon should quickly insert the screw to stop bleeding, abandon the procedure and send the patient for an angiogram. If the damaged VA is the non-dominant one or is hypoplasic, the procedure can be continued, but the surgeon should change the strategy for the controlateral side (hooks or laminar screws).

3. Nerve root:

   The nerve root cannot be visualized during the screw insertion, so respecting the safe quadrant and choosing the right screw size are mandatory.

4. Facet joint:

   Respecting the facet joint is mandatory for keeping good segmental motion. The inserted screw should not enter into the articular rim; otherwise, the movement will be compromised. The surgeon should keep in mind the oblique direction of the facet joints. The right oblique direction can be checked by fluoroscopy.

Specific perioperative considerations

An appropriate radiological workup is necessary. Standard films are easily performed in any emergency center and available for a first evaluation of the cervical alignment. CT scans offer more accurate evaluation of bone integrity and can also detect some indirect signs of instability (disc rupture, increased interspinous distance, etc.). MRI is mandatory in the presence of a neurological deficit and in case of suspected disco-ligamentous injuries. If MRI results are equivocal or MRI contraindicated, a CT myelogram can be used.

During anesthesia induction, extension maneuvers should be avoided. Fiber optic intubation should always be implemented in case of cervical instability or severe stenosis. Motor-evoked potentials and/or sensory-evoked potentials can be an additional resource to avoid neurological impairment during induction and surgery. Neuronavigation can also be added as a useful tool to reduce the rate of screw misplacement.

In postoperative care, antibiotics are continued for 24 h. Patients are placed in a rigid Minerva collar to wear for 6 weeks after surgery. A postoperative CT scan is performed the day after surgery to check the screw's positioning. Patients usually stay in the hospital for up to 1 week. A physical therapist schedules daily sessions to help patients learn safe ways to move, dress and carry out activities without putting extra strain on the neck. Patients are able to return home when their medical condition is stable. However, they are usually required to keep their activities to a minimum. Outpatient physical therapy is usually started 4 to 6 weeks after the date of surgery. Upright AP and LL x-rays are used for the follow-up.

Specific information to give to the patient about surgery and potential risks

Patients should be informed and give their consent to surgery. The surgical procedure should be anticipated by the

patient. The risks of the prone position (pressure points, shoulder stretching, etc.) should be mentioned. General risks of surgery are detailed (problem with anesthesia, infections, hematoma, thrombophlebitis, etc.). Specific potential risks associated with lateral mass screw fixation are: vascular injury (vertebral artery), spinal cord and nerve root injury, screw misplacement or failure, facet joint injury, and CSF leak.

Key points

- Lateral mass screw placement is a safe and effective fixation technique for cervical subaxial lesions associated with instability.
- The nerve root, vertebral artery and facet joints are in danger during this procedure.
- The Magerl technique, with the divergent and oblique trajectory of the screw, may reduce the risk for VA and nerve root injury.
- The "safe quadrant" should always be identified.
- Screw insertion should be performed under fluoroscopic guidance.
- Bicortical screw purchase is recommended.
- If distorted, anatomical landmarks should be restored.
- In case of VA injury, the procedure should be abandoned or an alternative technique chosen.
- Postoperative immobilization in a Minerva collar for 6 weeks is recommended.
- Upright AP and LL x-rays are used for the radiological follow-up.

Conflicts of interest None.

References

1. Abdullah KG, Nowacki AS, Steinmetz MP, Wang JC, Mroz TE (2011) Factors affecting lateral mass screw placement at C-7. J Neurosurg Spine 14:405–411
2. An H (1994) Anatomy and the cervical spine. In: An HSSJ (ed) Surgery of the cervical spine. Williams & Wilkins Baltimore, pp1-40
3. An HS, Gordin R, Renner K (1991) Anatomic considerations for plate-screw fixation of the cervical spine. Spine (Phila Pa 1976) 16:S548–S551
4. Ebraheim NA (1999) Posterior lateral mass screw fixation: anatomic and radiographic considerations. The University of Pennsylvania Orthopaedic J 12:66–72
5. Ebraheim NA, Tremains MR, Xu R, Yeasting RA (1998) Lateral radiologic evaluation of lateral mass screw placement in the cervical spine. Spine (Phila Pa 1976) 23:458–462
6. Heller JG, Silcox DH III, Sutterlin CE III (1995) Complications of posterior cervical plating. Spine (Phila Pa 1976) 20:2442–2448
7. Ishikawa Y, Kanemura T, Yoshida G, Ito Z, Muramoto A, Ohno S (2010) Clinical accuracy of three-dimensional fluoroscopy-based computer-assisted cervical pedicle screw placement: a retrospective comparative study of conventional versus computer-assisted cervical pedicle screw placement. J Neurosurg Spine 13:606–611
8. Jeanneret B, Magerl F, Ward EH, Ward JC (1991) Posterior stabilization of the cervical spine with hook plates. Spine (Phila Pa 1976) 16:S56–S63
9. Jones EL, Heller JG, Silcox DH, Hutton WC (1997) Cervical pedicle screws versus lateral mass screws. Anatomic feasibility and biomechanical comparison. Spine (Phila Pa 1976) 22:977–982
10. Pal GP, Routal RV, Saggu SK (2001) The orientation of the articular facets of the zygapophyseal joints at the cervical and upper thoracic region. J Anat 198:431–441
11. Bauer R, Kerschbaumer F, Poisel S (1993) Fusion of the cervical spine: Posterior fusion. Atlas of spinal operations. Thieme
12. Bauer R, Kerschbaumer F, Poisel S (1993) Posterior approach to the cervical spine with occipitocervical junction. Atlas of spinal operations. Thieme
13. Rauschning W (1991) Anatomy and pathology of the cervical spine. In: Frymoyer JW (ed) The adult spine. Raven Press, New York, pp 907–929
14. Ungkyu Chang MCL, Daniel H, Kim (2006) Posterior approach to the cervical spine. In: Daniel H, Kim JSH, Vaccaro AR, Dichman CA (ed) Surgical anatomy & Techniques to the spine. Elsevier, pp 57–64
15. Wang MY, Levi AD (2006) Minimally invasive lateral mass screw fixation in the cervical spine: initial clinical experience with long-term follow-up. Neurosurgery 58:907–912, discussion 907–912
16. Zhang J, Tsuzuki N, Hirabayashi S, Saiki K, Fujita K (2003) Surgical anatomy of the nerves and muscles in the posterior cervical spine: a guide for avoiding inadvertent nerve injuries during the posterior approach. Spine (Phila Pa 1976)

Acta Neurochir (2011) 153:1701–1711
DOI 10.1007/s00701-011-0978-5

EXPERIMENTAL RESEARCH

Microsurgical and endoscopic anatomy of Liliequist's membrane and the prepontine membranes: cadaveric study and clinical implications

Ihsan Anik · Savas Ceylan · Kenan Koc · Mehtap Tugasaygi · Gozde Sirin · Nurperi Gazioglu · Bulent Sam

Received: 21 December 2010 / Accepted: 15 February 2011 / Published online: 6 March 2011

Abstract
Background Liliequist's membrane is mostly described as having a diencephalic leaf, mesencephalic leaf, and diencephalic-mesencephalic leaves in the literature. Also different descriptions of the prepontine membranes were reported. In this study, we visualized the regular structural forms of membranes without disturbing any attachments and defined infrachiasmatic and prepontine safety zones. We discussed the clinical significance of these structures.
Materials and methods The study was carried out on 24 adult human cadavers at the Morgue Specialization Department of the Forensic Medicine Institution following the initial autopsy examination. Liliequist's membrane and the prepontine membranes were explored after retraction of the frontal lobes. Dissections were performed under the operative microscope. A 0- and 30-degree, 2.7-mm angled rigid endoscope (Aesculap, Tuttlingen, Germany) was advanced through the prepontine cistern from the natural holes of membranes, or small holes were opened without damaging the surrounding structures.
Results The basal arachnoid membrane (BAM) continued as Liliequist's membrane (LM) without any distinct separation in all specimens. The LM coursed over the posterior clinoids and split into two leaves as the diencephalic leaf (DL) and mesencephalic leaf (ML) in 18 specimens; the medial pontomesencephalic membrane (MPMM) coursed anterolaterally as a continuation of the ML and attached to the medial surfaces of the fifth and sixth nerves, joining with the lateral pontomesencephalic membrane (LPMM), which was also a posterolateral continuation of the ML in all specimens. The medial pontomedullar membrane (MPMdM) and lateral pontomedullar membrane (LPMdM) were observed in 21 specimens. The MPMdM membrane was a continuation of the MPMM, and the LPMdM was a continuation of the LPMM in all 21 specimens.
Conclusion We observed that the LM is a borderless continuation of the BAM. The MPMM and LPMM split from the ML without any interruptions. The MPMdM and LPMdM were a single membrane continuing from the MPMM and LPMM. We determined infrachiasmatic and prepontine areas that can be important for inferior surgical approaches.

Keywords Liliequist membrane · Endoscope · Skull base · Prepontine

I. Anik · S. Ceylan (✉) · K. Koc
Department of Neurosurgery, Kocaeli University,
School of Medicine,
41380 Umuttepe, Kocaeli, Turkey
e-mail: ssceylan@yahoo.com

M. Tugasaygi · G. Sirin · N. Gazioglu · B. Sam
National Forensic Institute of Ministry of Justice,
Istanbul, Turkey

N. Gazioglu
Cerrahpasa School of Medicine, Istanbul University,
Istanbul, Turkey

Introduction

The anatomy of Liliequist's membrane (LM) and the membranous structures in the prepontine structures is of essential importance in minimally invasive neurosurgery. The importance of these anatomic structures has increased with the introduction of neuroendoscopic and endoscopic transphenoidal procedures [13, 28, 29]. An

endoscopic approach through the cisterns requires detailed knowledge of the BAM, LM and prepontine cistern anatomy [13, 23, 28].

Magendie [21] first described the arachnoid mater as a specific layer of the meninges and arachnoidal cisterns in 1842. Key and Retzius [16] described the arachnoid mater and cisterns, and illustrated a distinct arachnoid membrane that divided the interpeduncular cistern into deep and superficial portions. The cisternal anatomy, which is comprised of the arachnoid structures, is described in the literature [15, 22, 24, 33].

In the literature, the LM is mostly defined as a group of anatomically distinct arachnoid sheets [13, 17]: a diencephalic leaf (DL), a mesencephalic leaf (ML) and a pair of diencephalic-mesencephalic leaves (DML). Different descriptions of the lateral pontomesencephalic membrane (LPMM),medial pontomesencephalic membrane (MPMM), medial pontomedullar membrane (MPMdM) and lateral pontomedullar membrane (LPMdM) in the prepontine cistern and their connections forming the cisterns have been described in the literature.

Several authors [27] described the basal arachnoid membrane (BAM), which is important especially in endoscopic skull base surgery, and recently Wang et al. [32] defined the hypothalamic membrane in addition to the other membranes.

In our cadaveric study, we determined the variations of LM, BAM and membranous structures located in the prepontine cistern. We discussed the clinical significance of our findings for endoscopic skull-base procedures and endoscopic third ventriculostomy.

Materials and methods

We studied 24 adult human cadavers in the Morgue Specialization Department of the Forensic Medicine Institution in Istanbul following the initial autopsy examination and approval of the forensic medicine team. Age of 18 years or older and no history of head trauma and/or cranial surgery were the selection criteria for the cadavers. Liliequist's membrane and the prepontine membranes were explored after retraction of the frontal lobes. Dissections were performed under the operative microscope, and a 0- and 30-degree, 2.7-mm angled rigid endoscope (Aesculap, Tuttlingen, Germany) was advanced through the prepontine cistern from the natural holes of membranes, or small holes were opened without damaging the surrounding structures. This allowed us to visualize the regular structural forms of membranes without disturbing any attachments. Surgical procedures were recorded with a digital video camera system.

Results

Basal arachnoid membrane The BAM arose from the superior wall of the cavernous sinus and optic canals covering the tuberculum sellae and anterior clinoid process, and then continued as the LM without any distinct separation in all specimens (Fig. 1). Arachnoid sleeves arose from the BAM to chiasmatic cistern and constituted the anterior wall of the chiasmatic cistern (Fig. 2a). The pituitary stalk coursed to the pituitary gland, penetrating the BAM.

Liliequist's membrane The LM coursed over the posterior clinoids and split into two leaves as the DL and ML in 18 specimens, separated the DL and ML only in 3 specimens and coursed as the ML in 3 specimens. These leaves of the membrane attached to the corpus mamillare at the posterior inferior edges, basilar artery bifurcation anterior-inferiorly, extended to the tentorial edges anterosuperolaterally and attached to the medial uncus inferolaterally (Fig. 1).

Diencephalic leaf The DL was observed in 21 specimens, but not in 3. It had a trabecular form in 4 specimens, was thick in 13 and opaque in 4 (Fig. 2b).

Posterior projections

The DL coursed posterosuperiorly towards the diencephalon, extended upwards and attached to the floor of the third ventricle at the mammillary bodies. The posterior edge of the DL was attached to the mammillary bodies directly in 17 specimens and attached to the pia of the diencephalon between the infundibulum and mammillary bodies in 4 specimens.

Lateral projections

The DL coursed laterally covering the medial third nerve in 14 specimens and gave rise to arachnoid trabeculations of the third nerve in 7 specimens. In three specimens the DL was not observed; thus, the LM continued as the ML. In three specimens the DL coursed from the dorsum sellae to the mammillary bodies as a single membrane.

It merged with the ML superolaterally and coursed in an anterior-inferior direction, forming the DML in 17 specimens.

Mesencephalic leaf The ML leaf was observed in all specimens. The membrane was thick in 14 specimens and opaque in 10. It had various free edges in 7 specimens, trabecular attachments in 5 and was closed totally in 12 (Fig. 2b).

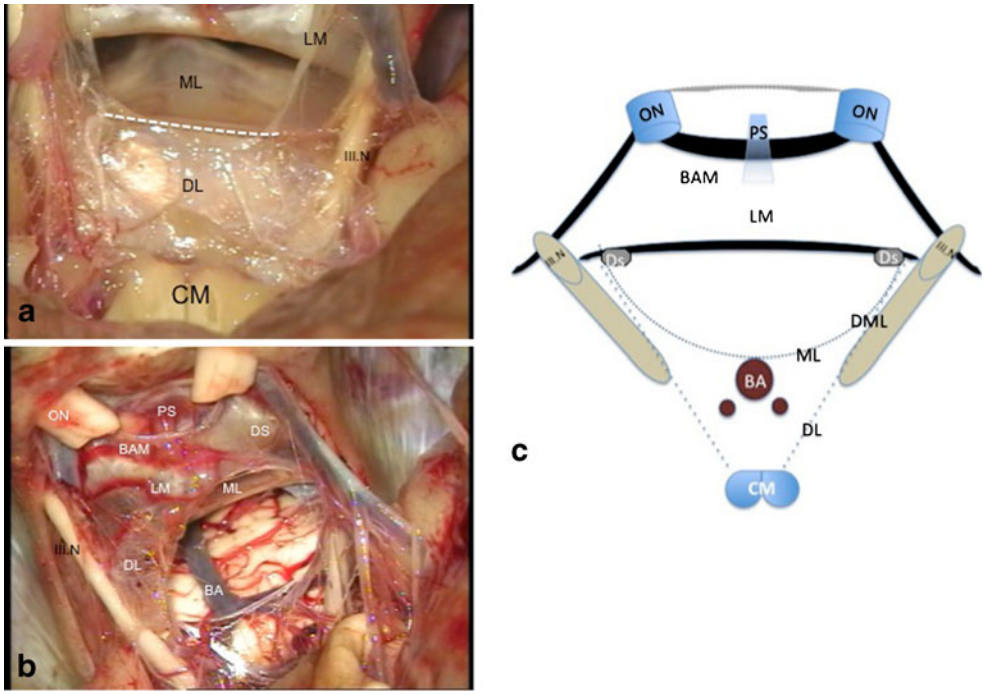

Fig. 1 **a** Optic chiasma was removed. The LM coursed as a continuation of the BAM over the posterior clinoids and split into two leaves as the DL and ML (a large part of a single piece of the LM was removed to visualize the ML). The LM extended laterally and covered the proximal third nerve. The DL attached to the corpus mamillare posteriorly, extending laterally to cover the distal part of the third nerve and attached to the tentorial edges anterosuperolaterally. It attached to the medial uncus inferolaterally. The ML attached to the basilar artery anterior-inferiorly and continued through the prepontine cistern. **b** The optic chiasma was removed. The LM coursed as a continuation of the BAM over the posterior clinoids and split into two leaves as the DL and ML (a large part of the DL was removed to visualize the ML). The DL coursed over the distal part of the third nerve and attached to the medial uncus inferolaterally. The ML coursed towards to the basilar artery-vertebral artery junction through the prepontine cistern. **c** Illustrative drawing of the LM and surrounding structures. BAM: Basal arachnoid membrane, LM: Liliequist's membrane, PS: pituitary stalk, ON: optic nerves, PS: pituitary stalk, BAM: basal arachnoid membrane, DS: dorsum sellae, III.N: third nerve, ML: mesencephalic leaf, DL: diencephalic leaf, CM: corpus mamillare, BA: basilar artery. Horizontal elliptical blue area represents the infrachiasmatic area; vertical elliptical blue area represents the prepontine area

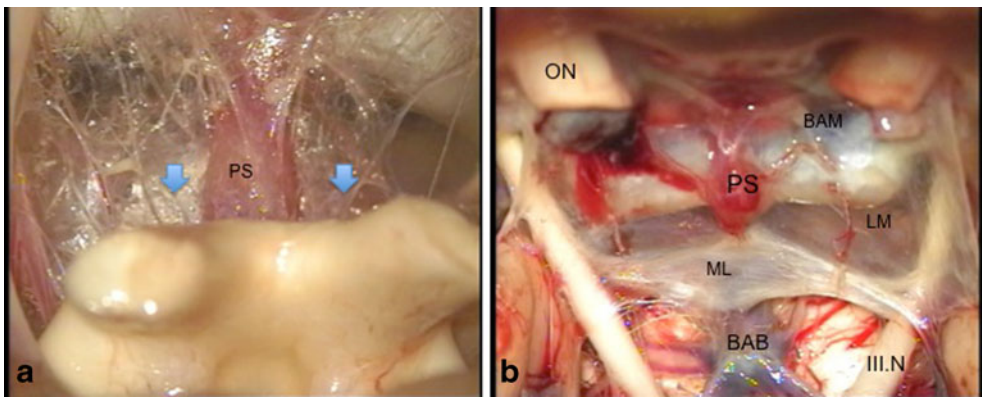

Fig. 2 **a** Arachnoid sleeves arose from the BAM to chiasmatic cistern and formed the anterior wall of the chiasmatic cistern covering the pituitary stalk superiorly (arrows). The pituitary stalk coursed to the pituitary gland, penetrating the BAM. **b** View of the BAM, which was separated from the tuberculum sellae and coursed over the superior wall of the cavernous sinus, optic canals and anterior clinoid process, and continued as the LM without any distinction. The ML attached to the basilar artery bifurcation. The DL is absent, and the ML and LM attached to the uncus laterally covering the third nerve. BAM: Basal arachnoid membrane, LM: Liliequist's membrane, PS:pituitary stalk, ON: optic nerves, PS: pituitary stalk, BAM: basal arachnoid membrane, BAB: basilar artery bifurcation

Anterior projection

In 15 specimens, the ML split from the anterior portion of the LM. The ML coursed anteriorly to the basilar bifurcation in 8 of 12 and coursed towards to the basilar artery-vertebral artery junction in 4 of 12 specimens. In three specimens the ML coursed as a single membrane and attached to the anterior part of the basilar bifurcation.

In eight specimens, the ML was split from the posterior part of the LM and coursed anterior to the basilar bifurcation.

In one specimen there were two MLs, one split from the anterior portion and attached to the basilar artery at the level of the vertebral artery bifurcation, and the other split from the posterior portion of the LM and attached to the basilar artery bifurcation.

Lateral projections

The ML coursed in a posterior-lateral-inferior direction, forming the DML in 17 specimens. It attached with the DL superiorly. Lateral projections of the ML also included the MPPL and LPMM. The ML continued anterolaterally as the MPMM and LPMM posterolaterally in all specimens (Fig. 3). These membranes covered the fifth and sixth nerves medially and laterally.

Diencephalic-mesencephalic leaf The DML was observed in 17 specimens (Fig. 3a). It was located anteroinferolaterally on the distal part of the oculomotor nerve and gave arachnoid sheets to the anteromedial surface of the oculomotor nerve. The posterosuperior part of the leaf was the contination of the DL, and the anterosuperior part of the membrane was the pair of the ML. It was attached to the LPMM inferolaterally. The inferior border of the membrane was located on the anterolateral surface of the pons. In four specimens, arachnoid sleeves attaching to the corpus mammillare formed the DL of the membrane.

In three specimens where the mesencephalic and diencephalic leaves coursed separately as single membranes, an interpeduncular cistern was formed as a single closed room bordered by the DML inferolaterally and the medial carotid artery laterally and superolaterally, the DL posteriorly and ML anteriorly.

Medial and lateral pontomesencephalic membranes (Figs. 3b, 4a)

The MPMM coursed anterolaterally as a continuation of the ML and attached to the medial surfaces of the fifth and sixth nerves, joining with the LPMM between these nerves in all specimens.The LPMM was a continuation of the ML in the posterolateral direction in all specimens. It extended laterally and attached to the lateral edges of the trigeminal and abducens nerves. The LPMM attached to the MPMM between the fifth and sixth nerves anteriorly in all specimens and continued as the LPMdM anteroinferiorly in 21 specimens. The fourth nerve coursed to penetrate the LPMM beneath the tentorium. The LPMM joined the formation of a ring that covered the third nerve, attaching to the DL on the distal posterior surface of the nerve and attaching to the parahippocampal gyrus coursing lateral to the uncus.

Medial and lateral pontomedullar membranes

The MPMdM and LPMdM were observed in 21 specimens. The MPMdM membrane was a continuation of the MPMM, and the LPMdM was a continuation of the LPMM in all 21 specimens (Fig. 4b, c, d).

Lateral and medial pontomedullar membranes continued as a single membrane in all specimens. They continued

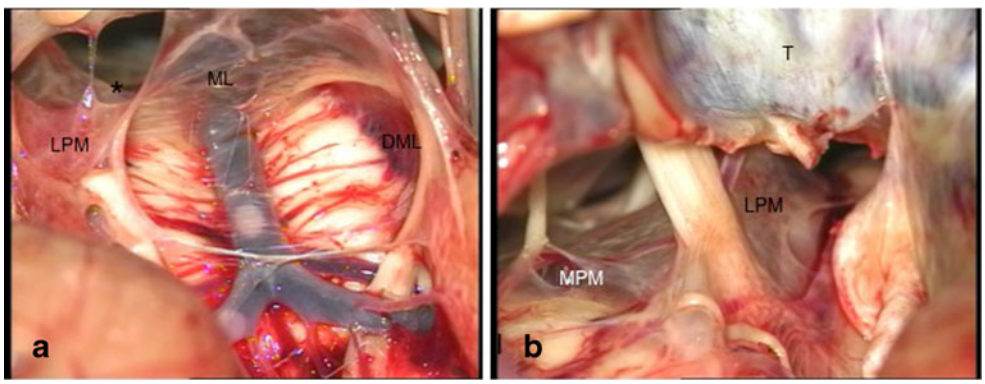

Fig. 3 **a** Microscopic view of the MPML and LPML, which are contiguous with the ML (proximal part of the third nerve was cut). The ML continued anterolaterally as the MPMM and LPMM posterolaterally. It is attached to the basilar artery inferiorly. **b** The LPMM was localized at the lateral edges of the trigeminal and abducens nerves. The MPMM was localized at the medial part of these nerves. The tentorium was cut to clarify the course of the LPMM. The fifth nerve coursed to penetrate the LPMM, and the LPMM was divided into two parts at this point. *MPMM, T: tentorium

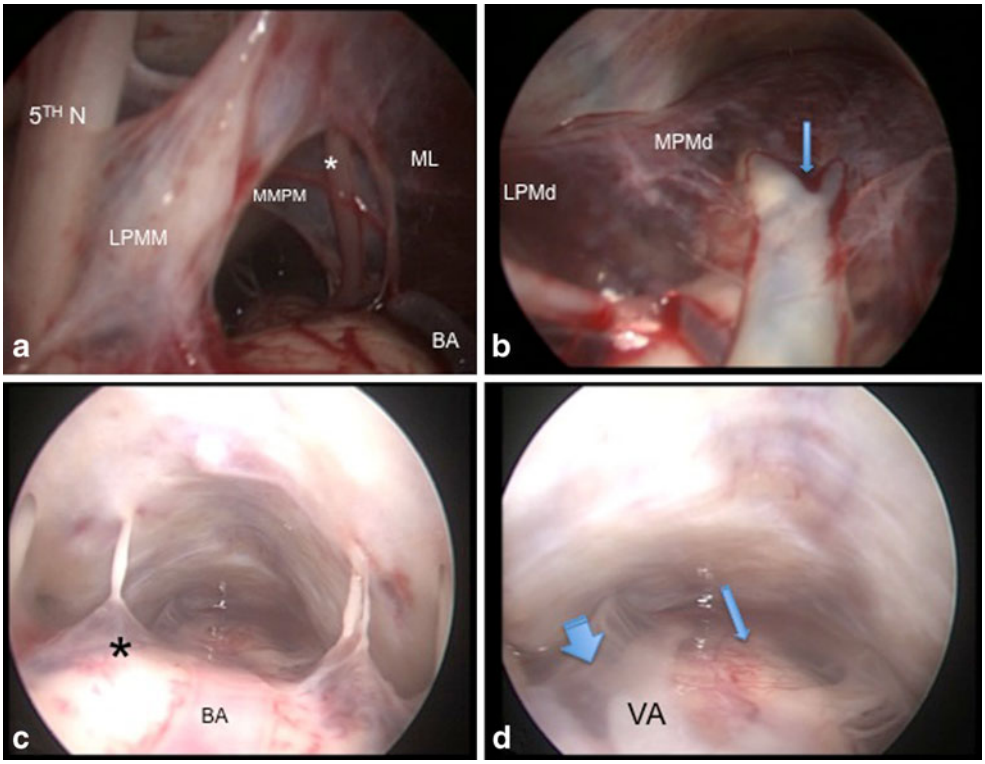

Fig. 4 **a** Endoscopic view of the MPMM and LPMM, which split from the LM. The MPMM covered the sixth nerve laterally (*) and attached to the fifth nerve medially. The LPMM covered the fifth nerve laterally. **b** Membranes representing the medial pontomedullar (MPMdM) and lateral pontomedullar (LPMdM) junction at the level of the basilar artery (BA). Vertebral artery (VA), bifurcation (arrow). **c**, **d** Endoscopic view of the membranes in the prepontine area. A: MPMM (*) coursing over the basilar artery (BA) and continuing as the MPMdM; B: LPMdM (short big arrow) coursing over the vertebral artery (VA) laterally and the MPMdM (thin arrow) coursing between the vertebral arteries. Note that these two membranes cannot be separated

laterally covering the cranial nerves and coursed through the premedullary area in 17 specimens anteriorly, but attached the dura behind the clivus in 4 specimens inferiorly below the level where the vertebral arteries exit.

Occulomotor nerve

We separated the course of the third nerve into three parts (Fig. 5):

1. The entrance point (EP) represents the area between the oculomotor nerve entrance through the porus at the level between the anterior clinoid process and the posterior clinoids. This part was covered with the BAM medially in all cases.
2. The proximal part represents the area between the interpeduncular cistern and EP. If the mesencephalic and diencephalic leaves were separated from the anterior portion of the LM beneath the dorsum sellae, a single part of the LM covered the superior proximal part of the nerve. In case of a posterior separation level, a superior single part of the LM and lateral aspect of the ML covered the proximal posterior surface of the nerve (8 specimens), and the DL covered the inferior part of the proximal part of the nerve. The proximal anteromedial surface of the nerve was covered with ML in all cases.On the proximal anterior surface, the oculomotor nerve coursed between two leaves: medially the ML and laterally the LPMM. The

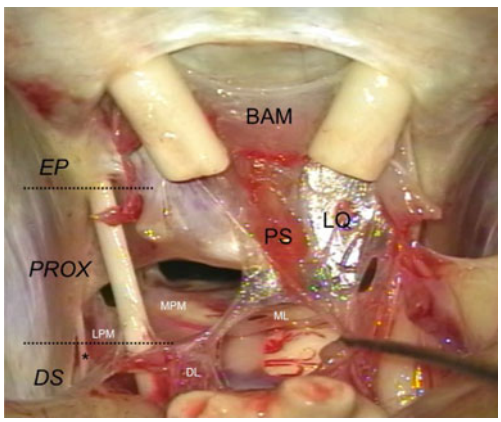

Fig. 5 The course of the third nerve was separated into three regions: the entrance point (EP) represents the area between the occulomotor nerve entrance through the porus at the level between the anterior clinoid process and the posterior clinoids. The proximal part (PROX) represents the area between the interpedincular cistern and EP. The distal part (DS) represents the region in the interpedincular cistern. The ML continued anterolaterally as the MPMM and posterolaterally as the LPMM. The MPMM attached to the anterior and anteromedial part of the proximal part of the third nerve. The LPMM extended backwards, covering the third nerve posterolaterally and laterally. It formed a ring with arachnoid sleeves attaching the DL on the distal posterior surface of the nerve. The DL covered the distal posterior surface of the nerve in the interpedincular cistern. The fourth nerve (*) coursed beneath the tentorium penetrating the LPM. BAM: Basal arachnoid membrane, PS: pituitary stalk, ML: mesencephalic leaf, DL: diencephalic leaf, LPM: lateral pontomesencephalic membrane, MPM: medial pontomesencephalic membrane

proximal lateral surface of the nerve was covered with LPMM in all cases.

3. Distal part represents the region of the interpeduncular cistern. If mesencephalic and diencephalic leaves were separated from the anterior portion of the LM beneath the dorsum sellae, the DL covered the distal part of the medial and posteriomedial surface of the nerve (13 specimens). Otherwise, in the case of a posterior separation level, the DL covered only the distal posterior surface of the nerve in the interpeduncular cistern (8 specimens).The distal anteromedial surface of the nerve in the interpeduncular cistern was covered with DML in 17 specimens. The distal lateral surface of the nerve was covered with LPMM in all cases. DL covered the distal part of the medial and posteriomedial surface of the nerve.

Infrachiasmatic and prepontine areas

We determined two important safety zones in this anatomical study (Fig. 6): the infrachiasmatic and prepontine areas. The infrachiasmatic area is an anatomical region formed by the BAM, LM, DL and ML extending from the optic canal and tuberculum sella to the corpus mamillare. The borders of this area are made up of the optic chiasma, stalk and tuber cinereum superiorly; the diaphragmatic sella-dorsum sella and interpeduncular cisterns inferiorly; the internal carotid artery, posterior communicating artery and oculomotor nerve laterally; and corpus mamillare posteriorly. The BAM, LM, ML and DL, central infindibulum, superior hypophyseal artery and perforating branches are located in this area.

The prepontine area represents the region between the clival dura, mesencephalic leaf and prepontine membranes.

Discussion

In the literature there are various descriptions of Lillequist's membrane [2, 3, 13, 16–20, 27–31, 34]. General consideration of the descriptions includes that the Liliequist membrane is a complicated arachnoid structure formed by a group of arachnoid sheets: a diencephalic leaf, a mesencephalic leaf and diencephalic-mesencephalic leaves [13, 17].

Song-Tao et al. [27] described that the BAM covers the diaphragma sellae and courses to cover the tuberculum

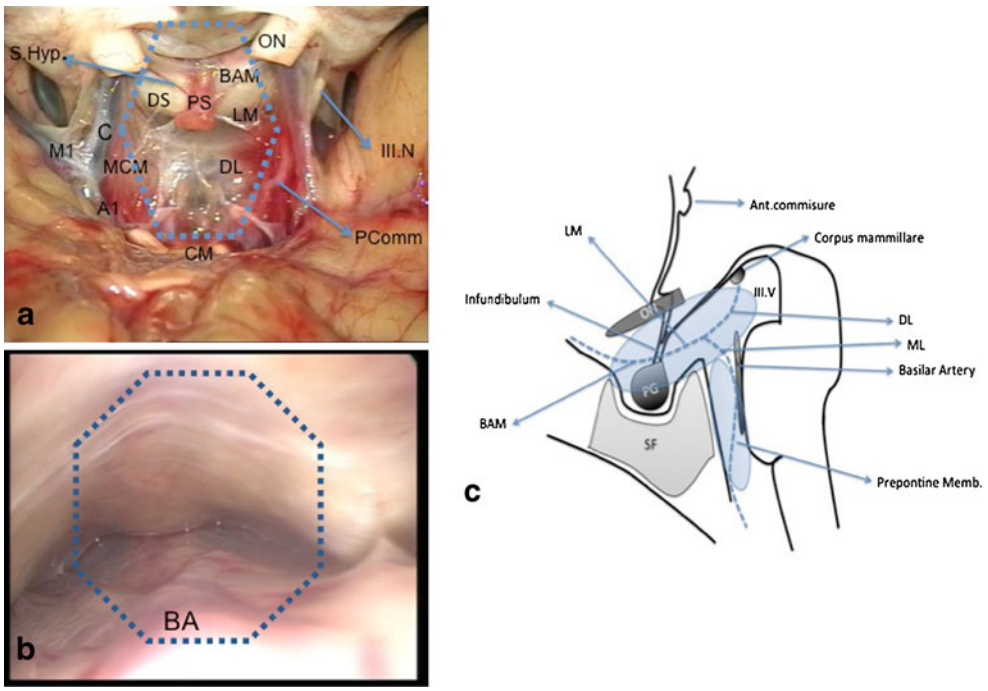

Fig. 6 **a** Infrachiasmatic safety zone: The borders of this area are made up of the optic chiasma (removed), pituitary stalk (PS) and tuber cinereum superiorly, diaphragmatic sella-dorsum sella (DS), interpedincular cisterns inferiorly, internal carotid artery (C), posterior communicating artery (PComm), oculomotor nerve (III.N) laterally and corpus mamillare (CM) posteriorly. Basal arachnid membrane (BAM), Liliequist's membrane (LM), mesencephalic leaf, diencephalic leaf (DM), central pituitary stalk, superior hypophyseal artery (S. Hyp) and perforating branches are located in this area. **b** The prepontine area represents the region between the clival dura, mesencephalic and prepontine membranes, which cover the basilar artery (BA). **c** Illustrative drawing demonstrating the infrachiasmatic (horizontal blue) and prepontine (vertical blue) area. III.V: Third ventricle, SF: sphenoid sinus, PG: pituitary gland

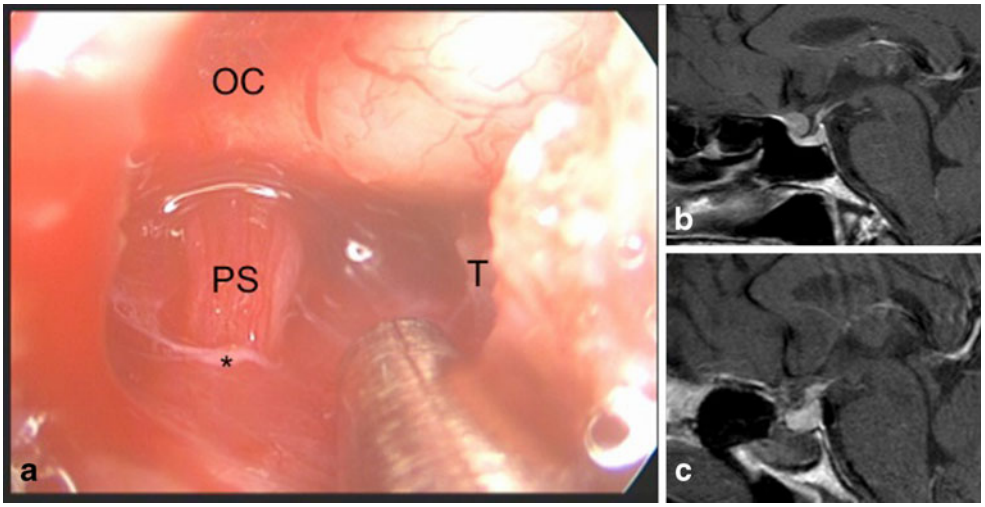

Fig. 7 Intraoperative (**a**), preoperative (**b**) and postoperative (**c**) views of a patient with tuberculum sellae meningioma. OC: Optic chiasma, PS: pituitary stalk, T: residue tumor. *BAM

sellae and anterior clinoid processes. The LM arose from the BAM, covering the dorsum sellae and posterior clinoid processes, and is anteriorly adjacent to the tentorial edge.

In our study we did not observe any distinct separation of the LM and BAM. In all our specimens, the BAM continued as the LM without any attachment or border. The BAM continued over the anterior clinoids and tuberculum sellae, and attached to the anterior-inferior part of the optic nerves at the level of the optic canal entrance.

Wang et al. defined the DL as usually being attached to the ML from underneath, and above the DL it was usually a pair of hypothalamic membranes extending superomedially [32].

In our cadaveric study, we observed that the LM coursed as a single membrane covering the dorsum sellae and posterior clinoid processes. It continued anterior- superiorly to the pituitary stalk covering the dorsum sella and coursed along to the optic canals and tuberculum sella in all specimens. The LM coursed posteriorly and separated into two leaves as the DL and ML either close to the dorsum sella (anterior) or at a distance from the dorsum sella (posterior).

Lü et al [17] described the MPMM as being located in the midline and joining the BA and pons at the bottom of the ML of the LM. The LPMM is reported to be located between the superior cerebral artery, and the trigeminal nerve was free or attached to the lateral end of the MPMM. Froelich et al. [13] demonstrated that the LPMM was a continuation of the LM.

In all our specimens, we observed that the ML separated into two parts forming the MPMM and LPMM. The ML coursed anterolaterally as the MPMM and attached to the trigemineal and abducens nerves. The ML coursed posterolaterally as the LPMM. Lateral and medial pontomesencephalic membranes attached between the 5th and 6th nerves in the lateral part of the prepontine cistern.

Lü, Zhu et al. [20] described that the medial pontomedullar membrane is located in the midline of the pontomedullary sulcus, the superior extremity of the medulla

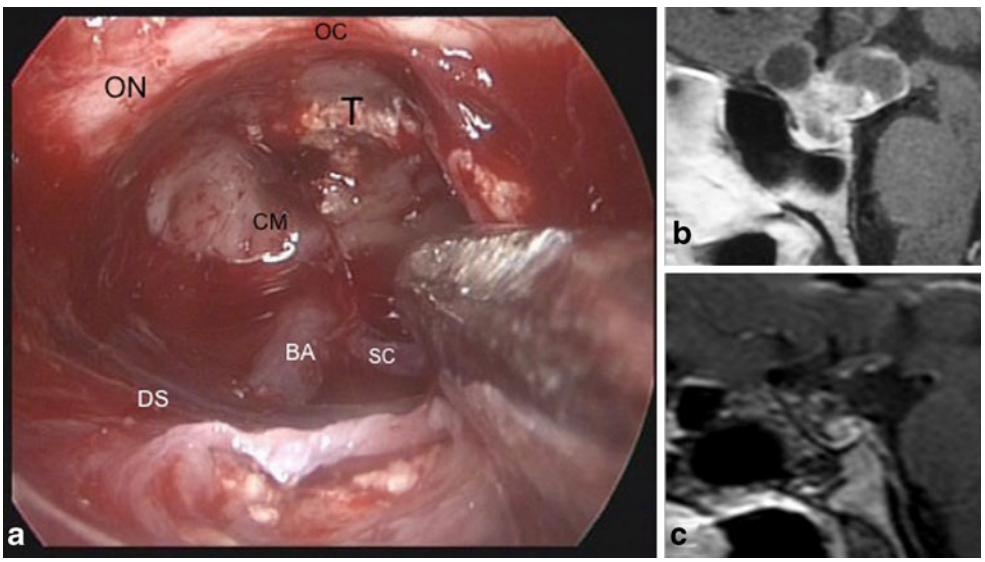

Fig. 8 Intraoperative (**a**), preoperative (**b**) and postoperative (**c**) views of a patient with pre-retro infindibular craniopharyngioma. OC: Optic chiasma, PS: pituitary stalk, T: calcified residue tumor, DS: diaphragma sellae, CM: corpus mamillare, BA: basilar artery, SC: superior cerebellar artery

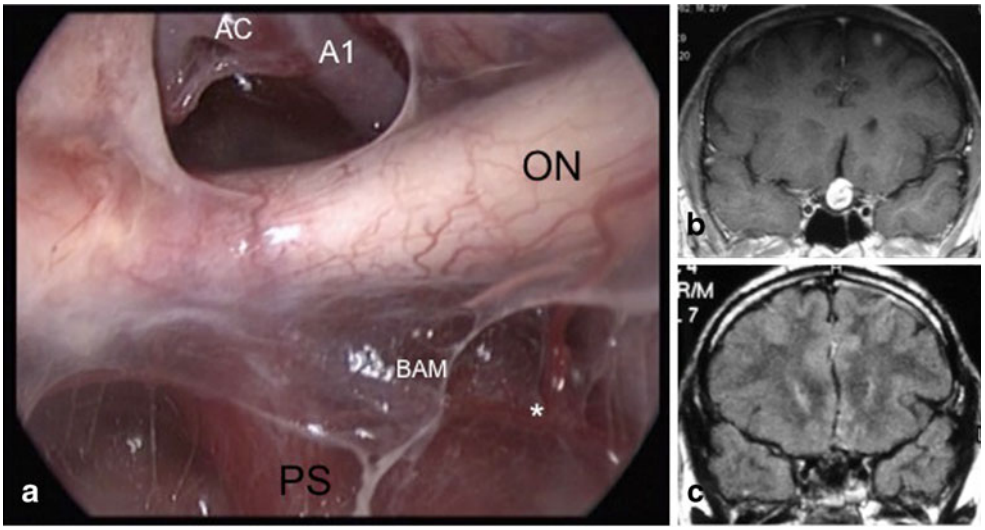

Fig. 9 Intraoperative (**a**), preoperative (**b**) and postoperative (**c**) views of a patient with dermoid tumor extended to the suprasellar area. Intraoperative view of the interpeduncular cistern after the tumor removal. PS: Pituitary stalk, BAM: basal arachnoid membrane, AC: anterior communicating artery, A1: right anterior cerebral artery, *superior hypophyseal artery with the arterial root to the optic nerve

oblongata and basilar membrane, which is perpendicular to the ventral surface of the pons and approximately parallel to the basilar artery. They also demonstrated that the lateral pontomedullar membrane is a paired membrane, which is located in the lateral portion of the pontomedullary sulcus.

In our study we did not observe a separate basilar membrane. The ML coursed as a membrane towards the basilar artery, which may represent the basilar artery membrane.

Also other differences from the literature were the formation of the medial and lateral pontomedullar membranes. The medial pontomedullar membrane was a continuation of the medial pontomesencephalic membrane, and the lateral pontomedullar membrane was the continuation of the lateral pontpmesencephalic membrane in 21 specimens. These membranes coursed through the prepontine cistern as a single membrane and attached to the dura covering the superior aspects of the cranial nerves laterally.

Actually, different descriptions of the LM may be related to the complex structural formation of the ML. In our study, we observed that this formation of the ML provided the continuation of the ML leaf to the neighboring membranes.

Clinical implications

Extended endoscopic transphenoidal approach for skull base lesions

An extended endoscopic transphenoidal approach is needed for skull base lesions extending to the suprasellar area such as craniopharyngeomas, suprasellar cysts, pituitary adenomas with suprasellar extension and tuberculum sellae meningiomas [5–8, 12]. One of the drawbacks of this approach is the limited visibility of the posterior part of the lesions. In the last decade, use of endoscopic approaches for sellar and parasellar lesions has increased.

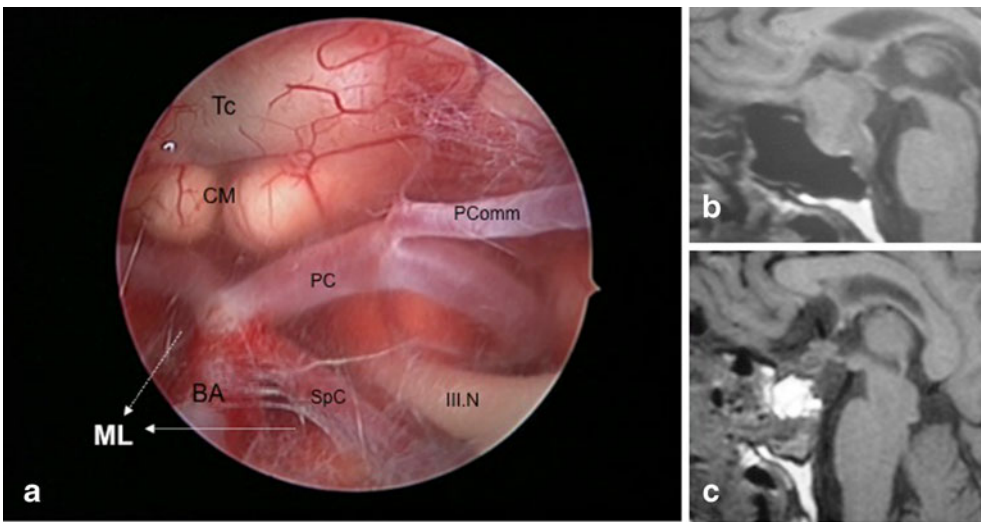

Fig. 10 Intraoperative (after removal) (**a**), preoperative (**b**) and postoperative (**c**) views of a patient with suprasellar pituitary adenoma. Dashed arrows: Mesencephalic leaf. Tc:Tuber cinereum, CM: corpus mamillare, BA: basilar artery, PComm: posterior communicating artery, PC: posterior cerebral artery, III.N: oculomotor nerve

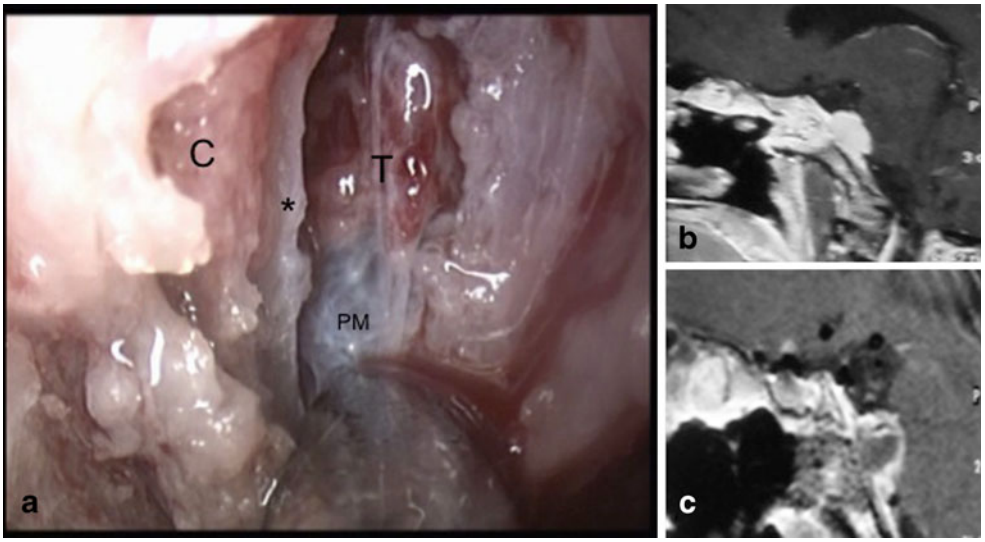

Fig. 11 Intraoperative (**a**), preoperative (**b**) and postoperative (**c**) views of a patient with clival meningioma. T: Tumor, C: clivus, PM: prepontine membrane, * clival dura

In our clinic, we have been performing the endoscopic endonasal transphenoidal approach since 1997 and the extended/expanded endoscopic transphenoidal approach for the last 8 years [4, 5]. Extended and expanded endoscopic transsphenoidal approaches are used for midline skull base lesions from the lamina cribrosa to foramen magnum and have been improved by the development of a standard endoscopic technique and increased experience.

There are still many critics of the extended endoscopic endonasal transphenoidal approach, especially for lesions with an intradural location (meningiomas, craniopharengiomas, etc.) [5–8, 12]. These critiques include that these lesions can be removed much more easily and confidently via traditional approaches; dissection and prevention of neurovascular bundles located behind the tumor are performed much more easily, and complication rates including CSF leakage are lower. These criticisms can be justifiable for intradural anterior midline skull base lesions including olfactory groove meningiomas.

However, EETS provides an important alternative route for operating on the lesions (e.g., tuberculum sella meningiomas, craniopharengioma, pituitary adenomas, etc.) located in the infra-chiasmatic region, extending to the third ventricle, corpus mamillare and prepontine area. In these approaches, the optic chiasma and persistance of the prefix chiasma are important limitations of the transcranial or supraorbital keyhole approaches.

The BAM and LM are important barriers protecting the optic chiasm and these arteries. The infrachiasmatic area is an important surgical safety zone for inferior approaches to this area. In this region, the superior hypophyseal arteries ascend along with the infindibulum; perforating arteries ascend along with the chiasma, tuber cinereum and corpus mamillare [25, 26].

In our clinic, we preferred the extended endoscopic endonasal transsphenoidal approach especially for infrachiasmatically located tumors including the tuberculum sella, diaphragma sella meningiomas, craniopharyngiomas and other tumors [5, 6]. In this region in pre-infundibular (Fig. 7) or retro-infundibular lesions (Fig. 8) up to the corpus mamillare and basilar bifurcation , more secure entrances are provided by the BAM and LM. It was observed that in tuberculum sellae meningiomas, the BAM is displaced inferiorly; however, in pituitary adenomas, craniopharyngiomas and dermoid tumors, it is displaced superiorly (Fig. 9). In pituitary adenomas extending to this region, the mesencephalic membrane is a leading and protecting layer (Fig. 10).

The BAM is an important structure for these lesions because it can cover the posterior-superior surface of the lesions and forms a critical border that avoids damage to the structures located posterior and superior to the lesions during the surgical procedures. In our study, the BAM continued as the LM without a distinct border, and this flexibility of the membrane avoids its laceration during tumor growth. Intactness and elasticity of the membrane may allow the extension of these structures rather than invasion.

There is a significance of the prepontine area for the pathologies located at the clivus intradurally or lesions involving this region with extra- and intradural spreading. These membranes provide protection of vascular structures both in the opening of the clival dura and in tumor dissection (Fig. 11).

Endoscopic third ventriculostomy

The DL is the main component of endoscopic third ventriculostomy. Opening of the tuber cinereum may not always be sufficient to provide CSF diversion in cases with

a dense DL [9–11, 14]. Moreover, as Froelich et al. [13] described, in some cases the DL is opened during the puncture of the tuber cinereum. In these cases, the surgeon observes the ML directly. Since the communication between the anterior basal cisterns is variable according to the anatomy of the LM, the success of the third ventriculostomy is also related to the CSF diversion through the prepontine area [9, 14]. In our study, the interpeduncular cistern was observed as a single closed space covered by the DL, ML, DML and medial carotid membrane in three specimens. In these cases opening of the DL may not provide sufficient CSF diversion, and the ML becomes a significant structure like the DL.

CSF accumulation through the prepontine cistern is also important for third ventriculostomy [1, 14]. In our cadaveric study, it was observed that prepontine cisterns are mostly formed as a single membrane, and in four specimens pontomedullary membranes were attached to the dura behind the clivus, creating a wide prepontine cistern surrounded by the membranes.

Conclusion

1. The continuity of the BAM, LM, DL and ML and the relation of the ML and prepontine membranes were described. The structural formation of these membranes and their variations are important for the efficiency of endoscopic third ventriculostomy.
2. We have determined the borders of the infrachiasmatic and prepontine areas, which are described as safety zones for inferior approaches. The surgical importance of these areas was emphasized by extended endoscopic transphenoidal approaches.

Conflicts of interest None.

References

1. Anik I, Etus V, Anik Y et al. (2011) Role of Interpeduncular and Prepontine Cistern Cerebrospinal Fluid Flow Measurements in Prediction of Endoscopic Third Ventriculostomy Success in Pediatric Triventricular Hydrocephalus. Pediatr Neurosurg doi:10.1159/000323413 (in Press)
2. Brasil AV, Schneider FL (1993) Anatomy of Liliequist's membrane. Neurosurgery 32:956–961
3. Buxton N, Vloeberghs M, Punt J (1998) Liliequist's membrane in minimally invasive neurosurgery. Clin Anat 11:187–190
4. Ceylan S, Koc K, Anik I (2010) Endoscopic endonasal transsphenoidal approach for pituitary adenomas invading the cavernous sinus. J Neurosurg 112(1):99–107 (Erratum in: 2010, 112(1): 210)
5. Ceylan S, Koc K, Anik I (2009) Extended endoscopic approaches for midline skull-base lesions. Neurosurg Rev 32 (3):309–319
6. Ceylan S, Koc K, Anık I (2011) Extended endoscopic transphenoidal approach for tuberculum sellae meningiomas. Acta Neurochir (Wien) 153(1):1–9
7. de Divitiis E, Cappabianca P, Cavallo LM, Esposito F, de Divitiis O, Messina A (2007) Extended endoscopic transsphenoidal approach for extrasellar craniopharyngiomas. Neurosurgery 61(5 Suppl 2):219–227
8. de Divitiis E, Cavallo LM, Esposito F, Stella L, Messina A (2008) Extended endoscopic transsphenoidal approach for tuberculum sellae meningiomas. Neurosurgery 62(6 Suppl 3):1192–1201
9. Dinçer A, Kohan S, Ozek MM (2009) Is all "communicating" hydrocephalus really communicating? Prospective study on the value of 3D-constructive interference in steady state sequence at 3 T. Am J Neuroradiol 30(10):1898–1906
10. Etus V, Ceylan S (2005) The role of endoscopic third ventriculostomy in the treatment of triventricular hydrocephalus seen in children with achondroplasia. J Neurosurg 103(3 Suppl):260–265
11. Etus V, Ceylan S (2005) Success of endoscopic third ventriculostomy in children less than 2 years of age. Neurosurg Rev 28 (4):284–288
12. Frank G, Sciarretta V, Calbucci F et al. (2006) The endoscopic transnasal transsphenoidal approach for the treatment of cranial base chordomas and chondrosarcomas. Neurosurgery 59(1 Suppl 1):ONS50-7; discussion ONS50-7
13. Froelich SC, Abdel Aziz KM, Cohen PD, van Loveren HR, Keller JT (2008) Microsurgical and endoscopic anatomy of Liliequist's membrane: a complex and variable structure of the basal cisterns.Neurosurgery 63(1 Suppl 1):ONS1-8; discussion ONS8-9
14. Fushimi Y, Miki Y, Ueba T, Kanagaki M, Takahashi T, Yamamoto A, Haque TL, Konishi J, Takahashi JA, Hashimoto N, Konishi J (2003) Liliequist membrane: three-dimensional constructive interference in steady state MR imaging. Radiology 229:360–365
15. Inoue K, Seker A, Osawa S, Alencastro LF, Matsushima T, Rhoton AL Jr (2009) Microsurgical and endoscopic anatomy of the supratentorial arachnoidal membranes and cisterns. Neurosurgery 65(4):644–664
16. Key A, Retzius G (1875) Studien in der Anatomie des Nervensystems und des Bindegewebes. Liliequist's Membrane. Stockholm, vol 1
17. Lü J, Zhu XI (2003) Microsurgical anatomy of Liliequist's membrane. Minim Invasive Neurosurg 46:149–154
18. Lü J, Zhu XL (2005) Characteristics of distribution and configuration of intracranial arachnoid membranes. Surg Radiol Anat 27:472–481
19. Lü J, Zhu XI (2005) Microsurgical anatomy of the interpeduncular cistern and related arachnoid membranes. J Neurosurg 103:337–341
20. Lü J, Zhu XL (2007) Cranial arachnoid membranes: some aspects of microsurgical anatomy. Clin Anat 20(5):502–511
21. Magendie F (1842) Recherches Physiologiques et Cliniques sur le Liquide Céphalorachidienou cérébrospinal. Libraire Medicale de Mequignon-marvis fils, Paris
22. Matsuno H, Rhoton AL Jr, Peace D (1988) Microsurgical anatomy of the posterior fossa cisterns. Neurosurgery 23:58–80
23. Perneczky A (1999) Keyhole concept in neurosurgery: with endoscope-assisted microsurgery and case study. Georg Thieme, Stuttgart
24. Rhoton AL (2000) The posterior fossa cisterns. Neurosurgery 47: S287–S297
25. Rhoton AL Jr (2002) The sellar region. Neurosurgery 51(4 Suppl):S335–S374
26. Rhoton AL Jr (2007) The cerebrum. Anatomy. Neurosurgery 61(1 Suppl):37–118

27. Song-tao Q, Xi-an Z, Hao L, Jun F, Jun P, Yun-tao L (2010) The arachnoid sleeve enveloping the pituitary stalk: anatomical and histologic study. Neurosurgery 66(3):585–589
28. Sufianov AA, Sufianova GZ, Iakimov IA (2009) Microsurgical study of the interpeduncular cistern and its communication with adjoining cisterns. Childs Nerv Syst 25(3):301–308
29. Vinas FC, Dujovny N, Dujovny M (1996) Microanatomical basis for the third ventriculostomy. Minim Invasive Neurosurg 39:116–121
30. Vinas FC, Dujovny M, Fandino R, Chavez V (1996) Microsurgical anatomy of the infratentorial trabecular membranes and subarachnoid cisterns. Neurol Res 18:117–125
31. Vinas FC, Dujovny M, Fandino R, Chavez V (1996) Microsurgical anatomy of the arachnoidal trabecular membranes and cisterns at the level of the tentorium. Neurol Res 18:305–312
32. Wang SS, Zheng HP, Zhang FH, Wang RM (2011) Microsurgical anatomy of Liliequist's membrane demonstrating three-dimensional configuration. Acta Neurochir (Wien) 153(1):191–200
33. Yasargil MG, Kasdaglis K, Jain KK, Weber HP (1976) Anatomical observations of the subarachnoid cisterns of the brain during surgery. J Neurosurg 44:298–302
34. Zhang M, An PC (2000) Liliequist's membrane is a fold of the arachnoid mater: study using sheet plastination and scanning electron microscopy. Neurosurgery 47:902–909

Acta Neurochir (2011) 153:1713
DOI 10.1007/s00701-011-0971-z

LETTER TO THE EDITOR

Radiological factors related to recurrence of chronic subdural hematoma

Kimihiro Nagatani · Satoru Takeuchi · Fumihiro Sakakibara · Naoki Otani · Hiroshi Nawashiro

Received: 4 February 2011 / Accepted: 7 February 2011 / Published online: 24 February 2011

We read with great interest the article titled "Use of twist-drill craniostomy with drain in evacuation of chronic subdural hematomas: independent predictors of recurrence" by Escosa et al. [1]. The authors analyzed factors related to the recurrence of hematoma in 312 consecutive patients with chronic subdural hematoma (CSDH) who were treated with twist-drill craniostomy (TDC) with a drain. They measured the radiological parameters of CSDH, namely, hematoma width, midline shift, and hematoma side, before and after the operation, and concluded that preoperative and postoperative hematoma width and midline shift are independent predictors of recurrence. We completely agree with the viewpoint of Escosa et al., and we wish to provide further comment on this issue. Nakaguchi et al. [3] reported that they classified CSDHs into four types according to the internal architecture and density of hematomas, and defined the "separated type" as a hematoma containing two components of different densities separated by a clear boundary—that is, a lower density component located above a higher density component. Among all the CSDH types, the separated type had the highest recurrence rate (36%), as reported by some previous studies [2, 4]. We have also reported the recurrence rates in 64 consecutive patients after CSDH evacuation [5]. Recurrence was noted in seven of the 64 (10.9%) patients after burr-hole craniostomy with a drain, and the separated type of CSDH was seen in three (42.9%) of the seven recurrent cases. Furthermore, Nomura et al. [4] analyzed the concentrations of fibrinogen, fibrin monomer, and d-dimer in patients with "layering-type" CSDH, which is equivalent to the separated type, and reported that the layering type of CSDH is active, has a high tendency to rebleed, and exhibits hyperfibrinolytic activity. Based on these reports, we consider that further investigation to determine the correlation of internal architecture and density of hematomas with the recurrence of CSDH may provide additional insight into the recurrence of CSDH after TDC with a drain.

K. Nagatani (✉) · S. Takeuchi · F. Sakakibara · N. Otani · H. Nawashiro
Department of Neurosurgery, National Defense Medical College, 3–2 Namiki,
Tokorozawa, Saitama 359–8513, Japan
e-mail: naval.kimi@gmail.com

Conflicts of interest None.

References

1. Escosa Baé M, Wessling H, Salca HC et al (2010) Use of twist-drill craniostomy with drain in evacuation of chronic subdural hematomas: independent predictors of recurrence. Acta Neurochir. doi:10.1007/s00701-010-0903-3
2. Fujioka S, Matsukado Y, Kaku M, Sakurama N, Nonaka N, Miura G (1981) CT analysis of 100 cases with chronic subdural hematoma with respect to clinical manifestation and the enlarging process of the hematoma. Neurol Med-Chir 21:1153–1160
3. Nakaguchi H, Tanishima T, Yoshimasu N (2001) Factors in the natural history of chronic subdural hematomas that influence their postoperative recurrence. J Neurosurg 95:256–262
4. Nomura S, Kashiwagi S, Fujisawa H, Ito H, Nakamura K (1994) Characterization of local hyperfibrinolysis in chronic subdural hematomas by SDS-PAGE and immunoblot. J Neurosurg 81:910–913
5. Sakakibara F, Tsuzuki N, Uozumi Y, Nawashiro H, Shima K (2011) Chronic subdural hematoma:recurrence and prevention. Brain Nerve 63:69–74

Acta Neurochir (2011) 153:1715–1716
DOI 10.1007/s00701-011-1013-6

LETTER TO THE EDITOR

Misdiagnosed shoulder tip pain: complication of a ventriculoperitoneal shunt

Jozsef Lorant Lang · John Amaechi Emelifeonwu · Richard Herford Hatfield · Paul Leach

Received: 9 February 2011 / Accepted: 1 April 2011 / Published online: 13 April 2011

Dear Editor,

More than 100 medical conditions can cause shoulder pain and some are due to referred pain [7] such as cardiac and gallbladder conditions, liver abscess and ectopic pregnancy. Similar pain can be a complication of ventriculo-peritoneal (VP) shunts [3, 9]. We report such a case of recurrent shoulder tip pain with a discussion of the likely mechanisms.

A 29-year-old female with benign intracranial hypertension had a frontal VP shunt inserted at the age of 13 and revised 14 years later. A year after the revision she was seen in the clinic with intermittent severe right upper quadrant abdominal plus shoulder pain made worse by coughing, sneezing and taking deep breaths. She was experiencing episodes every 2–3 weeks, which lasted for a couple of days. Plain abdominal films plus a computerised tomography scan of her chest and abdomen were negative. The tip of the peritoneal catheter of the VP shunt was seen in the left side of the abdomen.

She was reviewed by the general surgical team and an ultrasound revealed a gallstone for which she underwent a laparoscopic cholecystectomy. Postoperativly she developed pancreatitis that was managed conservatively.

In spite of the cholecystectomy her right shoulder tip pain recurred. Urgent abdominal imaging was performed and confirmed that the shunt tubing was lying under the right diaphragm (Fig. 1). She underwent repositioning of the peritoneal catheter. There was no evidence of infection and the catheter was not tethered. The catheter was reintroduced into the peritoneum via a left subcostal incision. Her excruciating shoulder tip pain immediately resolved.

Despite an abundance of research on the topic, the precise mechanisms underlying referred pain remain elusive. Several theories have been proposed; one of the most popular is the convergent-projection theory, which suggests that somatic and visceral afferent nerve fibres converge on the same central neurone [7]. This leads to nociceptive visceral activity being mis-intepreted as originating from the somatic area with which that visceral structure is neuronally connected. In our case, afferent fibres from the phrenic nerve innervate central portions of the diaphragm (septum transversus). This association occurs because the septum transversum has its origins in the embryonic cervical region and becomes innervated (by cervical nerve roots C3, C4 and C5, i.e. the phrenic nerve) as it migrates caudally. These afferents therefore enter the spinal cord and mediate pain that is referred to the shoulder, which derives its dermatomal innervations from some of these cervical nerve roots [2]. Further evidence of this phenomenon may be evident in laparoscopic surgery, in which shoulder tip pain is a common complication. Pain in these patients has been attributed to irritation and stretching of the diaphragm [8], with resultant phrenic nerve neuropraxia leading to shoulder tip pain [5]. As such, a peri-operative phrenic nerve block significantly reduces the incidence of shoulder tip pain [4], as does peri-operative infiltration of the peritoneum with local anaesthetic [6]. Ardalan et al. recently reported bilateral infusion-related shoulder and upper limb paraesthesia as a complication of peritoneal dialysis [1]. The authors attributed this to the referred pain from diaphragmatic irritation with dialysate fluid. The incidence of referred shoulder pain secondary to VP shunts is unknown. Based on

J. L. Lang (✉) · J. A. Emelifeonwu · R. H. Hatfield · P. Leach
Department of Neurosurgery,
University Hospital of Wales Cardiff,
Heath Park,
Cardiff CF14 4XW, UK
e-mail: jllang@sky.com

Fig. 1 Lateral abdominal plain X-ray confirming the shunt tubing lying under the right diaphragm (arrow). Abdominal imaging was performed when the patient was in pain

the above mechanism this may be a transient phenomenon in many cases and could well explain an underestimated clinical presentation. In the five previously published cases the average age was 17.4 years, suggesting that the condition affects younger patients, but it is unclear why more patients do not suffer from this complication.

Physicians and surgeons need to be aware of this complication of VP shunts when patients are admitted with shoulder tip and abdominal pain. The shunt tubing needs to be visualised by AP and lateral x-rays during an episode of pain.

The condition is easily treatable by repositioning the abdominal catheter and perhaps the peritoneal catheter should be directed towards the pelvis or the left abdominal cavity, especially in young patients, at the original procedure.

Conflicts of interest None.

References

1. Ardalan MR, Tubbs RS, Etemadi J, Shoja MM (2010) Referred shoulder pain in patients undergoing peritoneal dialysis. Biomedicine International 1:34–36
2. Hinsey JC, Phillips RA (1940) Observations upon diaphragmatic sensation. J Neurophysiol 3:175–181
3. Lim C, O'Sullivan GJ (2005) Shoulder tip pain:under-reported complication of ventriculoperitoneal shunt. Br J Neurosurg 19:354–356
4. Matsui K, Yoshida M, Maemura Y, Ichihara Y, Yamagami M, Kikuchi H (1994) Significance of phrenic nerve block in the anaesthetic management of laparascopic cholecystectomy. Masui 43:1718–1721
5. Mourton WG, Bessell JR, Otten KT, Maddern GJ (1999) Pain after laparoscopy. Surg Endosc 13:445–448
6. Pasqualucci A, de Angelis V, Contardo R, Colo F, Terrosu G, Donini A, Pasetto A, Bresadola F (1996) Preemptive analgesia: intraperitoneal local anaesthetic in laparoscopic cholecystectomy. A randomized, double-blind, placebo-controlled study. Anesthesiology 85:11–20
7. Ruch TC (1961) Pathophysiology of pain. In: Ruch TC, Patton HD, Woodbury JW, Towe AL (eds) Neurophysiology. WB Saunders, Philadelphia, pp 350–368
8. Sarli L, Costi R, Sansebastiano G, Trivelli M, Roncoroni L (2000) Prospective randomized trial of low-pressure pneumoperitoneum for reduction of shoulder-tip pain following laparascopy. Br J Surg 87:1161–1165
9. Tubbs RS, Wellons JC III, Blount JP, Grabb PA, Oakes WJ (2005) Referred shoulder pain from venriculoperitoneal shunts. Report of three cases. J Neurosurg (Pediatrics 2) 102:218–220

Acta Neurochir (2011) 153:1717–1718
DOI 10.1007/s00701-011-1014-5

LETTER TO THE EDITOR

Histologically demonstrated skull bone integration in a hydroxyapatite prosthesis in a human

Giuseppe Messina · Ivano Dones · Angelo Nataloni · Angelo Franzini

Received: 28 March 2011 / Accepted: 1 April 2011 / Published online: 15 April 2011

Dear Editor,

Surgical treatment for skull bone defects consists of cranioplasty using different materials including polymethylmethacrylate, titanium, resin prostheses, polyesther and ceramics [1–4]. The increasing tendency to employ decompressive craniectomy for the treatment of cerebral trauma has led to the need for high-quality materials that can possibly be both resistant and biocompatible. An additional advantage could be osteoinductivity, with promotion of osteoblastic migration across the prosthesis. This property can be found in porous custom-made hydroxyapatite (HA) prostheses, which have been shown to induce osteogenesis in experimental animal models [4]. We had the opportunity to demonstrate that osteogenesis induced by bioceramic protheses occurs also in humans.

A 69-year-old woman had been operated on for left atypical parasagittal meningioma in 2006 at the Department of Neurosurgery of the Istituto Neurologico "Carlo Besta" in Milan. The need to remove the bone flap developed during surgery as the bone was infiltrated by the lesion. One year after her first surgery, the patient underwent cranioplasty with a previously manufactured custom-made hydroxyapatite ceramic new flap. The prosthetic bone flap was obtained by three-dimensional stereolithography based on a computerized tomography 3D model of the patient's skull and bone defect. The material consists of porous hydroxyapatite (including both macropores and micropores). Because of recurrence of the meningioma, she underwent Cyberknife therapy and, subsequently, further surgery 2 years after the first operation. The size of the lesion and the tight adherence of the ceramic material to the skull forced us to remove the prosthesis together with a portion of the surrounding skull, thus resulting into enlargement of the craniotomy. The removed flap was then sent for histological examination, which revealed the presence of fresh bone tissue along the superior margin of the prosthesis and of bone formation along the interface (Fig. 1).

The thickness (in frontal sections) of both the synthetic and the newly developed bone was 4.38 mm; the thickness of the autologous bone layer was 0.13 mm.

The search for perfect or nearly perfect bone integration in bone prostheses implanted as cranioplasty has led to the development of new materials that could help the fusion with the bone edges. In our patient porous hydroxyapatite showed these characteristics. The mainstay is obviously the bone integration at the interface with the used material, but in our case new bone formation occurred also along the superior surface of the prosthesis. Although several reports of radiologically demonstrated successful bone-prosthesis fusion exist [5], this is the first report in the literature of effective bone-HA integration in humans as demonstrated in the postoperative histological examination.

G. Messina (✉) · I. Dones · A. Franzini
Department of Neurosurgery, Fondazione Istituto Nazionale Neurologico "Carlo Besta",
Via Celoria 11,
20133 Milan, Italy
e-mail: giusmex@gmail.com

A. Nataloni
Biomedical Division, Fin Ceramica,
Faenza, Italy

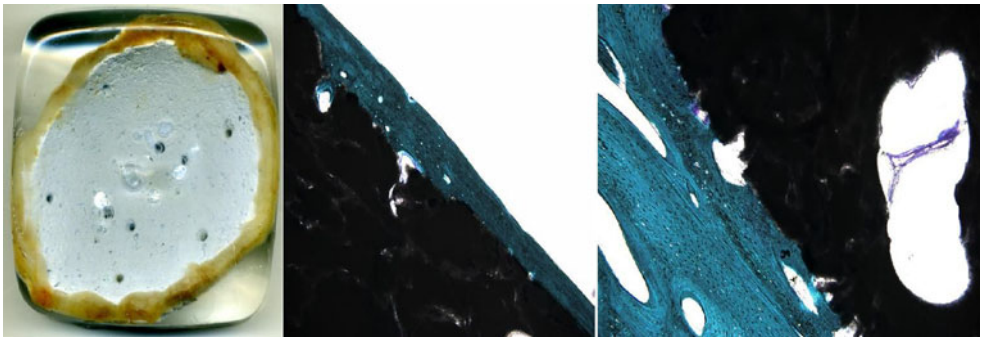

Fig. 1 *Left*: Macroscopic view of the implanted hydroxyapatite prosthesis surrounded by bone after surgical removal. *Middle*: Detail of histological section showing newly formed bone (blue) along the superior surface of the prosthesis (grey). *Right*: Detail of the frontal section of the prosthesis showing bone growth at the interface

Conflicts of interest None.

References

1. Ducic Y (2002) Titanium mesh and hydroxyapatite cement cranioplasty: a report of 20 cases. J Oral Maxillofac Surg 60:272–276
2. Fabbri M, Celotti GC, Ravaglioli A (1995) Hydroxyapatite-based porous aggregates: physico-chemical nature, structure, texture and architecture. Biomaterials 16:225–228
3. Iwama T, Yamada J, Imai S, Shinoda J, Funakoshi T, Sakai N (2003) The use of frozen autogenous bone flaps in delayed cranioplasty revisited. Neurosurgery 52:591–596, discussion 595–596
4. Marcacci M, Kon E, Zaffagnini S, Giardino R, Rocca M, Corsi A, Benvenuti A, Bianco P, Quarto R, Martin I, Muraglia A, Cancedda R (1999) Reconstruction of estensive long-bone defects in sheep using porous hydroxyapatite sponges. Calcif Tissue Int 64:83–90
5. Staffa G, Nataloni A, Compagnone C, Servadei F (2007) Custom made cranioplasty prostheses in porous hydroxy-apatite using 3D design techniques: 7 years experience in 25 patients. Acta Neurochir (Wien) 149(2):161–170, discussion 170

Acta Neurochir (2011) 153:1719–1720
DOI 10.1007/s00701-011-1042-1

LETTER TO THE EDITOR

Cerebral salt wasting syndrome in traumatic brain injury following therapeutic barbiturate coma

M. Kontogiorgi · P. Opsimoulis · E. Diamanti-Kandarakis · A. Karabinis

Received: 7 April 2011 / Accepted: 26 April 2011 / Published online: 9 June 2011

Dear Editor

We present a 22-year-old male with traumatic brain injury (TBI) treated with therapeutic barbiturate coma, who developed cerebral salt wasting syndrome (CSWS) within 24 h of stopping the pentobarbital infusion.

A brain computed tomography (CT) scan revealed subarachnoid haemorrhage and cerebral oedema. He was transferred to an intensive care unit (ICU), where his intracranial pressure (ICP) was found increased (ICP: 30 mmHg).

Despite the applied measures [2], ICP continued to increase and the patient was treated with pentobarbital. The patient remained for 3 days under barbiturate coma and the laboratory findings were unremarkable. After the ICP value was stabilized to 18 mmHg for 24 h, the cessation of pentobarbital infusion was decided. Within a few hours, a sudden steep rise of potassium levels (from 4 to 6.0 mEq/l) accompanied by hyponatremia (serum sodium 138 mEq/l falling to 125 mEq/l in 5 h) was observed. The biochemistry results and the values of right heart catheterization were in favour of the diagnosis of CSWS. Serum potassium concentration returned to normal within 7 h after administration of glucose-insulin infusion and calcium. Despite fluid volume correction with normal saline, the serum sodium dropped to 120 mEq/l. Hypertonic solutions were also administered in the effort to correct the hyponatraemia with a gradual response within 7 days. Finally, his general condition was improved, and he was transferred to the neurosurgery ward.

The early and correct differential diagnosis of hyponatremia in critically ill neurological patients is of major importance and includes the (CSWS) and the syndrome of inappropriate secretion of antidiuretic hormone (SIADH).

CSWS and SIADH share several diagnostic criteria (Table 1) with the two most important differences being extracellular volume and salt balance. CSWS is recognized as a distinct entity from SIADH, a transient phenomenon usually resolving within 3–4 weeks and a therapeutic goal in patients with acute craniocerebral injury.

Smith et al. [6] first proposed the role of atrial natriuretic factor (ANP) in the development of the CSWS. The biological effects of ANP include natriuresis, diuresis, vasodilation and suppression of renin and aldosterone secretion. The administration of pentobarbital induces effects on ANP synthesis gene expression and secretion. A single dose (30 mg/kg, i.p.) of pentobarbital sodium resulted in a suppression in the plasma levels of immunoreactive ANP for up to 1 week of administration and stimulates ANP gene expression and ANP synthesis of the atrium for up to 6 weeks [4]. After cessation of barbiturate

M. Kontogiorgi (✉)
Critical Care Department, Medical School of Athens University,
Evangelismos Hospital,
45–47 Ipsilantou Str,
Athens, Greece 10676
e-mail: kontoloi@otenet.gr

P. Opsimoulis
Critical Care Department, Sotiria Hospital,
Athens, Greece
e-mail: opsimous@yahoo.com

E. Diamanti-Kandarakis
Endocrinology Department, Medical School of Athens University,
Sotiria Hospital,
Athens, Greece
e-mail: e.diamanti.kandarakis@gmail.com

A. Karabinis
Critical Care Department,
Onasis Cardiac Surgery Center Hospital,
Athens, Greece
e-mail: karabinis291@hotmail.com

Table 1 Differential diagnosis of CSWS and SIADH

	CSWS	SIADH
Plasma volume	Decreased	Increased
Salt balance	Negative	Variable
Signs and symptoms of dehydratation	Present	Absent
Weight	Decreased	Increased or not change
Pulmonary capillary wedge pressure	Decreased	Increased or not normal
Central venus pressure	Decreased	Increased or normal
Hematocrit	Increased	Decreased or no change
Osmolality	increased or normal	Decreased
Blood urea nitrogen	Increased	Normal
Serum protein concentration	Increased	Normal
Urine sodium concentration	Increased	Increased
Serum potassium concentration	increased or no change	Decreased or no change
Serum uric acid concentration	Normal	Decreased

coma, an increased plasma ANP concentration is observed. In this case, the ANP levels could not be documented due to lack of facilities.

The hyperadrenergic status after the cessation of barbiturates might have contributed by altering arterial pressure to natriuresis [5].

According to the literature, some cases of patients with TBI presented a biphasic course of treated hypokalaemia, followed by rebound hyperkalaemia after cessation of barbiturate coma [1, 3]. In this case, hyponatraemia, hyperkalaemia and high natriuresis occurred also after cessation of pentothal without presenting hypokalaemia during pentobarbital infusion. We consider that the release of ANP in response to cessation of barbiturate coma mediated inhibition of aldosterone, followed by natriuresis and hyperkalaemia.

The broadly accepted treatment for patients with CSW is, generally, salt supplementation and water replacement.

The prevention and/or treatment of CSWS in patients with TBI appear to be a readily available therapeutic strategy with crucial significance for the neurological outcome. This case emphasizes to development of CSWS after cessation of barbiturate coma to patient with TBI. As possible mechanisms, we consider the realease of ANP and adrenergic surge after the cessation of pentothal. More studies must be completed in order to secure more save results.

Conflicts of interest None.

References

1. Cairns CJS, Thomas B, Fletcher S, Parr MJA, Finfer SR (2002) Life-threatening hyperkalaemia following therapeutic barbiturate coma. Intensive Care Med 28(9):1357–1360
2. Guidelines for the management of severe traumatic brain injury, 3rd edn (2007) J Neurotraum 24(Suppl 1)
3. Schaefer M, Link J, Hannemann L, Rudolph KH (1995) Excessive hypokalemia and hyperkalemia following head injury. Intensive Care Med 21:235–237
4. Seul KH, Cho KW, Kim SH, Hwang YA, Park CU, Koh GY (1993) Single injection of pentobarbital induces long–lasting effects on ANP synthesis and gene expression in the rat atria. Life Sci 52 (16):1351–1359
5. Singh S, Bohn D, Carlotti APCP, Cusimano M, Rutka JT, Halperin ML (2002) Cerebral salt wasting: truths, fallacies, theories, and challenges. Crit Care Med 30:2575–2579
6. Smith HW (1957) Salt and water volume receptors: an exercise in physiologic apologetics. Am J Med 23:623–652

Acta Neurochir (2011) 153:1721–1722
DOI 10.1007/s00701-011-1053-y

LETTER TO THE EDITOR

A simple and safe system for avoiding electrode dislodgement in patients undergoing peripheral nerve field stimulation for chronic pain

Ivano Dones · Giuseppe Messina · Angelo Franzini

Received: 7 March 2011 / Accepted: 16 May 2011 / Published online: 3 June 2011

Dear Editor,

Peripheral nerve field stimulation (PNFS) is a recently introduced minimally invasive surgical procedure used to treat chronic pain refractory to both drug therapy with painkillers or anticonvulsants and spinal cord stimulation [1–3]. It is based on the assumption that the subcutaneous application of an electric field can interfere with the transmission of pain, thus decreasing the local sensation of pain. Many off-label tools are available on the market to achieve this kind of stimulation and they are all characterized by the use of wire cylindrical multipolar electrodes connected to implantable electronic programmable stimulators (IPG). One of the possible reported complications of this procedure is the dislodgment of the electrode and sliding away from the initial determined site, thus bringing to the loss of effect on the painful area. The only remedy claimed by the literature and by some producers is to suture the tip of the electrode to the surrounding tissue by passing a readsorbable suture through the tip of the electrode itself and then suturing that to the subcutaneous tissue. This can be a valuable method, although it forces the surgeon to create an additional skin incision in correspondence to the tip of the electrode with a consequent possible exposure and infection of the electrode from that incision in the long term, but it needs an extra skin incision for every electrode implanted.

In this regard, we thought it would be useful to perform a very simple and quick method of fixing the electrode to the initial location through a transcutaneous reabsorbable suture around the distal part of the Tuohy needle used to insert the electrode once the needle is inserted (Fig. 1a). The electrode is then inserted into the needle and the needle is removed, leaving the electrode in place (Fig. 1b). The suture is then tightened to fix the distal part of the electrode with some subcutaneous tissue around the suture to preserve the electrode from any damage due to the suture itself (Fig. 1c). We could thus avoid a distal skin incision to fix the electrode and by adding a constant loop of the electrode wire at every skin incision along its way to the IPG, we could avoid any dislodgement of any electrode at various subcutaneous locations over the body. In fact, this method was used in the last ten cases submitted to subcutaneous nerve field stimulation in whom the electrodes were placed at both the face and the lumbar and thoracic level. Particularly, five cases affected by hemifacial chronic pain of different origin including postherpetic neuralgia (one case affected by a postherpetic neuralgia at the right arm and shoulder, two cases of post-thoracotomy pain, and two patients affected by median lumbar chronic pain as part of a picture of failed back surgery syndrome) were implanted with a system ranging from the use of one quadripolar subcutaneous electrode to the use of four quadripolar scattered electrodes to cover a wider area. In all these patients, we had no spontaneous or movement-induced dislodgments of the electrodes even on 1-year follow-up.

I. Dones · G. Messina (✉) · A. Franzini
Department of Neurosurgery,
Fondazione Istituto Nazionale Neurologico “Carlo Besta”,
Via Celoria 11,
20133 Milan, Italy
e-mail: giusmex@gmail.com

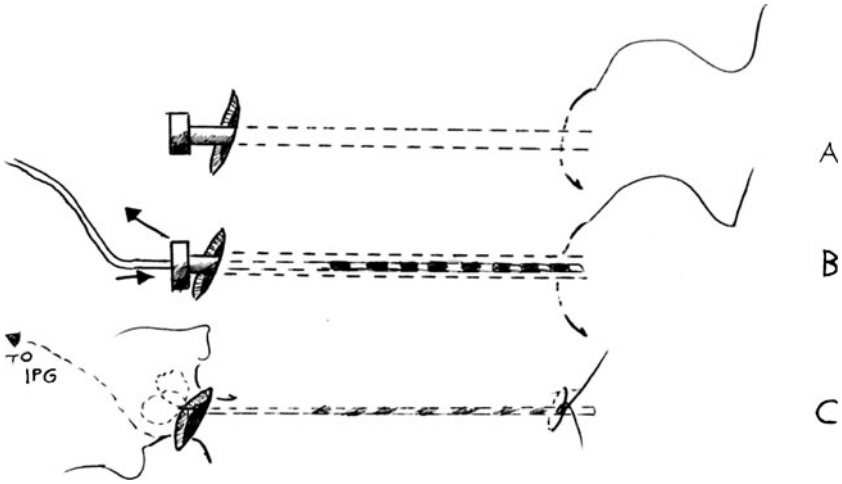

Fig. 1 **a** Insertion of the Tuohy needle for placement of the subcutaneous electrode; a readsorbable suture is positioned around the distal part of the needle. **b** The electrode inserted through the Tuohy needle. **c** Once the Tuohy needle is removed, the suture is tightened around the tip of the electrode to secure it

Conflicts of interest None.

References

1. Paicius RM, Bernstein CA, Lempert-Cohen C (2007) Peripheral nerve filed stimulation for the treatment of chronic low back pain: preliminary results of long-term follow-up: a case series. Neuromodulation 10(3):279–290
2. Slavin KV (2008) Peripheral nerve stimulation for neuropathic pain. Neurotherapeutics 5(1):100–106
3. Weiner RL, Reed KL (1999) Peripheral neurostimulation for control of intractable occipital neuralgia. Neuromodulation 2 (3):217–221.2

Acta Neurochir (2011) 153:1723–1724
DOI 10.1007/s00701-011-1058-6

LETTER TO THE EDITOR

Coexistence of spinal schwannoma with unusual malignant peripheral T-cell lymphoma within a lumbar spine lesion

Christian von der Brelie · Klaus Kuchelmeister · Harald Stein · Azize Boström

Received: 18 February 2011 / Accepted: 18 May 2011 / Published online: 3 June 2011

Dear Editor,

Concerning the central nervous system (CNS), there have been case reports of composite tumorous lesions [2]. We report an unusual case of spinal schwannoma being infiltrated with a T–cell non-Hodgkin's lymphoma (NHL) originating from a rare type of T follicular helper cells.

A 40-year-old male patient presented with sciatic pain and paraesthesia radiating into his left leg, as well as a slight weakness of the left quadriceps femoris muscle. The medical history revealed the onset of a Crohn's disease 10 years previously, treated with prednisone and azathioprine. He did not display clinical lymphoma symptoms. Magnetic resonance imaging (MRI) of the lumbar spine revealed an intradural tumor located at level L2/3, resembling spinal schwannoma (Fig. 1a, b).

A complete microsurgical resection was carried out via partial laminectomy L2 and L3. Intraoperatively the tumor originated in the L3 nerve root and showed findings unusual for schwannoma. The adjoining nerve roots were thickened, possibly by tumor infiltration, and the tumor affected six nerve roots.

C. von der Brelie (✉) · A. Boström
Department of Neurosurgery, University of Bonn,
Sigmund–Freud-Str. 25,
53105 Bonn, Germany
e-mail: Christian.von_der_Brelie@ukb.uni-bonn.de

K. Kuchelmeister
Department of Neuropathology,
University of Bonn Medical School,
Bonn, Germany

H. Stein
Department of Pathology, Campus Benjamin Franklin,
Charité Universitätsmedizin Berlin, Berliner Konsultations- und Referenzzentrum für Lymphknoten- und Hämatopathologie,
Berlin, Germany

Microscopically, the biopsy tissue showed dense sheets and nests of small round lymphoid cells with hyperchromatic nuclei and scant cytoplasm intermingled with histiocyte-like cells. The cells infiltrated a spindle cell tumor with fascicular architecture of tumor cells with hyperchromatic nuclei and ill-defined cytoplasm in a fibrillary eosinophilic matrix. The tumor tissue showed a dense network of argyrophilic reticulin fibers.

The spindle cells displayed S-100 protein-immunopositivity (Fig. 1c) and only rare Ki-67-positive nuclei. Schwannoma (WHO grade I) was diagnosed.

The lymphoid infiltrates consisted predominantly of CD3-immunopositive T cells (Fig. 1d) and there were also numerous CD68-immunopositive histiocytes. The T cells showed PD-1 immunopositivity and focal Ki-67 labeling indices of 10-20%. In molecular pathology, they proved to be a clonal T-cell population. An unusual small cell peripheral T-cell lymphoma originating from T follicular helper cells was diagnosed.

Therefore, the patient showed two tumors in one mass lesion: a schwannoma (WHO grade I) and a small cell peripheral T-cell lymphoma.

Postoperatively, the patient was free of symptoms. Hemato–oncological screening revealed no second focus of NHL or any other neoplasm. The patient underwent local radiation therapy and after 20 months there is no tumor recurrence.

Spinal tumors are uncommon. Spinal schwannomas account for about 25% of intradural spinal cord tumors in adults [1]. T-cell NHLs are a very heterogeneous group of malignancies derived from mature postthymic T–cells and natural killer cells. Peripheral T-cell lymphomas account for approximately 7% of all NHL. Spinal involvement of NHL occurs in 0.1–10% of the patients with NHL as metastatic lymphoma [8]. Primary NHLs arising in the spinal cord are

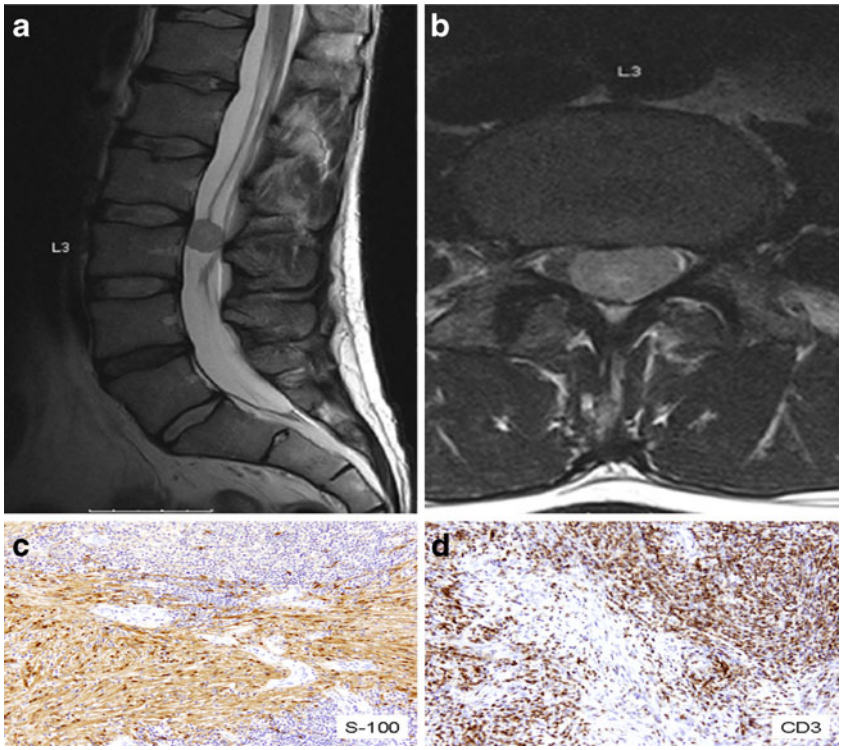

Fig. 1 **a** The saggital T2-weighted image shows a round, well-circumscribed, intradural lesion, which is located behind the L3 lumbar vertebral body. **b** The axial T1 contrast-enhanced image shows a homogenous enhancement. **c** S-100 protein immunopositivity of the schwannoma areas with unstained lymphoid infiltrates (S-100 protein immunohistology). **d** Immunopositivity of the lymphocytic cells with the T-cell marker CD3 with focal unstained schwannoma areas (CD3 immunhistology)

extremely rare [6]. Inflammatory lymphoid infiltrates are frequent in nerve sheath tumors [5]. However, the occurrence of a lymphocytic neoplasm arising in a schwannoma is extremely rare. Recently, a rare case of a schwannoma infiltrated with monoclonal plasma cells was described as a collision tumor. [7] The lymphoma in our case had not only infiltrated the schwannoma but probably also thickened adjoining cauda nerves. Various mechanisms have been proposed for the development of collision tumors, such as the "chance accidental meeting" of two primary tumors or the alteration of the microenvironment by the initial tumor, facilitating the development of a second primary neoplasm or seeding of metastatic tumor cells.

Purine analogues like azathioprine increase the standardized incidence ratios of developing immunosuppression-related NHL [3, 4]. However, whether the immunosuppression in this patient has facilitated the development of the NHL remains unclear.

The patient does not display any recurrent tumor after 20 months so far. Thus, we argue for combined treatment in such an unusual case.

Conflicts of interest None.

References

1. Conti P, Pansini G, Mouchaty H, Capuano C, Conti R (2004) Spinal neurinomas: retrospective analysis and long-term outcome of 179 consecutively operated cases and review of the literature. Surg Neurol 61:34–43, discussion 44
2. Drlicek M, Aichholzer M, Wurm G, Bodenteich A, Fischer J (2004) Collision tumour composed of glioblastoma and meningioma—a case report. Pathologe 25:402–405
3. Farrell RJ, Ang Y, Kileen P, O'Briain DS, Kelleher D, Keeling PW, Weir DG (2000) Increased incidence of non-Hodgkin's lymphoma in inflammatory bowel disease patients on immunosuppressive therapy but overall risk is low. Gut 47:514–519
4. Kandiel A, Fraser AG, Korelitz BI, Brensinger C, Lewis JD (2005) Increased risk of lymphoma among inflammatory bowel disease patients treated with azathioprine and 6-mercaptopurine. Gut 54:1121–1125
5. Labit-Bouvier C, Crebassa B, Bouvier C, Andrac-Meyer L, Magnan J, Charpin C (2000) Clinicopathologic growth factors in vestibular schwannomas: a morphological and immunohistochemical study of 69 tumours. Acta Otolaryngol 120:950–954
6. Mohile NA, Abrey LE (2007) Primary central nervous system lymphoma. Semin Radiat Oncol 17:223–229
7. Plaut J, Galloway M, Childerhouse A, Bradford R (2009) Schwannoma with monoclonal plasma cell infiltration. J Neurosurg 111:509–511
8. Yamashita T, Sakaura H, Oshima K, Iwasaki M, Yoshikawa H (2010) Solitary intradural extramedullary lymphoma of the cervical spine. J Neurosurg Spine 12:436–439

Acta Neurochir (2011) 153:1725
DOI 10.1007/s00701-011-1000-y

RETRACTION NOTE

Erratum to: Cemento-ossifying fibroma of the temporal bone

A. Mahore · R. Kansal · N. Dange

Published online: 21 April 2011

Erratum to: Acta Neurochir
DOI 10.1007/s00701-010-0634-5

It has been brought to our attention that the majority of this article has been previously published in the journal "*Turkish Neurosurgery*" (2010) Kansal R, Sharma A, Gaikwad N, Mahore A, Goel A Vol 20 No 2 pp 265–268

After carefully checking the circumstances with the responsible corresponding author this appears to be an unfortunate result stemming from a misunderstanding of the author in the course of submitting this paper to *Acta Neurochirurgica*.

In order to appropriately correct this situation and to comply with Springers policy of publishing integrity, which also follows the recommendations of COPE, we have therefore agreed with the author and with our colleagues at the Journal *of Turkish Neurosurgery* to the retraction of this article.

Acta Neurochirurgica sincerely regrets the circumstances that have led to this situation and any inconvenience that might have arisen.

The online version of the original article can be found at http://dx.doi.org/10.1007/s00701-010-0634-5.

A. Mahore · R. Kansal (✉) · N. Dange
Department of Neurosurgery, King Edward Memorial Hospital,
Seth G.S.Medical College,
Parel, Mumbai 400 012, India
e-mail: drkansal@yahoo.co.in